https://ntrs.nasa.gov/search.jsp?R=19790025402 2020-03-21T21:08:01+00:00Z

General Disclaimer

One or more of the Following Statements may affect this Document

- This document has been reproduced from the best copy furnished by the organizational source. It is being released in the interest of making available as much information as possible.

- This document may contain data, which exceeds the sheet parameters. It was furnished in this condition by the organizational source and is the best copy available.

- This document may contain tone-on-tone or color graphs, charts and/or pictures, which have been reproduced in black and white.

- This document is paginated as submitted by the original source.

- Portions of this document are not fully legible due to the historical nature of some of the material. However, it is the best reproduction available from the original submission.

Produced by the NASA Center for Aerospace Information (CASI)

Ford Aerospace
-955115-Final
Vol. 1 (Text)

(NASA-CR-162369) PHASE 1 OF THE FIRST SOLAR SMALL POWER SYSTEM EXPERIMENT (EXPERIMENTAL SYSTEM NO. 1). VOLUME 1: TECHNICAL STUDIES FOR SOLAR POINT-FOCUSING, DISTRIBUTED (Ford Aerospace and Communications) 294 p

N79-33573

G3/44 Unclas 38927

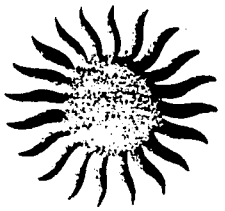

PHASE I OF THE FIRST (SOLAR) SMALL POWER SYSTEM EXPERIMENT

(EXPERIMENTAL SYSTEM NO. 1)

FINAL REPORT

VOLUME 1; TECHNICAL STUDIES FOR SOLAR POINT-FOCUSING, DISTRIBUTED COLLECTOR SYSTEM, WITH ENERGY CONVERSION AT THE COLLECTOR (CATEGORY C)

Prepared by
Ford Aerospace & Communications Corporation
Aeronutronic Division
Newport Beach, California 92663

Prepared for
California Institute of Technology
Jet Propulsion Laboratory
Pasadena, California 91103

Under Contract No.
~~95515~~ 955115

5 May 1979

Ford Aerospace &
Communications Corporation
Aeronutronic Division

Ford Road
Newport Beach, California 92663

PAGE IS
OR QUALITY

CONTENTS

CONTENTS (Continued)

FOREWORD

This final report documents the technical studies conducted by Ford Aerospace & Communications Corporation, Aeronutronic Division under Contract 955115 to the California Institute of Technology Jet Propulsion Laboratory (JPL) in Pasadena, California. The JPL Technical Manager was Mr. J. R. Womack.

This is a three volume report prepared by the Aeronutornic Division. Subcontractors were the WDL Division of Ford Aerospace & Communications Corporation, Palo Alto, California; United Stirling of Sweden (USS), Malmö, Sweden; Sundstrand Energy Systems, Rockford, Illinois.

The WDL Division was responsible for the concentrator and electrical subsystems. USS provided information on Stirling engines, and Sundstrand supplied information on organic Rankine-Cycle Engines. Additional supporting information was provided by Garrett AiResearch Manufacturing Company, Phoenix, Arizona (closed-cycle Brayton engines); Solar Turbines International, San Diego, California (open-cycle Brayton engines); and Williams Research, Walled Lake, Michigan (open-cycle Brayton engines). Also, the following divisions of the Ford Motor Company provided expertise: Glass Division, Scientific Research Laboratory, and the Manufacturing Planning Group.

The key personnel for the studies documented in this final report are listed below:

- Aeronutronic Division, Ford Aerospace & Communications Corporation

  N. L. Cowden - Program Manager

  R. L. Pons - Technical Manager and Systems Analysis

  T. B. Clark - Optics and Assistant Technical Manager

  D. B. Osborn - Thermodynamics

  E. D. Avetta - Design

  D. C. Jackson - Structures

- WDL Division, Ford Aerospace & Communications Corporation

  H. J. Sund - Subcontract Manager

  I. E. Lewis - Concentrator Subsystem

  J. L. Knorpp - Electrical Subsystem

- United Stirling (USS)

  W. Percival - Consultant to Aeronutronic and Marketing Representative of USS

  Y. Håland - Program Manager for Solar/Stirling Applications

- Sundstrand

  M. Santucci - Principal Investigator, Organic Rankine Engine

- Garrett

  L. Six - Principal Investigator, Closed-Cycle Brayton Engine

- Solar Turbines International

  M. Gramlich

- Williams Research

  R. Mandel

- Ford Motor Company Manufacturing Planning Group

  W. Nagle

T. B. Clark was the editor of these reports.

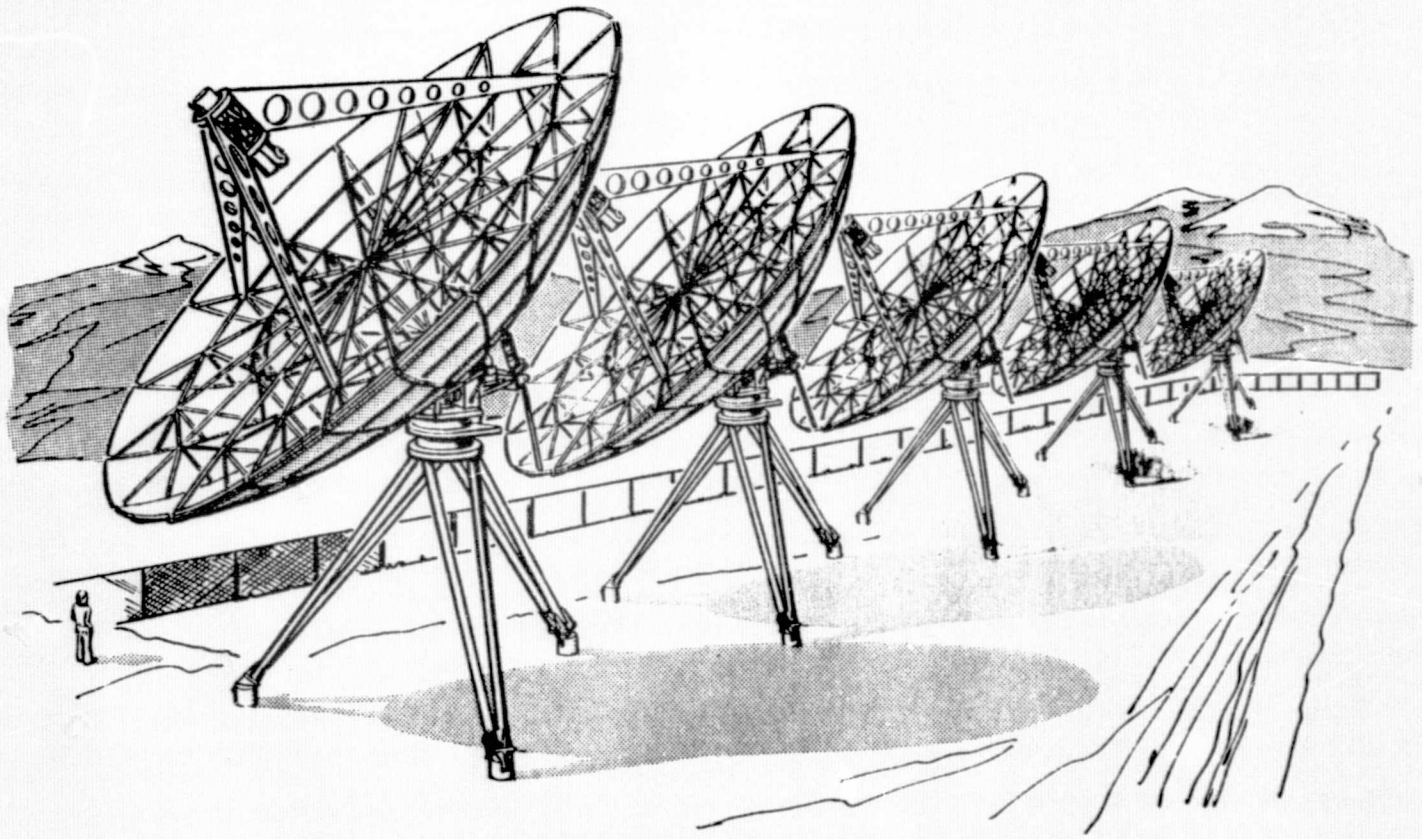

PROPOSED MODULAR DISH/STIRLING SOLAR POWER SYSTEM

SECTION 1

INTRODUCTION

This report presents the results of a ten month study carried out by the Aeronutronic Division of Ford Aerospace & Communications Corporation (FACC) for the Jet Propulsion Laboratory (JPL) under Contract No. 955115, Small Community Power System, Phase I, Engineering Experiment No. 1. Study results encompass an evaluation of the technical and economic feasibility of a solar electric power plant for a small community, together with the selection of specific system designs for further development and demonstration.

All of the systems investigated are defined as point-focusing, distributed receiver (PFDR) concepts, with energy conversion at the collector (JPL category C). An artist's concept of the preferred system is shown in the Frontispiece; it is comprised of multiple parabolic dish concentrators employing Stirling-cycle engines for power conversion. The engine, AC generator, cavity receiver, and integral sodium pool boiler/heat transport system are combined in a single package and mounted at the focus of each concentrator. The output of each concentrator is collected by a conventional electrical distribution system which permits either grid-connected or stand-alone operation, depending on the choice of storage system selected.

1.1 STUDY OBJECTIVES/REQUIREMENTS

The basic objective of this Phase I study is to identify and evaluate optimum small community solar electric power system(s) -- for further engineering development and demonstration testing.

Study requirements include specific tasks, specific development schedules, and criteria for selecting preferred system concepts. The two tasks reported under this contract are:

TASK 1 - Development of Preferred System Concepts.

- Perform the design and optimization analyses required to select preferred Category C concepts for three different plant start-up times (defined below). Nominal system rated power is 1.0 MWe with an annualized capacity factor (ACF) of 0.4.
- Review the development status of each major subsystem and identify the R&D effort necessary to bring them to maturity.
- Provide descriptions of the systems for each start-up time.

TASK 2 - Sensitivity Analysis.

- Analyze the effect of different plant rated power and annualized capacity factor on cost and performance. In addition to the above nominal values, consider rated power of 0.5 and 10.0 MWe and ACF of 0.7 and the value for zero storage.

Figure 1-1 is a detailed breakdown of the various time-phased tasks carried out on the program. All program objectives and requirements have been met during the contract period and are documented in this report. The plant start-up times specified for Task 1 are 3½, 4½ and 6½ years, beginning with the initiation of Phase I. The relationship between the various phases for each start-up time is shown in Figure 1-2. We have adjusted the relative periods of Phases II and III to reflect realistic schedules and lead times and an additional two months has been added between Phases I and II.

The specified system selection criteria, in order of decreasing importance, are (1) High operational reliability, (2) Minimum risk of failure, (3) Commercialization potential, and (4) Low program cost. Table 1.1 gives a further breakdown of the selection criteria. Within a given system concept, minimum life cycle energy cost, for a 30-year plant life, is the specified basis for choosing an optimum design.

1.2 METHOD OF APPROACH

The criteria identified in Table 1.1 represent an approximate balance between near-term considerations, (i.e. Phase III) and far-term, (i.e. ca. 1990) capability. For the near-term demonstration, a reliable low-risk, low-cost concept is desired. For the far term, the concept must offer high operational reliability and be capable of producing electricity at a cost competitive with conventional energy sources, for example, fossil and nuclear systems. To achieve this balance between near- and far-term capabilities, we have formulated an approach with the following key elements:

(1) Overall system selection is based on the criterion of best potential performance for least development cost. Performance is measured by levelized busbar energy cost (BBEC) and development cost includes all effort (Phase III and beyond) which is required to achieve the far term potential.

(2) Emphasis is placed on using state-of-the-art components and technology particularly where such technology has high cost impact for the near-term development/demonstration effort.

(3) Concentrate on critical, high-risk components by applying more in-depth analysis than is customary for conceptual design phase studies.

We have implemented the first element of the approach by selecting a high-efficiency heat engine (Stirling). This results in lowest concentrator cost;

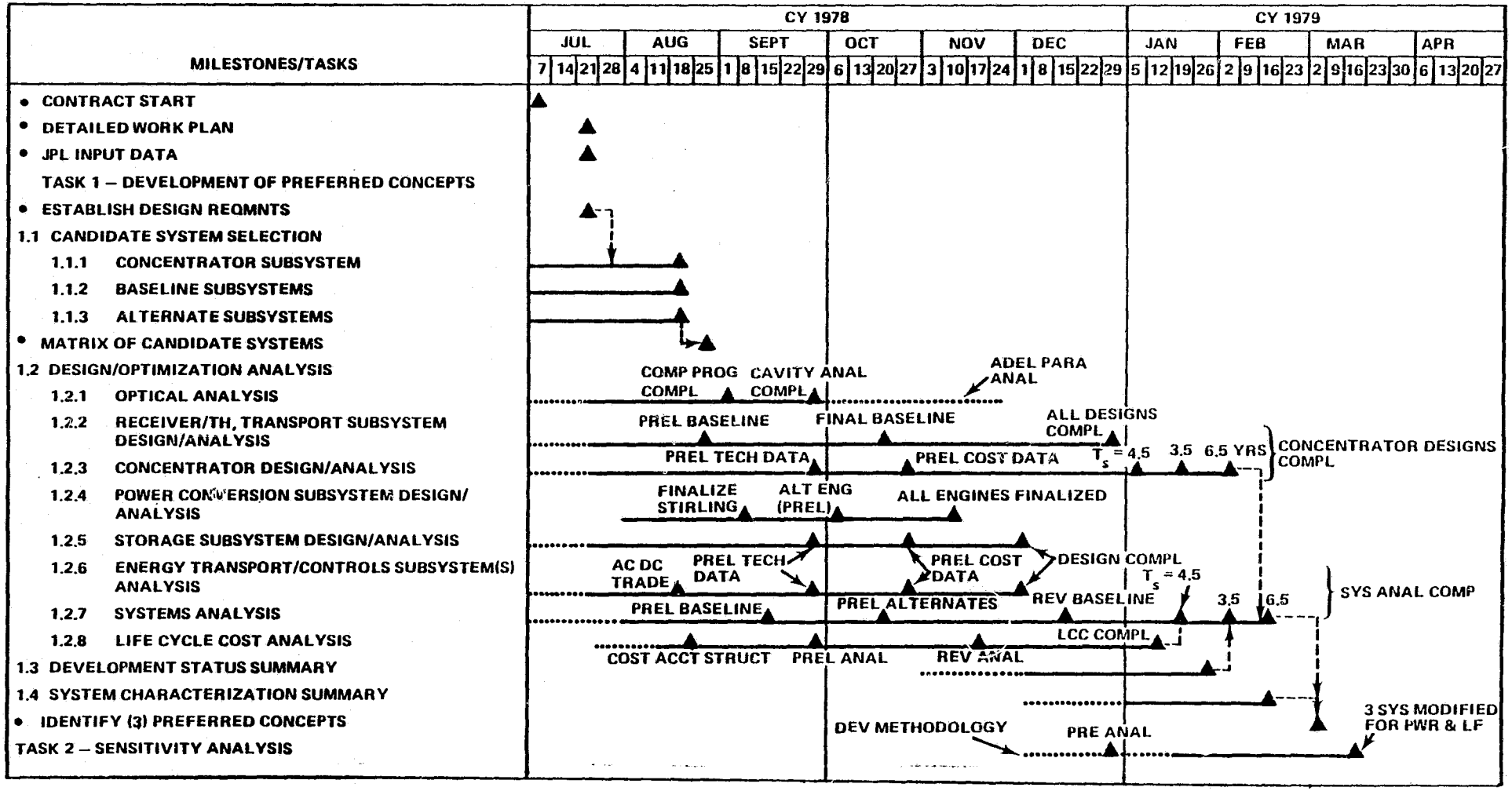

FIGURE 1-1. SPS PROGRAM SCHEDULE

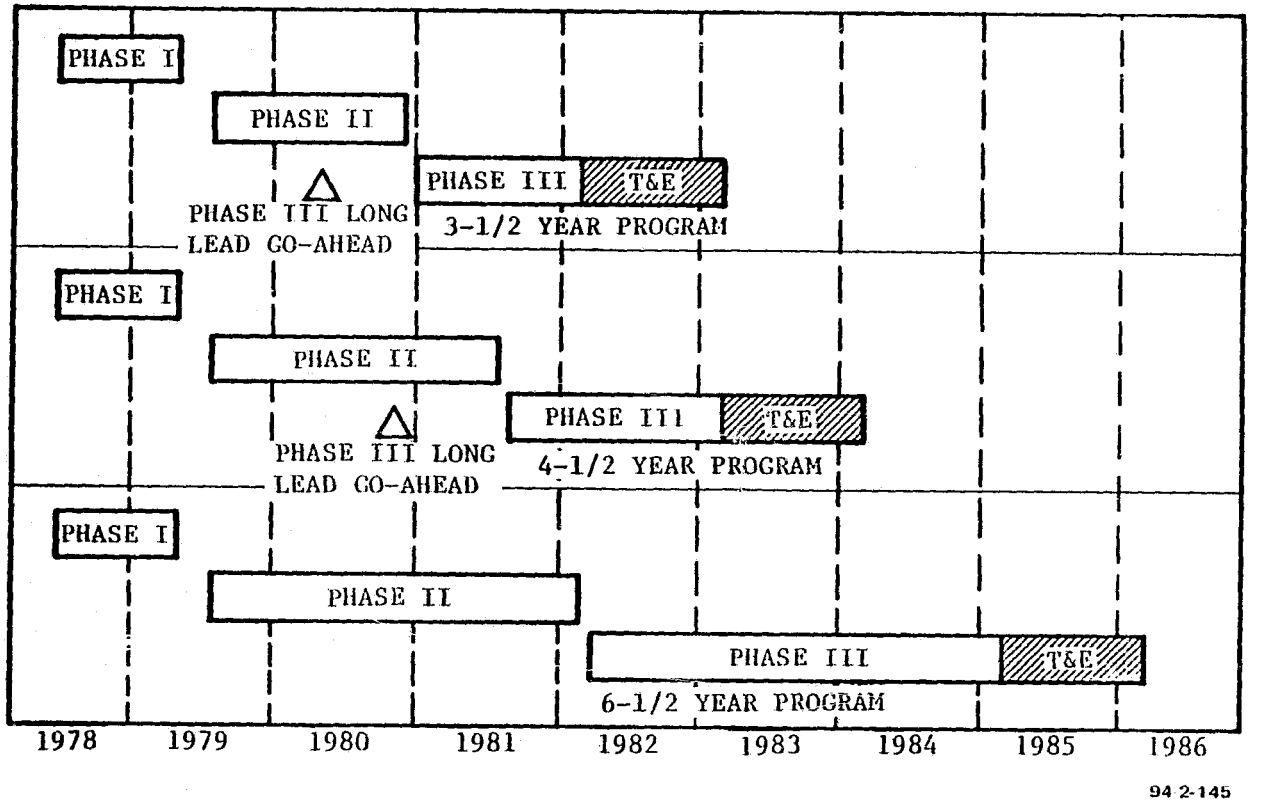

FIGURE 1-2. PROGRAM OPTIONS

TABLE 1.1. SYSTEM SELECTION CRITERIA

HIGH OPERATIONAL RELIABILITY

- Concept should lead to a SPS with ultimate reliability of a commercial power plant.
- Consider enhancement of reliability through redundancy associated with modular design (capability for incremental power operation at constant efficiency).
- Also applies to Engineering Experiment No. 1 (EE No. 1 must operate reliably for at least two years after start-up).

MINIMUM RISK OF FAILURE

- Concept subsystems developable within allotted Phase II schedule.
- Minimum risk of failure in bringing SPS on line at the selected start-up time.
- Consider concepts with available hardware of proven performance (minimize new hardware development within Phase II).

COMMERCIALIZATION POTENTIAL

- Concept should lead to eventual concept likely to achieve commercial success in late 1980s (Low capital costs and low energy costs for mass-produced plants).
- Compatibility with small community and utility applications requirements.
- Adaptable to applications other than utilities, for example stand-alone (Modularity of design should be a primary consideration).
- Simple plant operation, minimum operations/maintenance costs (Remote operation, if possible).

LOW PROGRAM COST

- Minimize total cost of Phase II and Phase III.
- Consider concepts with available hardware of proven performance (minimize development costs associated with Phase II).
- Minimize capital investment for actual hardware for EE No. 1.

together with a projected low production cost, the Stirling-based system shows lowest BBEC when compared with alternate systems, for example using either Brayton or Rankine cycle engines. In addition, the Stirling-based system benefits by the fact that the engine has been under separate development for nearly ten years and is close to volume production. Phase II/III engine costs are also lowest of the group and the Stirling system clearly meets the criterion of highest performance for least development cost.

The second element of the approach has been implemented by selecting state-of-the-art concentrator and electrical subsystems. The concentrator is the largest single cost item and it was decided to base its design on fully-established microwave antenna technology while reducing cost through redesign for mass production. All electrical components -- for example the AC generators, the electrical transport/distribution network and the central control subsystem -- are available state-of-the-art components.

A storage system is required to achieve the specified nominal value of ACF of 0.4. For the near-term effort, a conventional lead-acid system has been selected as the storage device although its far-term potential is poor. A number of alternate storage devices are applicable, including advanced batteries and flywheels; they have high far-term potential and are currently under development on other DOE-supported programs. However, since it is not clear at this time which of these devices will be the most cost effective, the lead-acid battery is selected, with provision for adding an advanced storage device in the future.

A related issue deals with the need for high values of ACF and the concomitant need for storage. There appears to be no clear-cut way to establish a quantitative evaluation of the merits of high ACF, that is greater than 0.4, for a grid-connected system. This is an important point, since the energy cost of this type of system will always be higher with storage than without it. From discussions with several large utilities, we conclude that the most cost effective approach is to initially develop these solar electric power plants without storage in order to displace the use of fossil fuel during daylight hours; storage systems -- particularly the external type favored by the PFDR, Category C concept -- could be added as they are developed and their cost is reduced. For the stand-alone case hybrid operation with a variety of fossil fuels, for example employing a combustion-heated receiver, would provide for 24-hour operation.

The Stirling Engine is not generally regarded as mature a technology as is the various Brayton and Rankine cycle engines. However, detailed examination of heat engines suitable for solar use in the sizes of interest to the PFDR application shows that all candidates require some development effort. None of the candidates can be considered off-the-shelf hardware. The outstanding performance of the Stirling engine thus tips the scale in its favor. An additional factor is engine availability for the different development schedules. The Stirling engine is the only one which could be obtained for all three plant start-up times.

The third element of the approach deals with the critical component -- the receiver. An in-depth transient thermodynamic analysis of the integrated receiver/boiler/thermal transport loop was conducted to determine system stability and fully identify system response to sudden changes in solar insolation. Comprehensive cyclic thermostructural analyses were carried out, together with safety analyses for a variety of different failure modes. Detailed performance maps of the engine were obtained and incorporated in a computer simulation (in 15-minute intervals) of system performance during one full year of operation at Barstow, California.

1.3 REPORT ORGANIZATION

Sections of this final technical report for the Phase I effort are organized to respond to the study objectives stated in Paragraph 1.1. Section 2 provides a summary of the baseline system. Section 3 contains the preferred system concepts (i.e. Task 1 study results). The sensitivity analysis (Task 2 results) is presented in Section 4 and finally Section 5 is a program summary, including cost estimates for subsequent phases.

Some of the important technical data generated on the program -- too voluminous to be included in the main report -- has been included in two volumes of Appendices. These are listed below.

APPENDIX	TITLE	VOLUME
A	Concentrator Subsystem Selection and Definition	2
B	Electrical Subsystem Selection and Definition	
C	Development History of the USS Stirling Engine	
D	Organic Rankine Cycle Engine for SPS Application	
E	Stirling Engine Control Analysis	3
F	Brayton Cycle Performance Models	
G	Determination of Station-Keeping Power	
H	Life Cycle Cost Equations	
I	Reliability Predictions for the SPS	
J	Study of Receiver Insulation Materials	

APPENDIX	TITLE	VOLUME
K	Buffer Storage Materials and Comparison	3
L	Transient Thermal Model for the Receiver/Transport Subsystem	
M	Shadowing Analysis for Parabolic Concentrator Fields	
N	Study of Sodium for High Temperature Applications	

SECTION 2

SUMMARY OF BASELINE SYSTEM

For SPS Engineering Experiment No. 1, FACC has selected a system which is comprised of multiple parabolic dish concentrators employing Stirling-cycle engines with direct-coupled AC generators for power conversion at the focal point of each concentrator. Each collector assembly, or module, includes the parabolic concentrator and a cavity receiver with an integral sodium pool boiler; the collector also houses the sodium thermal transport hardware and the engine/generator assembly. The vaporized sodium is transported by natural convection to the heater head of the engine, with condensate return to the boiler by gravity. A number of these collectors are grouped together to supply the required system electrical output (nominally 1 MWe).

The parabolic concentrator is a unique front-braced design* configured for mass production/installation techniques; it promises to reduce significantly the cost of the concentrator. Lead-acid batteries have been selected for energy storage for the demonstration phase of the program; the ca. 1990 operational system would employ either advanced batteries or composite flywheels.

The FACC baseline Stirling engine system is clearly superior to all competing approaches using the JPL-supplied evaluation criteria, and, based on the Phase I studies and analyses, can be carried forward into Phases II and III with high confidence of program success.

Key features of the FACC baseline P-75 system** are:

(1) High Commercialization Potential

- With State-of-the-Art Concentrator: Levelized Bus Bar Energy Cost (BBEC) = 53.5 mills/kWh (without storage)
  BBEC = 77.6 mills/kWh (with storage)
- With Advanced Concentrator ($60/m^2):
  BBEC = 38 mills/kWh (without storage)

(2) No Basic Module Development is Required Beyond Phase III

- USS P-75 Stirling engine will be in production by 1982 (pre-production engines available before 1982 for use in Phase II of the program)

---

*Patent applied for.

**The P-75 Stirling system is FACC's recommended concept for 4½ and 6½ year plant start-up times; the P-40 system is the recommended 3½ year concept.

- High engine thermal efficiency
- Baseline System is compatible with current DOE advanced energy storage development programs
- High overall system efficiency

(3) FACC Baseline System Allows Flexibility in Siting and Operation

- The basic module is site invariant
- System is easily adaptible to different storage concepts
- System can operate in grid-connected or stand-alone modes
- Module design permits high packing fraction with low energy loss
- Minimum site preparation required

(4) No Technical Breakthroughs are Required to Translate Concept to Real Hardware

- All technologies have been demonstrated
- All materials are available and are non-critical

(5) FACC Baseline System is a Simple, Reliable Design

- Module concept insures high system availability
- Design has limited amount of plumbing

A brief description of the FACC baseline system together with a summary of overall system performance is given in the following paragraphs.

2.1 SYSTEM DESCRIPTION

A field layout sketch of the 18 module, baseline P-75 engine system (without storage) is shown in Figure 2-1. For the 6 x 3 matrix shown, a 25 percent packing fraction (concentrator area to land area) is achieved without loss of energy due to blockage; the resulting land area is 4.85 acres. If required, the packing fraction can be increased to 50 percent with only a six percent loss in energy. The system would then occupy only about 2.4 acres. Figure 2-2 demonstrates the concept's siting flexibility by making use of very irregular terrain to locate the modules. The slight amount of additional electrical losses in the longer lines which connect the collectors in irregular terrain can be compensated for by using larger wires. This will result in only a small cost increase.

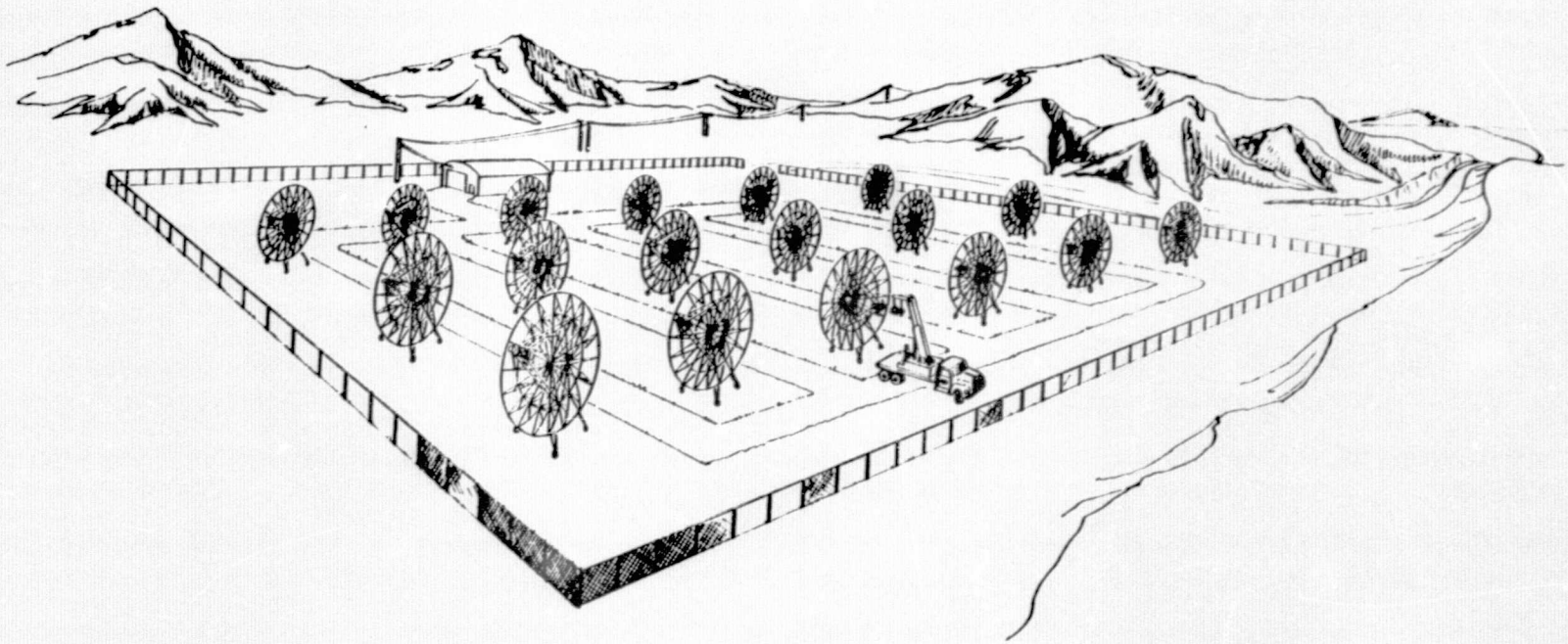

FIGURE 2-1. FIELD LAYOUT FOR BASELINE DISH - STIRLING SYSTEM

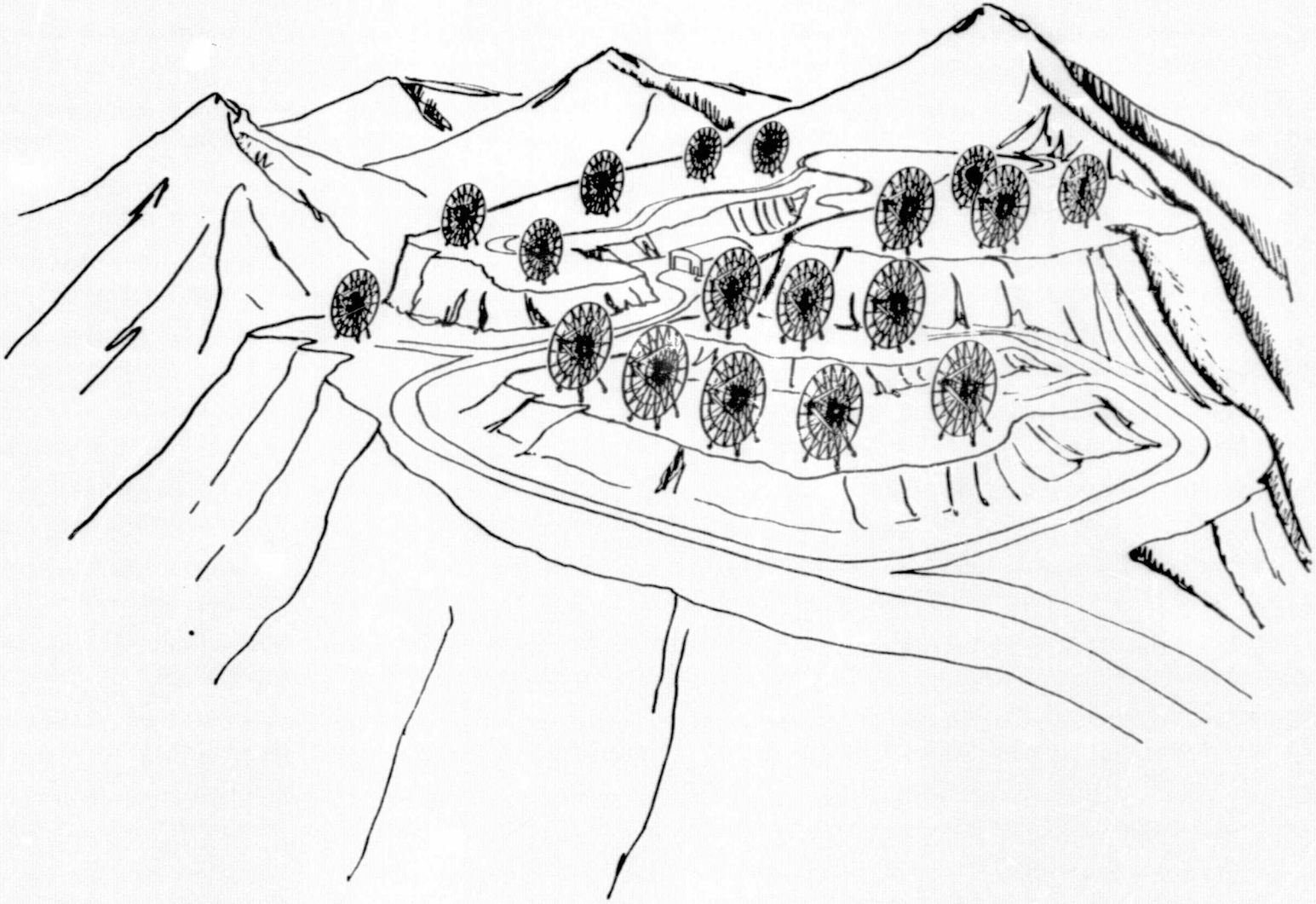

FIGURE 2-2. SYSTEM LAYOUT FOR HILLY TERRAIN

The collector subsystem consists of the concentrator and the cavity receiver. An artist's sketch of the concentrator is shown in Figure 2-3. Key parameters of the concentrator are as follows:

- It is an 18.6 meter diameter (11.2 meters for P-40 design) paraboloid with front-braced steel structure.
- An attached tripod supports the receiver/power conversion equipment (power module) including the Stirling engine.
- The concentrator is supported by a 3-leg elevation-over-azimuth (AZ-EL) type mount.
- Rim angle is 65 degrees.
- Geometric concentration ratio of the concentrator/receiver is 1950:1.
- The reflector surface is composed of back-surfaced, high-reflectivity (95 percent) draw-fusion glass mirror segments.
- Mirror segments are pressed (or sagged) while heated to form the required 2-dimensional shape, and bonded to structural sandwich panels composed of galvanized steel surface sheets and an interior filled with a stabilized structural foam.
- Major concentrator errors (one sigma) are 2.62 mrad (0.15 deg.) in reflector surface slope and 1.75 mrad (0.10 deg.) in pointing.
- Sun tracking is accomplished by open-loop programmed tracking (from central microprocessor) combined with sun sensors for fine adjustment.
- Total concentrator cost in mass production including shipping, field installation/check-out and maintenance equipment is $\$134/m^2$. The equivalent cost of the 11.2 meter P-40 configuration is $\$107/m^2$.

A sketch of the receiver/thermal transport equipment and power conversion hardware (power module) is shown in Figure 2-4. The key parameters for the cavity receiver are as follows:

- Design consists of concentric cylinders fabricated of Type 316 stainless steel with sodium filling the annulus.
- The receiver is designed for a 15 year life, optimized for lowest life cycle energy cost.
- The maximum operating temperature is $830^{\circ}C$ and the cavity area to aperture area ratio is 13.5, which achieves an effective solar absorptivity (α_{EFF}) and effective emissivity (ϵ_{EFF}) equal to 0.987.

ORIGINAL PAGE IS
OF POOR QUALITY

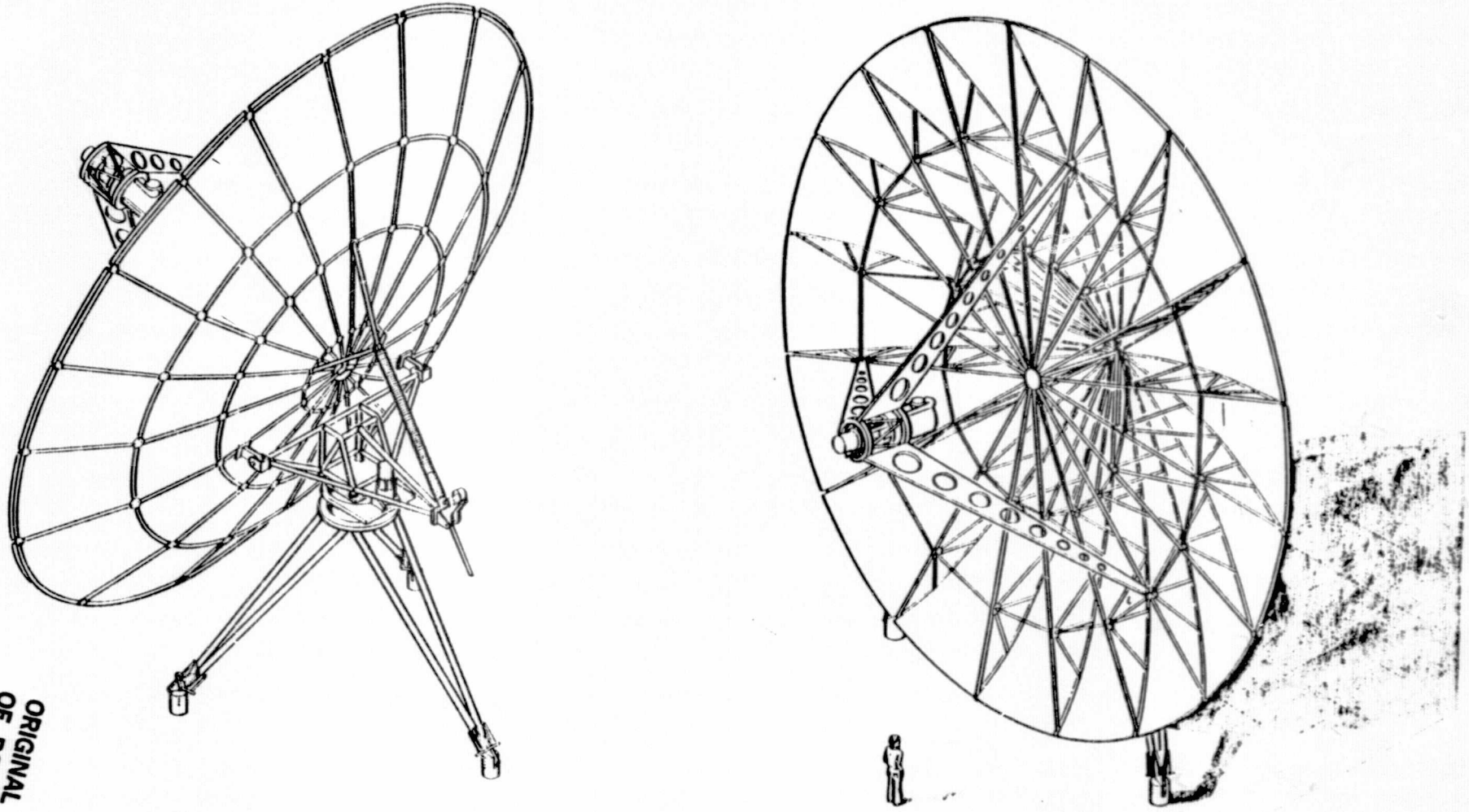

FIGURE 2-3. 18.6 M COLLECTOR MODULE FOR BASELINE SYSTEM WITH P-75 STIRLING ENGINE

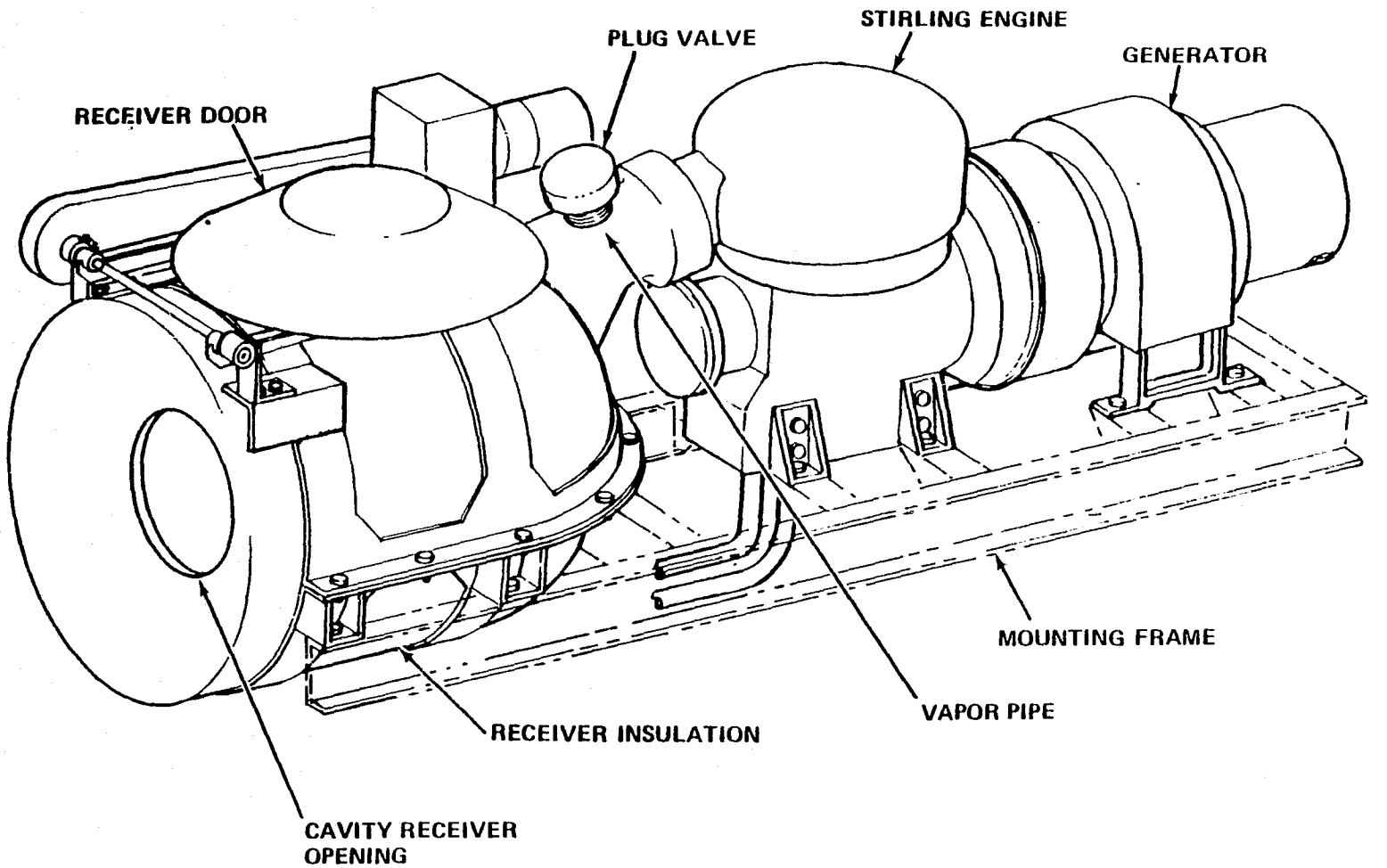

FIGURE 2-4. STIRLING ENGINE RECEIVER/THERMAL TRANSPORT/POWER CONVERSION (POWER MODULE)

- System physical characteristics are:

	P-75 design	P-40 design
Overall Diameter, meter (m)	1.06	0.72
Aperture Diameter, (m)	0.422	0.254
Weight, kg (incl. sodium)	310	201

- A remotely actuated, totally enclosed "plug" valve is located in the vapor pipe to shut off vapor flow to the engine during nighttime and periods of inclement weather.

- The receiver operates without pumps in any required solar attitude; energy is transported via sodium vapor to the engine heater head by natural convection and the liquid sodium is returned to the receiver by gravity.

- A well-insulated electric motor-driven cover (door) is placed in the receiver aperture at night and during long periods of cloud cover to minimize radiation/convection losses from the receiver cavity.

- In mass production the P-75 receiver/thermal transport subsystem cost is projected at about $2400/unit and the P-40 design is projected at about $1800/unit.

The power conversion subsystem consists of the Stirling engine and the direct-coupled AC generator (see sketch in Figure 2-4). Key parameters of these elements are:

- The baseline Stirling engine is the USS P-75 engine operating at a rated shaft power of 63.4 kW at 1800 rpm and about 115 atmospheres mean pressure level using helium as the working fluid. (Unit is rated at 800 W/m^2 solar insolation on a 44.6°C. day.

- The P-75 engine has a maximum power developed of 79.3 kW. (Unit-operating at 1000 W/m^2 solar insolation and 150 atmospheres mean pressure level in the engine.)

- The maximum heater head temperature is 800°C.

- The projected engine life is 75,000 hours which is equivalent to about 27 years at an Annualized Capacity Factor (ACF) of 0.4.

- The P-40 engine is essentially a scale-down version of the P-75; rated shaft power at 1800 rpm is 21.9 kW and maximum power is 27.3 kW.

- The P-75 engine cost in mass production is estimated at $2500 and the P-40 cost estimate is $1800.

- The generator for the P-75 system is a direct-coupled, 75 kW, 480V, 3-phase, 60 Hz synchronous AC machine operating at 1800 rpm; mass-production cost with voltage regulator is $2690. The generator for the P-40 system is a 30 kW unit; its cost with voltage regulator is $1290.

The energy transport and distribution subsystem has the following key parameters:

- The power cables are single-conductor stranded aluminum, typically No. 4/0 and 250 MCM sized, with 480 volt RHW-USE 600V insulation.
- Direct burial of conductors.
- A high voltage, 1250kVA/1000 kW commercial transformer, switchboard, instrumentation and protective devices are provided to interface the system with the utility grid.
- An electrical system block diagram for the baseline 1 MWe power plant is shown in Figure 2-5 for a system with battery storage. Key component parameters are shown in the figure.

Key parameters of the central microprocessor based digital control subsystem are:

- Microprocessor typical of Cromemco CS-3 computer with 64 K memory will be used.
- System will use two 8-inch floppy discs and a S-100 bus system for interface with other components.
- Control subsystem concept will provide accurate power flow control, station diagnostics and comprehensive data logging.

The far-term battery storage system would employ advanced batteries (sodium/sulfur or other type). However, these will not be available for Phases II and III, so conventional lead-acid cells were selected. The lead-acid battery system has the following key parameters:

- Batteries are grouped in 180 cell strings at a float voltage of 2.25 V/cell.
- Conditioning equipment includes SCR phase-control rectifiers and SCR 3-phase double-bridge inverters.

2.2 SYSTEM PERFORMANCE

Operational system performance for the P-40 and P-75 Stirling power plants, based on 5000 systems manufactured and installed per year, circa 1990, is summarized below in Table 2.1.

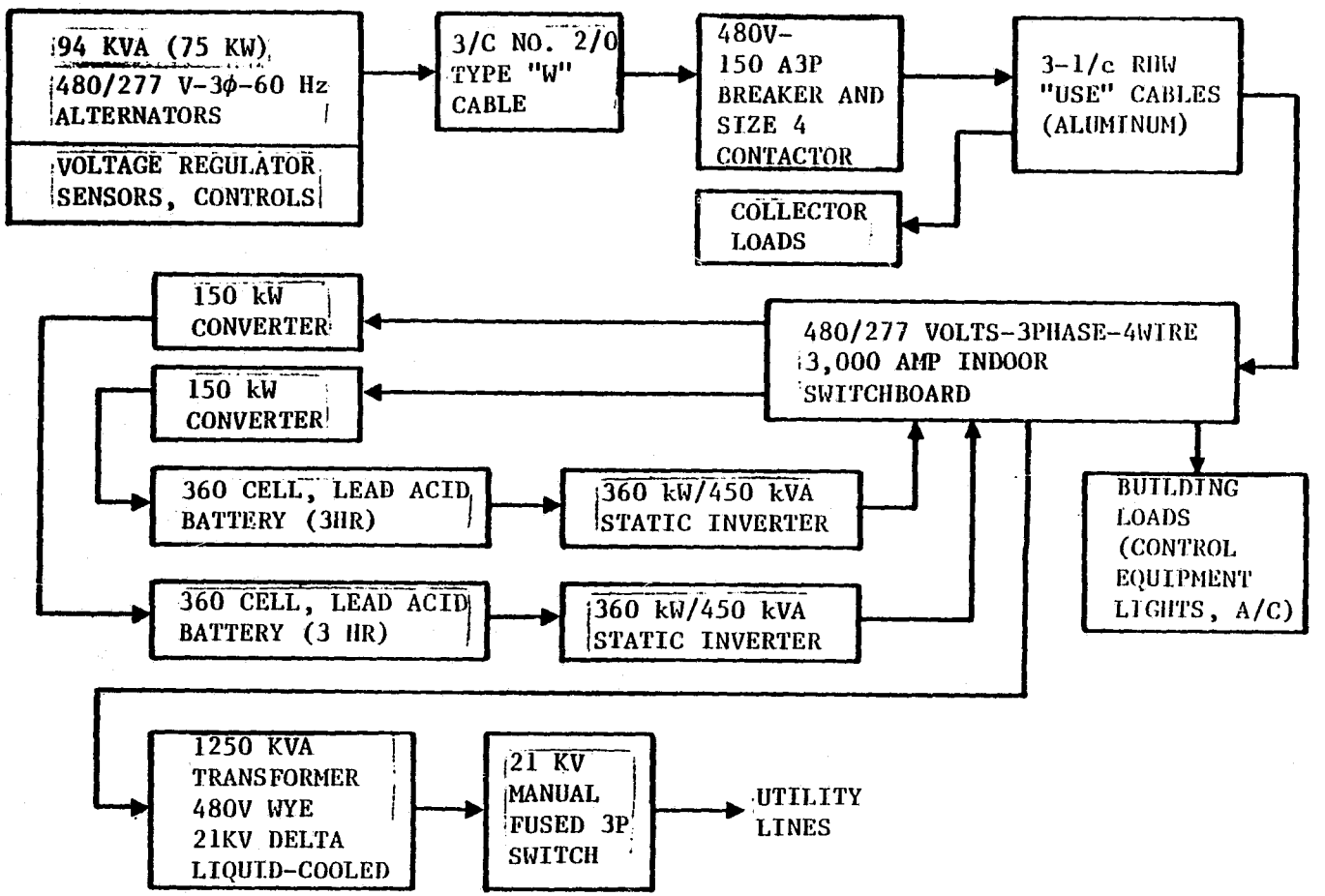

FIGURE 2-5. SPS ELECTRICAL SYSTEM BLOCK DIAGRAM

94-2-165

TABLE 2.1. BASELINE SYSTEM PERFORMANCE @ 1 MWe and ACF ≈ 0.4 (with storage)

Stirling Engine	USS P-40	USS P-75
Overall System Efficiency, η_{SYS}	0.228	0.256
CI (1986), ($)	1,683,200	1,406,900
CI_{PV}, ($)	3,426,900	2,773,000
$\overline{BBEC}_C$, (mills/kWh)	85.68	70.00
$\overline{OM}$, (mills/kWh)	15.60	7.58
$\overline{BBEC}$, (mills, kWh)	101.28	77.58

The terms in the table are defined as:

CI (1986) = Capital investment at time of plant construction, 1978 dollars.

CI_{PV} = Present value of total capital investment, 1978 dollars.

$\overline{BBEC}_C$ = Levelized bus bar energy cost due to capital investment only.

$\overline{BBEC}$ = Total levelized bus bar energy cost

$\overline{OM}$ = Levelized operating and maintenance cost

2.3 SYSTEM SELECTION

The major "driver" in selecting the PFDR, Category C system is the choice of a heat engine; it is the major influence on BBEC by virtue of the effect of engine efficiency on required concentrator area and it dictates the type, size and cost of the associated receiver and thermal transport subsystem. The choice of a concentrator was deliberately limited to derivatives of state-of-the-art microwave technology as explained in paragraph 1.2. The selection of the lowest cost design is described in detail in Appendix A.

The basis for selecting the Stirling engine over the Brayton and Rankine cycles is developed in detail in the following sections of this report. In summary, however, the Stirling engine gives much lower energy costs as well as lower development costs. A comparison of the energy costs and the development costs for the major system components (excluding design costs) is shown in Table 2.2.

TABLE 2.2. SYSTEM ENERGY COST AND B&P DEVELOPMENT COST FOR MAJOR HARDWARE ELEMENTS(1) (WITHOUT STORAGE)

ENGINE	ca. 1990 ENERGY COST,(2) $\overline{BBEC}$, (mills/kWh)	DEVELOPMENT COST, PH. II/III (millions of $)			
		ENGINES(3)	CONCENTRATORS	ELECTRICAL	TOTAL
CLOSED-CYCLE BRAYTON (P_{o_r} = 30kW)	95.1	7.315	4.040	0.678	12.033
ORG. RANKINE (P_{o_r} = 77.5kW)	85.4 (79 @ P_{o_r} = 37.2kW)	3.260	4.161	0.352	7.773
P-75 STIRLING (P_{o_r} = 63.4kW)	53.5	2.650*	2.681	0.471	5.80

(1) Excludes design cost (Hardware Only)

(2) Based on ACF for $P_G \gtrless P_{G_R}$

(3) Assumes one engine for Phase II and 39 engines for Brayton, 15 engines for Rankine and 18 engines for Stirling for Phase III.

* Note that the data given in Table 2.2 are consistant with a 4½ year development schedule. For a 6½ year schedule, production P-75 engines would be available and the Phases II/III engine cost would drop from $2.65 M to $1.03 M; total hardware cost (excluding receivers) would then drop to $4.182 M.

SECTION 3

TASK 1 STUDY RESULTS - DEVELOPMENT OF PREFERRED SYSTEM CONCEPTS

This section presents the results of the Task 1 Study effort. It includes the system/subsystem/component analysis and design work, a review of the development status of the individual subsystems and a complete definition/characterization of the preferred systems for 3½, 4½, and 6½ year start-up times.

3.1 SYSTEM DESIGN & OPTIMIZATION ANALYSES

The baseline SPS has a nominal rated power of 1 MW_e and an annualized capacity factor (ACF) of 0.4. The analyses presented in this subsection deal with the performance of a far-term system, ca. 1990, which closely reflects the actual hardware selected for each preferred 3½, 4½, and 6½ system. The major differences between these development-phase systems and the ca. 1990 version are the reductions in cost projected with mass production components and improvement in the performance of some components, e.g., AC generator efficiency from 0.90 to 0.94. All analyses are carried out for a grid-connected system. However, consideration is also given to the stand-alone case and recommendations in the area of storage are made for accommodating this case.

The system analysis logic used to optimize the SPS throughout the design process is presented in Figure 3-1. The performance and cost trade analyses made for each of the subsystems have been integrated into an overall optimization analysis to determine the lowest cost system. The results of this analysis were continually fed back to each of the subsystems for refinement of the design until an optimum system was obtained.

3.1.1 SYSTEMS ANALYSIS/DESIGN

The following paragraphs summarize the system related analyses, which have been carried out for the nominal 1 MW_e, ACF = 0.4 concepts.

3.1.1.1 Fundamental Optical/Thermal Performance Trades. Detailed optical analyses are required in two general areas:

(1) Computation of flux distributions within the cavity receiver for input to receiver thermo-structural analyses.

(2) Computation of flux distributions on the focal plane for input to system analyses which seek to determine optimum values for intercept factor, concentrator rim angle, concentrator slope error, etc.

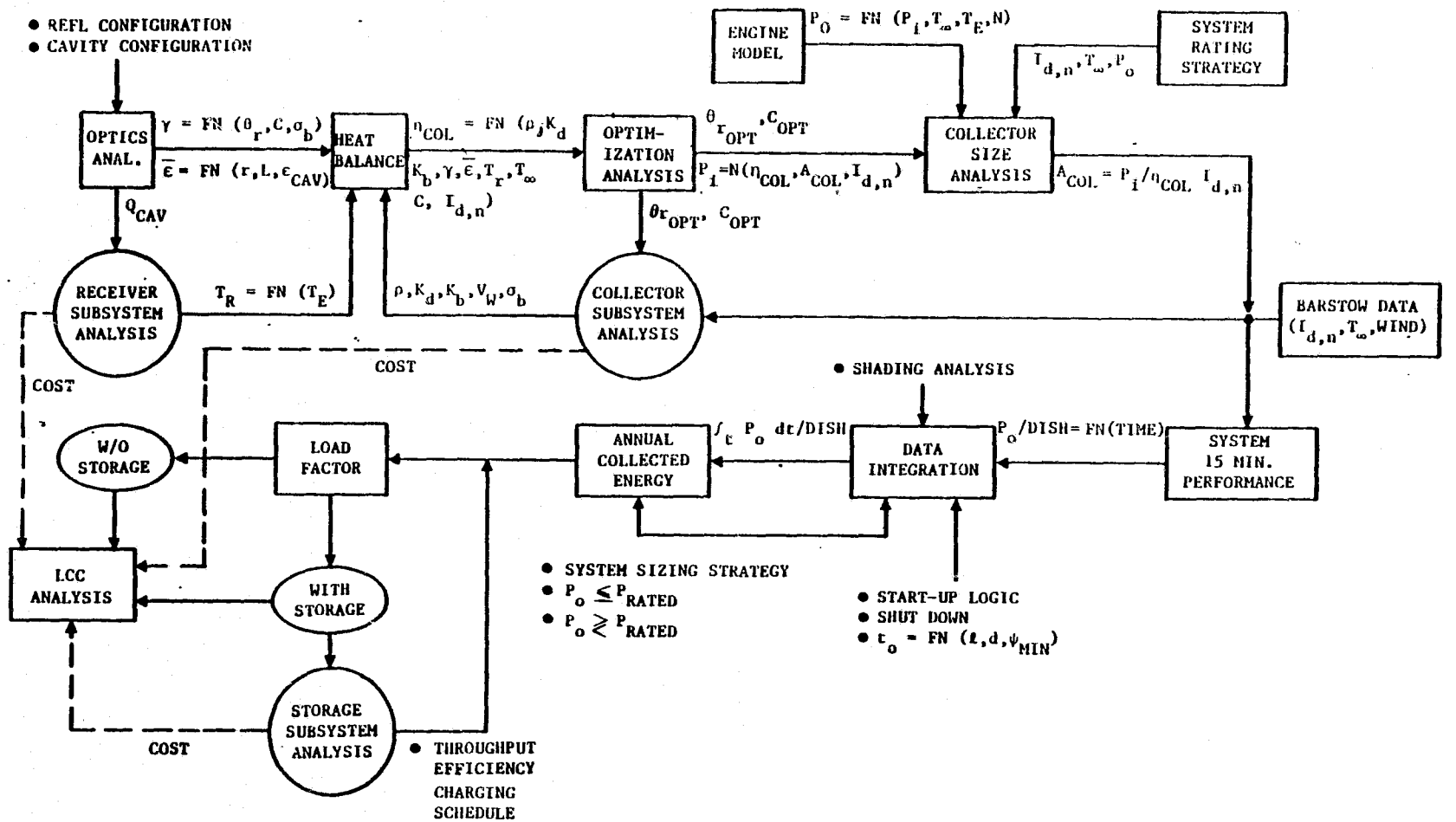

FIGURE 3-1. SYSTEM ANALYSIS LOGIC

The computation of flux distributions generally requires an optics code because the statistics of the errors in the system and the associated mathematical complexity preclude the use of closed-form analytical expressions. The various optic codes used in the SPS design are discussed in Paragraph (a) below. For system trade study analyses, the code results have been used to develop simple analytic expressions; together with previously-published empirical formulas these expressions permit rapid optical-thermal system optimization, as described in the following paragraphs.

a. Optical Techniques. There are two recognized types of computer programs used to obtain accurate flux distributions at the focal plane and on receiver surfaces of parabolic solar concentrators (parabolic dishes). These are the Monte Carlo "ray trace" technique (for example, References 3-1 and 3-2), and the "cone optics" approach (for example, References 3-3 and 3-4). An evaluation of these two approaches resulted in the decision to use a version of the Cone Optics Program for determining the flux distributions for the SPS Program.

The cone optics approach has been under development by Dr. G. L. Schrenk since the early 1960's. Unpublished results for the focal plane flux distribution and intercept factor have been obtained from Dr. Schrenk for 159 cases consisting of rim angles between 35 degrees and 60 degrees, slope errors between 0 and 30 minutes of arc, and various pointing angle errors (typical results are presented in Reference 3-5). This information was computed using an early, but complete, version of the program, and the output is referred to as "exact" cone optics since this represents the most accurate results currently available. An approximate version of the cone optics program was prepared for Aeronutronic. This proprietary program, called OPTICSFORD1 is available through Dr. Schrenk on time share. It is similar in many respects to the "exact" code except for the important difference that the concentrator surface errors (that is, the mirror slope errors) are approximated by specifying a larger sun angle than normal. By doing this, the time-consuming statistics analysis is avoided, thus saving a factor of 10 to 15 in the running time. The code computes the flux distribution at any arbitrary plane, including the interior of a cavity receiver. Comparisons between the "exact" and approximate codes are summarized.

Systems trade studies require the use of an analytical expression for the focal plane intercept factor, γ. This factor is the fraction of the total incident power within a defined area. The discrete values of γ computed by cone optics codes are not well suited for this purpose because it is difficult to fit accurate curves through the existing computer data over the desired range of values. However, a semi-empirical expression for the intercept factor has been derived by Aparisi (Reference 3-6). The original Aparisi equation for the focal plane intercept factor is

$$\gamma = 1 - \mathrm{EXP}\left[- \frac{\mathrm{SIN}^2\theta_r}{2\sigma_b^{\,2}} \left(\frac{r}{R}\right)^2 \right] \qquad (3\text{-}1)$$

where:

γ = Focal plane intercept factor = $\int_0^A I\, dA \Big/ \int_0^\infty I\, dA$

A = Focal plane area = πr^2, units of m^2

C = Geometric concentration ratio = $A_{\text{dish aperture}} / A_{\text{receiver}} = (R/r)^2$

I = Solar intensity at focal plane for unity reflectivity

r = Radius of receiver opening (or radial coordinate at focal plane), m

R' = Radius of parabolic concentrator, m

θ_r = Rim angle of the parabolic concentrator, degrees

σ_b = Angular standard deviation of energy distribution within a solar beam reflected from the concentrator surface

= $\left(\sigma_{\text{Sun}}^2 + 4\sigma_{\text{Slope}}^2 + \sigma_{\text{Point}}^2 + \sigma_{\text{Spec}}^2\right)^{\frac{1}{2}}$, rad.

σ_{Sun} = Angular standard deviation of the distribution of radiation across the diameter of the sun:
With solar limb darkening $\cong$ 2.176 mrad(0.1247 deg.)
Without limb darkening $\cong$ 2.9046 mrad(0.1667 deg.)

σ_{Slope} = Value of angular tangential and radial surface slope errors of the reflector (one sigma), rad.

σ_{Point} = Standard deviation of the angular misalignment of the concentrator with the solar vector. A value of 1.745 mrad (0.10 deg.) is used for the baseline system.

σ_{Spec} = Standard deviation of the angular departure of the reflected beam from specularity; $\cong$ 0.2 mrad (0.0286 deg.) for glass mirrors.

Figure 3-2 presents a comparison of Equation (3-1) and the two cone optics results ("exact" and approximate) for a typical case of 60 degrees rim angle and 10 minute (2.909 mrad) slope error. The important conclusion is that the simple Aparisi expression gives more accurate results than the approximate cone optics.

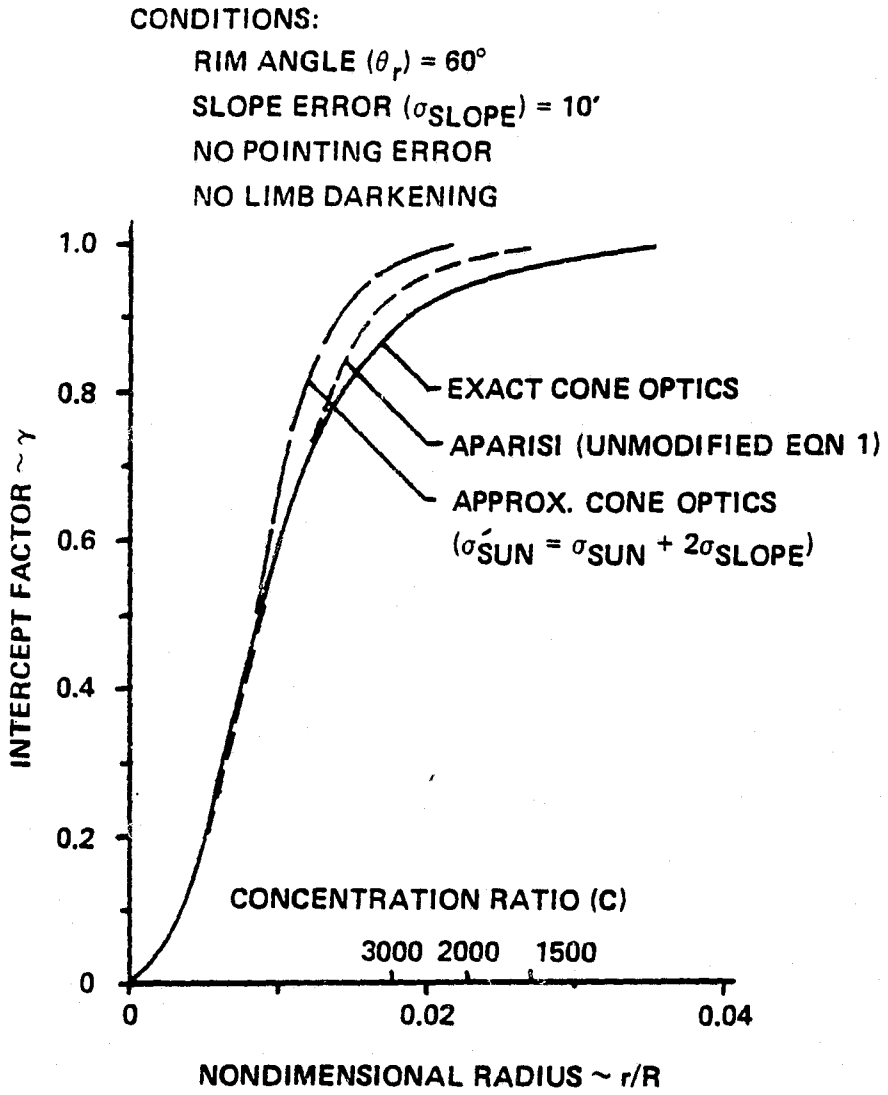

FIGURE 3-2. COMPARISON OF EXACT AND APPROXIMATE CONE OPTICS WITH APARISI

As previously stated, the approximate code requires the use of a larger sun angle than normal to simulate the slope errors. A variety of approximations were used to determine the best fit (see Reference 3-7), and the following gave the closest results to exact cone optics:

$$\sigma'_{Sun} = \sigma_{Sun} + 2\sigma_{Slope} \tag{3-2}$$

Where σ'_{Sun} is the increased value for the solar angle used in the approximate code to simulate the slope error.

Comparison of the original Aparisi equation was made with exact cone optics for rim angles of 45 degrees up to 60 degrees. It was found that the comparison was best at 45 degrees but the error increased up to rim angles of 60 degrees. (Note that Figure 3-2 shows that unmodified Aparisi is still better than approximate cone optics for this worst-case condition of 60 degrees rim angle.) Figure 3-3 illustrates the Aparisi/exact cone optics comparison at rim angles of 45 degrees and 60 degrees for a geometric concentration ratio of 2000. Since the original (unmodified) Aparisi equation was not as accurate as desired at rim angles near 60 degrees, a series of different modifications were investigated to determine if a better fit could be obtained. The best results were found using the following equations:

$$\gamma = 1 - EXP\left[-\frac{SIN^2\theta_r}{2\,\sigma_{b'}^2}\left(\frac{r}{R}\right)^2\right] \text{ , Modified Aparisi} \tag{3-3}$$

Which is the same as Equation (3-1) except for the beam error which becomes

$$\sigma'_b = \sigma_b + 0.003\left(\frac{\theta_r}{45^o} - 1\right) \text{ , } 45^o \lesssim \theta_r \lesssim 70^o \tag{3-4}$$

And σ_b is the same as defined above. The term inside the brackets in Equation (3-4) removes the modifying factor at $\theta_r = 45^o$. At $\theta_r = 60^o$ the modified value for σ'_b is $\sigma_b + 0.001$. This simple change results in the circled points for the 60^o rim angle case shown in Figure 3-3. As seen from the figure, the results using the modified equation are accurate over the entire range of surface errors. Additional comparisons for different concentration ratios are shown in Reference 3-7.

The approximate cone optics code, OPTICSFORD1, was used to compute the incident flux on the interior walls of a cavity receiver. However, since it has been shown that the approximate code is subject to errors due to the simulation of slope errors by a larger sun angle, an initial comparison was made with a cavity analysis using the exact code results published in

- CONCENTRATION RATIO = 2000

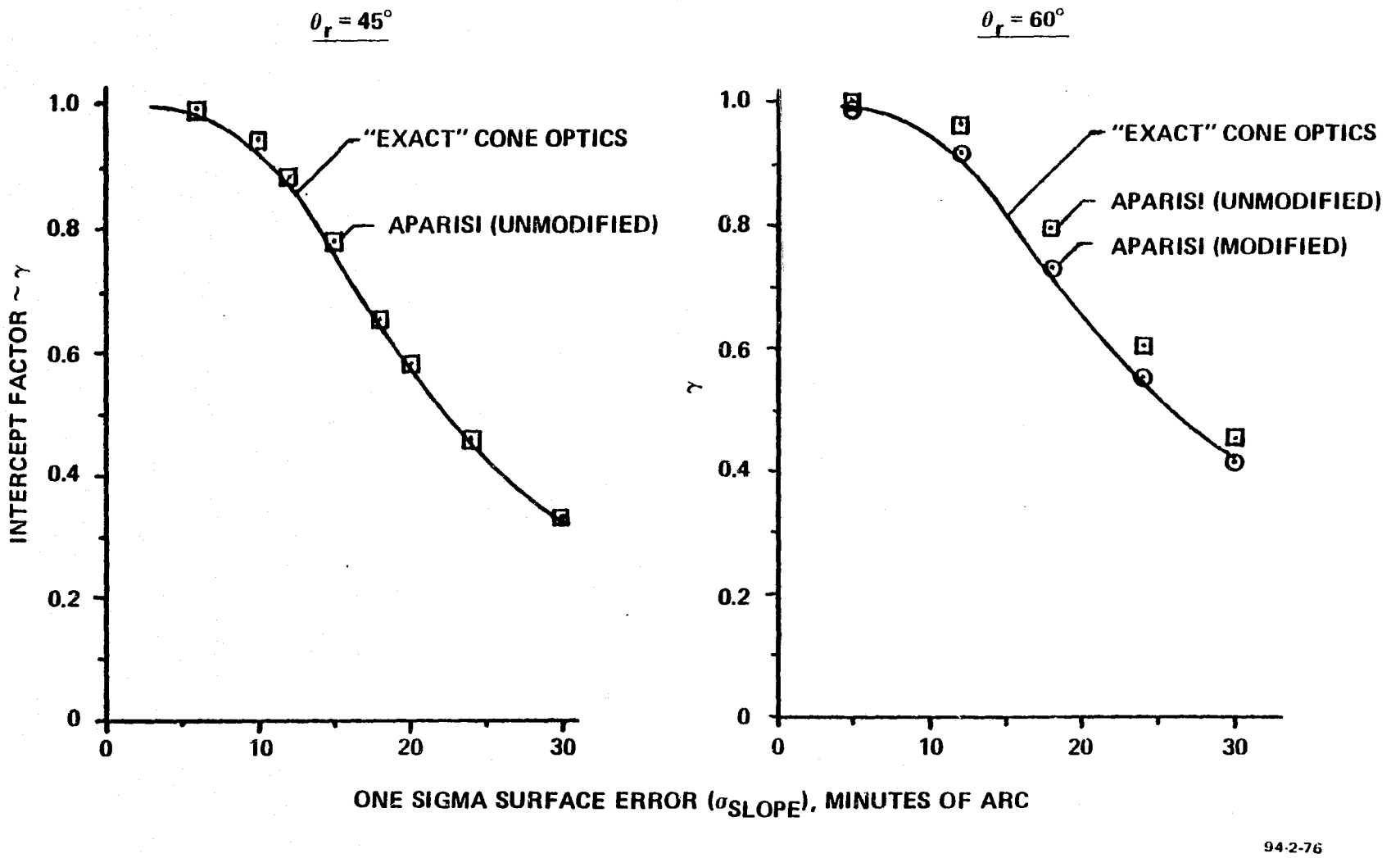

FIGURE 3-3. COMPARISON OF APARISI WITH EXACT CONE OPTICS

Reference 3-3. It was concluded that approximate cone optics gives reasonable cavity flux profiles (peak flux within 10 percent of exact cone optics and similar flux profiles) if the surface slope errors were simulated by the larger sun angle relationship given in Equation (3-2).

Flux profiles for a typical cavity receiver for Stirling engine applications are shown in Figure 3-4. Three different cavity wall radii (r_c) were used so that the reduction of intensity with r_c could be evaluated. The effect is pronounced, showing that the peak flux can be significantly reduced by increasing the cavity radius, but of course with the disadvantage of increased interior area and external size. Reduction of the peak flux is actually of little consequence for a sodium receiver because the burnout point is over one order of magnitude higher than the peak flux shown in the figure. However, burnout is a much greater problem for receivers which have a lower heat transfer coefficient to the working fluid (for example, Brayton receivers using air or argon), and for these cases the radius of the receiver is of prime importance.

In summary, the unpublished exact cone optics results serve as a basis of comparison for Aparisi and the fast-running approximate cone optics code. It has been shown that the Aeronutronic modification to the Aparisi equation for intercept factor, γ, is very accurate over a range of rim angles between 45 degrees and 60 degrees and is the recommended technique for computing γ. Cavity flux calculations using approximate cone optics are in reasonable agreement with the results from the exact cone optics code.

b. Optical Trade Studies. The design of the SPS is predicated on the results of several major trades relating to the optical and thermal characteristics of the point-focusing concept. The governing equations for the combination of a parabolic reflector and a cavity receiver are discussed here. Equation (3-3) relates the intercept factor, γ, to the reflector rim angle, θ_r, the geometrical concentration ratio, C, and the error in the reflected beam angle, σ_b'. As discussed previously, this is the Aparisi equation, modified according to the results of the exact cone optics program to represent more accurately the larger reflector rim angles, that is, $\theta_r \geq 45$ deg.

The collection efficiency for the concentrator/receiver is determined by the equation:

$$\eta_{COLL} = \rho\alpha_{eff}K_dK_b\gamma - \frac{\left[\sigma\varepsilon_{eff}(T_R^4 - T_\infty^4) + h(T_R - T_\infty)\right]}{I_{d,n}} - \frac{Q_{Cond}}{A_{Con}I_{d,n}} \qquad (3\text{-}5)$$

Where the terms not previously defined are:

ρ = Reflectivity of concentrator surface.

α_{eff}, ε_{eff} = Effective cavity absorptivity and emissivity

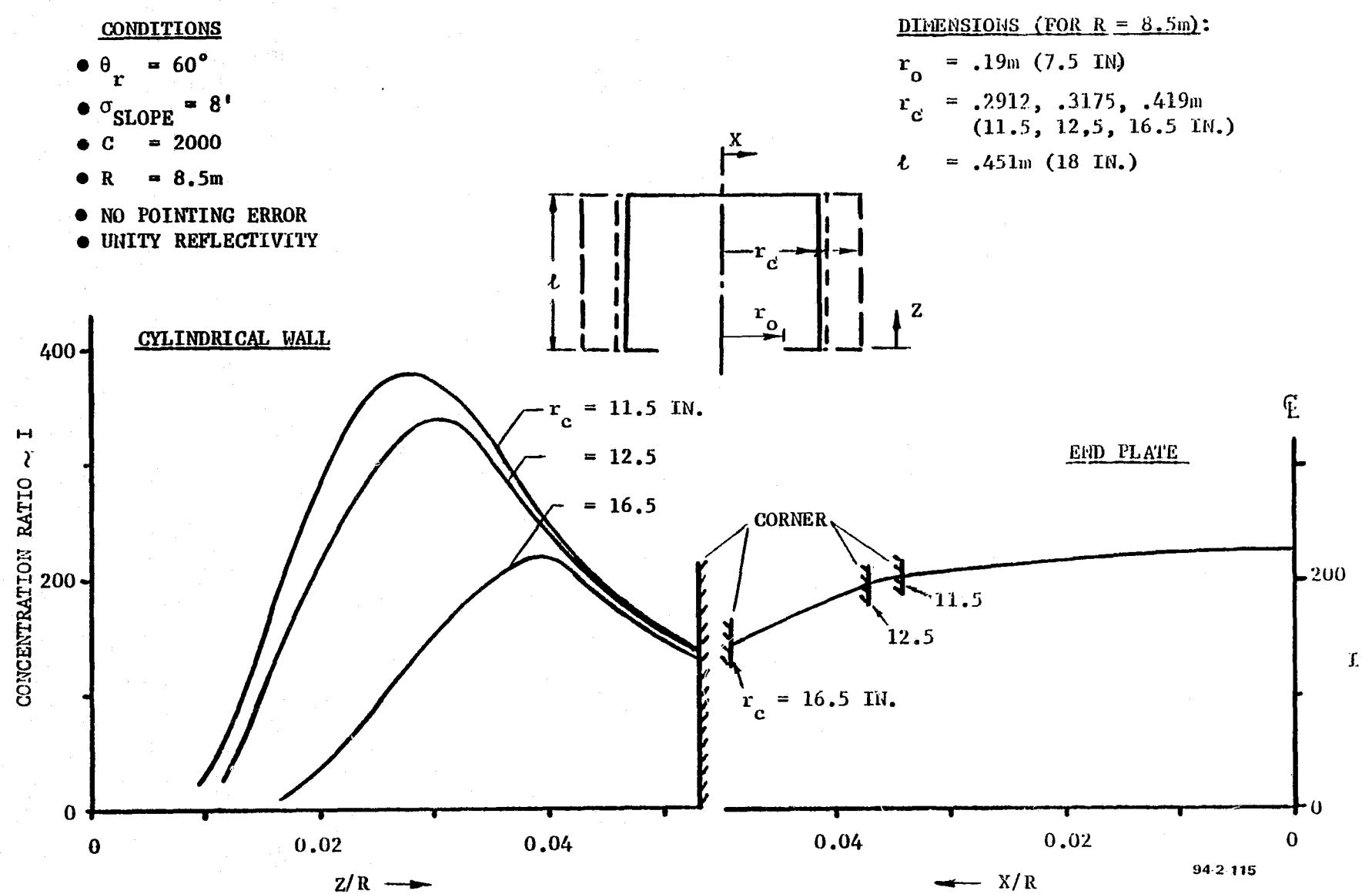

FIGURE 3-4. INCIDENT FLUX ON A TYPICAL CYLINDRICAL CAVITY

K_d = Dust correction factor (estimated = 0.95).

K_b = Concentrator structure solar shadowing/blockage factor (=0.92 for the baseline front-braced paraboloid).

σ = Stefan-Boltzmann constant (5.67×10^{-8} $W/m^2-{}^oK^4$).

T_R = Receiver inner (cavity) surface temperature, ^oK.

T_∞ = Ambient temperature, ^oK.

h = Convective heat transfer coefficient for cavity aperture ($\cong 16$ $W/m^2 - {}^oK$).

$I_{d,n}$ = Direct solar insolation at normal incidence, W/m^2.

Q_{Cond} = Thermal conduction loss ($Q_{Cond}/A_{Con} \cong 3$ W/m^2 for the baseline Stirling, where A_{Con} used as the reference area).

A_{Con} = Concentrator aperture area, m^2.

Equation (3-5) is derived from an energy balance on the concentrator and cavity receiver. Equations (3-3) and (3-5) can be combined to demonstrate: (1) that maximum collection efficiency occurs when $\gamma < 1$, as mirror quality degrades and (2) that there is an optimum concentration ratio which varies with concentrator rim angle, mirror quality and receiver temperature. The influence of intercept factor is shown in Figures 3-5 and 3-6. Optimum performance occurs when the energy lost by "spillover" ($\gamma < 1$) due to reduced cavity aperture size is compensated by reduced radiation and convection losses. Figure 3-7 shows the effect of concentration ratio on collection efficiency for different values of rim angle. At $\theta_r = 65$ degrees the maximum collection efficiency for the baseline system is $\cong 0.740$ and occurs at $C_{Opt} = 1951$. General expressions for C_{Opt} and $\eta_{COLL}(max)$ can be derived from the preceding equations and are:

$$C_{Opt} = \left[\frac{SIN^2\theta_r}{2(\sigma_b')^2}\right] \frac{1}{\ell n\ B} \qquad (3\text{-}6)$$

$$\eta_{COLL}(max) = \left(\rho\ \alpha_{Eff} K_d K_b\right)\left[1 - \frac{1 + \ell n\ B}{B}\right] - \frac{3}{I_{d,n}} \qquad (3\text{-}7)$$

Where $$B = \left\{\frac{\rho\ K_d K_b \alpha_{Eff}\left[SIN^2\theta_r/2(\sigma_b')^2\right] I_{d,n}}{\sigma\varepsilon_{Eff}(T_R^4 - T_\infty^4) + h(T_R - T_\infty)}\right\}$$

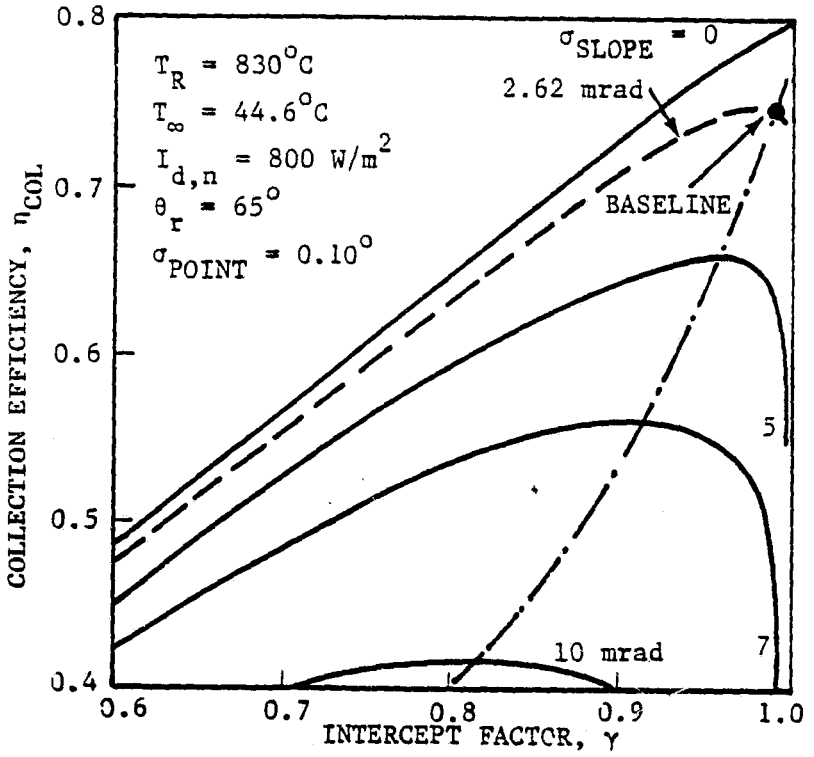

94-2-71

FIGURE 3-5. OPTIMUM INTERCEPT FACTOR TRADEOFF

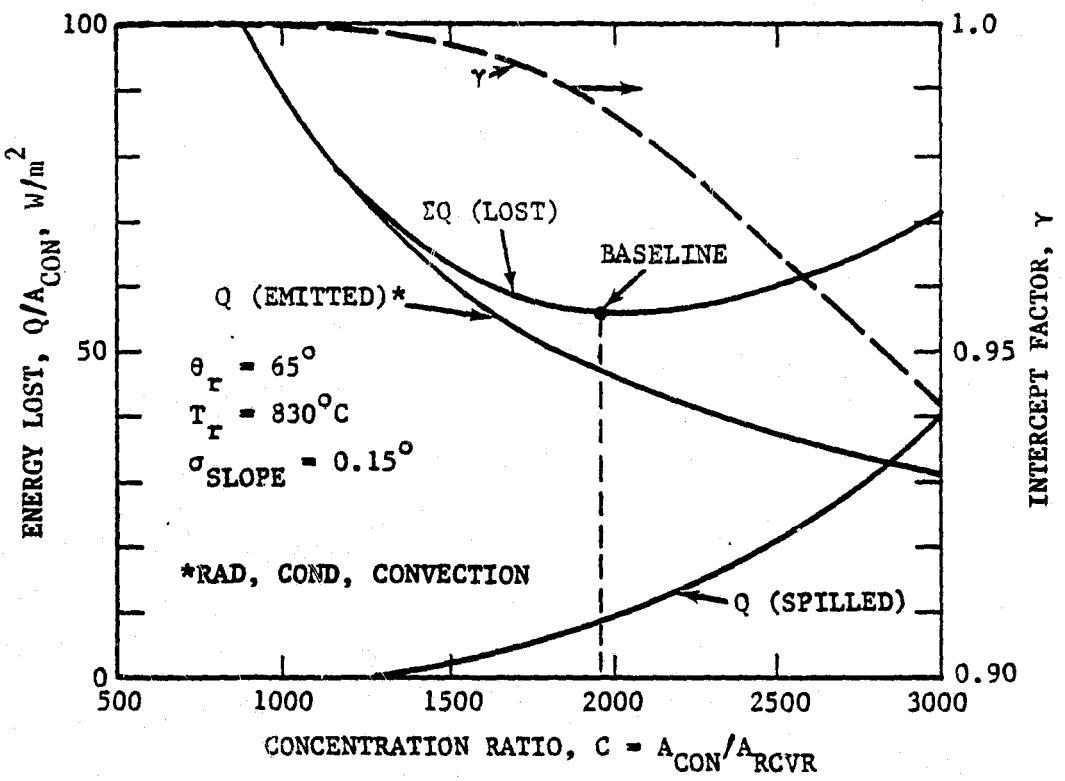

94-2-70

FIGURE 3-6. RECEIVER APERTURE OPTIMIZATION

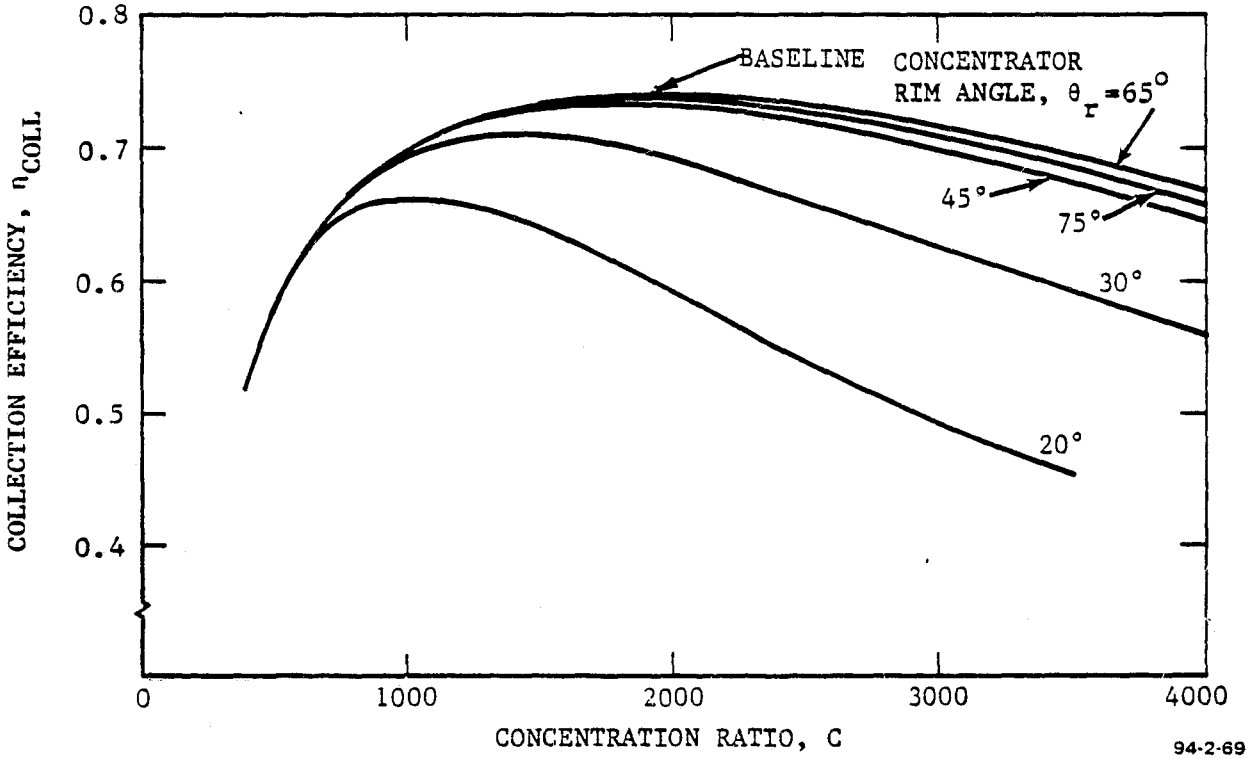

FIGURE 3-7. CONCENTRATION RATIO TRADEOFF

From Equation (3-6), the optimum concentration ratio is shown in Figure 3-8 as a function of σ_{Slope} and receiver temperature. Note that the combination of high concentrator quality and high temperature results in a large value for C_{Opt}; for a given power level (concentrator diameter), therefore, the resultant receiver will be small resulting in less solar blockage, lower weight (for a given generic design) and lower cost.

The governing equations also yield the influence of rim angle; as shown in Figure 3-9, optimum rim angle occurs at values above ~50 degrees but the influence is not a strong one for reflector slope errors of interest. Separate design/cost analyses were carried out with the result shown in Figure 3-10. Lowest system energy cost occurs at $\theta_r \cong 65$ degrees. This result is primarily due to the reduction in weight and associated solar blockage of the tripod structure carrying the receiver/power conversion package compensating for the increased cost of the reflector surface. Figure 3-11 shows the effect of reflector slope error on system energy cost; lowest system cost occurs at $\sigma_{Slope} \cong 3.0$ mrad. This trade-off is due primarily to the influence of slope error on concentrator cost (see Paragraph 3.1.3) but note that reduced σ_{Slope} results in reduced C_{Opt} and the receiver increases in size, thus increasing both its cost and amount of solar blockage.

Trade studies made to evaluate the effect of reflectivity and specularity of the concentrator surface on system performance demonstrated that maximum values are optimum, consistent with the type of reflective surface used. Draw fusion glass has been selected for the mirror, which has a reflectivity about as high as can be achieved (95 percent) and the corresponding specularity is also excellent ($\cong$ 0.2 mrad, 1σ). The pointing accuracy selected as the nominal is a compromise between the energy spill-over and the errors in the tracking and pointing system. A 1σ value of 1.745 mrad (0.1 deg) was selected for the SPS.

All of the preceding trades were carried out at the nominal receiver temperature of 830 degrees Centigrade, corresponding to an engine temperature of 800 degrees Centigrade. Figure 3-12 shows the influence of receiver temperature on both collection efficiency and Stirling engine efficiency; collection efficiency is particularly sensitive to reflector slope error. The two efficiencies can be combined into an overall system efficiency as shown in Figure 3-13. For the baseline concentrator quality ($\sigma_{Slope} = 2.618$ mrad), Figure 3-13 shows that η_o continues to increase with temperature beyond the maximum 800 degrees Centigrade limit currently placed on the metallic heater head. If ceramic heater heads are developed in the future, performance gains of several percentage points (over 30 percent overall system efficiency) can thus be expected. At the nominal $\sigma_{Slope} = 2.618$ mrad, overall efficiency (sun-to-electricity) is approximately 25.6 percent at rated power conditions which is essentially the same value for system efficiency computed on an annual basis at Barstow.

Figure 3-14 shows the influence of the geometric deployment of collectors on mutual sun shading and associated system energy loss (see Appendix M).

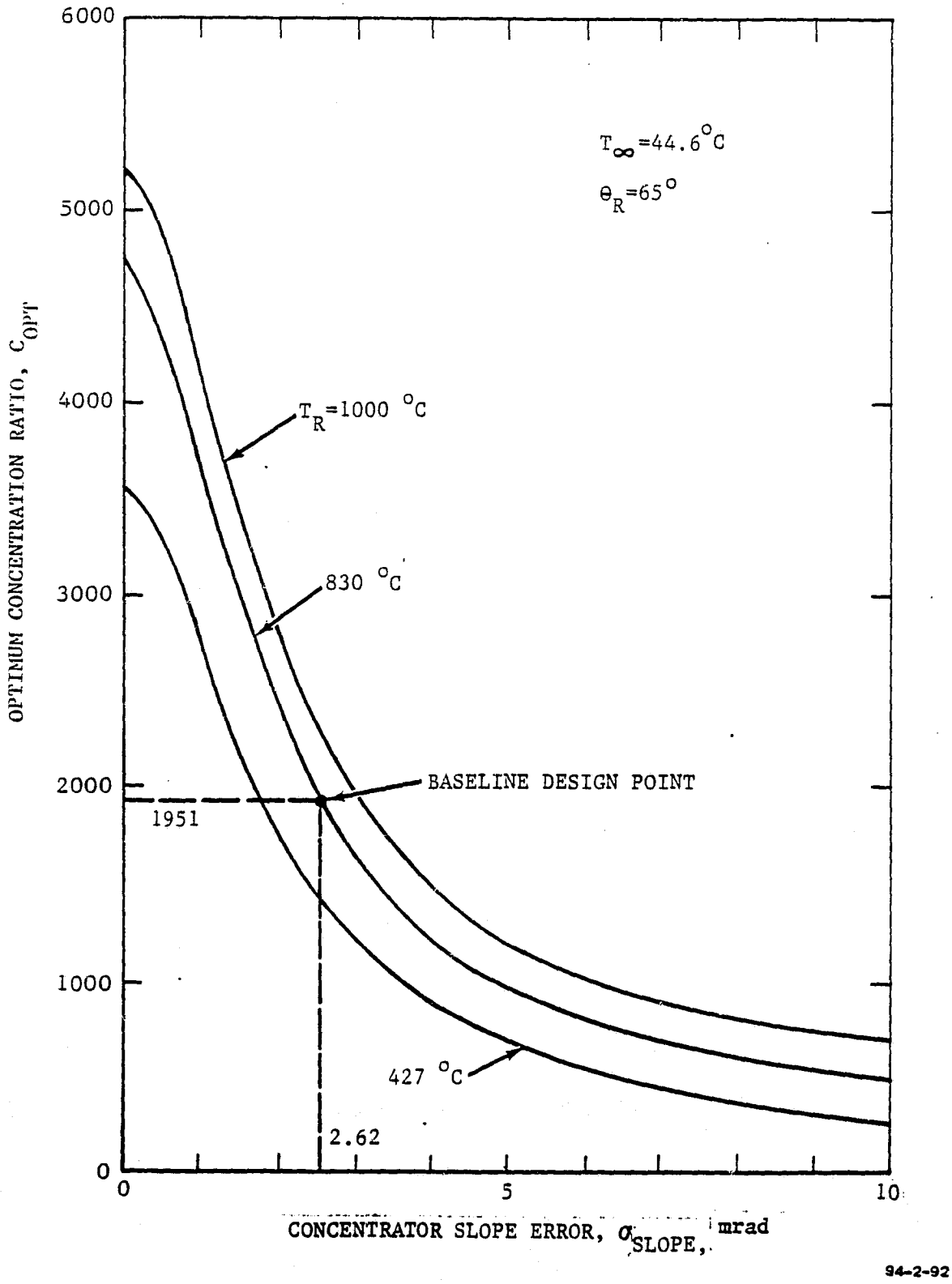

FIGURE 3-8. EFFECT OF REFLECTOR QUALITY ON OPTIMUM CONCENTRATION RATIO

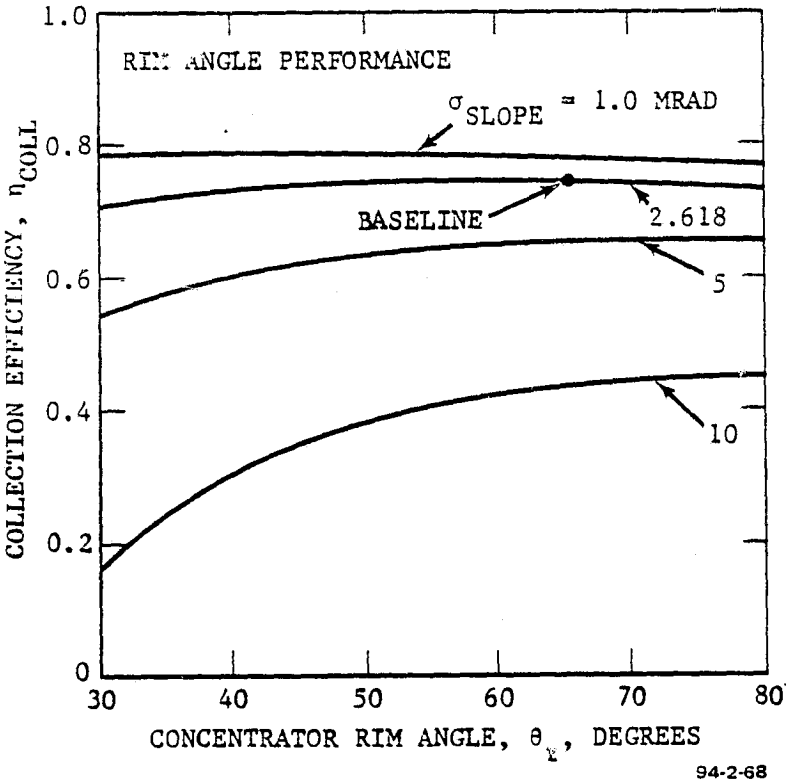

FIGURE 3-9. CONCENTRATOR RIM ANGLE SENSITIVITY

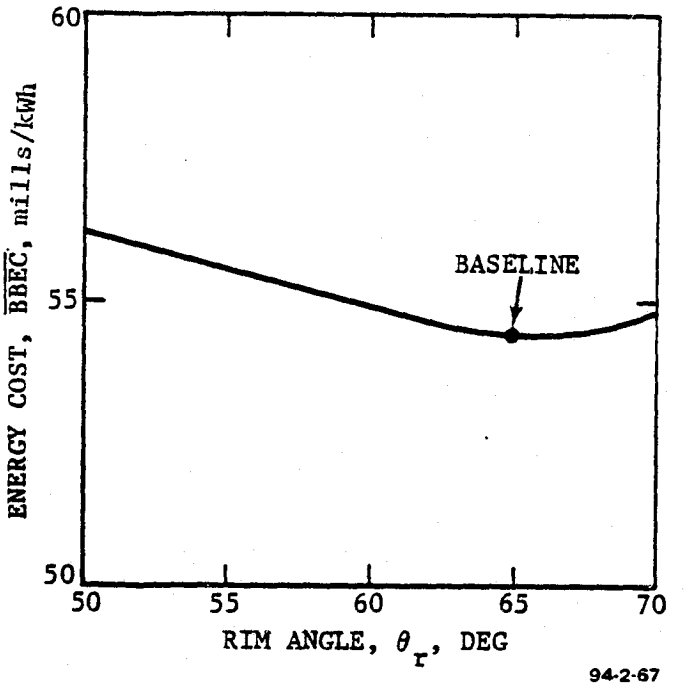

FIGURE 3-10. TRADEOFF BETWEEN CONCENTRATOR RIM ANGLE AND LIFE CYCLE ENERGY COST

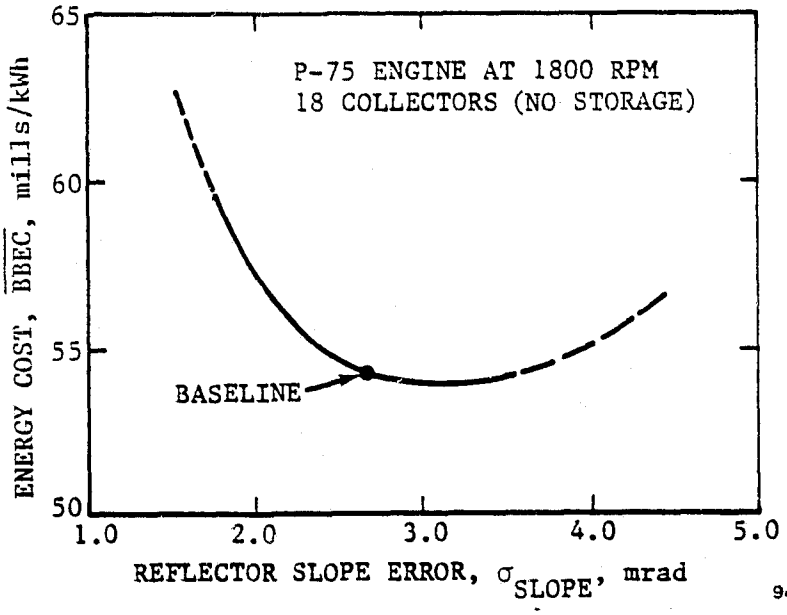

FIGURE 3-11. TRADEOFF BETWEEN REFLECTOR QUALITY AND LIFE-CYCLE ENERGY COST

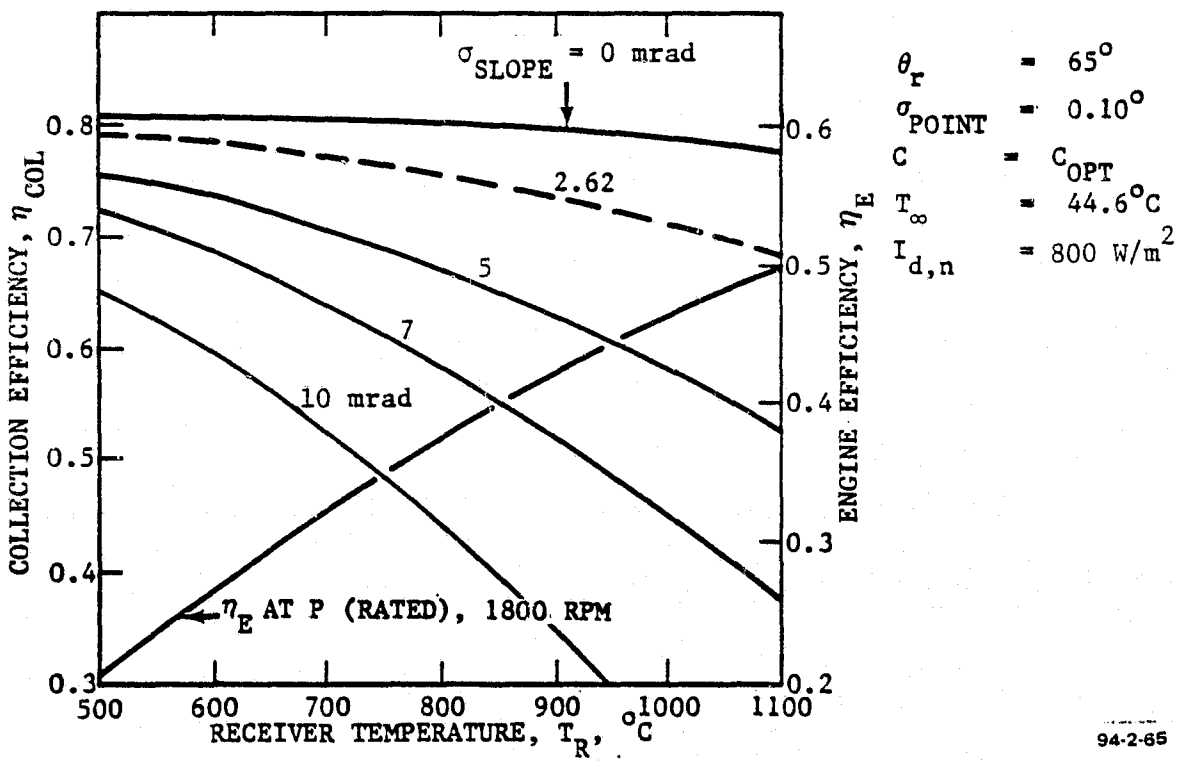

FIGURE 3-12. EFFECT OF RECEIVER TEMPERATURE ON COMPONENT EFFICIENCY

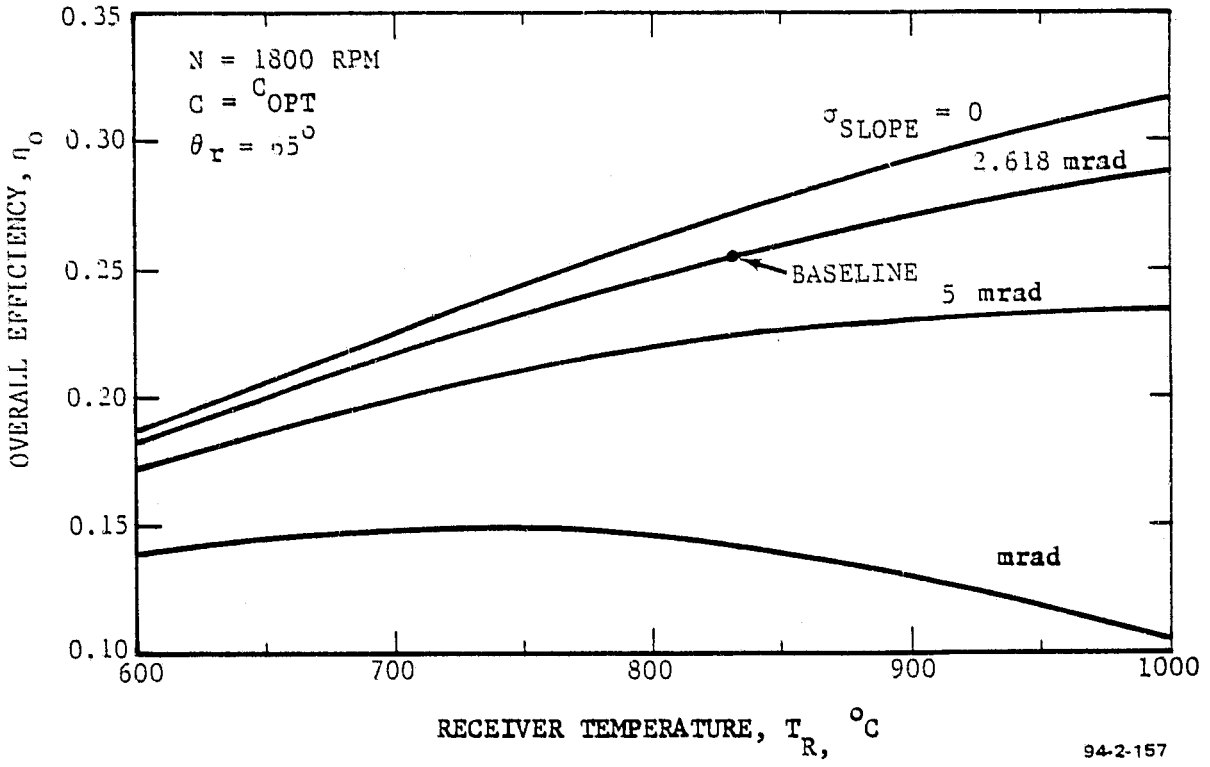

FIGURE 3-13. OVERALL SYSTEM EFFICIENCY

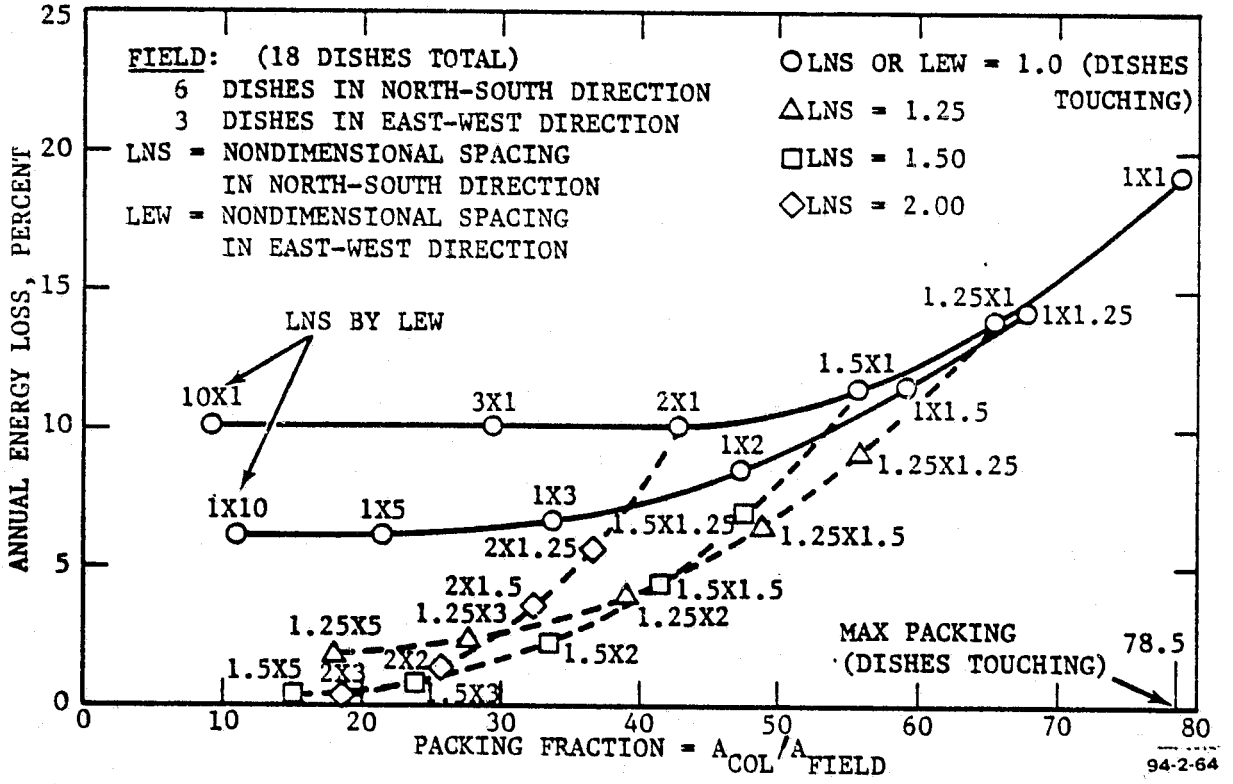

FIGURE 3-14. COLLECTOR PACKING FRACTION TRADE-OFF

The calculations were made for an 18 dish ("basic module") system arranged in a 6(N-S) by 3(E-W) matrix with varying N-S and E-W spacings (expressed proportional to dish diameter) between dishes. Note that at 25 percent packing fraction (concentrator area-to-land area) there is virtually no energy loss at the optimum spacing; even at 50 percent packing fraction, the loss is only six percent. At the specified $5000/acre land cost and including cabling cost for the electrical transport subsystem, trade-off analysis shows that lowest system cost occurs at about 25 percent packing fraction. This requires 4.85 acres for a field of 18 dishes, each 18.6 m in diameter. Land costs would have to rise substantially, that is, to about $30,000/acre, to justify a 50 percent packing fraction.

Collection efficiency at rated power can be evaluated from Equation 3-7 given in Paragraph 3.1.1.1; engine efficiency at rated power can be determined by combining Equation 3-9 with the engine correlation equations given in paragraph 3.1.4.1 System size data for the two baseline systems without storage are summarized in Table 3.1; performance data are computed at rated condition.

TABLE 3.1. SYSTEM SIZE DATA (NO STORAGE)

Engine	P-40	P-75
N_o (Number of Basic Modules)	55	18
η_{COLL_r}	0.740	0.740
η_{E_r}	0.373	0.393
P_{o_r}(kW)	21.9	63.4
P_G(kW) (Grid Power per Collector)	18.2	55.6
A_{con}(m^2) (Concentrator Area)	99	272.5
D_{con}(m) (Concentrator Diameter)	11.2	18.6

b. System Performance (Without Storage). Program SPEEL computes system performance in 15 minute intervals, as a function of the time-dependent ambient temperature (T_∞) and solar insolation ($I_{d,n}$); the influence of T_∞ and $I_{d,n}$ on engine performance as well as on receiver performance is accounted for in the computer programs. Receiver performance, however, is not a strong function of these time-dependent variables, as shown in Figure 3-15. For normal days at Barstow, $I_{d,n}$ is above 500 W/m^2 for most of the operating day and T_∞ has a negligible effect on collection efficiency and it is much less than receiver temperature (T_R). The major time-variable effect, therefore, is on engine performance. The major impact here, however, is associated with the specified definition of rated power, i.e., which requires that no more than rated power be delivered to the grid when $I_{d,n} \geq$ 800 W/m^2. Program SPEEL was thus formulated to compute the following: (1) the net energy (E_{G_2}) generated by all collectors which would be delivered to the grid regardless of power level,

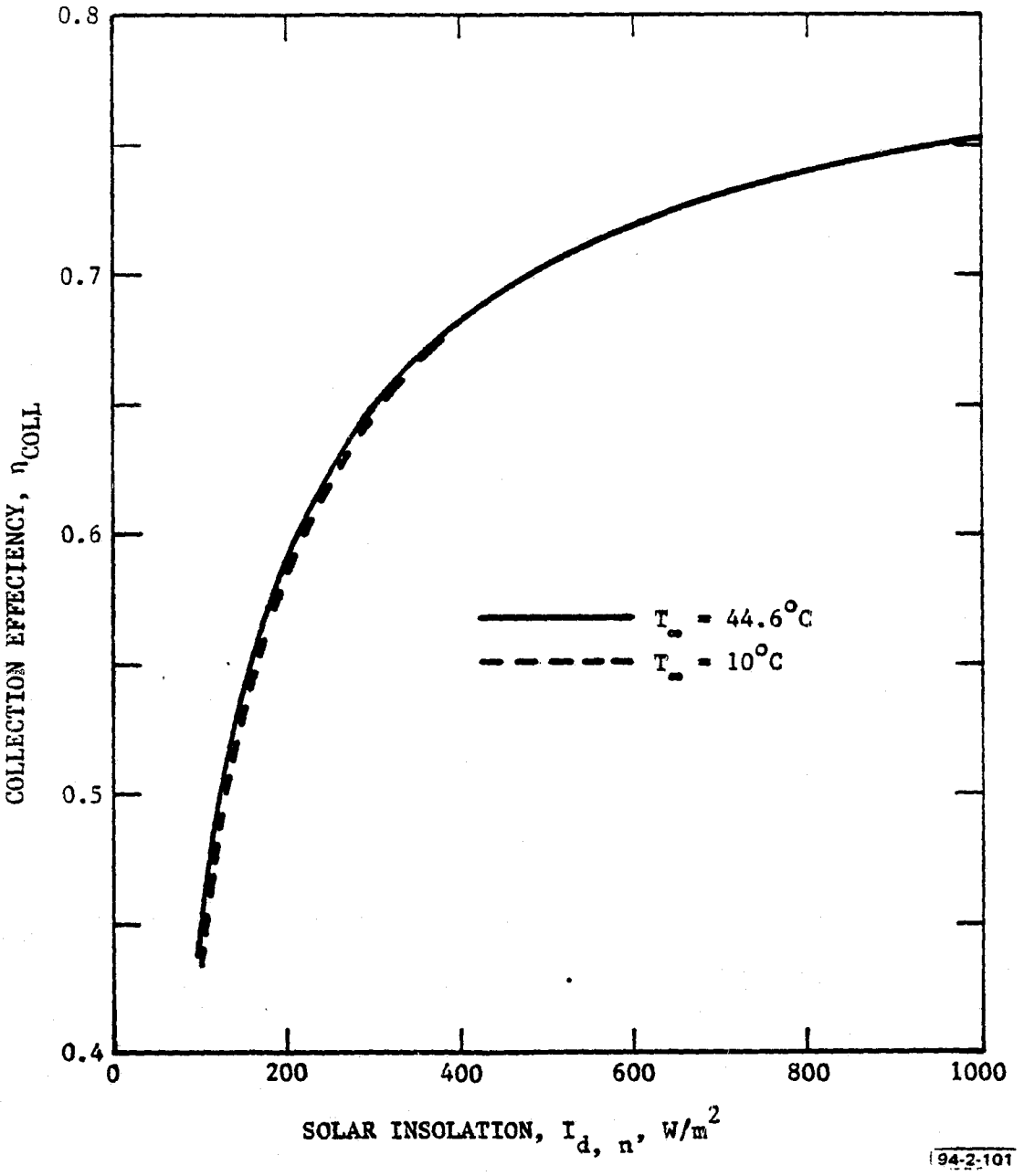

FIGURE 3-15. EFFECT OF SOLAR INSULATION ON COLLECTION EFFICIENCY

i.e., $P_G \gtrless P_{G_r}$; (2) the net energy E_{G_1} delivered to the grid only when the power level is equal to or below rated power, i.e., $P_G \leq P_{G_r}$; and (3) E_{G_S}, the difference between E_{G_2} and E_{G_1}, which represents the "excess energy" which can be diverted to storage or dumped or not collected by de-focussing one or more collectors. However, adherence to the doctrine that $P_G \leq P_{G_r}$ is not cost-effective in the absence of a storage system; it is obviously much better for the grid to accept all of the energy generated by the solar plant rather than to throw energy away.

Program SPEE1 includes the station-keeping power (= 1.5 N_O + 8) in its computation of E_{G_2}, E_{G_1} and E_{G_S}. Typical daily energy outputs for the P-75 baseline system are shown in Figures 3-16 and 3-17; monthly energy output is shown in Figure 3-18 and tabulated in Tables 3.2 and 3.3 for the P-75 and P-40 engine systems, respectively. The tabular data permit ready determination of the annualized capacity factor (ACF), as shown in Equation (3-11).

3.1.1.2 Annualized Performance. System performance calculations were carried out on an annualized basis accounting for the actual temporal variations in solar insolation, the actual variation in ambient temperature which influences engine performance, and, to a lesser extent, receiver performance. Performance based on 15 minute data tapes compiled for Barstow, California in 1976 was determined using computer program SPEE1. The computational procedure is based upon the system analysis logic presented in Figure 3-1 and is defined in the following paragraphs.

a. System Size. The system is first sized at the defined rated power conditions, i.e., on the hottest day (44.6°C) when $I_{d,n}$ = 800 W/m^2. (This assures that system rated power (1MW$_e$) will always be met for $I_{d,n}$ = 800 W/m^2). The net power delivered to the grid by a single collector, P_G, is:

$$P_G = \eta_{EL} P_{o_r} - P_{STA} = \frac{1000}{N_o} \text{ , kW} \qquad (3\text{-}8)$$

where:

P_{o_r} = Engine shaft output power at rated conditions, kW

η_{EL} = Electrical system efficiency (ca.1990, high production rates) including a 94% efficient generator, = 0.9065

P_{STA} = Station-keeping power per collector, = 1.5 + 8/N_o, kW, (See Appendix G)

N_O = Number of collectors required to deliver rated power direct to grid (basic modules).

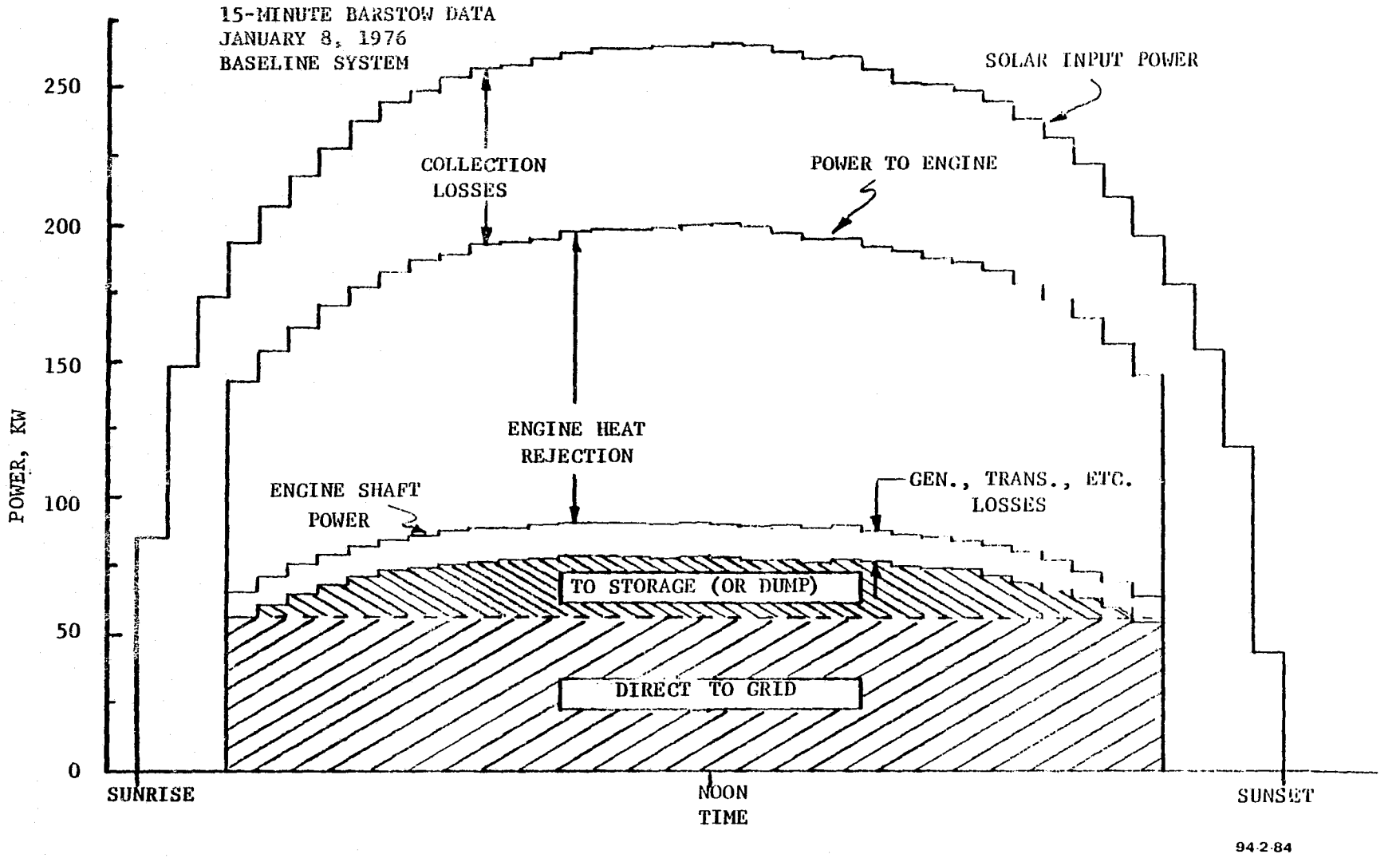

FIGURE 3-16. SYSTEM PERFORMANCE FOR A TYPICAL DAY

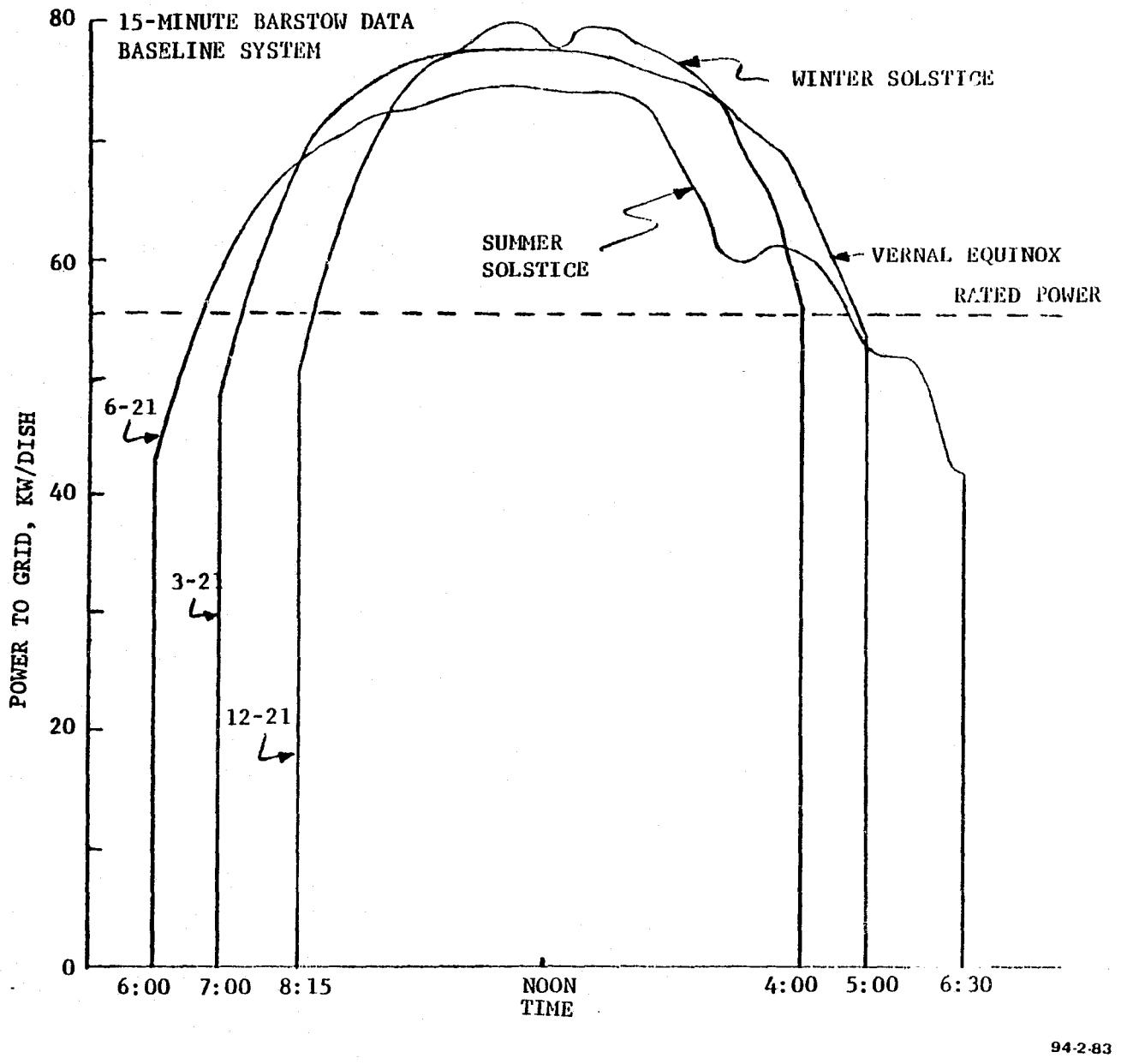

FIGURE 3-17. SYSTEM PERFORMANCE BY SEASON

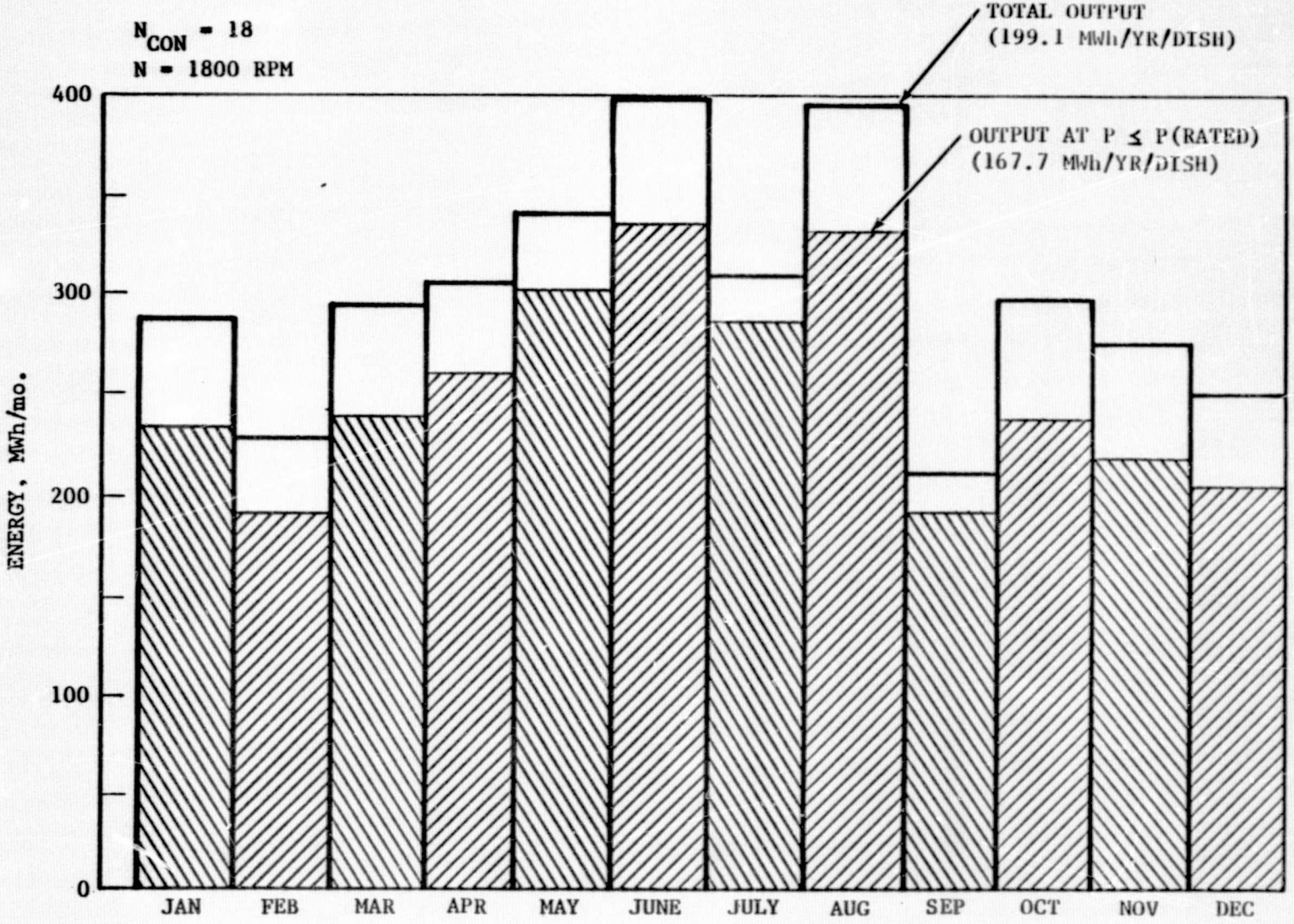

FIGURE 3-18. SYSTEM MONTHLY OUTPUT

94 2 100

TABLE 3.2 P-75 SYSTEM OUTPUT AT BARSTOW (1976)

(Ca. 1990 PERFORMANCE)

Month	E_{G_2} $\left(\frac{\text{MWh}}{\text{mo-dish}}\right)$	E_{G_1} $\left(\frac{\text{MWh}}{\text{mo-dish}}\right)$	E_{G_s} $\left(\frac{\text{MWh}}{\text{mo-dish}}\right)$
January	15.766	12.694	3.073
February	12.482	10.245	2.237
March	16.148	13.131	3.017
April	17.120	14.578	2.541
May	19.161	16.917	2.244
June	22.100	18.787	3.313
July	17.274	15.541	1.732
August	21.890	18.368	3.522
September	11.814	10.648	1.166
October	16.160	13.367	2.793
November	15.100	12.287	2.813
December	14.075	11.154	2.921
TOTALS	Σ = 199.089	Σ = 167.718	Σ = 31.371

E_{G_2} = Net energy delivered to grid regardless of power level

E_{G_1} = Net energy to grid only when power level is equal to or below rated power

$E_{G_s} = E_{G_2} - E_{G_1}$ = "Excess" energy diverted to storage or thrown away if there is no storage.

TABLE 3.3 P-40 SYSTEM OUTPUT AT BARSTOW (1976)

(Ca. 1990 PERFORMANCE)

Month	E_{G_2} $\left(\frac{\text{MWh}}{\text{mo-dish}}\right)$	E_{G_1} $\left(\frac{\text{MWh}}{\text{mo-dish}}\right)$	E_{G_s} $\left(\frac{\text{MWh}}{\text{mo-dish}}\right)$
January	5.088	4.105	0.983
February	4.009	3.288	0.721
March	5.192	4.211	0.981
April	5.505	4.684	0.821
May	6.167	5.422	0.745
June	7.204	6.082	1.122
July	5.580	4.992	0.588
August	7.164	5.972	1.192
September	3.789	3.408	0.381
October	5.247	4.325	0.922
November	4.898	3.986	0.912
December	4.542	3.605	0.938
TOTALS	Σ = 64.385	Σ = 54.079	Σ = 10.306

thus:

$$P_{o_r} = \frac{1008/N_o + 1.5}{\eta_{EL}} \qquad (3\text{-}9)$$

and

$$A_{con} = \frac{P_{o_r} \times (10)^3}{I_{d,n_r}\ \eta_{E_r}\ \eta_{coll_r}} \qquad (3\text{-}10)$$

where:

A_{con} = Concentrator aperture area, m^2

η_{E_r} = Engine efficiency at rated power

η_{Coll_r} = Collection efficiency at rated power

$$ACF = \frac{\Sigma\ N_o\ E_{G_1}\ \bar{A}}{8784^*}, \quad \text{for } P_G \leq P_{G_r} \qquad (3\text{-}11)$$

and

$$ACF = \frac{\Sigma\ N_o\ E_{G_2}\ \bar{A}}{8784^*} \quad \text{for } P_G \geq P_{G_r} \qquad (3\text{-}12)$$

Where $\bar{A}$ = effective availability of the system ($\simeq$ 0.99). The ACFS for the two systems are therefore:

Case:	ACF P-40 Engine	ACF P-75 Engine
$P_G \leq P_{G_r}$	0.335	0.340
$P_G \gtrless P_{G_r}$	0.399	0.404

These data show that both systems demonstrate ACFs of 0.4 without storage for $P_G \gtrless P_{G_r}$. For the specified $P_G \leq P_{G_r}$ doctrine, the amount of storage needed to achieve 0.4 is obviously small, however the cost to achieve this is substantial.

---

* 1976 was a leap year

c. System Performance (With Storage). The data of Tables 3.2 and 3.3 also permit easy computation of ACF for any specified storage system. For example, it is assumed that there are N_0 basic modules providing direct energy to the grid (ΣE_{G_1}) with their "excess" energy (ΣE_{G_S}) diverted to the storage system as previously mentioned. In addition there are N_1 "dedicated" dishes whose entire output (ΣE_{G_2}) is delivered to the storage system.**

Total net output of the system (delivered to the grid), ΣE, (MWh/yr) is thus:

$$\Sigma E = \eta_0 \Sigma E_{G_1} + \eta_S \eta_0 \Sigma E_{G_S} + \eta_S \eta_1 \Sigma E_{G_2} - E_1(10)^{-3} \qquad (3\text{-}13)$$

where η_S is the end-to-end efficiency of the storage system and E_1 is the additional station-keeping energy (kWh/yr) to accomodate the air conditioning and other loads associated with the storage system. As shown in Appendix G, E_1 for a battery system (typical lead-acid) is

$$E_1 = C_1 \bar{E}_B D_{yr} \qquad (3\text{-}14)$$

where

C_1 = Constant (= 0.177)

$\bar{E}_B$ = Average daily energy delivered to the grid from the batteries, kWh/day

D_{yr} = Number of operating days per year

and $\bar{E}_B$ can be defined as

$$\bar{E}_B = \eta_S [\eta_0 \Sigma E_{G_S} + \eta_1 \Sigma E_{G_2}] \frac{10^3}{D_{yr}} \qquad (3\text{-}15)$$

Equations 3-13, 3-14, and 3-15 can be combined to yield

$$\Sigma E = \eta_0 [\Sigma E_{G_1} + \eta_S \Sigma E_{G_S} (1 - C_1)] + \eta_1 [\eta_S \Sigma E_{G_2} (1 - C_1)] \qquad (3\text{-}16)$$

and

$$ACF = \frac{\Sigma E A}{8784} \qquad (3\text{-}17)$$

** This is a mathematical artifice; all collectors deliver to a single bus, from which some energy is diverted to storage and some delivered directly to the grid

The size (and cost) of the storage system is dictated by the highest daily energy delivered to the grid from storage, $E_b(max)$(kWh/day):

$$E_b(max) \cong \eta_S [N_O E_{G_S} + N_1 E_{G_2}] \frac{10^3}{D_{mo}} \qquad (3\text{-}18)$$

Inspection of Tables 3.2 and 3.3 shows that $E_B(max)$ occurs in either June or August, depending on the relative values of N_1 and N_O, which are in turn determined by ACF and the type of storage system. For ACF $\sim$ 0.4, $E_b(max)$ occurs in August for both battery and flywheel systems. Table 3.4 summarizes the performance characteristics of the P-40 and P-75 systems for both storage system concepts.

Table 3.4 shows an advantage for the composite flywheel over the advanced battery system in that fewer collectors are required to achieve the same ACF. This is due to the higher value of η_S and the assumption that $E_1 = 0$ for the flywheel. As shown in subsequent paragraphs, there is an associated cost advantage with the flywheel. However the flywheel data are projections based on on-going studies rather than on hardware and our present conclusion is that the flywheel and the advanced battery system have about the same performance/ cost characteristics.

TABLE 3.4 SYSTEM PERFORMANCE @ ACF $\sim$ 0.4 (WITH STORAGE)

	P-40 Engine		P-75 Engine	
Parameter	Battery (η_S = 0.775)	Flywheel (η_S = 0.82)	Battery	Flywheel
N_O	55		18	
N_1	5	2	1	0
ACF	0.399	0.400	0.395	0.392
E_b(max (kWh/day)	2534	2184	2132	1677
Σ E (MWh/yr)	3505	3514	3470	3443
P(STA), (kW)	134.5	93.5	74.3	35

d. Alternate Engine Comparison. The annualized performance of systems employing the alternate Brayton and Organic Rankine power plants as described in Paragraph 3.1.4.3 was also determined using the previously discussed methodology. The data for E_{G_2}, E_{G_1} and E_{G_S} for these systems are given in Tables 3.6, 3.7 and 3.8. A summary comparison of the performance of the various systems (without storage) is given below in Table 3.5.

TABLE 3.5 COMPARATIVE SYSTEM PERFORMANCE (NO STORAGE)

Parameter	Brayton		Rankine*	Stirling	
	Closed	Open		P-40	P-75
P_{o_r}	30.2	30.2	77.5	21.9	63.4
N_O	39	39	15	55	18
$A_{con}(m^2)$	207.8	185.4	450.	99.	272.5
$D_{con}(m)$	16.3	15.4	23.9	11.2	18.6
$N_O \cdot A_{con}$ (m^2)	8104	7231	6750	5445	4905
η_{E_r}	0.251	0.281	0.250	0.373	0.393
η_{COLL_r}	0.723	0.723	0.793	0.740	0.740
η System (Annualized)	0.160	0.145	0.193	0.228	0.256
ACF $(P_G \leq P_{G_r})$	0.346	0.309	0.347	0.335	0.340
ACF $(P_G \gtrless P_{G_r})$	0.416	0.336	0.418	0.399	0.404

Note the low value of ACF (annualized capacity factor) for the open-cycle Brayton; this is due primarily to the poor part-load efficiency of this power plant when Turbine Inlet Temperature (TIT) control is employed. Also, the lower operating temperature for the Organic Rankine System (427°C) results in a higher value for collection efficiency, partly compensating for the low engine efficiency. Table 3.5 also shows that both Stirling Systems show higher overall system efficiency than achieved with the alternate engine systems.

* Variable turbine and fan speeds

TABLE 3.6 CLOSED CYCLE BRAYTON SYSTEM OUTPUT AT BARSTOW (1976) (Ca.1990 PERFORMANCE)

Month	E_{G_2} $\left(\frac{MWh}{Mo\text{-}Dish}\right)$	E_{G_1} $\left(\frac{MWh}{Mo\text{-}Dish}\right)$	E_{G_S} $\left(\frac{MWh}{Mo\text{-}Dish}\right)$
January	7.57	5.94	1.63
February	6.01	4.84	1.17
March	7.76	6.20	1.56
April	8.20	6.87	1.33
May	9.10	7.98	1.12
June	10.37	8.76	1.61
July	8.13	7.30	0.83
August	10.24	8.54	1.70
September	5.63	5.03	0.60
October	7.66	6.25	1.41
November	7.19	5.78	1.46
December	6.77	5.22	1.55
TOTALS	94.63	78.66	15.97

E_{G_2} = Net energy generated to grid regardless of power level

E_{G_1} = Net energy generated to grid only when power level is equal to or below rated power

E_{G_S} = $E_{G_2} - E_{G_1}$ = "excess" energy diverted to storage or thrown away if there is no storage

TABLE 3.7 OPEN CYCLE BRAYTON SYSTEM OUTPUT AT BARSTOW (1976) (Ca.1990 PERFORMANCE)

Month	E_{G_2} $\left(\frac{MWh}{Mo\text{-}Dish}\right)$	E_{G_1} $\left(\frac{MWh}{Mo\text{-}Dish}\right)$	E_{G_S} $\left(\frac{MWh}{Mo\text{-}Dish}\right)$
January	6.21	5.46	0.75
February	4.76	4.25	0.51
March	6.04	5.38	0.66
April	6.57	5.99	0.58
May	7.18	6.77	0.41
June	8.45	7.99	0.46
July	6.45	6.22	0.23
August	8.51	8.03	0.48
September	4.47	4.22	0.25
October	6.27	5.74	0.53
November	6.01	5.38	0.63
December	5.52	4.81	0.71
TOTALS	76.44	70.24	6.20

TABLE 3.8 ORGANIC RANKINE SYSTEM OUTPUT AT BARSTOW (1976) (Ca.1990 PERFORMANCE)

Month	E_{G_2} $\left(\frac{MWh}{Mo\text{-}Dish}\right)$	E_{G_1} $\left(\frac{MWh}{Mo\text{-}Dish}\right)$	E_{G_S} $\left(\frac{MWh}{Mo\text{-}Dish}\right)$
January	19.37	15.44	3.93
February	15.55	12.62	2.93
March	20.11	16.19	3.92
April	21.41	17.93	3.48
May	24.07	20.93	3.14
June	27.32	22.91	4.41
July	21.53	19.17	2.36
August	26.95	22.28	4.67
September	14.91	13.21	1.70
October	20.08	16.30	3.78
November	18.65	14.91	3.74
December	17.28	13.58	3.70
TOTALS	247.24	205.48	41.77

3.1.1.3 Design and Cost Analysis. The following paragraphs detail the design/cost analyses carried out to select the preferred 3.5, 4.5, and 6.5 year systems. The basic approach, described in Section 1.2, is to select a concept on the basis of lowest energy cost projected for a commercialized, ca. 1990 system, with suitable consideration of development cost, hardware availability and risk associated with the three different development schedules.

a. Generalized Engine Study. Although there are only a few specific engines available (or soon to be available) which are suitable for use with Engineering Experiment No. 1, the basic question to be addressed in a modular solar system of the type studied herein is the selection of the optimum size of engine to be employed. A generalized systems analysis was thus carried out using rubber engines, for instance, with varying output power (P_{o_r}) but with the same efficiency and general performance characteristics as the candidate engines summarized in Paragraph 3.1.4 For simplification, the analysis is restricted to the zero storage case (where $P_G \gtrless P_{G_r}$).

1. System Sizing. Expressions for grid power (P_G), engine rated power (P_{o_r}) and concentrator aperture area (A_{con}) were given previously in Equations 3-8, 3-9, and 3-10, respectively. Concentrator diameter, D_{con}, and receiver cavity aperture diameter, D_r, are determined by:

$$D_{con} = \left(\frac{4A_{con}}{\pi}\right)^{0.5} \qquad (3\text{-}19)$$

$$D_r = \frac{D_{con}}{\sqrt{C_{opt}}} \qquad (3\text{-}20)$$

where C_{opt} = Optimum concentration ratio, defined in paragraph 3.1.1.1.

These equations provide the necessary means for determining basic component size variations as engine rated power is varied. The size variation then permits determination of component costs and ultimately system energy costs.

2. Governing Cost Equations. The derivation of the applicable set of cost equations is given as Appendix H. The baseline scenario postulates that the 1 MW_e power plant is constructed in two years, starting in 1986 with the following schedule* implementation:

***The schedule is shown specifically for the Stirling engine, which requires maintenance/replacement at various times during the life of the plant.**

SCHEDULE FOR 1 MW_e PLANT

YEAR	FUNCTION	TYPE OPERATION
1986	Build Plant	Capital
1988	Start Operations	
1997 (j=10)	Replace Engine Heater Head(s) @ 25,000 hrs. (9 years.)	Maintenance
2003 (j=16)	Replace Receivers	Capital
2006 (j=19)	Replace Engine Heater Head(s)	Maintenance
2015 (j=28)	Replace Engine @ 75,000 hrs. (27 yrs.)	Capital
2018	End of plant first life	

The j-functions constitute exponents on some of the cost equations given in Appendix H; 1978 is the base year, that is, all costs are in 1978 dollars. The part of levelized busbar energy cost, due to capital investment alone, $\overline{BBEC}_c$ (mills/kWh), can be expressed for this plant as:

$$\overline{BBEC}_c = 9.9759\ (10^{-6}) \left(\frac{CI_{PV}}{ACF} \right) \qquad (3\text{-}21)$$

where ACF = Annualized capacity factor including allowance for nonscheduled maintenance ($\overline{A} \approx 0.99$)

CI_{PV} = Summarized present value of total capital investment in the plant, adjusted to constant base year dollars

= 1.83477 CI(1986) + 1.21528 CI(2003) + 0.90866 CI(2015)

CI(YR) = Specific year capital investment.

As shown above, capital investments are made in 1986 (original plant), 2003 (new receivers) and 2015 (new engines). The constant in Equation (3-21) includes the specified annualized fixed charge rate, $\overline{FCR}$ of 0.1565. The contribution of maintenance costs* to the overall energy cost can be written as:

$$\overline{OM} = 5.4491(10^{-6}) \left(\frac{MNT_{PV}}{ACF} \right) \qquad (3\text{-}22)$$

where MNT_{PV} = Present value of recurrent costs of maintenance

*Since the plant is unmanned and remotely operated, no operating costs are identified.

For the Stirling engine-based plant, the maintenance costs are of two types: (1) cost outlays that grow approximately uniformly over the system lifetime and (2) cost outlays that occur at discrete times and do not exhibit uniform growth. Category (1) accommodates the annual maintenance expenses, M_{ANN}, for instance, for cleaning the concentrators, annual replacement of engine seals/rings, etc. Category (2) accommodates the expenditure of M_t dollars, for instance, for replacing engine heater heads at 25,000 hours; it is treated in the cost analysis exactly as a capital expenditure. MNT_{PV} is thus expressed as:

$$MNT_{PV} = 47.274\ M_{ANN} + 3.1797\ M_t \qquad (3\text{-}23)$$

Total energy cost, $\overline{BBEC}$, is thus;

$$\overline{BBEC} = \overline{BBEC}_c + \overline{OM} \qquad (3\text{-}24)$$

Equations (3-21) through (3-24) provide the basis for costing the candidate systems.

3. Generalized Stirling Results. The individual component cost equations (in $) are as follows:

CI(1986)

- Receivers = $N_o \left[1500 + 4960\ D_r^2\right]$, (See Paragraph 3.1.2.3)
- Engines = $N_o \left[1641.8 + 0.554\ P_{o_r}^{1.77}\right]$, (Figure 3-19)
- Concentrators = $N_o A_C \left[8.45\ D_{Con} + 1021.89/D_{Con} - 79.5\right]$, (Figure 3-20)
- Electrical* = $\left[113{,}000 + 4000\ N_o\right]$, (See Appendix B)
- Building = 20,000
- Land & Site Prep = $5.436\ N_o A_C$ (Land is 5000/acre, site prep is 500/acre and packing fraction is 25 percent)

CI(2003)

- Receivers (Same as above)

CI(2015)

- Engines (Same as above)

*Includes generators, transport and control subsystems.

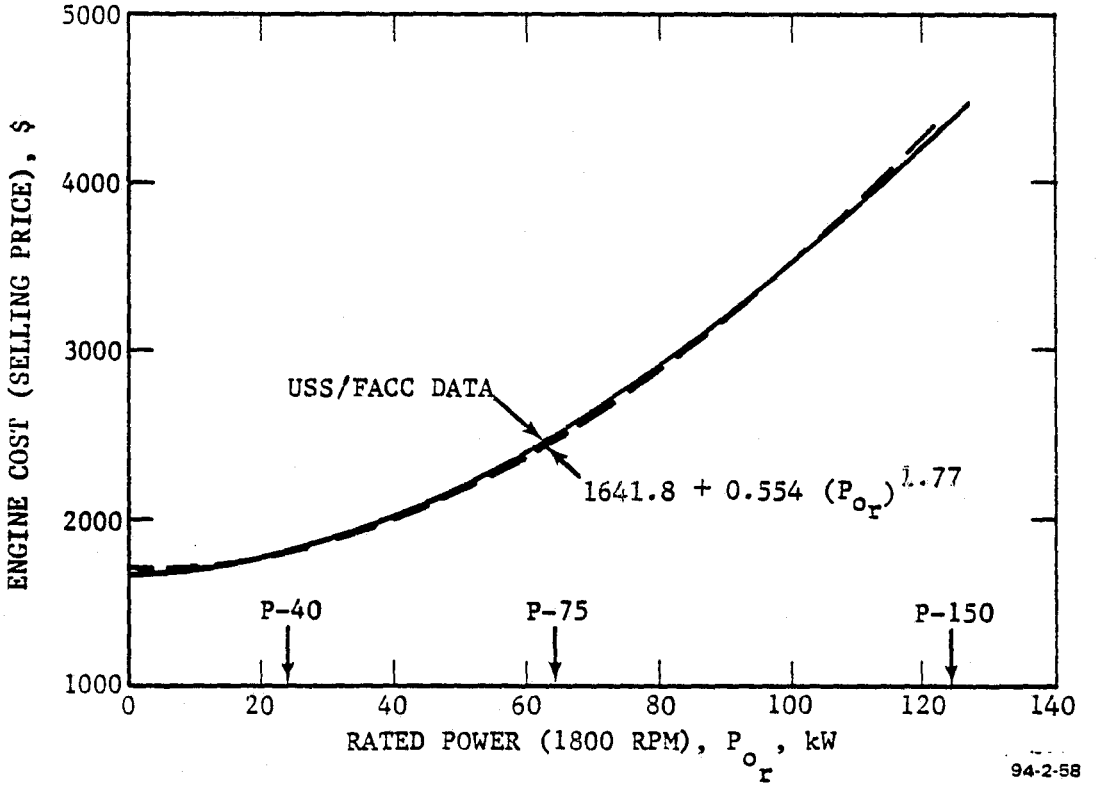

FIGURE 3-19. FACC PROJECTED STIRLING ENGINE COST IN MASS PRODUCTION, CA 1990

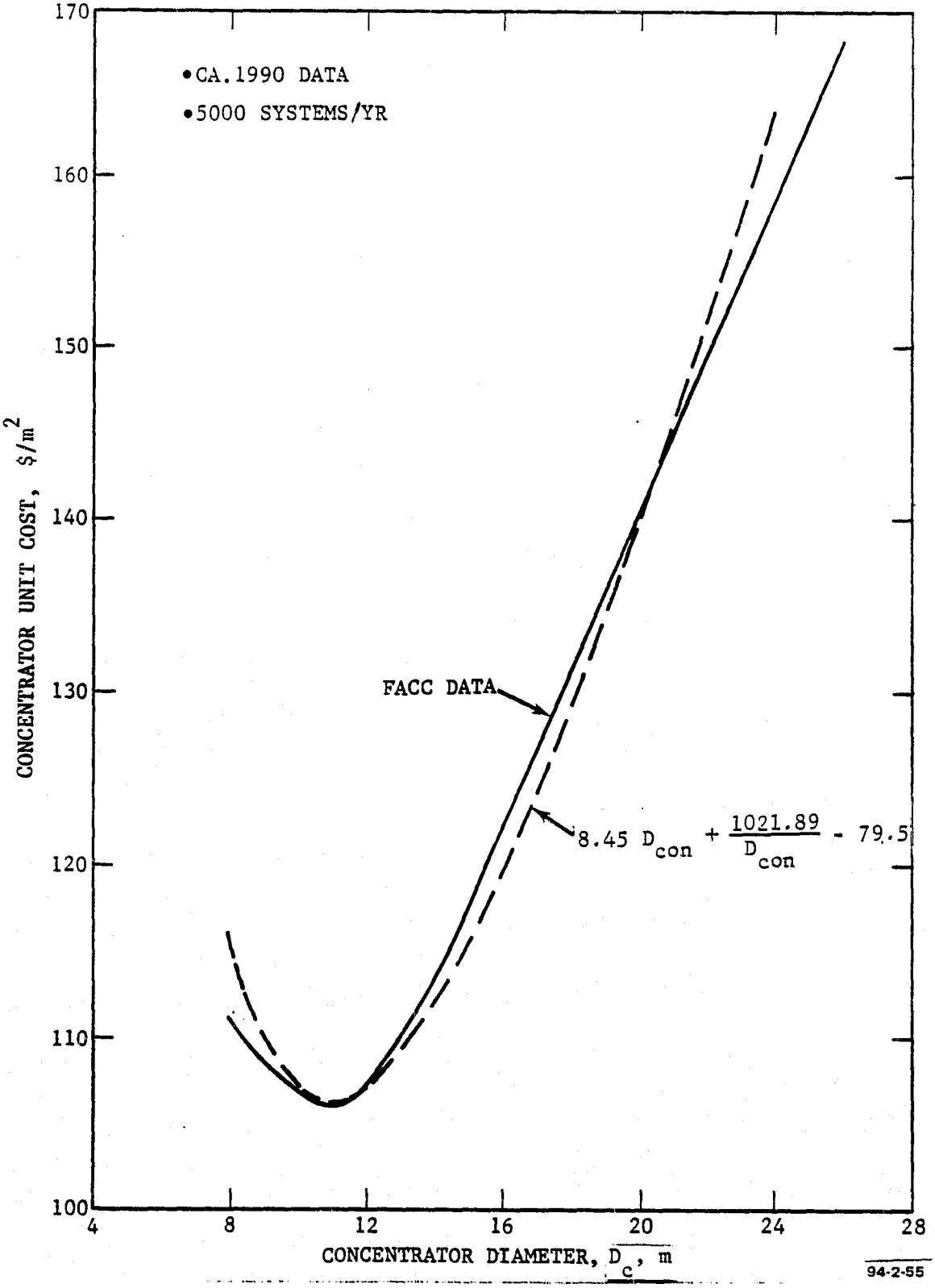

FIGURE 3-20. FACC PROJECTED CONCENTRATOR COST IN MASS PRODUCTION, CA. 1990

$$M_{ANN}\ (\text{Engine})\ \$/yr = N_o\ [115 + 0.19\ (P_{o_r})^{1.456}],\ \text{Figure (3-21)}$$

$$M_{ANN}\ (\text{Concentrators})\ \$/yr = 1202 + 104.7N_o + 0.427\ N_oA_c,$$
(Curve fit to maintenance cost data given in Paragraph 3.1.3.)

$$M_t\ (\text{Engine})\ \$ = N_o\ [1381.47 + 0.55\ (P_{o_r})^{1.68}],\ \text{(Figure 3-21)}$$

The results of the analysis are shown in Figure 3-22; the lowest cost Stirling system ($\approx$ 53 mills/kWh) occurs at a rated power level of 50-70 kW corresponding to concentrator diameters on the order of 18 m. The P-75 engine with P_{o_r} = 63.4 kW at 1800 rpm is thus close to optimum for this application. The P-40 engine at P_{o_r} = 21.9 kW at 1800 rpm is obviously not as good a choice. This is a result of an increase in both the capital investment and maintenance costs associated with many small modules.

4. Alternate Engines. Similar generalized analyses were carried out for the alternate Brayton and organic Rankine (ORC) engines, with some additional assumptions and simplifications (favorable to the alternates) as follows:

- 30 year engines
- ~30 year receivers (15 yr designs given in para. 3.1.2)
- Fixed engine cost/kW
- Fixed engine maintenance cost/kW.

Specific cost and parameter data used for these engines are given in Table 3.9. Figure 3-23 shows the results of the comparative analysis. The data clearly show that there is no justification for engines less than approximately 30 kW. If size-variable cost/performance data had been employed for the alternate engines, the optimum point would shift to still higher power levels. The data also show that neither Brayton cycle engine approaches the performance of the Stirling; the cost ratio between them is nearly 2 to 1 and it would take a dramatic improvement in efficiency (receiver as well as engine) to narrow the gap. The use of ceramic components and significantly higher temperature would help considerably. A major weakness of the Brayton system appears to be the receiver. It is larger, heavier and more costly than either of the other two receivers -- mostly due to the larger surface area needed to transfer the solar energy to the gaseous working fluid as well as the geometry required to minimize the direct impingement solar flux. It is recommended than an additional stage of heat exchange (secondary fluid) be considered -- preferably a liquid metal system similar to the one employed for the Stirling -- for analysis of any future Brayton/point focusing concepts. On the basis of the present study, however, the Brayton cycle must be considered least attractive.

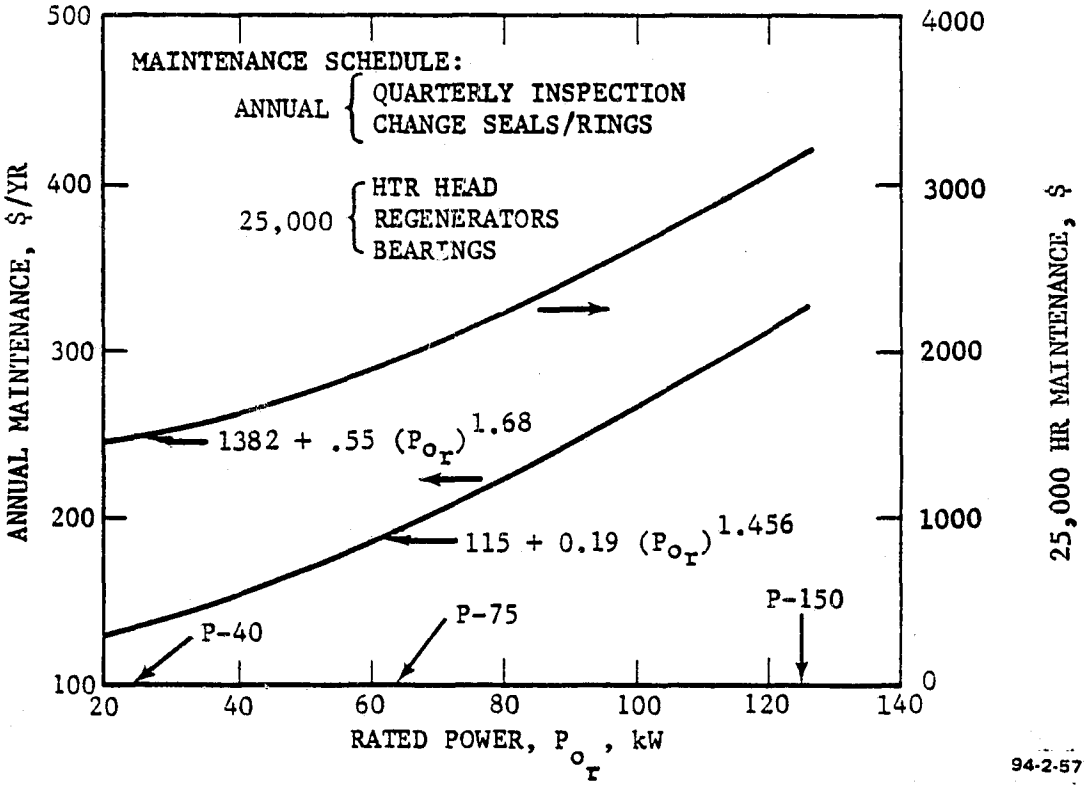

FIGURE 3-21. PROJECTED STIRLING ENGINE MAINTENANCE COSTS FOR PRODUCTION ENGINE, CA 1990

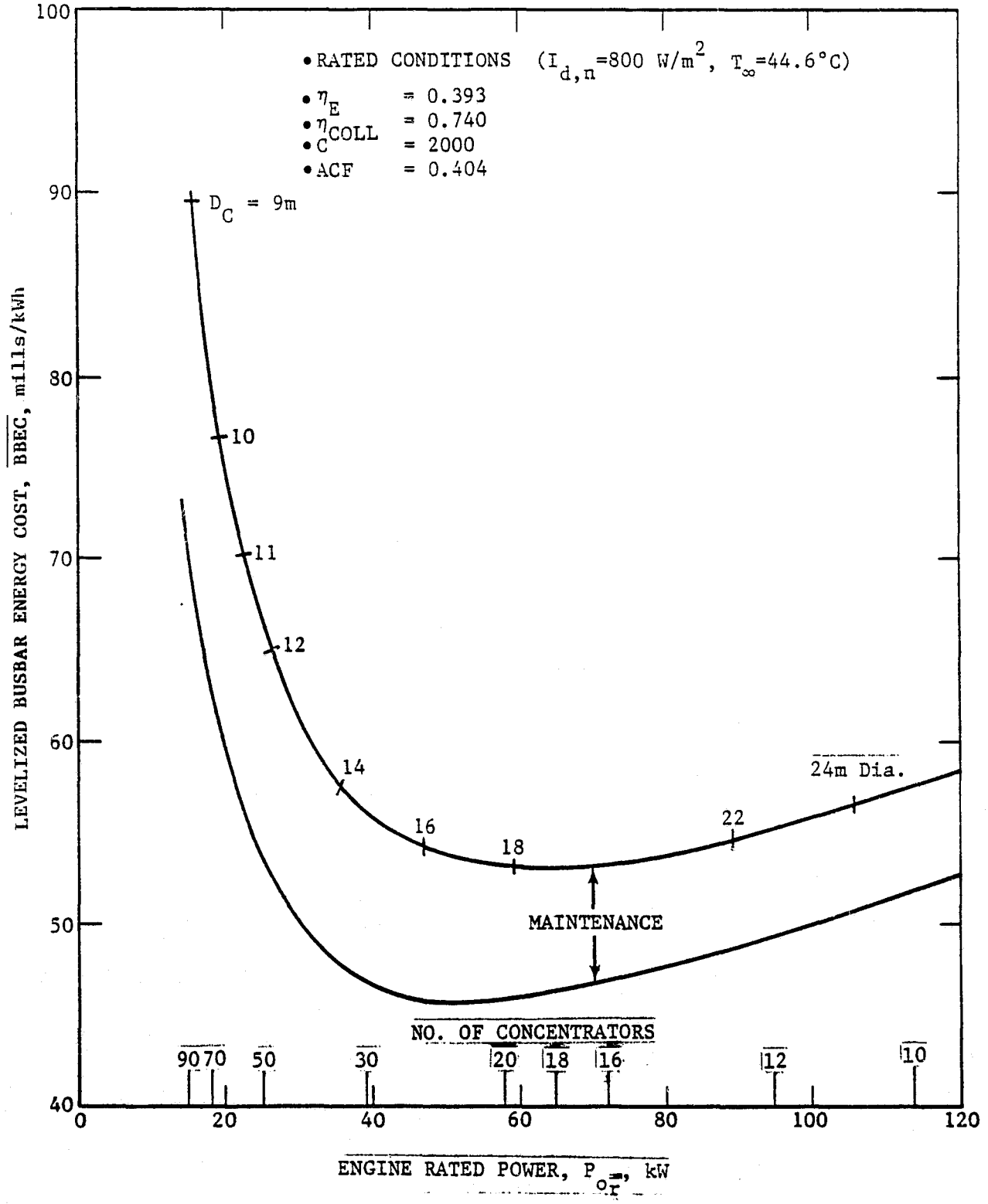

FIGURE 3-22. SYSTEM LIFE-CYCLE ENERGY COST WITH STIRLING ENGINES

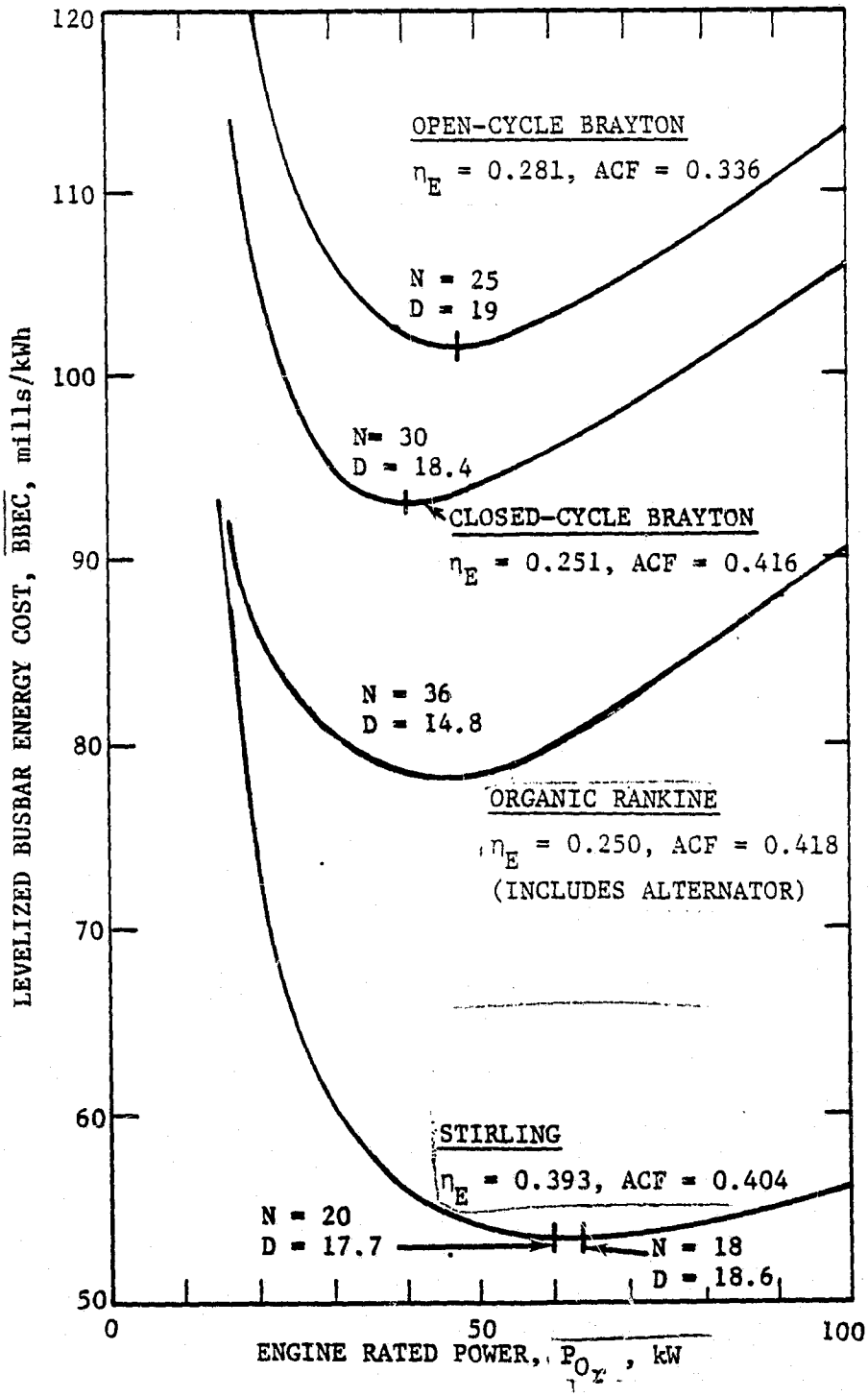

FIGURE 3-23. COMPARATIVE ENERGY COST WITH ALTERNATE ENGINES 94-2-94

TABLE 3.9 ALTERNATE ENGINE COST/PARAMETER DATA (Ca. 1990)

PARAMETER	BRAYTON		ORGANIC RANKINE
	CLOSED	OPEN	
$\tilde{\eta}_{E_r}$	0.251	0.281	0.250*
$\tilde{\eta}_{COLL_r}$	0.723	0.723	0.793
$\tilde{\eta}_{EL}$	0.9065*	0.9065*	0.964
T_R, ^oC	909	909	457
ACF ($P_G \gtrless P_{G_r}$)	0.416	0.339	0.418**
Receiver Cost, $	6000 + 37,641 D_r^2		1500 + 7300 D_r^2
Engine Cost ($/kW)	183	150	400
Engine Maint. Cost ($/kW/YR)	5	5	5.38
Elec. System Cost, $	113,000 + 4000 N		75,571 + 3392 N

* Includes alternator

** With variable speed turbine/fan

Figure 3-23 shows the ORC engine to be a possible alternative to the Stirling although it is nearly 40 percent more costly. Although the Sundstrand engine design is at a higher power level than the optimum (77.5 kW vs. 37.2 kW) the insertion of size-variable performance parameters will undoubtedly shift the optimum point to higher power. One of the prime benefits of the ORC system is the higher collection efficiency due to the lower receiver temperature. The receiver requires further design effort to try to reduce its cost and complexity. The reliability of the ORC system when compared with either the Brayton or Stirling is also questionable; further effort is necessary to obtain better data in this area. In summary, it is clear that the Stirling-based system has the best potential for producing low-cost energy and the USS P-75 engine is an excellent candidate for this application because its size is near the optimum. Note that for lower power levels, the USS P-40 engine also shows better performance than is achievable with the alternate engines.

b. Baseline Stirling System at ACF$\approx$0.4. Since the concentrator and receiver designs are the same for all three program schedules, the major technical issues concern the selection of the engine and the means for achieving the required ACF. The selection of an engine is basically a question of which Stirling engine is available. From the foregoing analysis, the P-75 engine is the obvious best choice. However, the only engine available for the 3.5 year program is the P-40 and thus it was chosen. The achievement of ACF = 0.4 is a more complex issue. As stated previously, the specified definition of system rated power results in throwing away energy in the absence of a storage system, which is not a very cost-effective approach. Perhaps a more important point relates to the desirability of high load factors, since it is clear that the addition of any storage system will increase $\overline{\text{BBEC}}$. Figure 3-24 shows $\overline{\text{BBEC}}$ versus ACF for the P-75 system with various battery options as well as the advanced flywheel concept. From these results it is obvious that:

- Battery cycle life is a major cost driver.
- The cost of the required electrical conditioning equipment (converter, inverter, etc.) is a major cost driver.
- The advanced (composite) flywheel is attractive, probably because it is still mostly on paper.
- The use of storage to achieve high ACF will always increase $\overline{\text{BBEC}}$ - even if all the storage-related equipment is free.

The amount of energy which must be stored per day also sets the discharge time (for constant power delivery); the discharge time in turn influences the cost of both the (lead-acid) battery and the electrical conditioning equipment as shown in Figures 3-25 and 3-26. A lead-acid battery system has been selected for the demonstration phase of the development program because it's the only practical external storage system available in the

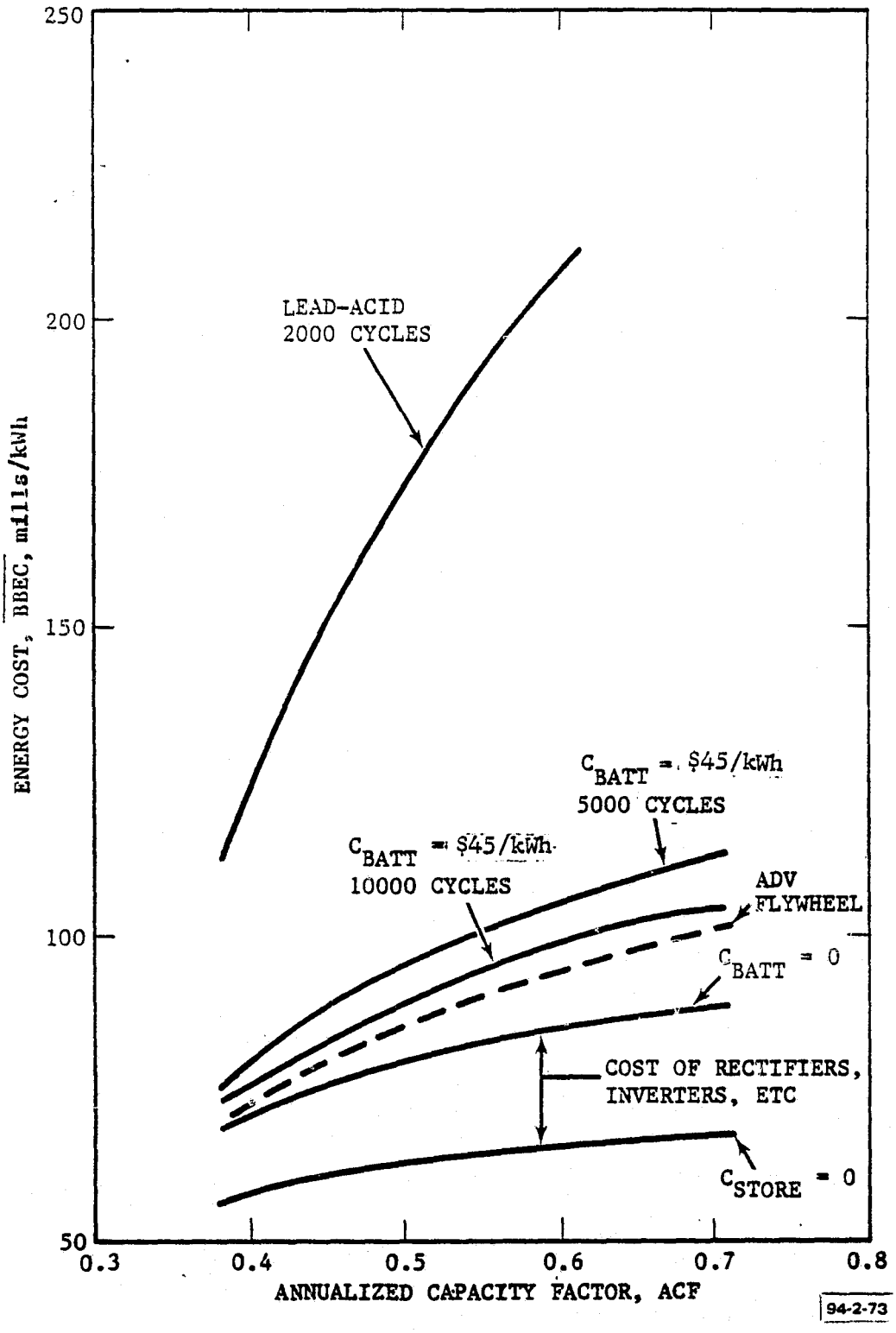

FIGURE 3-24. ENERGY COST BREAKDOWN FOR ALTERNATE DISH/STIRLING SYSTEM WITH STORAGE CONCEPTS

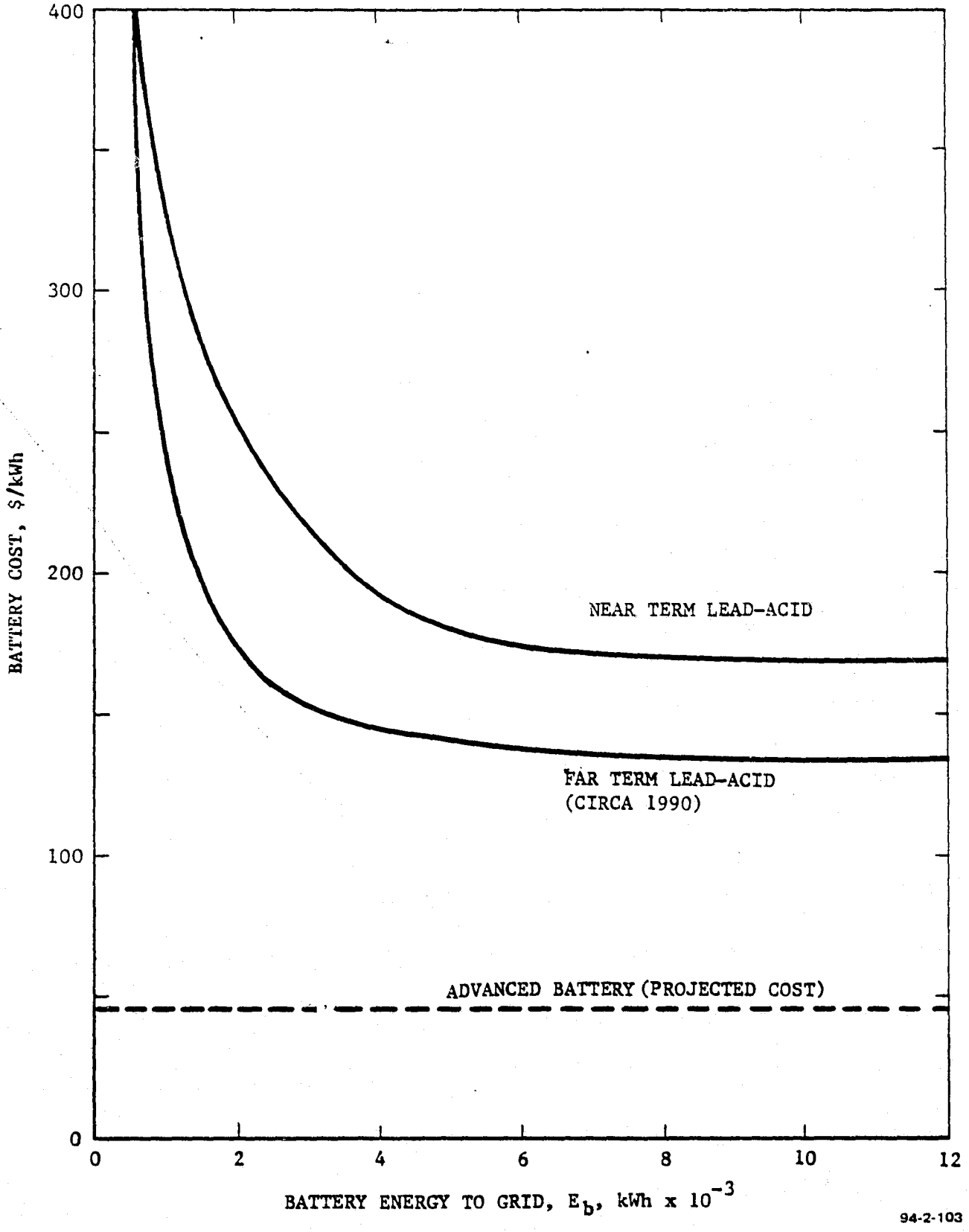

FIGURE 3-25. STORAGE BATTERY SPECIFIC COST DATA

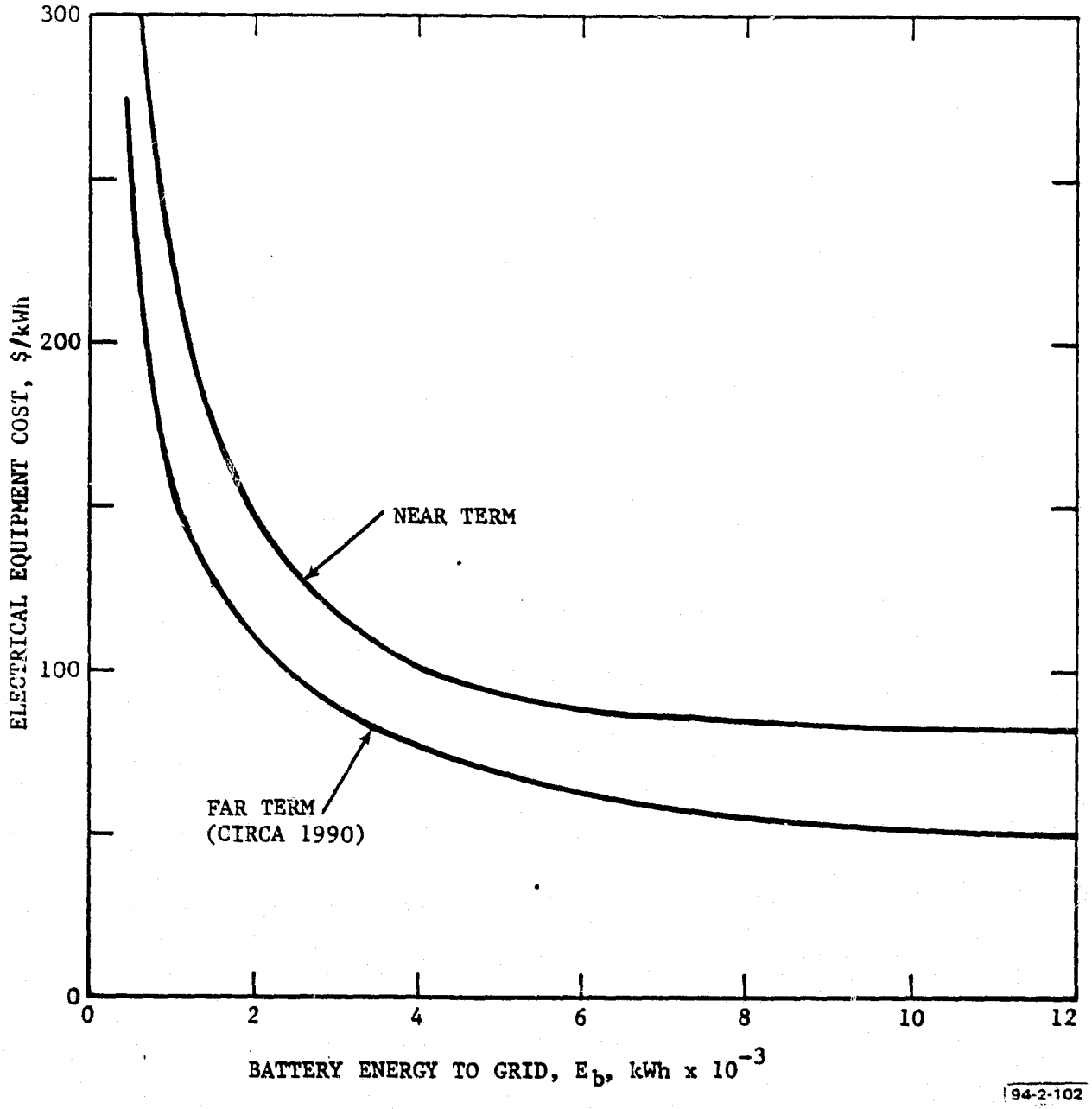

FIGURE 3-26. SPECIFIC COST OF BATTERY SUPPORTING ELECTRICAL EQUIPMENT (CONVERTERS, INVERTERS, CABLING, ETC.)

time allotted. This permits the system concept to be fully demonstrated, with provision for switching to advanced batteries (or flywheels) at a later date, as these concepts are developed.

Table 3.10 summarizes the cost elements for the P-40 and P-75 systems for achieving ACF = 0.4. All costs are ca. 1990 figures based on production/ installation of 5000 systems per year. As noted previously, the P-40 system is more expensive because of increased capital costs and maintenance cost due to the substantially increased number of units. Although the concentrator size is closer to optimum (11.2 m) the reduced concentrator cost is offset by increased power conversion, transport and control system costs as shown in Table 3.10.

TABLE 3.10 DETAILED COST BREAKDOWN FOR STIRLING SYSTEMS
(WITH STORAGE)

Subsystem	Baseline P-75 Engine, $		P-40 Engine, $	
Collector		737,900		738,600
• Concentrators	692,600		629,600	
• Receivers	45,300		109,000	
Power Conversion		129,600		243,900
• Engines	47,500		108,000	
• Alternators (With Volt. Reg)	51,100		77,300	
• Elect. Equip.	26,000		55,800	
Sensors	(11,100)			
Circuit Brkers	(2,500)			
Contactors	(7,400)			
Motor Starter	(4,000)			
Lightning Prot.	(1,000)			
• Cables	5,000		2,800	
Transport		87,800		169,200
• Cables	8,900		23,300	
• Elect. Equip.	34,000		34,000	
Switchboard	(9,000)			
Transformer	(19,000)			
Switch	(3,000)			
Mtrs/Instr	(3,000)			
• Shipping	3,400		7,300	
• Field Assembly	39,700		102,800	
Installation	(33,100)			
Check/Test	(6,600)			
• Recurring Eng'g	1,800		1,800	

TABLE 3.10 DETAILED COST BREAKDOWN FOR STIRLING SYSTEMS (CONT.)
(WITH STORAGE)

Subsystem	Baseline P-75 Engine, $		P-40 Engine, $	
Control		21,600		55,700
• Cables	7,400		31,300	
• Computer	9,700		9,700	
• Remote Assy.	4,500		14,700	
Storage		317,900		355,000
• Batteries	95,900 (E_b=2132 kWh)		114,000 (E_b=2534 kWh)	
• Elect. Equip.	222,000		241,000	
Converter	(35,000)			
Inverter	(58,000)			
Wiring	(9,000)			
Racks	(29,000)			
Ship	(68,000)			
Installation	(18,000)			
Check/Test	(5,000)			
Other		112,000		120,800
• Control Room	20,000		20,000	
• Battery Room	64,000		68,500	
• Land	25,600		29,400	
• Site Prep	2,500		2,900	
• CI (1986) ($)		1,406,900		1,683,200
• CI_{PV} ($)		2,773,000		3,426,900
• $\overline{BBEC_c}$ (mills/kWh)		70.00		85.68
• $\overline{OM}$ (mills/kWh)		7.58		15.60
• $\overline{BBEC}$ (mills/kWh)		77.58		101.28

3.1.1.4 Design. This paragraph presents a summary of the design studies conducted on the Power Conversion Subsystem. The major items considered in this study include: The design and installation methods for interfacing the Power Conversion Subsystem with the concentrator tripod structure; and the cavity receiver and its interface with the Stirling engine including blocking valve, bellows, and a new design for a Stirling engine heater head. In addition to the Stirling engine, alternate systems including the closed-cycle Brayton and organic Rankine were studied. Design details for these alternate systems are presented.

a. Power Conversion Subsystem Installations. The P-75 Stirling Engine Power Conversion System, selected as the baseline unit for the 4.5 and 6.5 year plans, is shown in position in the full collector system drawing of Figure 3-27, and is shown in more detail in Figure 3-28. This design shows the relationship of the engine heater head, the expansion bellows, the blocking valve and the receiver core which are assembled into a single unit at manufacture. The receiver support unit, the engine (without the heater head assembly) and the generator with its weather cover are assembled to the frame first. Then the sodium transport system (receiver, valve and duct, and heater head assembly) already charged with sodium but in a cold condition, is installed in the support unit and the heater head connected to the engine. The nichrome heater strips and other electrical lines are connected and the insulation sections are attached. Installation of the receiver door (lid) and its drive system and all remaining electrical and coolant line connections is then completed. The power conversion unit, assembled into a single replaceable module, is then ready for installation on the concentrator or can be stored as a spare for later use.

Installation of the module in the mounting rings of the collector is relatively simple. The unit is lifted into position as illustrated in Figure 3-29, and moved forward onto the guide rails attached to the mounting rings. The rollers on the main frame permit free motion of the assembly forward to the correct axial position, and the adjustment screws provided on the frame are used to center the module radially coincident with the concentrator focal point. The frame is fastened to the guide rails with shims and eight heavy duty bolts and the electrical and coolant lines are connected to complete the installation. The sodium transport system is sequentially heated (from the receiver end toward the heater head end) to a temperature sufficient to liquify the frozen sodium and preclude burnout condition (~450°C). At that point, the blocking valve and the receiver door are opened, and the collector may be pointed at the sun to begin full systems operation. (Note that electrical heating is not used during normal operation - except for several days of inclement weather - because the sodium does not freeze.) The P-75 baseline power conversion system, mounted to the guide rails with all electrical and coolant lines connected, door open and in full operating condition is shown in Figure 3-30.

The P-40 Stirling Engine Power Conversion System, selected for the 3.5 year plan, is essentially a scaled-down version of the P-75 design. All of the major elements, the receiver, the blocking valve, the expansion bellows, the heater head and the generator are appropriately sized to conform with the P-40

ORIGINAL PAGE IS
OF POOR QUALITY

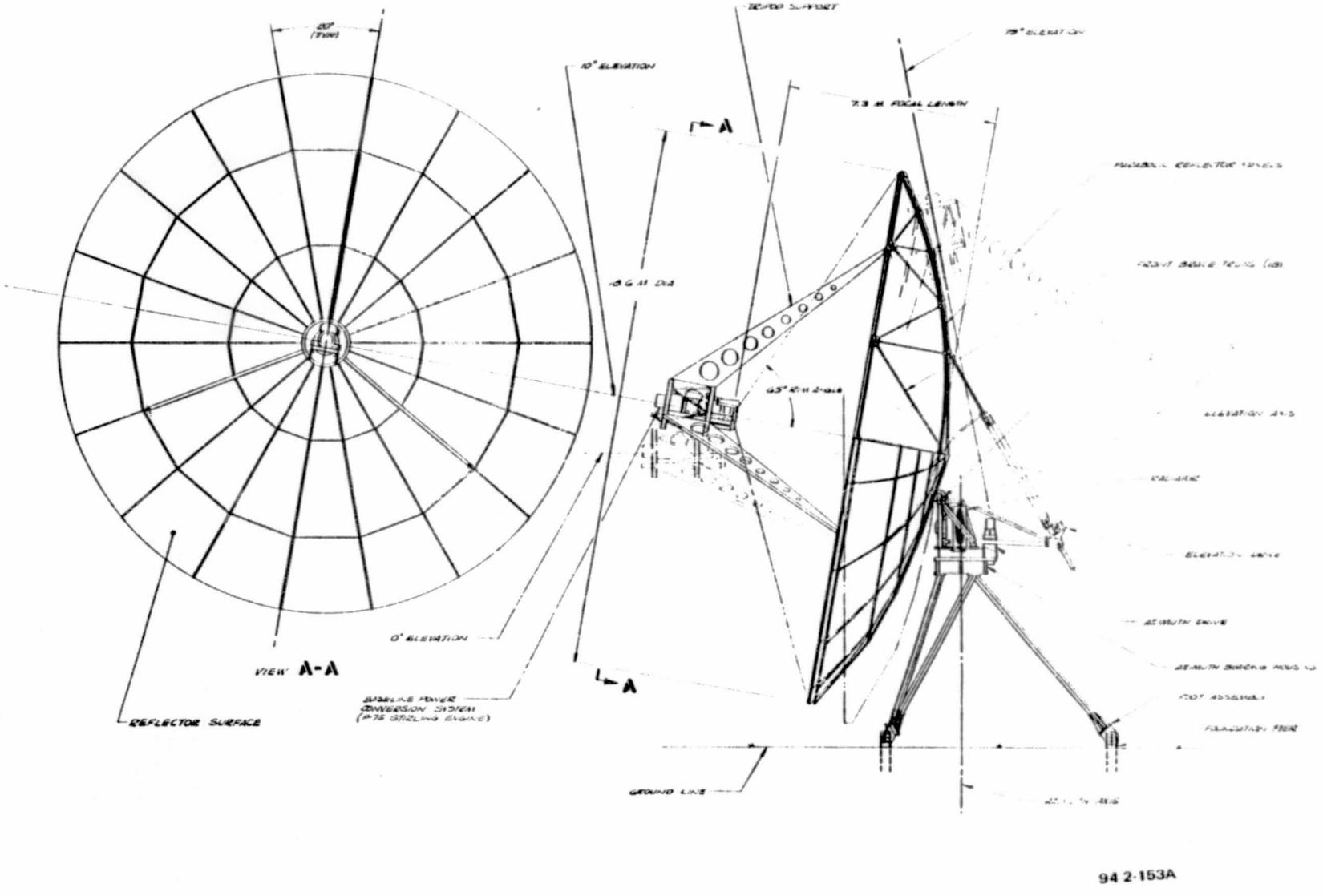

FIGURE 3-27. BASELINE COLLECTOR SYSTEM (18.6m DIAMETER, P-75 STIRLING ENGINE)

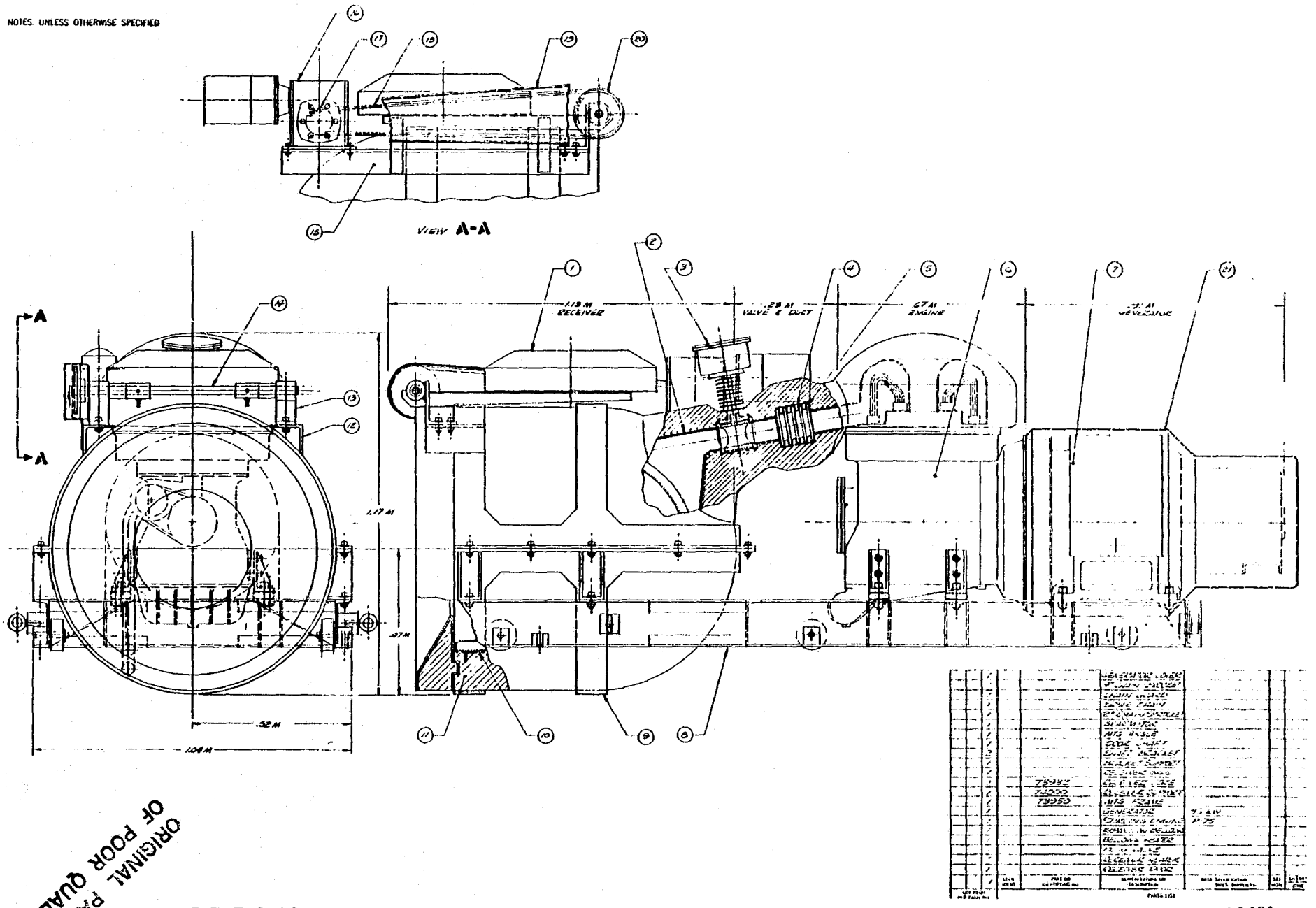

ORIGINAL PAGE IS OF POOR QUALITY

FIGURE 3-28. POWER CONVERSION MODULE FOR STIRLING ENGINE BASELINE SYSTEM (P-75)

94-2-124

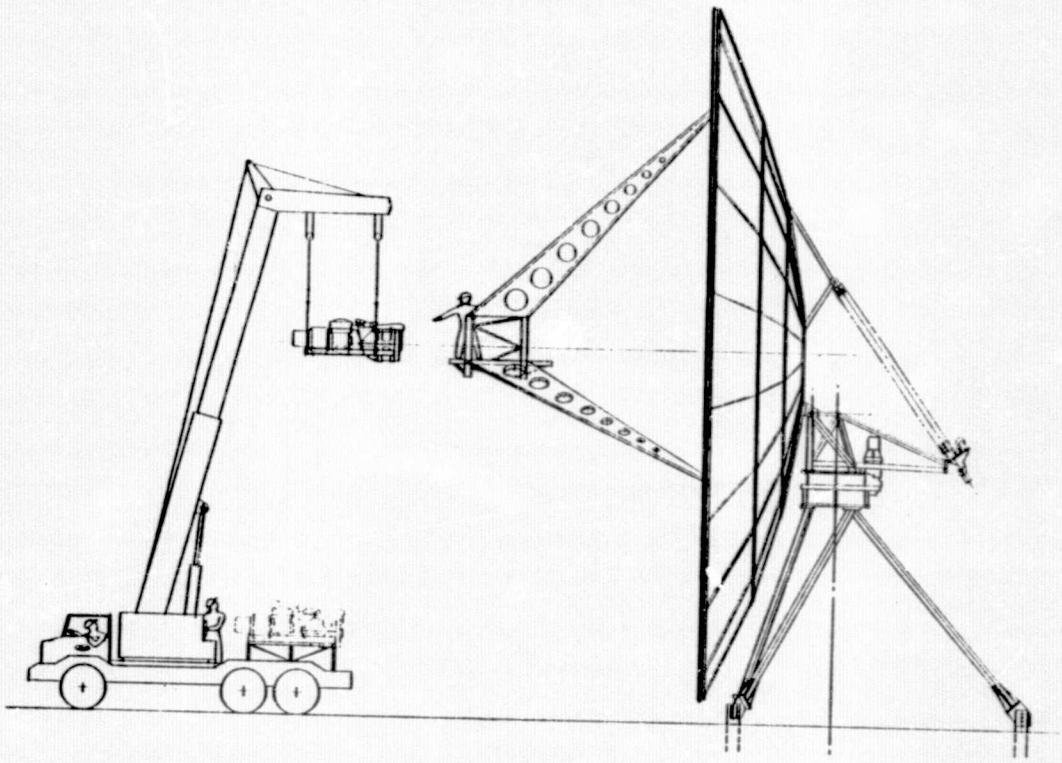

94-2-125

FIGURE 3-29. INSTALLATION OF POWER MODULE

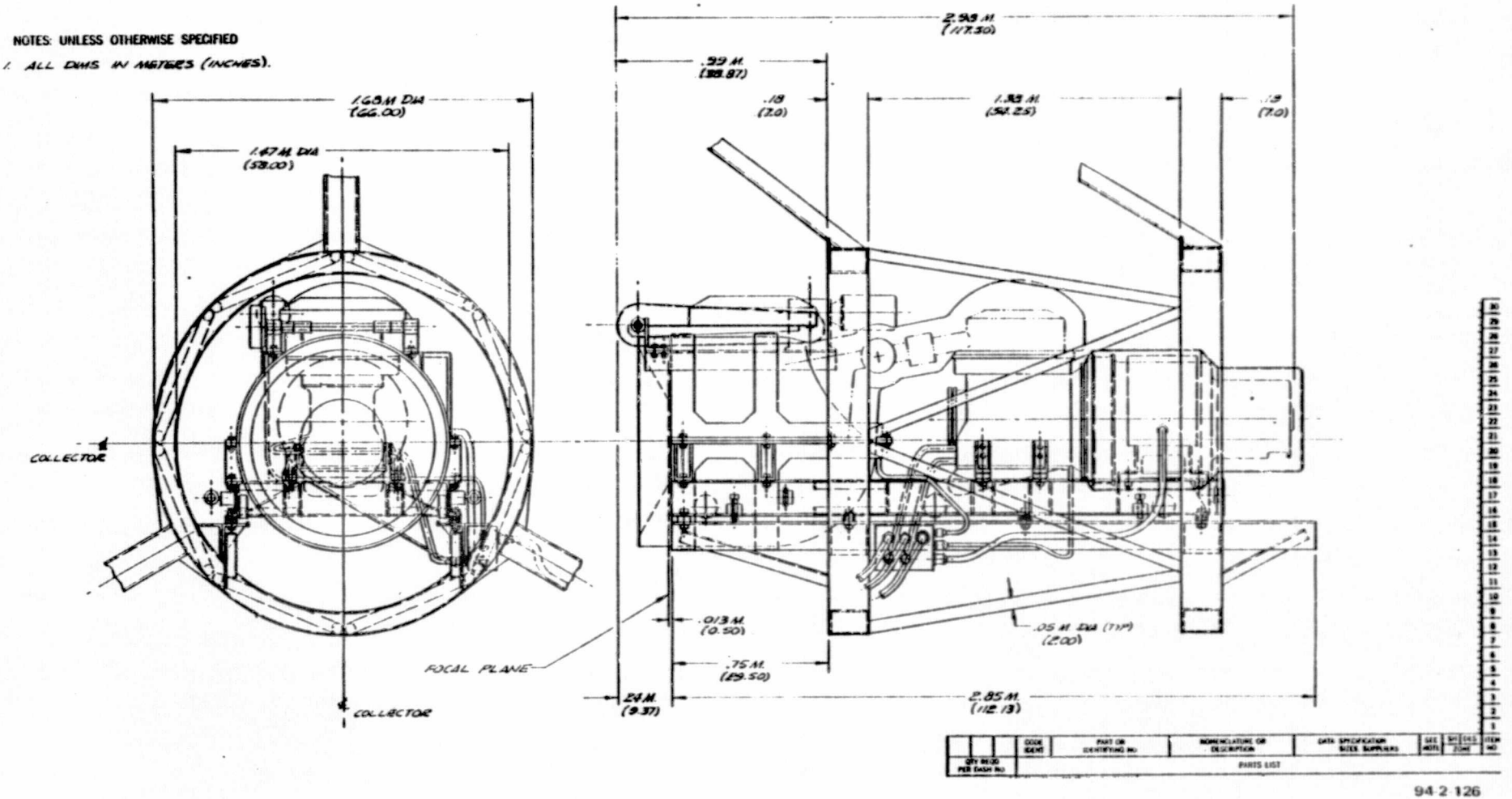

FIGURE 3-30. FIXED MOUNTING CONCEPT FOR BASELINE SYSTEM

engine performance characteristics. The system configuration, Figure 3-31, in keeping with the replaceable module concept, possesses the same ease of installation and removal and the same preheating and operational modes as the P-75 Baseline System.

Major components of the power module (the receiver, the engine and the generator) are fastened to a common mounting frame. This frame for the P-75 Baseline System is shown in Figure 3-32. The mounting frame for the P-40 power conversion system, shown previously in Figure 3-31, is similar in form but scaled to accept the smaller system components. Side channels of the frame contain the roller mounting blocks, adjustment screw blocks and the lifting eye assemblies. The frame is cross braced with sections of channel and with angle iron to provide lateral stiffness and torsional resistance. Although the engine will be mounted on automotive-type vibration isolators, the generator and the receiver support are bolted directly to the frame and enhance the stiffness of the assembly. The open area between the engine mounts permits easy access to the underside of the engine for routine maintenance, replacement of seals, and minor repairs without removing the engine or power conversion module from the concentrator.

b. Receiver. The configuration for the P-75 baseline receiver core is shown in Figure 3-33 and the P-40 receiver core are shown in Figure 3-34. This version does not contain provisions for buffer storage and is, therefore, of a simple design which is easy to manufacture. Both designs consist of two concentric cylinders joined at the forward end by a half-torus with concentric half-spheres forming the inner and outer rear portion of the cylinders. A conical vapor dome section and a lengthened cylinder have been added to provide a greater expansion volume for the sodium vapor.

This receiver concept is relatively easy to fabricate as compared to a multitube system. Each tube connection of a multitube system must be welded to a manifold section, greatly increasing the amount and complexity of the welds and the likelihood of leaks. The double cylinder-sphere design employs easily accessed continuous welds between the major receiver sections (compatible with machine welding techniques) and is, therefore, inherently more reliable than the multitube design.

The two mounting rings surrounding the outer cylinder add structural strength to the receiver and are convenient to attach points for mounting the unit to the receiver support shown in Figure 3-35. The core is attached to the support at seven places. One rigid connection at the rear of the core locates it axially with respect to the lower half of the receiver support, which in turn is bolted to the mounting frame. Six radial flex-locators, three at the front core attachment ring and three at the rear ring, permit the core to expand axially through slight flexure of the S-curved section. Radial expansion is accommodated by slotted bolt holes in each flex-locator, with the slots pointed toward the receiver-collector center-line. This mounting system holds the receiver core centered within the support yet permits it to expand freely in both the radial and axial directions.

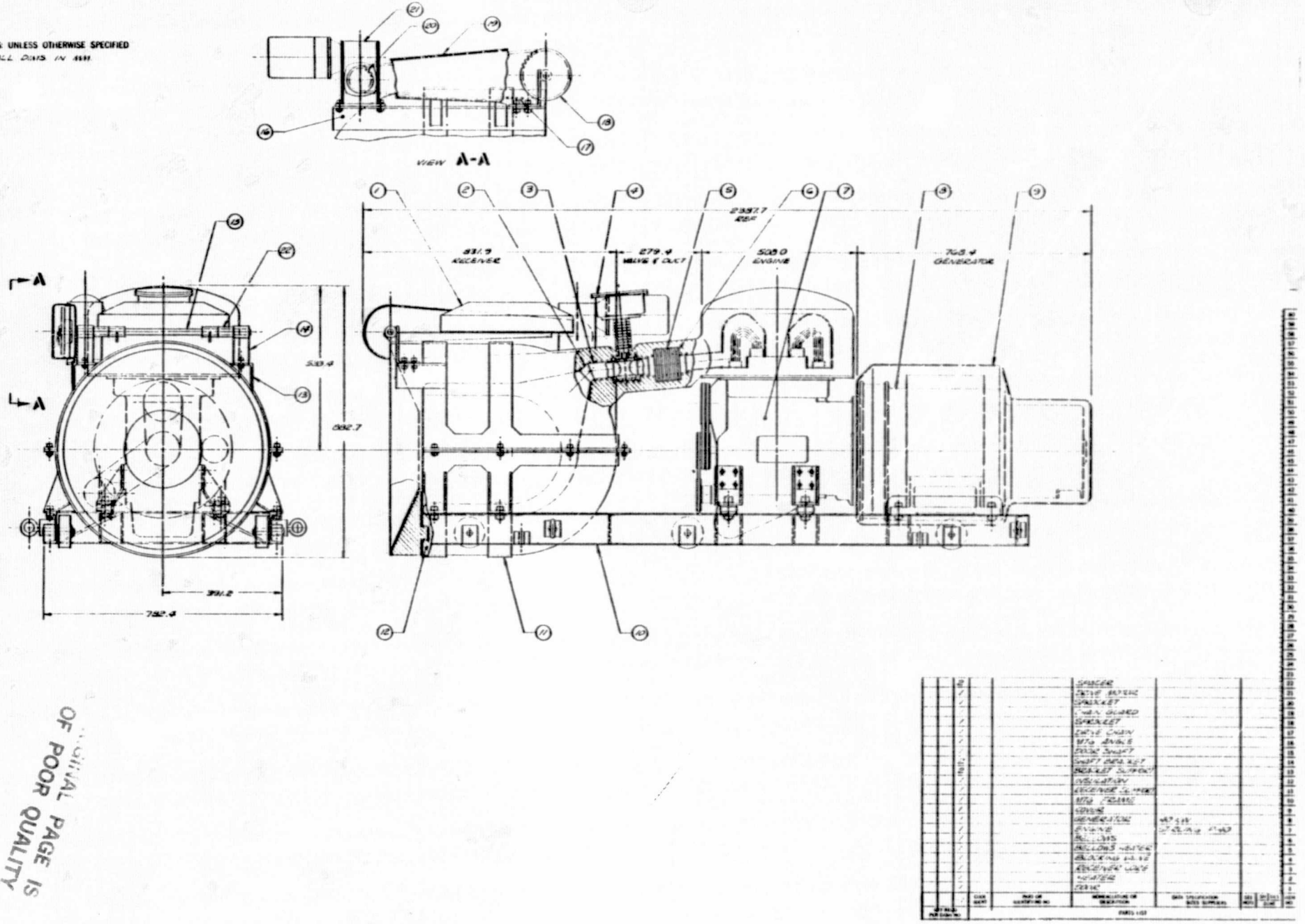

ORIGINAL PAGE IS POOR QUALITY

FIGURE 3-31. P-40 POWER MODULE

94-2-127

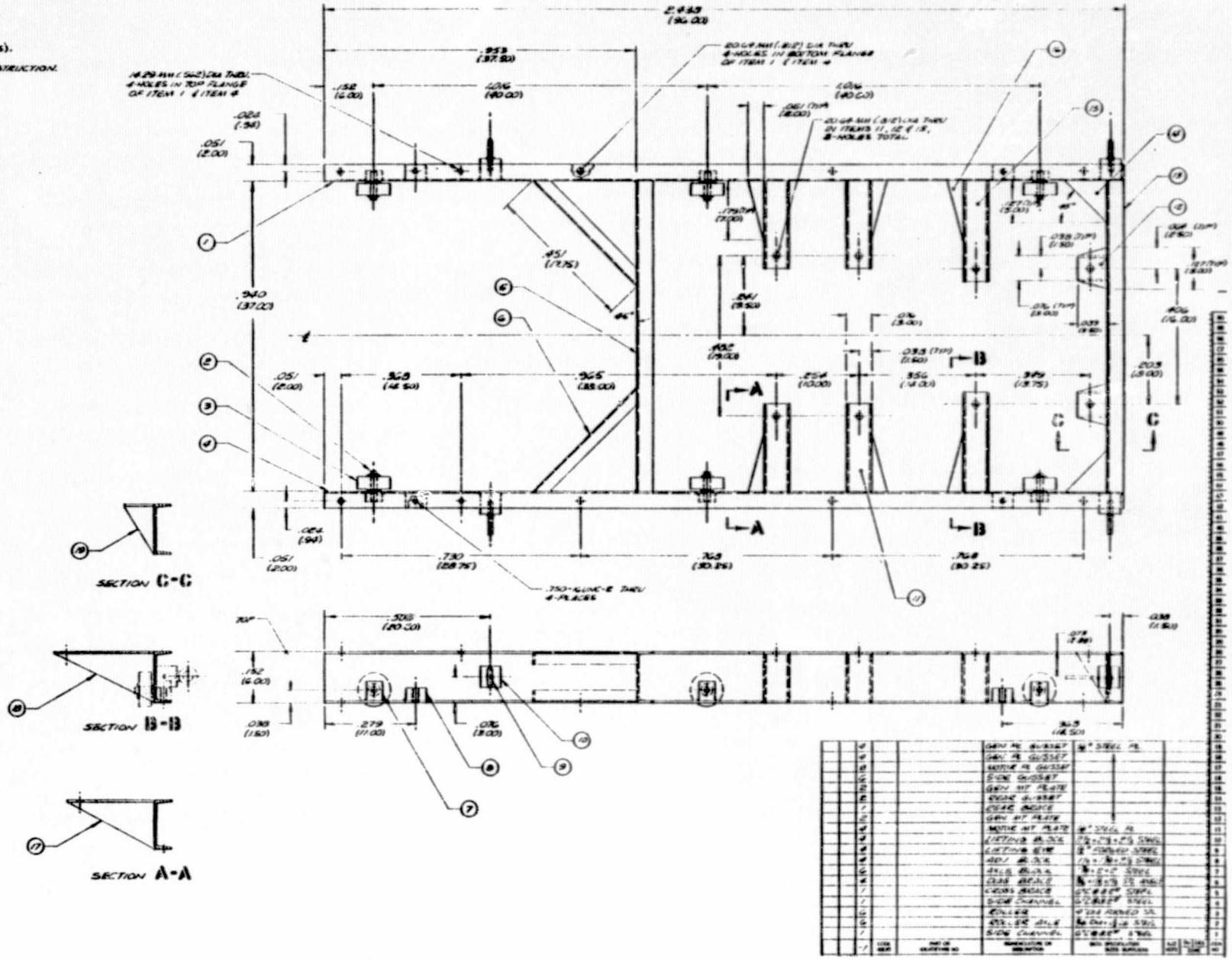

FIGURE 3-32. MOUNTING FRAME FOR POWER MODULE (P-75 ENGINE)

94-2-133

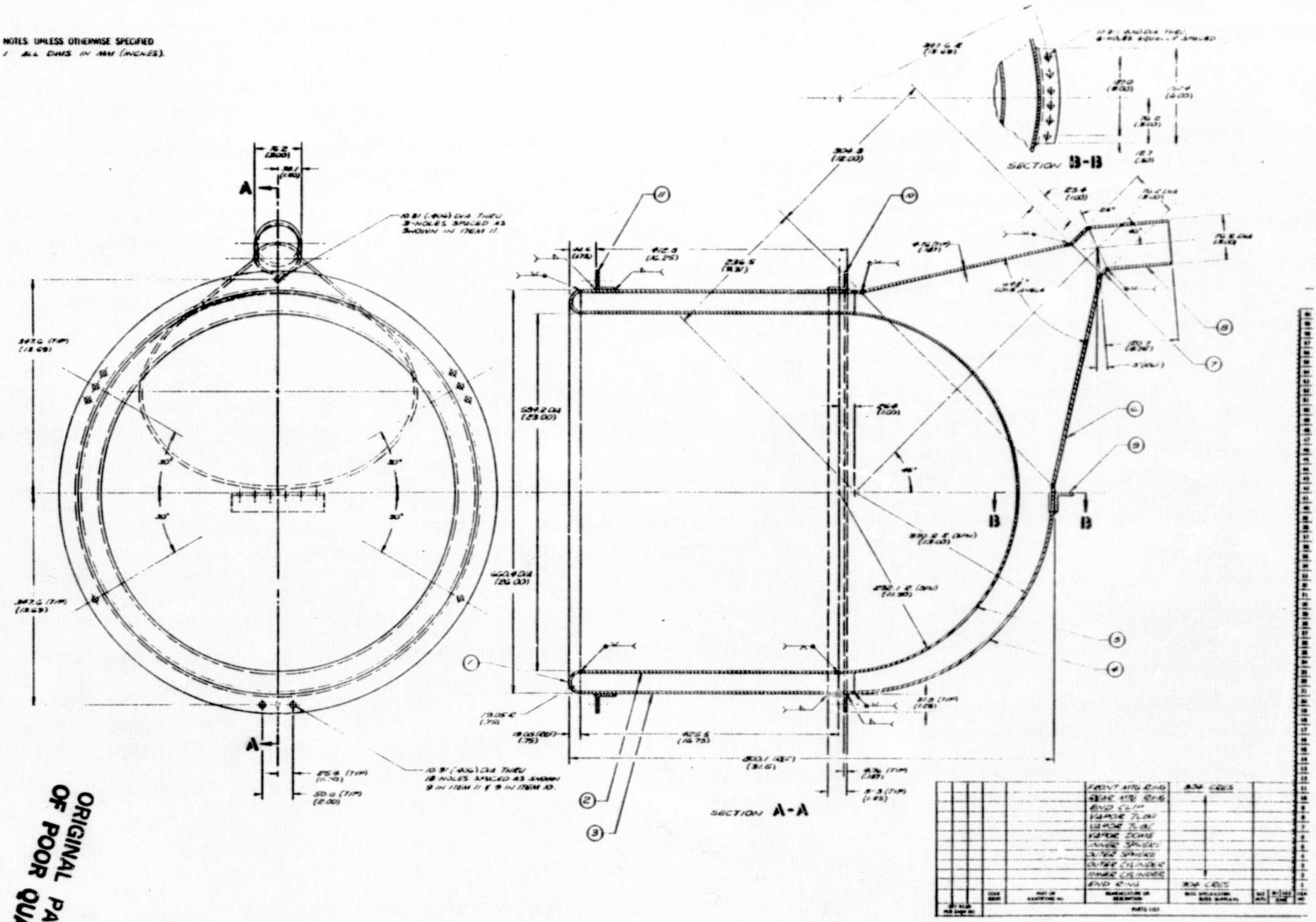

94-2-128

FIGURE 3-33. RECEIVER CORE FOR P-75 ENGINE

ORIGINAL PAGE IS OF POOR QUALITY

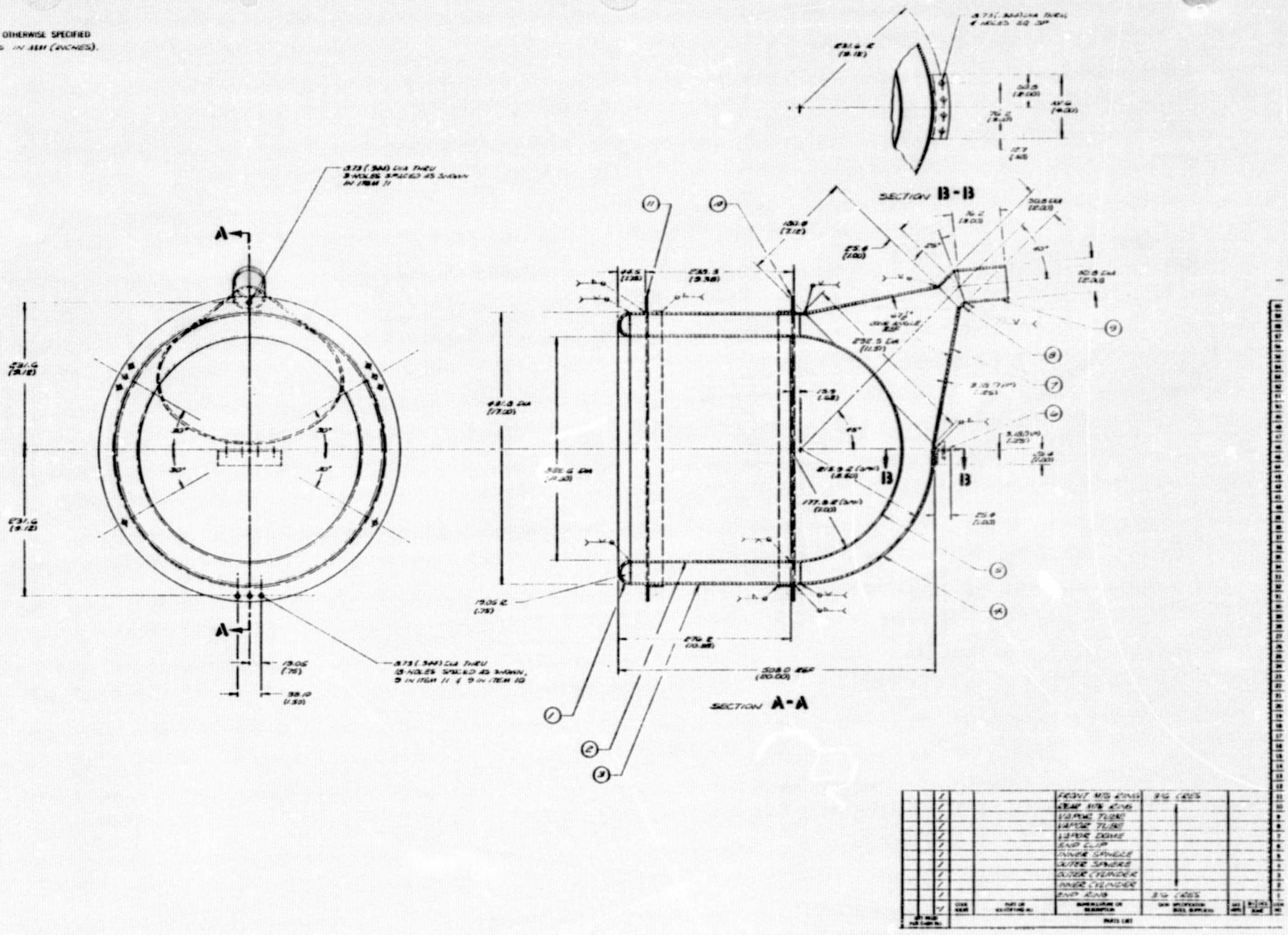

FIGURE 3-34. RECEIVER CORE FOR P-40 ENGINE

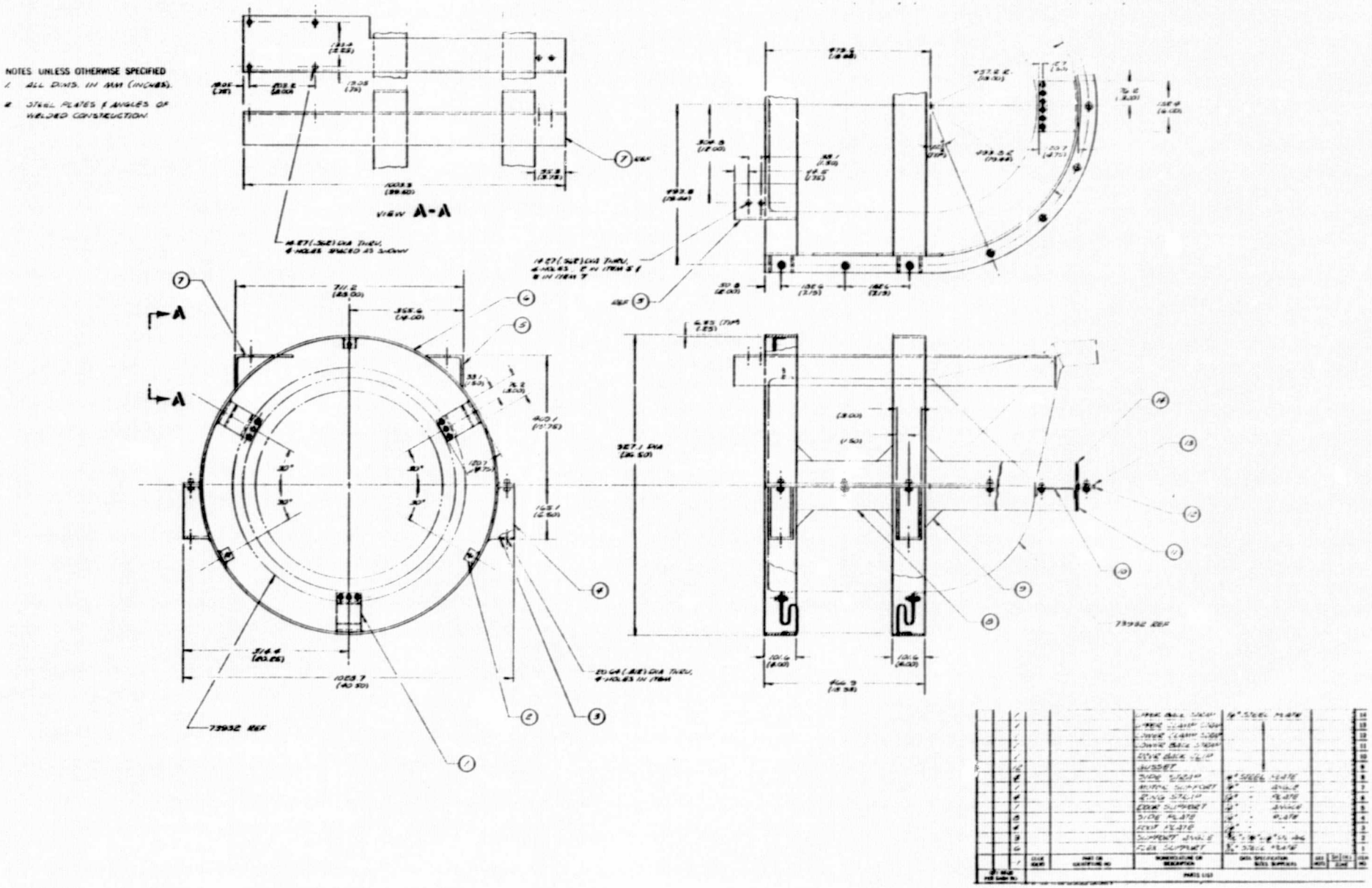

FIGURE 3-35. RECEIVER SUPPORT FOR BASELINE SYSTEM

The nose piece of the receiver insulation section, to which the door must interface when closed, is attached to the forward ring of the support. This nose section is rigid with an external ceramic or graphite material covering a formed insulation base. Attachment bolts, cast into the insulation base, attach the section to the mounting clips on the support forward ring. The nose piece, fixed to the same forward ring as the door axle mounting brackets, will properly register with the door as it is moved to the closed position.

The door actuating mechanism consists of an 115-230 volt ac gear-head motor attached to a right-angle single stage reduction unit operating a chain drive. The drive system is designed to operate in any collector elevation position, and is sized to assure full opening or closure of the door under all environmental conditions. The time required to close the door is a function of gear reduction ratios and motor size selected to meet operational requirements. Door position indicators are located independently of the drive mechanism to assure that the door is actually in the fully open or in the fully closed condition before other operational procedures commence.

A second receiver design for the P-75 Stirling engine, containing provision for add-on buffer storage, is shown in Figure 3-36. This design and mounting requirements are essentially the same as that for the baseline receiver core, but the core is enlarged to accommodate a series of sealed tubes located internally containing a eutectic salt. The fabrication techniques required for the receiver shell are the same as for the baseline core; however, the fabrication of the salt tubes is considerably more complex. Each tube must be filled with salt during the manufacturing process, the tube purged with argon gas, and then sealed. These tubes must be installed in the shell as it is welded together, forming a permanent assembly. Any subsequent tube leaks would require major and very expensive rework of the system to replace the leaking element. The buffer storage receiver core is larger, heavier, more expensive to fabricate, a high risk item from a reliability standpoint and, therefore very unattractive considering that add-on buffer storage provides only a few additional minutes of system operating time at full power.

c. Blocking Valve. During the study several blocking valve types were considered. The first one analyzed was a shutoff "Y" valve used in the nuclear reactor industry for liquid sodium systems. Subsequent analysis indicated that a complete seal of the sodium vapor flow was not required and a ball or butterfly valve with a small amount of leakage would be adequate. The ball valve was attractive because of the unrestricted vapor flow when in the open position; however, manufacturing costs were high due to the difficulty in machining the spherical ball and seat. The butterfly valve was less costly to manufacture but the vane remained in the vapor stream when in the open position presenting some flow restriction. The most practical configuration is a variation of the ball design called a plug valve, which is shown in Figure 3-37. A cylindrical plug is substituted for the ball, eliminating the spherical surfaces and the requirement to split the outer housing. Manufacturing tolerances can be very loose because the small amount of sodium vapor passing through the valve when in the closed position is insignificant. This results in a low manufacturing cost for the body of the valve which consists of four easily machined parts. In operation, the cylinder or plug is turned through

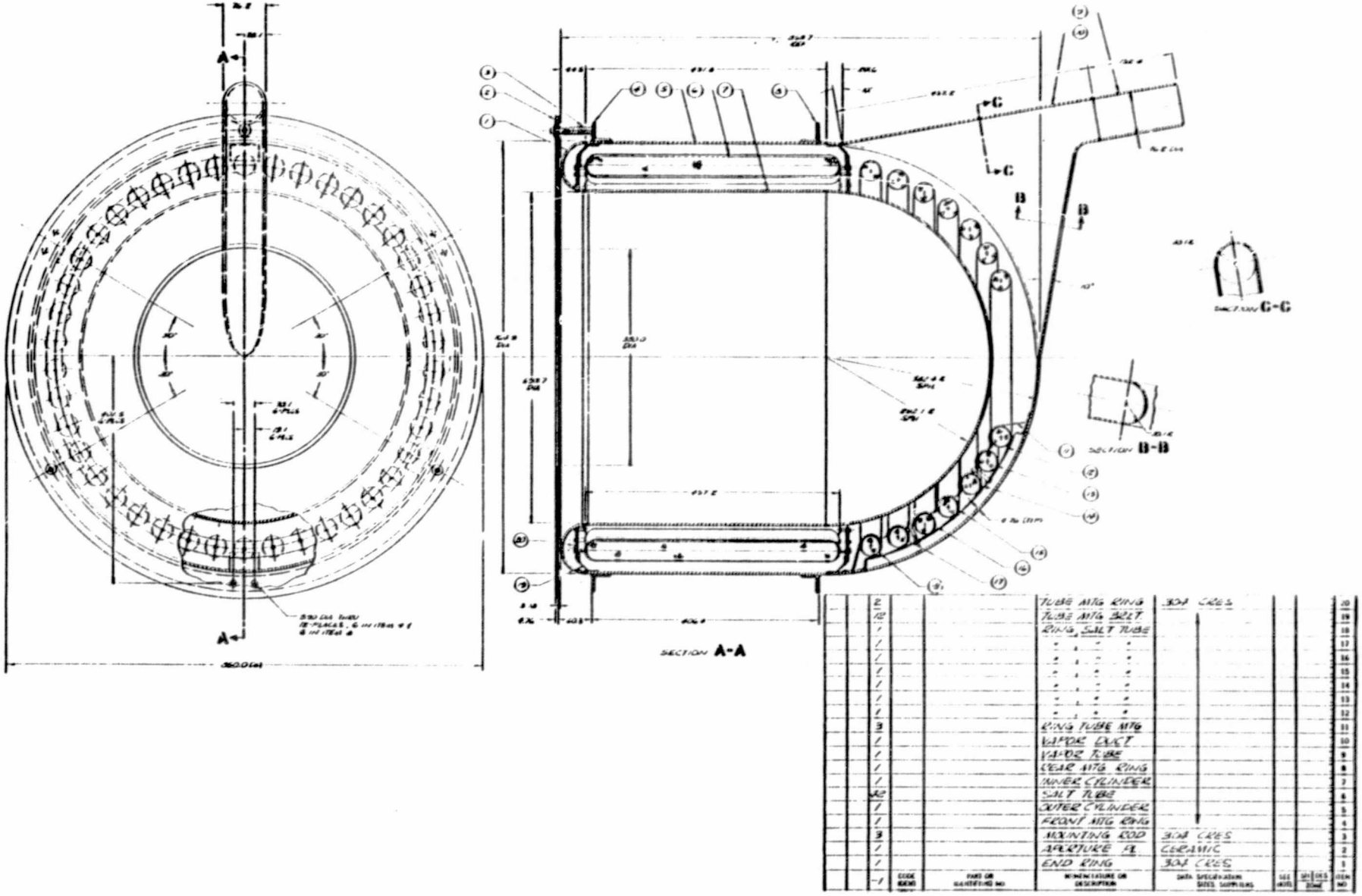

FIGURE 3-36. SODIUM RECEIVER WITH EUTECTIC SALT BUFFER STORAGE

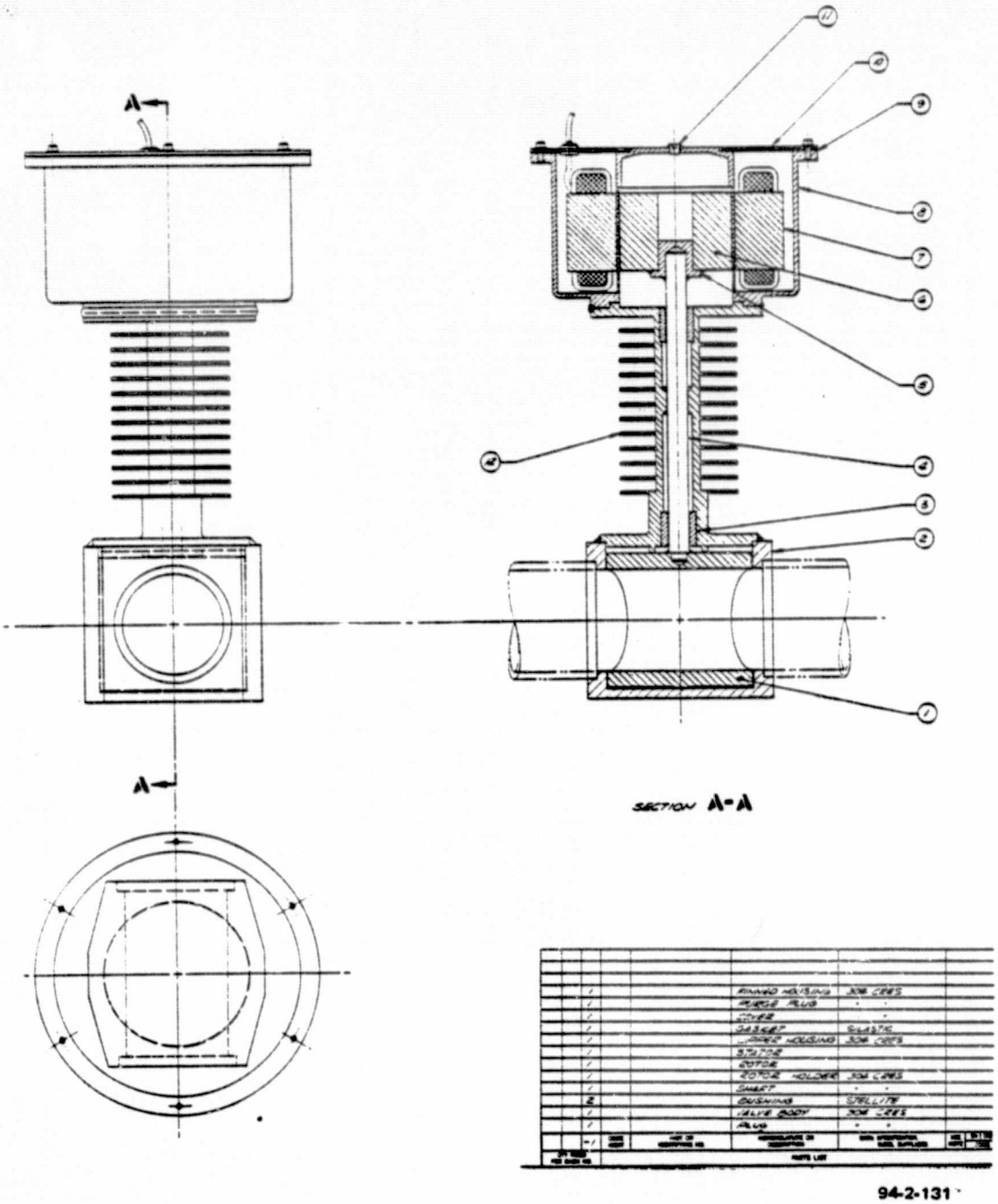

FIGURE 3-37. PLUG-TYPE BLOCKING VALVE

90 degrees by an electromagnetic actuator located at the top of the valve. The actuator rotor is attached to the upper end of the valve stem with the cylinder at the lower end. The upper housing contains the rotor, the finned housing (to freeze the sodium vapor) and the valve body; all are sealed from the external environment. Thus, the moving parts of the valve are totally enclosed within the sodium transport system, eliminating troublesome penetrations through the system walls. The exact location of the freeze zone around the valve stem and the sizing of the finned area to force freezing of the sodium vapor at that point will be determined in detail design.

d. Bellows. The bellows seal, shown in position between the blocking valve and the engine heater head in Figure 3-28, is designed to accommodate differential expansion between the heater head and the receiver core. The distance between these two major heat transport components will compress by approximately 6 mm at full system operating temperature over ambient conditions. This small amount of expansion between the core and the heater head will be easily abosrbed by compression of the multi-bellows design. A preliminary concept has been designed with a bellows manufacturer which uses a double ply type 316 stainless steel bellows wall welded onto 316 stainless steel end rings, sized to slip over the 76.2 mm (3.0 inch) diameter transport pipe. This design is similar to bellows units previously fabricated by the manufacturer and will be relatively inexpensive in large quantities.

e. Engine Heater Head Assembly. A conceptual design of the heater head, shown in Figure 3-38, has been developed based upon the P-75 and P-40 engine data received from United Stirling of Sweden. An array of helium filled pipes passing from the tops of the two regenerator heads to the cylinder head is exposed to the sodium within the enclosure top. The pipe pedestals are rigidly fixed (brazed) to the top of the regenerator and cylinder heads but are attached by flexible bellows to the floor plate of the enclosure. The enclosure is doughnut shaped with an access hole in the center to permit removal of the inner group of regenerator and cylinder head bolts. A combination argon purge, evacuation and sodium fill valve attachment will be located on the heater head enclosure. After initial purging and charging of the system with sodium, the valve will be closed and welded shut.

f. Alternate Systems. During the course of the study, both Brayton and organic Rankine Engine Systems were considered and analyzed. The Brayton system design concept was configured about the Garrett Corporation model CCPS-40 closed cycle engine. Open cycle engines were also studied but the CCPS-40 engine served as the packaging/integration model. The organic Rankine system design concept was based upon the Sundstrand Corporation Combined Rotating Unit (CRU) and its system components packaged in a long cylindrical form.

(1) Brayton System. The Brayton System design using the Garrett Corporation CCPS-40 engine is shown in Figure 3-39. This design employs a smaller, less efficient engine than the Stirling P-75 or P-40 engines but requires a considerably larger and much heavier receiver. The receiver core required for the Brayton system is shown in Figure 3-40. The large number of

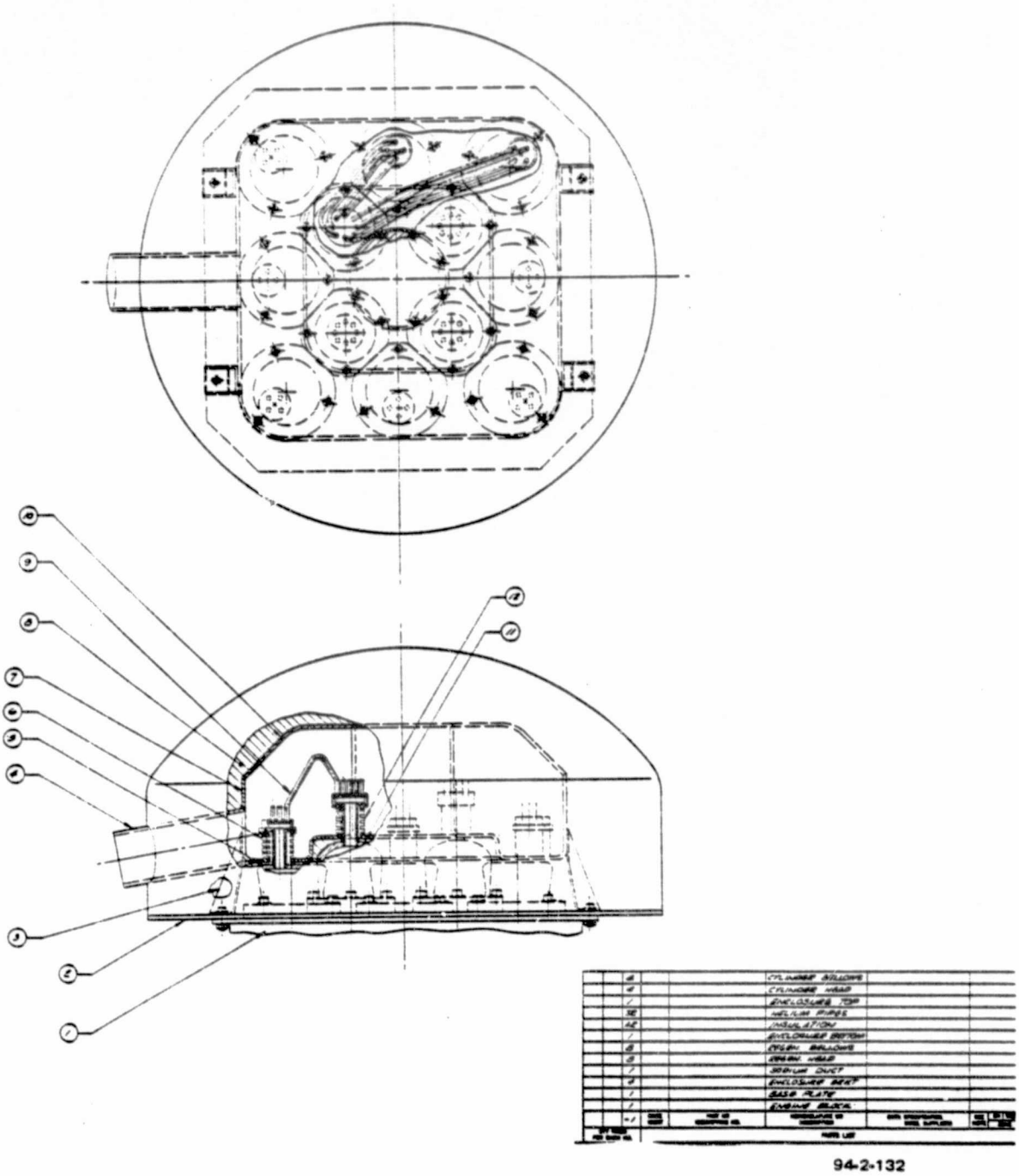

FIGURE 3-38. SODIUM HEATER HEAD DESIGN FOR P-75 STIRLING ENGINE

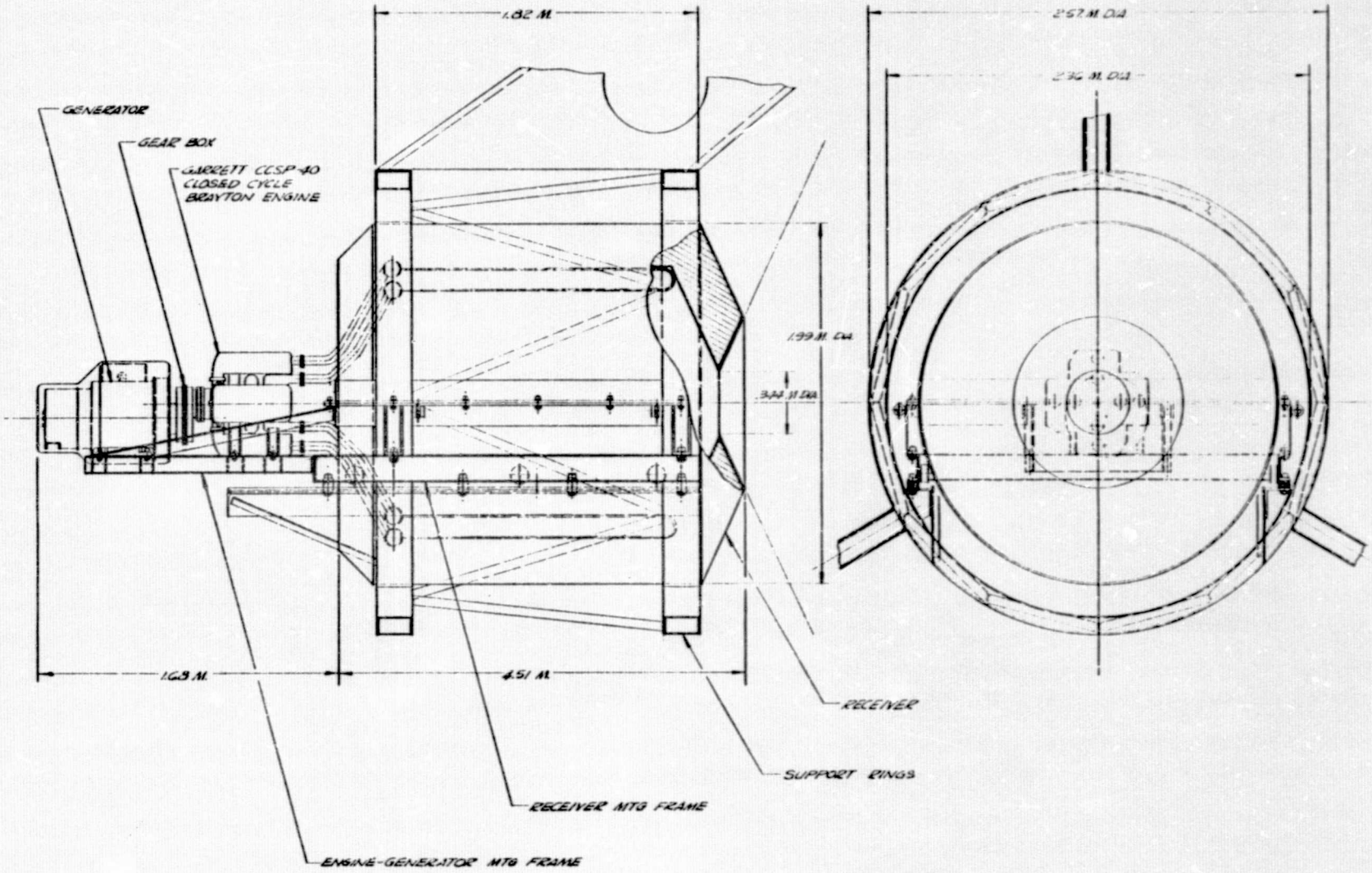

FIGURE 3-39. CLOSED CYCLE BRAYTON POWER CONV. SYSTEM

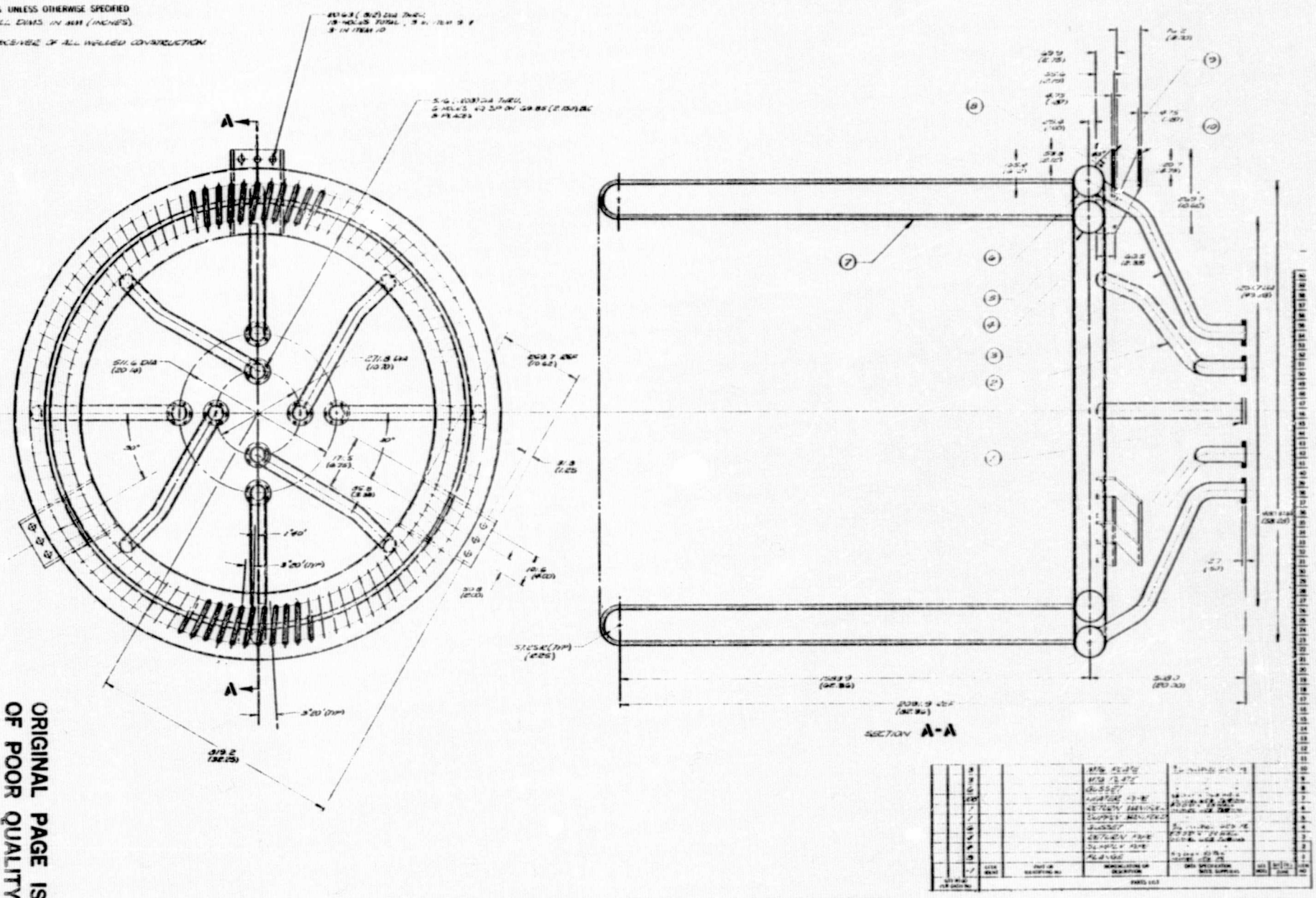

FIGURE 3-40. RECEIVER CORE FOR BRAYTON SYSTEM

94-2-134

ORIGINAL PAGE IS
OF POOR QUALITY

heater tubes* (108) and the large amount of welding of the tubes, manifolds and feed pipes increase the cost of this unit significantly over that of the P-75 or P-40 Stirling engine receiver cores. In addition, the receiver support structure is substantially increased in both size and weight to hold the receiver rigidly in position at the collector focal point. The large difference in size of the receiver versus the engine and generator combination requires an "add-on" mounting frame for the latter units, cantilevered off the back of the receiver mounting rails and receiver support. The end result is a very heavy system, awkward to handle and best separated into two sections (receiver and engine-generator) in order to be installed or removed. An additional component, a gear box, will be required to reduce the high speed of the CCPS-40 output shaft to drive an 1800 rpm existing 30 kW ac generator. The gear box could be eliminated but a high speed ac generator would be required with a frequency converter and controller in order to interface the system with a 60 Hz utility grid. The Brayton system concept shown does permit ready access to the engine or generator for routine maintenance and the units can be removed without disturbing the receiver. However, any heavy maintenance of the receiver would require the task of removing the entire system from the concentrator.

(2) Organic Rankine System. An organic Rankine system design was developed around the Sundstrand Corporation unit and is shown in Figure 3-41. This system is also larger than the P-75 Stirling Baseline System, and slightly heavier. The receiver core shown in Figure 3-42, although larger in physical size, is only about 16 kg heavier than the P-75 receiver core. However, the Rankine receiver core, involving eight interwoven heater tubes in helix form, is not a simple design to manufacture and align and would be more costly than the P-75 receiver core. The supporting structure for the receiver is larger and heavier and the mounting rails must be of larger cross section to support the weight. To keep the system envelope within reasonable limits and to eliminate additional structure, the supporting frames for the Sundstrand unit and the receiver are bolted directly to the frame channels forming one main frame. The entire assembly could have been moved further back (away from the concentrator) which would permit shorter mounting rails, support structure, and frame channels, but

* It is possible that the tube design can be replaced with a plate-fin heat exchanger design at substantial savings in weight; further analysis is needed to verify this design approach but it is doubtful if the Brayton receiver could be made competitive with the Stirling at the same power level.

NOTES UNLESS OTHERWISE SPECIFIED

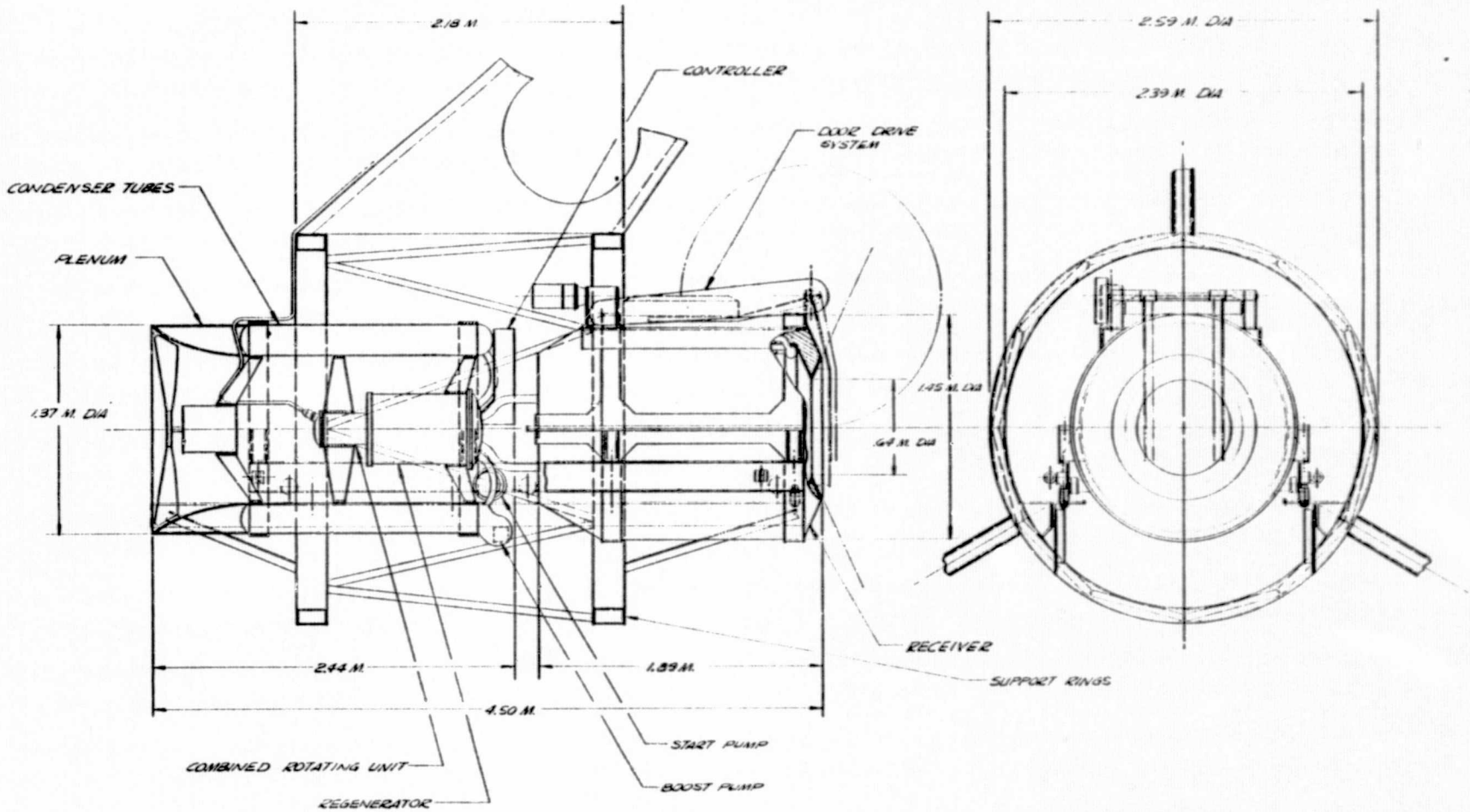

FIGURE 3-41. POWER MODULE FOR ORGANIC RANKINE SYSTEM

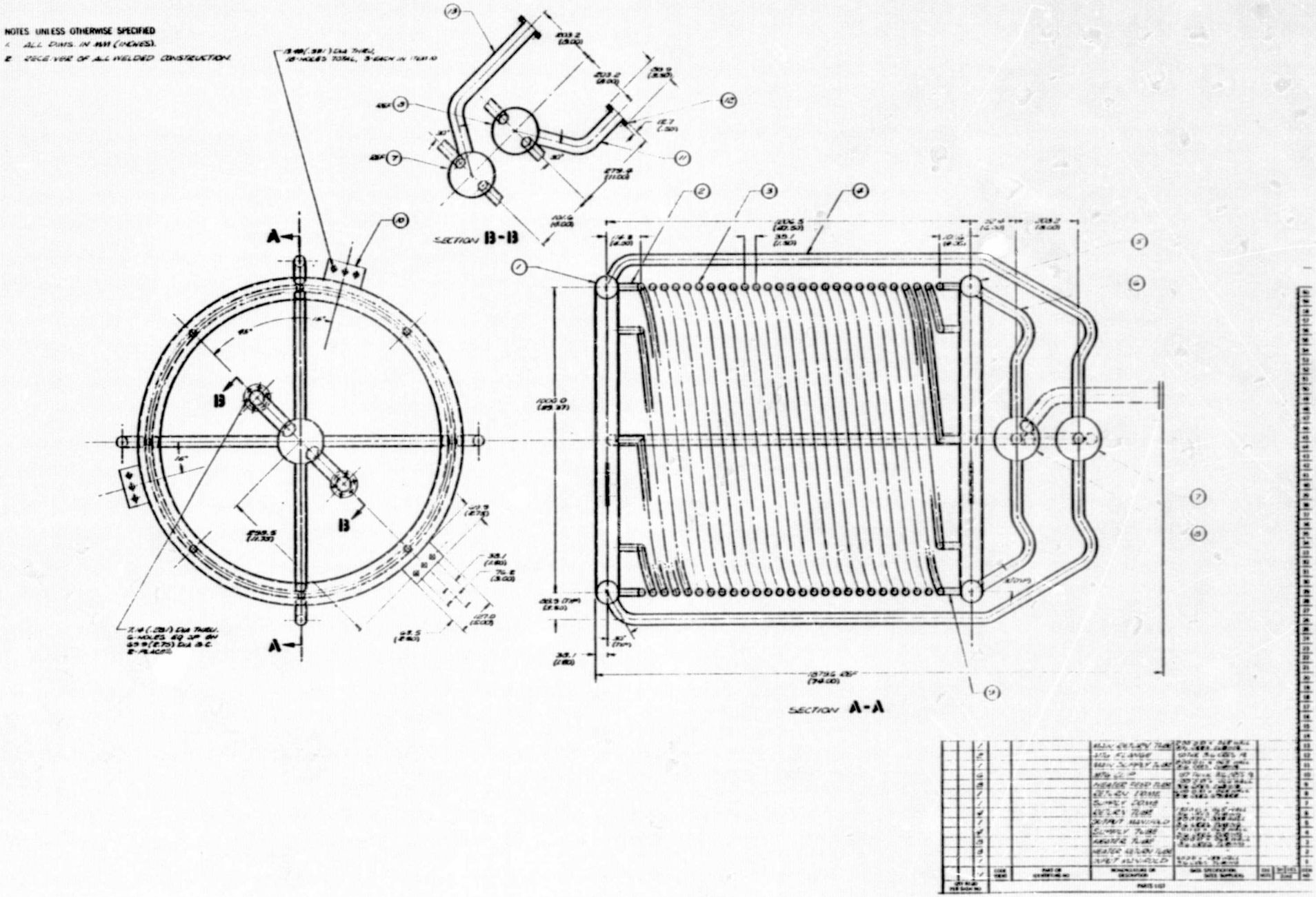

FIGURE 3-42. RECEIVER CORE FOR ORGANIC RANKINE SYSTEM

94-2 136

the requirement for a receiver door with its necessary clearance dictated the system position within the support rings. The rings are sized to clear the door actuating mechanism. The rings could be made smaller but only at the expense of additional complexity in the actuating mechanism.

Routine maintenance for the regenerator and the combined rotating unit is difficult because the units are enclosed within the condenser tube structure. The condenser system would have to be designed to permit ready access to the components inside or the entire power conversion system would have to be removed from the concentrator support rings. This would be a very costly and time consuming procedure.

g. Weight Statement. The Stirling Engine power conversion system is the smallest in size and the lightest in weight; the organic Rankine system ranks second and the Brayton System third. Weight data for all three systems are given in Table 3.11. All weights include receiver working fluids.

TABLE 3.11. SYSTEM WEIGHT DATA (kg)

	P-40 STIRLING (P_{O_r} = 21.9 kW)	P-75 STIRLING (P_{O_r} = 63.4 kW)	BRAYTON SYSTEM (P_{O_r} = 30 kW)	ORGANIC RANKINE SYSTEM (P_{O_r} = 77.5 kW)
Engine	225	315	124	538 (1)
Generator	259	522	259	
Receiver Core	80	111	325	127
Sodium Inventory	20	33	-	-
Receiver Support	68	113	537	245
Blocking Valve	10	16	-	-
Mounting Frame	89	147	320	357
Insulation	52	86	720	169
Door System	39	64	-	91
Total	842 kg	1407 kg	2267 kg	1527 kg (1491 without toluene)

(1) Rankine Engine-Generator System Includes:

Condenser	286
Fan/Motor	57
CRU	32
Regenerator	59
Start Pump	34
Controller	14
Miscellaneous	20
Inventory (Toluene)	36
Total	538

h. Receiver Preparation and Filling. Commercial sodium is available and can be purchased in brick form (1, 5, 12, 25 pound sizes) and cast solid form. These forms are available in regular purity and argon (reactor) purity grades. The argon (reactor) grade sodium has fewer impurities than the regular grade and will be used in the baseline receiver tank.

The brick forms of sodium are packed and delivered in returnable 55-gallon steel barrels. These barrels are fitted with airtight covers to maintain a protective nitrogen atmosphere. Cast solid sodium is available in 55-gallon steel drums and in 5-gallon steel pails. Sodium delivered in these non-returnable containers can be heated directly and dispensed as a liquid. Figure 3-43 shows a sodium-filling system which is currently being used at FACC to service experimental sodium/sulfur battery cells. This system will be utilized to fill the baseline sodium receiver tank. The closed-filling-system illustration shown in Figure 3-43 reduces handling costs and eliminates oxide formation during the filling procedure. The empty 5-gallon sodium pails must be cleaned free of sodium before disposal or other use. Reference 3-8 describes safety precautions which pertain to container cleaning.

The corrosion data presented in the previous sections of this report indicates the importance of minimizing the oxygen level (ppm) and oxides formed when filling the sodium (baseline) receiver. In an effort to minimize these corrosion reactants the following surface cleaning treatment and filling procedure is recommended:

(1) Vapor degrease component parts of receiver tank prior to welding with trichloracthlyene for 45 minutes.

(2) Abrasive cleaning of all welded joints by impinging with aluminum oxide material (No. 60). This process should be done during the assembly sequence to all welds exposed to sodium.

(3) Nitric acid (technical grade) dip of completely assembled receiver tank.

(4) Rinse receiver in distilled water and then in ethylene alcohol.

(5) Dry receiver in oven.

After the above steps are completed the receiver tank is ready to be filled. To eliminate and remove oxides, the following filling procedure is recommended:

(Refer to Figure 3-43)

(1) Remove trapped air in the system - Close valve D first; then, in the following sequence, open valves C, B, and A. This will allow the entire system to be evacuated by the vacuum accumulator.

C-2

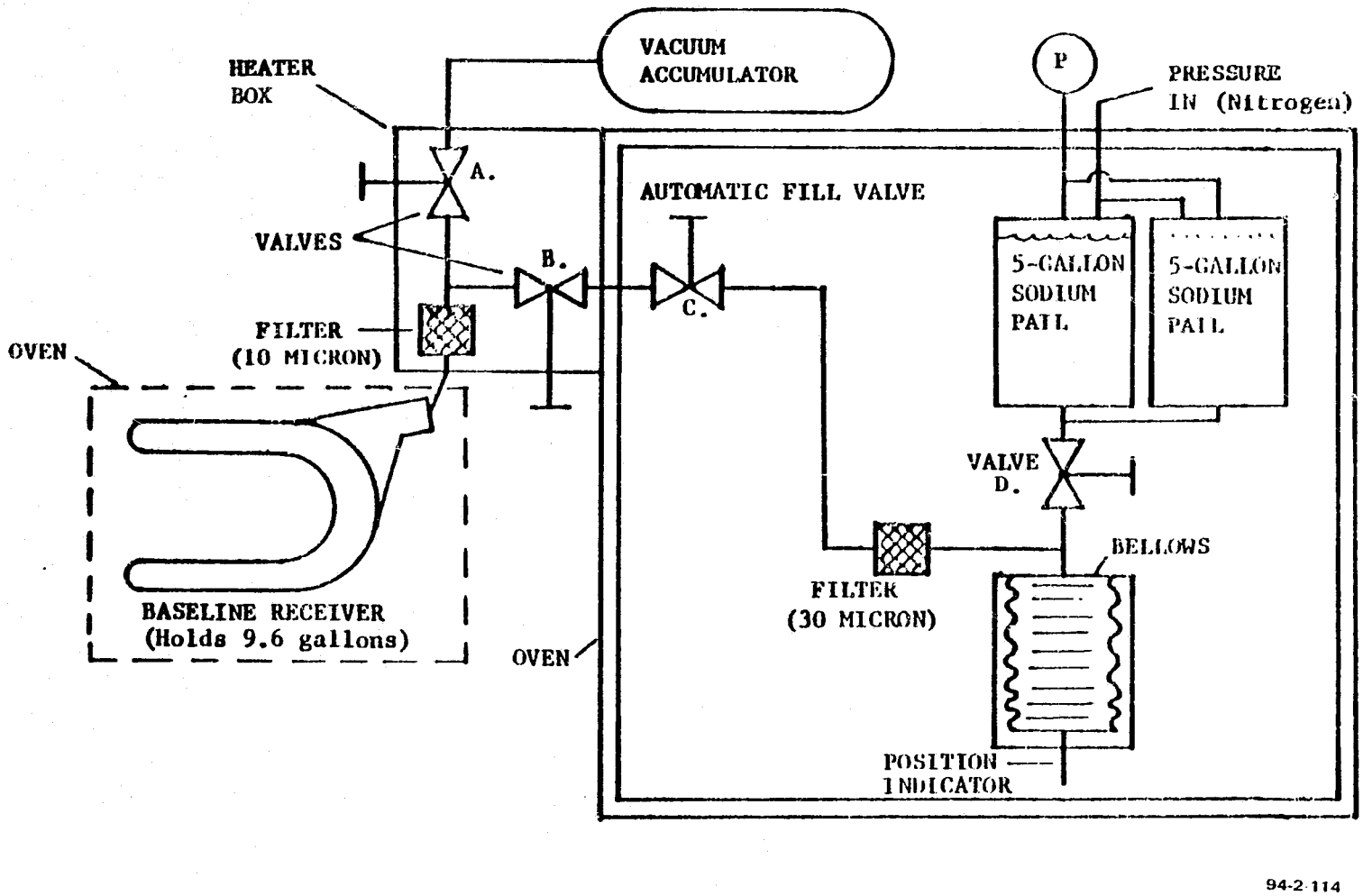

FIGURE 3-43. SODIUM FILLING SYSTEM

(2) Fill bellows with molten sodium - Close all valves except valve D. The volume of molten sodium flowing into the bellows is indicated by the position indicator. When the bellows maximum capacity is reached, valve D is closed.

(3) Remove trapped air inside receiver tank - The receiver tank is connected to the system fill line shown in the Figure 3-43. To evacuate the tank, valves B and C remain closed; and valve A is opened.

(4) Fill receiver tank with molten sodium - Close Valves A and D, cycle bellows with nitrogen gas pressure and pump molten sodium into tank. To obtain the required sodium purity, the sodium is pumped through a 30 micron and 10 micron filter.

After the receiver tank is filled to the correct level, the intake pipe is capped-off; and the tank is agitated for approximately 15 minutes. During this time, the oxide layer on the inside surface of the receiver will be removed by the hot sodium and carried in suspension. After approximately 30 minutes, the hot sodium and oxide impurities are removed from the receiver tank leaving an oxide-free surface. The sodium removed from the receiver tank can be filtered and reused. After completing steps (3) and (4) once again, the receiver tank is filled and ready to be mated with the other components.

3.1.1.5 Control/Operating Sequence. This section contains a summary of the control and operating sequence of the baseline Stirling engine system. Additional information on the control system is contained in Paragraph 3.1.7.

a. System Control. The system will operate under the control of a master power controller (MPC) using a microprocessor. The microprocessor will have several functions: store ephemeris data and keep time for tracking purposes; monitor sensor inputs from various components (for example, engines, AC generators, battery subsystem, electrical output, solar insolation, and weather data); receive status and alarm signals; and produce output signals and controls. The interface between the microprocessor and the Stirling engine/alternator is shown in Figure 3-44. This block diagram only shows a single engine/alternator unit; the interfaces are repeated for each of the other units in the system.

The power output of a Stirling engine is controlled by varying the mean pressure of the working gas (helium in this application). The power control consists of the following components:

- Helium reservoir
- Compressor
- Control valve
- Electronic control unit

A schematic of these items is shown in Figure 3-45. When the engine power output is to be increased, the control valve is set so that helium flows from the reservoir into the cylinders. To reduce power, the control valve allows the compressor to pump the gas back into the bottle.

This basic control scheme of valving gas in and out of the engine is used for any Stirling engine, whether powered by combustion or solar energy; however, a new method of implementing the engine control was developed for SPS. It was developed so that all the available solar energy can be utilized. It is both impractical and undesirable to try to vary the sun's input to the engine: impractical because of the difficulty of either shuttering the solar input or of bypassing part of the receiver heat transfer fluid, for example sodium, and undesirable because of the reduced efficiency and power output. The baseline engine control technique is to "slave" the existing Stirling engine power control loop to the engine head temperature; this arrangement permits output power (torque) to follow the solar input while maintaining constant system temperature. Head temperature control is ideal for the solar application because of the near-isothermal characteristics of the sodium loop. Background information and additional details on the development of the particular control scheme employe is contained in Reference 3-9 (Appendix E).

The station is designed for unattended operation therefore, it is fully controlled by the MPC. At the start of each day's operation, the station's main circuit breaker will be closed, the concentrators will be directed to

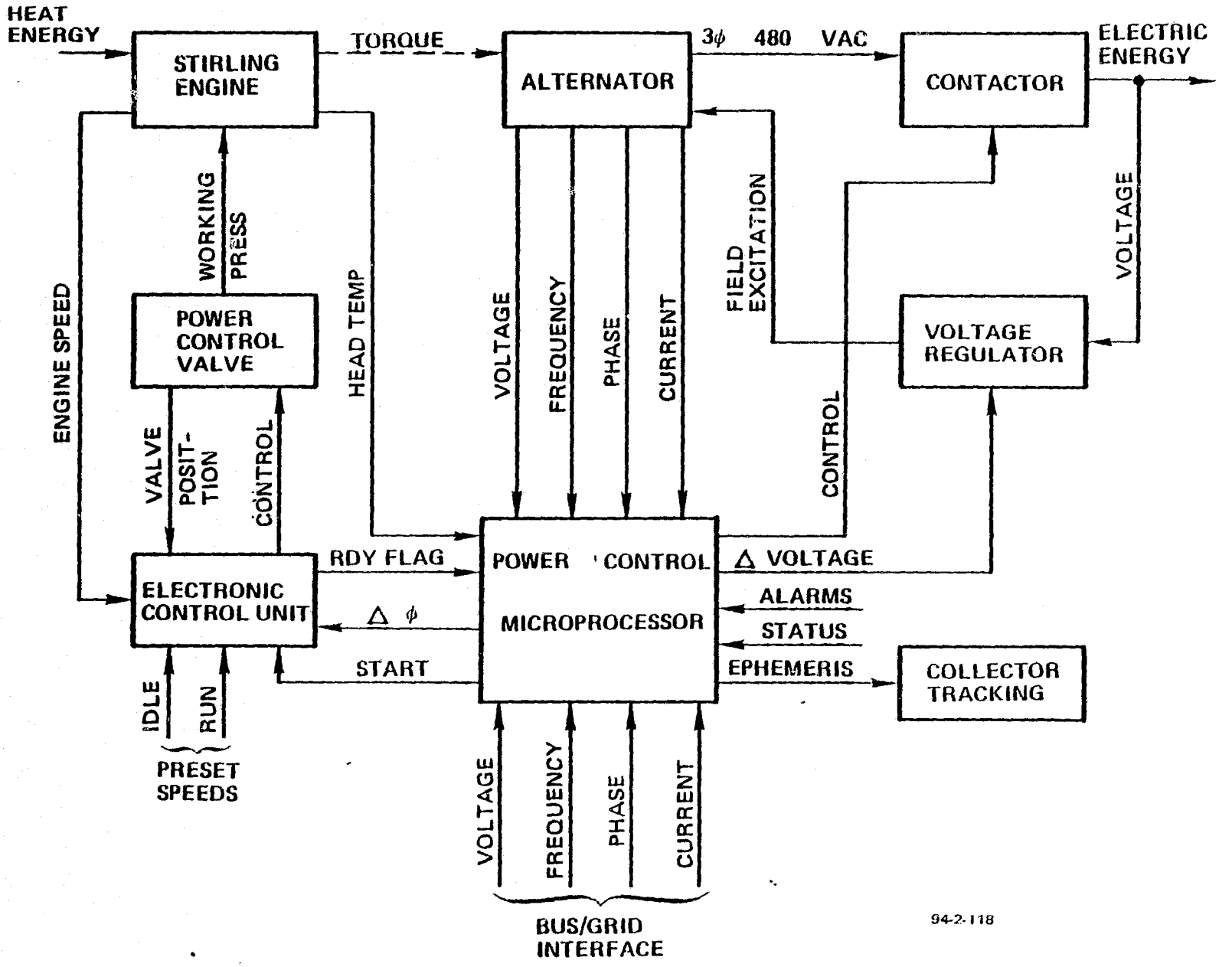

FIGURE 3-44. CONTROL INTERFACE—ENGINE/GENERATOR

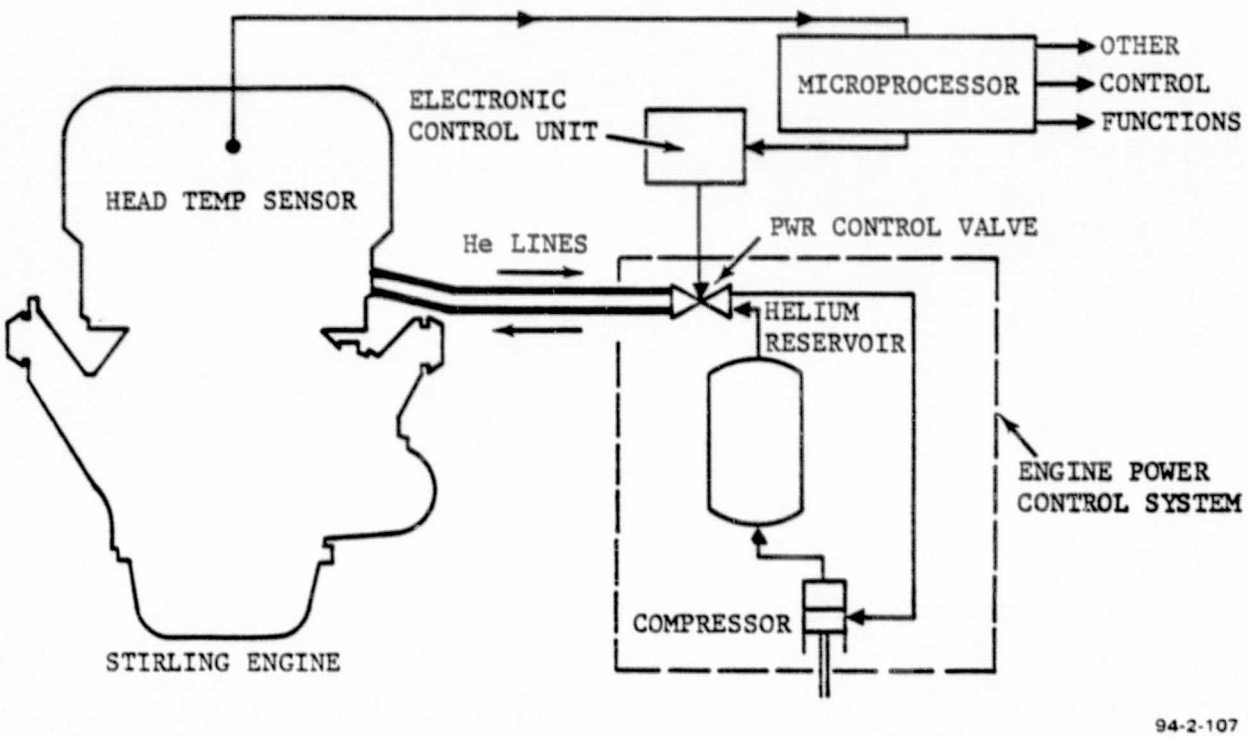

FIGURE 3-45. THE SOLAR-STIRLING CONTROL SCHEME

point to the sun's position at the appropriate point in the sky (~5 to 10 degrees above the horizon) and the receiver door will be opened to start collecting energy for warm-up prior to starting the engines. Special requirements for system start-up and grid synchronization are discussed below.

b. Start-up and Operating Sequence. Early each morning the computer monitors the status of all units (and the storage subsystem) and compares the output with a preprogrammed operating schedule to determine which units should be started first and placed on line. Clock time and solar insolation level will be monitored and when preselected values are reached, control signals will be sent to each power conversion system to open its receiver lid and sodium blocking valve, and start tracking the sun. Engine head temperature will be monitored and when it reaches approximately 450 degrees C, a start (cranking) signal will be sent to the engine. The engine will first operate at idle speed, only developing sufficient power to overcome internal friction as well as the drag of the alternator (the alternator field is not excited). As engine head temperature continues to increase, the power control valve is opened to increase the helium pressure in the engine thereby increasing engine torque and speed until the (excited) alternator output frequency, voltage and phase are matched to grid values by the MPC. The line switch is closed to lock onto the grid at low power level. All units will operate in a scramble mode, that is placed on-line as soon as conditions are matched and each engine is operating at the proper conditions. Once the system is placed on-line, all alternators must operate in phase synchronism with the utility grid and with each other. The MPC will control the excitation of each alternator so it will operate at the correct terminal voltage and the same power factor as the load. This is accomplished by a voltage regulator which senses alternator output terminal voltage and combines it with a current compensation offset signal from the MPC to determine the proper amount of field excitation current.

When the engine head temperature reaches a temperature of ~800 degrees C, the power control valve is opened further to increase engine torque (engine speed is held constant by the grid at 1800 rpm). The increased engine torque will advance the displacement angle of the alternator and increase the electrical power output. Subsequent changes in solar flux will be sensed by a change in the engine head temperature and the power control valve setting will be automatically changed (torque varied) to maintain a constant engine head temperature. The constant heater head temperature control scheme results in engine torque (and equivalently, the alternator power) being directly proportional to the solar insolation level.* The engine, receiver and concentrator are sized and matched to handle the peak power on the day of maximum solar insolation and coolest ambient temperature without engine overload. A safety override is provided to defocus the collectors

---

*As discussed in paragraph 3.1.1.2, there is also a change in collection efficiency with solar insolation; however, the change is a slight one and engine output is essentially linear with insolation.

and shut the system down in the event of failure of the MPC.

c. Cloud Passage, Shut-down, and Emergency Conditions. Passage of a cloud will cause the solar input power to the receiver to drop to zero, and the temperature in the receiver and heater will also drop. Engine power will reduce as the control system attempts to maintain ~800°C head temperature. However, the temperature will quickly drop below the level required for normal power-generating operation and an "idle-sequence" will be initiated. In this sequence, the helium pressure in the engine will decrease until a preselected minimum value is reached. The engine/alternator will still be connected to the grid although the power level will be minimal. Also, the receiver lid will be closed to reduce the heat loss from the receiver. If the cloud passes, the receiver lid is reopened quickly allowing an increase in the temperature level to the normal steady-state range (~800°C). If the cloud persists, the head temperature will reach the lower operational limit (~30 minutes) and at which time the units are stopped (no need for idle-sequence in this case). Also, the units are automatically stoppped when the sun is approximately 10 degrees above the horizon even though the power level is above the minimum. This is necessary to prevent the receiver from tilting to attitudes which would preclude transport of sodium vapor to the engine.

In the event of sudden disconnect from the grid or other emergency conditions such as overheat, engine overspeed is avoided by quickly moving the power control valve so as to release the working fluid from the engine to the reservoir, while at the same time rapidly defocusing the receiver ("emergency defocus") and keeping the cavity lid open to increase energy loss. The sodium blocking valve is closed to stop heat transfer to the engine, preventing engine overheat. Provisions for storing or dissipating some electrical output from the alternators may be required during a brief period, pending futher detailed analysis. Step-by-step control sequences have been developed for various operating scenarios (including emergency defocus) and summarized in Reference 3-10.

3.1.1.6 Reliability. This section summarizes the results of the Phase I reliability analyses and trade studies conducted on the various SPS configurations. The estimated cumulative-mean-time-between-failure (CMTBF), cumulative-mean-time-to-recover (CMTTR) and uptime (availability) probability for the various SPS systems at the end of one year test period have been determined.

The baseline (Nominal) SPS, rated at 1.0 megawatt electrical (mW_e) output with an annual capacity factor of 0.40, is basically the same system for the 4.5 and 6.5 year program. The main difference between the baseline system and the 3.5 year system is the complexity related to the number of collectors and power conversion subsystem. The basic data and predicted results used in this section are based on the detailed analysis given in Appendix I.

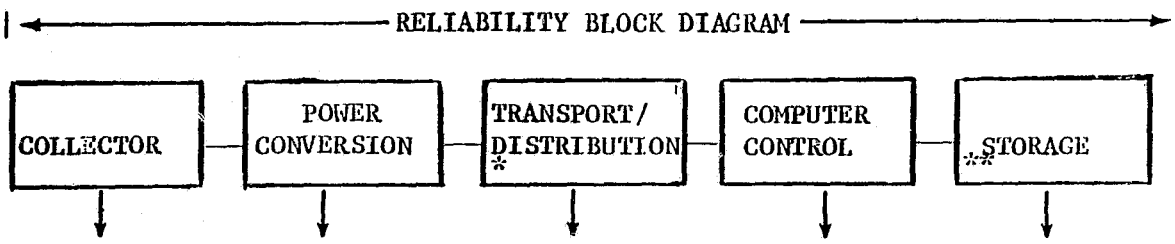

SYSTEM DESCRIPTION		UNITS PER SUBSYSTEM					REMARKS
PLANT SIZE	ACF						
0.5 MWe	0.34	9	9	1	1	0	
	0.40	10	10	1	1	1	
	0.70	20	20	1	1	1	
1.0 MWe	0.34	18	18	1	1	0	
	0.36	55	55	1	1	0	Applicable to 3.5 year program.
	0.40	60	60	1	1	1	Applicable to 3.5 year program.
	0.40	19	19	1	1	2	Baseline System. Applicable to 4.5 and 6.5 year program.
	0.70	40	40	1	1	2	
10.0 MWe	0.34	180	180	1	1	0	
	0.40	190	190	1	1	20	
	0.70	400	400	1	1	20	

*Subsystem unit complexity will vary with the number of power circuit breakers, HV transformer and HV switches required.

**Subsystem unit complexity will vary with the number of battery banks required based on the ACF.

FIGURE 3-46. SPS RELIABILITY BLOCK DIAGRAM WITH THE RELATED SUBSYSTEM COMPLEXITY DATA

a. Assessments. The reliability assessments encompass eleven different system configurations. A generalized reliability block diagram, reflecting the rated power delivery for one year test period, was established and used in the derivation of the CMTBF, CMTTR, availability (uptime probability) and recovery time probability.

b. Reliability Block Diagram. The generalization reliability block diagram of Figure 3-46 identifies the SPS subsystems. The block diagram is configured as a serial-type model; thus any subsystem failure or malfunction is assumed to preclude the delivery of full rated power. Total system reliability for this model is the product of the individual subsystem reliabilities. The CMTBF, CMTTR and availability (uptime probability) derived by the serial model are restricted to the full rated power output condition. Figure 3-46 also summarizes the various SPS configurations evaluated and provides the subsystem complexity data. The SPS reliability and availability analyses are based on the conditions and assumptions stipulated for the respective mode. The reliability model assumes that all failure modes are catastrophic in nature causing complete power outage. The predicted results are therefore considered to be quite conservative. A more detailed failure mode effects and criticality analysis would be needed to assess each possible failure mode and its effect on system operation and rated power output.

c. Definitions, Equations and Calculations. The following definitions and equations, were used to calculate the various parameters.

(1) Annualized capacity factor. The ACF determines the plant operative duration. The daily power delivery periods for each corresponding ACF is listed below.

	TIME (HOURS)		
ACF	Solar Source	Storage Source	Total
0.34	8.6	None	8.6
*0.36	8.6	None	8.6
0.40	8.6	1.0	9.6
0.70	8.6	8.2	16.8

*Applicable to the 3.5 year program system

(2) Cumulative-mean-time-between-failure. The CMTBF is defined as:

$$CMTFB = \frac{T_o}{\Sigma F}$$

where T_o = total time a given system delivers rated power output as determined by the ACF, and

ΣF = cumulative number of failures anticipated during one year of system operation.

(3) Cumulative-mean-time-to-recovery. The CMTR is defined as:

$$CMTR = \frac{\Sigma T_d}{\Sigma F}$$

where T_d = the total time per year required for recovery, or restoration to full rated system operation after in-service failure or malfunction.

(4) Uptime Probability. P(u), generally known as availability, is a measure of the time a system is operable (uptime) to the time/ scheduled for operation. It is defined as:

$$P(u) = A = \frac{CMTBF}{CMTBF + CMTTR}$$

(5) Recovery Probability. P_R is based on the assumption that the recovery time of a maintained system for most of the failures can be repaired in a relatively short time. Failures that occur infrequently take longer time to recover, correct or repair. It is therefore assumed that the recovery actions are exponentially distributed.

$$P_R(t) = 1 - \exp(-ut),$$

where P_R = the recovery probability as a function of time,

u = recovery rate, and

t = time interval being evaluated

Then the probability of completing a recovery action during a time interval (t, t+dt) is ut.

The calculated reliability parameters for the various SPS systems are summarized in Tables 3.12 and 3.13. The discussions of these results are in the paragraphs to follow.

d. Configuration Trade-offs. The Baseline Solar SPS is the 1.0 MW_e, 0.4 ACF power plant, designed for reliable operation, characterized by high uptime probability of 0.9868, CMTBF of 222 hours and CMTTR of 2.96 hours. The probability of no system failure per operational day is 0.958.

TABLE 3.12. SOLAR SPS RELIABILITY PREDICTION SUMMARY

System Description			Prediction		
Plant Size, MW_e	ACF	Storage	CMTBF (Hours)	CMTTR (Hours)	Full Rated Uptime Probability
0.5	0.34	No	466	3.20	0.9931
0.5	0.40	Yes	395	2.85	0.9928
0.5	0.70	Yes	315	2.72	0.9914
1.0	0.34	No	257	3.40	0.9869
*1.0	0.36	No	90	3.55	0.9621
*1.0	0.40	Yes	83	3.37	0.9610
**1.0	0.40	Yes	222	2.96	0.9868
1.0	0.70	Yes	170	2.81	0.9837
10.0	0.34	No	28	3.64	0.8849
10.0	0.40	Yes	24	3.13	0.8846
10.0	0.70	Yes	18	2.93	0.8600

*Applicable to the 3.5 year program (uses P40 engine)
**Baseline system, applicable to the 4.5 and 6.5 year programs (uses P75 engine).

TABLE 3.13. SUBSYSTEM RELIABILITY PREDICTION SUMMARY

A. Baseline System: 1.0 MW_e, 0.4 ACF (P-75)

Subsystem	Units	CMTBF (Hours)	CMTTR (Hours)	P(u)
Collector	19	650	3.56	0.99455
Power Conversion	19	612	4.00	0.99351
Transport/Distrib.	1	5028	0.88	0.99983
Computer Control	1	2707	1.00	0.99963
Storage	2	1293	1.04	0.99920
System:		222	2.96	0.9868

B. System: 1.0 MW_e, 0.36 ACF, no storage (P-40)

Subsystem	Units	CMTBF (Hours)	CMTTR (Hours)	P(u)
Collector	55	201	3.56	0.98260
Power Conversion	55	190	4.00	0.97938
Transport/Distrib.	1	1980	0.65	0.99971
Computer Control	1	2688	1.00	0.99963
System:		90	3.55	0.9621

C. System: 1.0 MW_e, 0.40 ACF (P-40)

Subsystem	Units	CMTBF (Hours)	CMTTR (Hours)	P(u)
Collector	60	191	3.56	0.98170
Power Conversion	60	189	4.00	0.97927
Transport/Distrib.	1	1694	0.63	0.99963
Computer Control	1	2707	1.00	0.99963
Storage	2	1290	1.04	0.99919
System:		83	3.37	0.9610

The trade-off results, Figures 3-47 and 3-48, present the predicted Baseline System reliability parameters relative to the ACF for various plant sizes. The following discussion presents the four major points illustrated in Figures 3-47 and 3-48.

(1) CMTBF. The CMTBF is highest for the least complex system having the minimal performance requirements, for example, system without storage capability (0.34 ACF). The CMTBF is the lowest for the most complex system having the most storage capability. For any plant size, the biggest change in CMTBF is observed between the no storage system and the minimal storage system. For a given plant size, the slope of the CMTBF curve indicates system sensitivity to ACF. The 0.5 MW_e plant is most sensitive to the increase of the ACF and the 10.0 MW_e plant is the least sensitive. The Baseline System CMTBF is situated at an optional level where the plant can deliver both direct solar conversion and storage power without being extremely complex. System design simplicity is a key reliability enhancing feature that can minimize initial costs as well as long term maintenance costs.

(2) CMTTR. The CMTTR is highest for the least complex system due to having proportionately higher percentage of items requiring longer recovery time in the event of a failure. The biggest change in CMTTR is observed between the no storage system and the minimal storage capability. Beyond the point of minimal storage, the rate of CMTTR change is relatively small. The Baseline System CMTTR is optimized for a system having both direct solar conversion and storage power delivery capabilities.

(3) Uptime Probability, P(u). The P(u) of any system is determined by the CMTBF and CMTTR relationship defined above. Generally, the P(u)s of the various Solar SPSs are significantly affected by the CMTTR. For the 10.0 MW_e system, P(u) becomes extremely sensitive to CMTTR since it becomes significant at lower CMTBF. This condition is observed when the ACF is greater than 0.4 ACF. The Baseline System P(u) reflects optimal CMTBF and CMTTR based on the simplest design configuration possible with emphasis on ease of maintenance for a system having direct solar as well as storage power delivery capabilities.

(4) Recovery Probability. The recovery probability (P_R) of the SPS is the probability of system recovery, given a specified recovery time interval. The Baseline System (P_R) is relatively higher at any recovery time interval when compared to the 1.0 MW_e, 0.34 MW_e system. The result reflects the optimized Baseline System repair rate which is directly related to the smallest possible system CMTTR. The higher the system CMTTR, the lower the system recovery probability for a given recovery time interval.

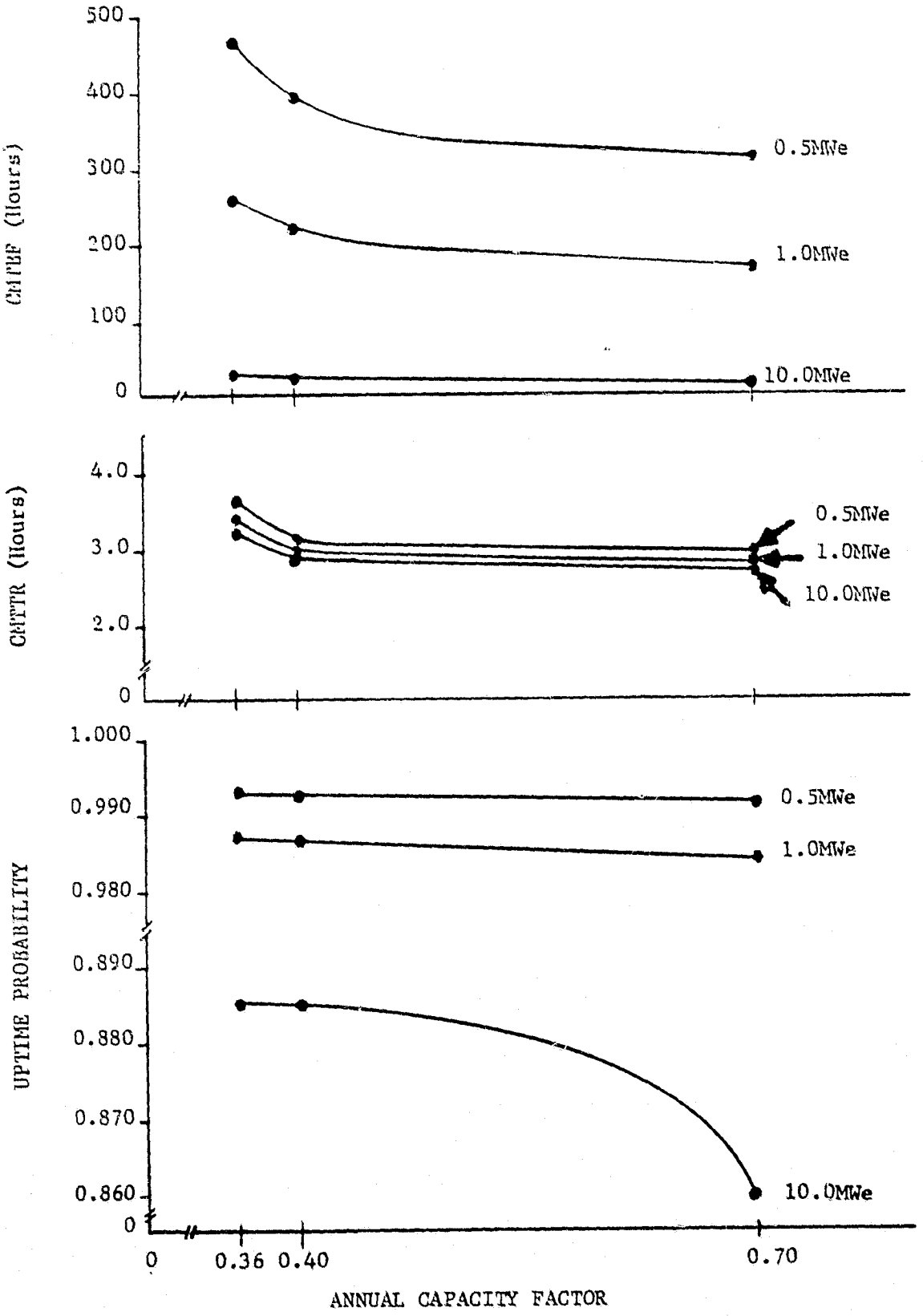

FIGURE 3-47. EFFECT OF ANNUAL CAPACITY FACTOR ON CMTBF, CMTTR AND UPTIME PROBABILITY

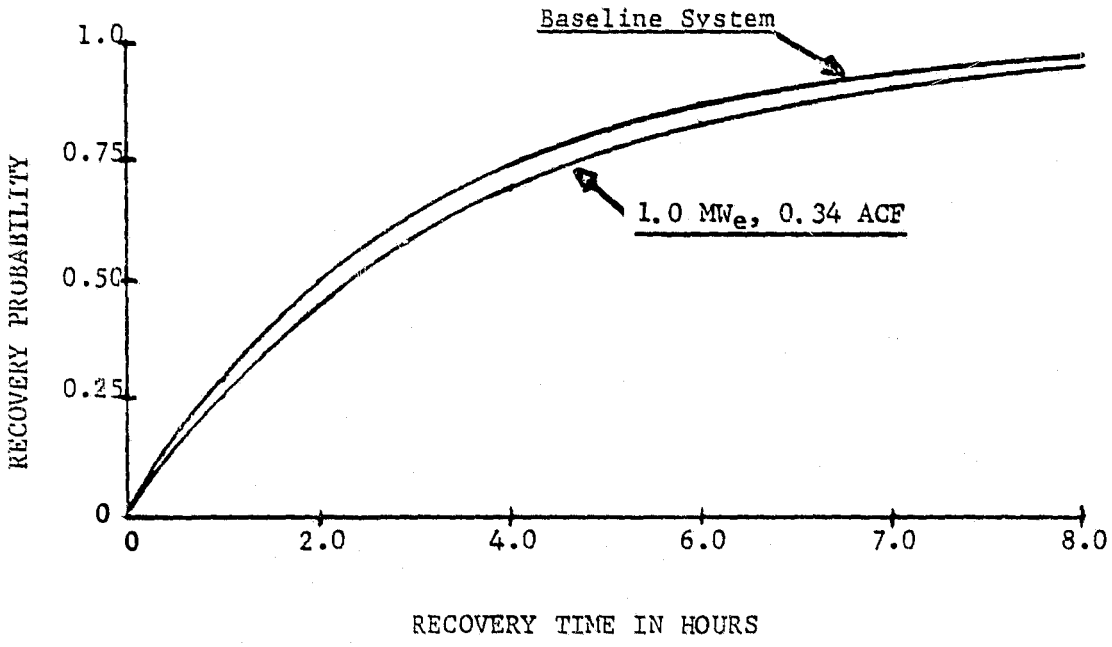

FIGURE 3-48. SYSTEM RECOVERY PROBABILITY SUBSEQUENT TO IN-SERVICE FAILURE

e. Reliability Enhancement by Modularization. Inherent in the baseline SPS is the unique capability of providing continuous power (no power outage) even when a portion of the collector field, the power conversion or the storage subsystem, is out for corrective maintenance action during the scheduled power delivery time period.

This continuous power delivery capability is achieved by effective modularization of the collector and power conversion units and connecting these units in the redundant configuration. The block diagram of Figure 3-49 shows 19 actively redundant sets of a collector unit serially connected to a power conversion unit. The system uptime probabilities for the following conditions are shown in Figure 3-49.

(1) 18 out of 19 collector/power conversion sets and the remaining subsystems must operate.

(2) 17 out of 19 collector/power conversion sets and the remaining subsystems must operate.

The output capacity for condition (1) is down to 94.7 percent of the full rated output only during the time one collector/conversion set is out for corrective maintenance. Hence the uptime probability for condition (1) is greater than 0.9928.

The output capacity for condition (2) is down to 84.7 percent of the full rated output only during the time when two collector/conversion sets are simultaneously out for corrective maintenance. Hence the uptime probability condition (2) is greater than 0.9948.

Figure 3-50 shows the P(u) relative to the baseline system capacity. Theoretically, the collector/power conversion subsystem P(u) will be approaching 1.00 as more than two sets are down simultaneously. Then system uptime probability will be limited to the P(u)s of the remaining subsystems which is 0.9986. Higher system P(u)s can be achieved by considering redundancy in the area of single point failure items, for example, HV transformers, HV switch and computer.

The probability of a baseline system failure during a continuous operating interval (9.6 hours) causing total power outage is calculated to be 0.0017. This total outage condition assumes only the failures caused by the single point failure items.

f. Program Start Up Effects. The 4.5 and 6.5 year system are assumed to be similar to the baseline system discussed in the previous section on the basis of similar equipment complexity as noted previously. For the 3.5 year program system, the higher complexity of the collector and the power conversion subsystems is due to the proposed use of the lower output capacity of the P-40 Stirling engine, which is the only engine available in the program time frame. More engines will be required to accomodate the equivalent plant capacity requirement of 1.0 MW_e, 0.4 ACF. The quantity of units required for the collector and power conversion units are significantly higher as shown previously.

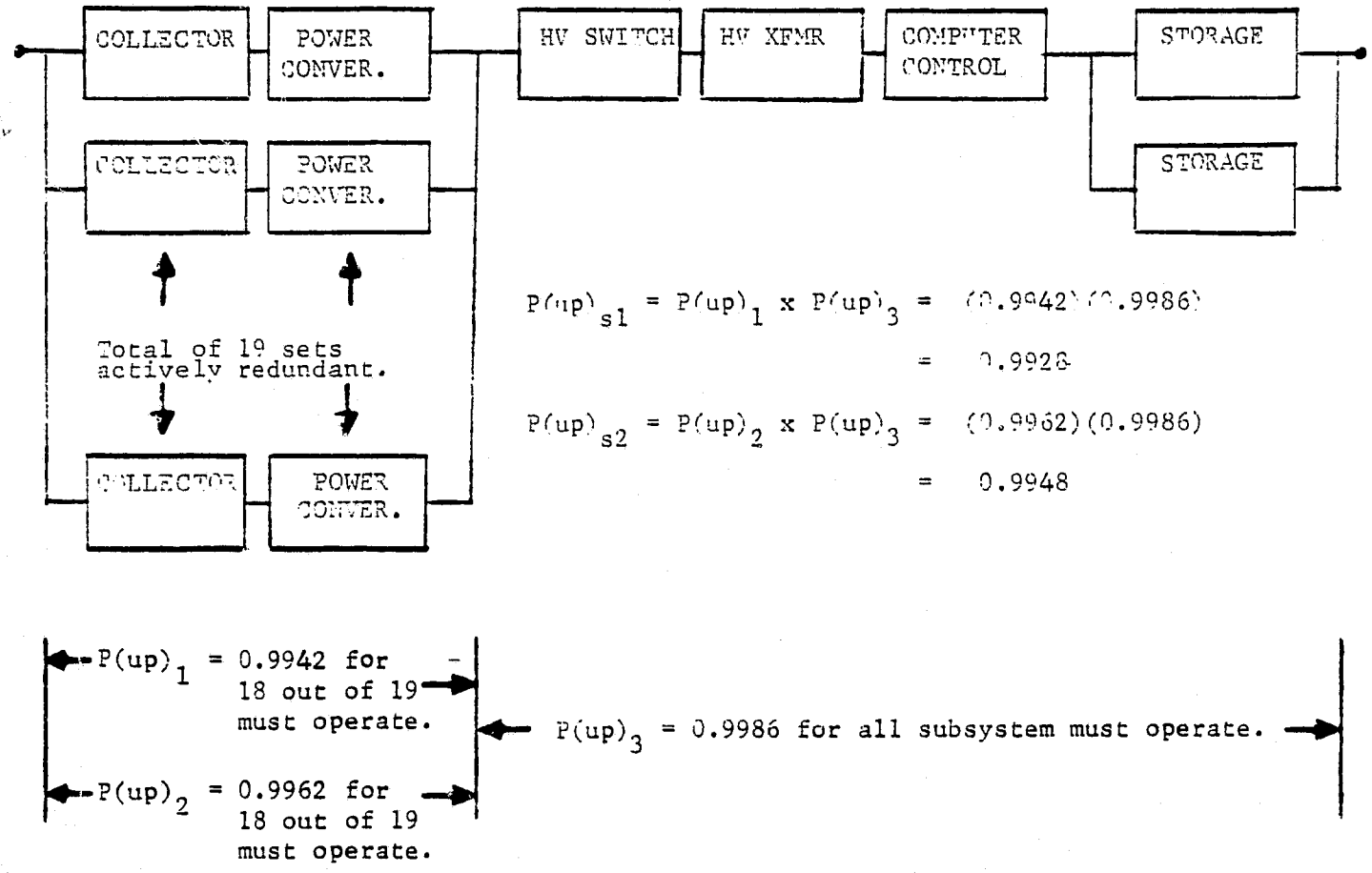

FIGURE 3-49. EFFECTS OF MODULARIZATION ON UPTIME PROBABILITY

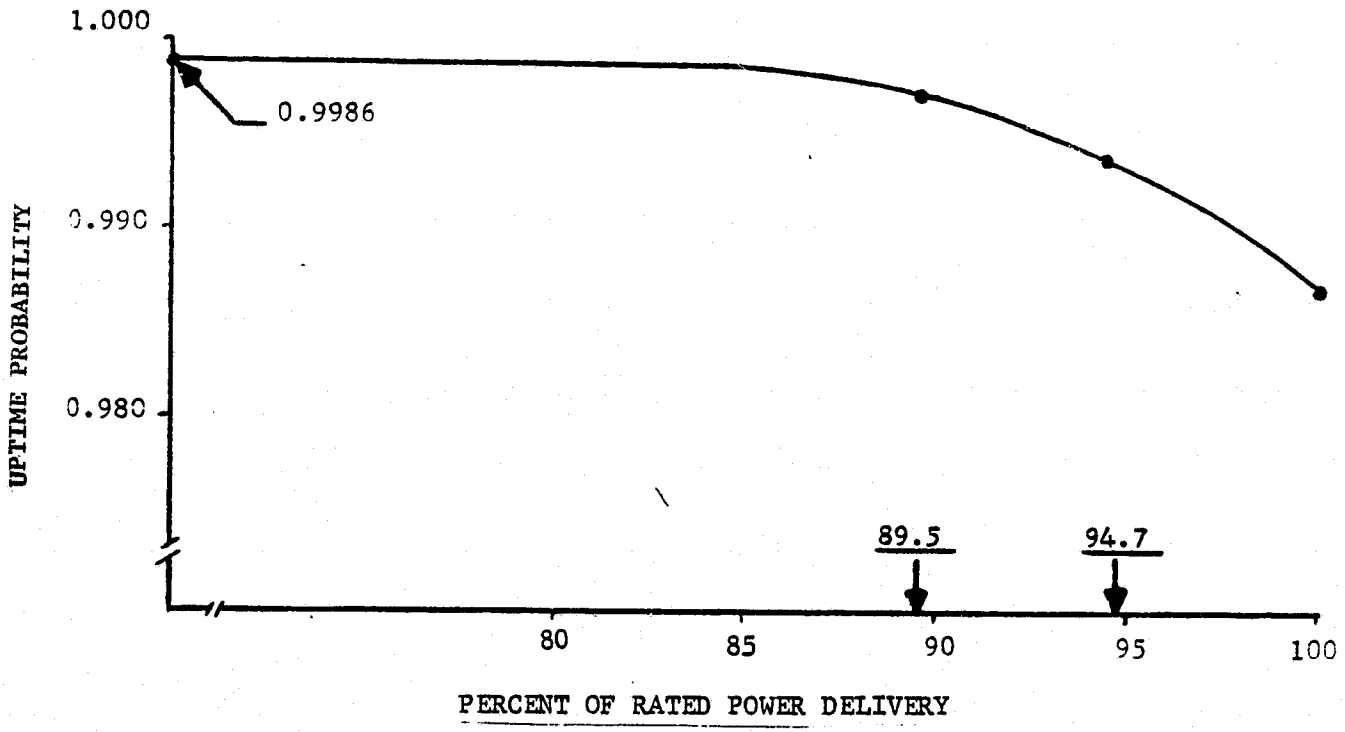

FIGURE 3-50. EFFECT OF REDUNDANCY ON UPTIME PROBABILITY

Table 3.13 summarizes the system and subsystem reliability parameters. Figure 3-51 compares the predicted CMTBF and uptime probabilities by the program involved and by the no-storage and storage configuration. The low CMTBF for the 3.5 year system is due to the effect of significantly high system complexity (unit count) in the area of collector and power subsystems. The 3.5 year system is inherently more complex and less reliable than the system proposed for the 4.5 and 6.5 year programs.

g. Maintenance Approach. Preventive maintenance will be planned for performance at regular intervals when the plant is idle at night in order to maintain the system in a condition consistent with its built-in level of performance, reliability, availability and safety. Preventive maintenance will involve servicing, inspections and minor or major overhauls during which:

- regular care will be provided to normally operating subsystems and components requiring such attention, for example, lubrication, cleaning, adjustments, alignments, etc.,
- periodic check or test will be planned and performed to ascertain the functional integrity of the subsystems,
- repair, removal or replacement action will be done on marginal or erratic components, and
- repair or overhaul action on all components approaching wearout will be performed.

Corrective (unscheduled) maintenance is necessitated by system operational failure or malfunction and requires immediate restoration of the system to full operational status. Restoration of the system requires replacement, repair or adjustment action on the subsystem or equipment causing interruption of service. Four levels of corrective maintenance shown in Table 3.14 are established for the SPS.

The design of the SPS is functionally partitioned or modularized to facilitate maintenance. Accessibility to all functional hardware will be provided. Remote sensing will be incorporated to localize and isolate failed or malfunctioning elements and to provide system checkout capability. The modular aspect of the design can reduce the subsystem CMTTR by reducing long on-site recover/repair time to a mere module replacement time.

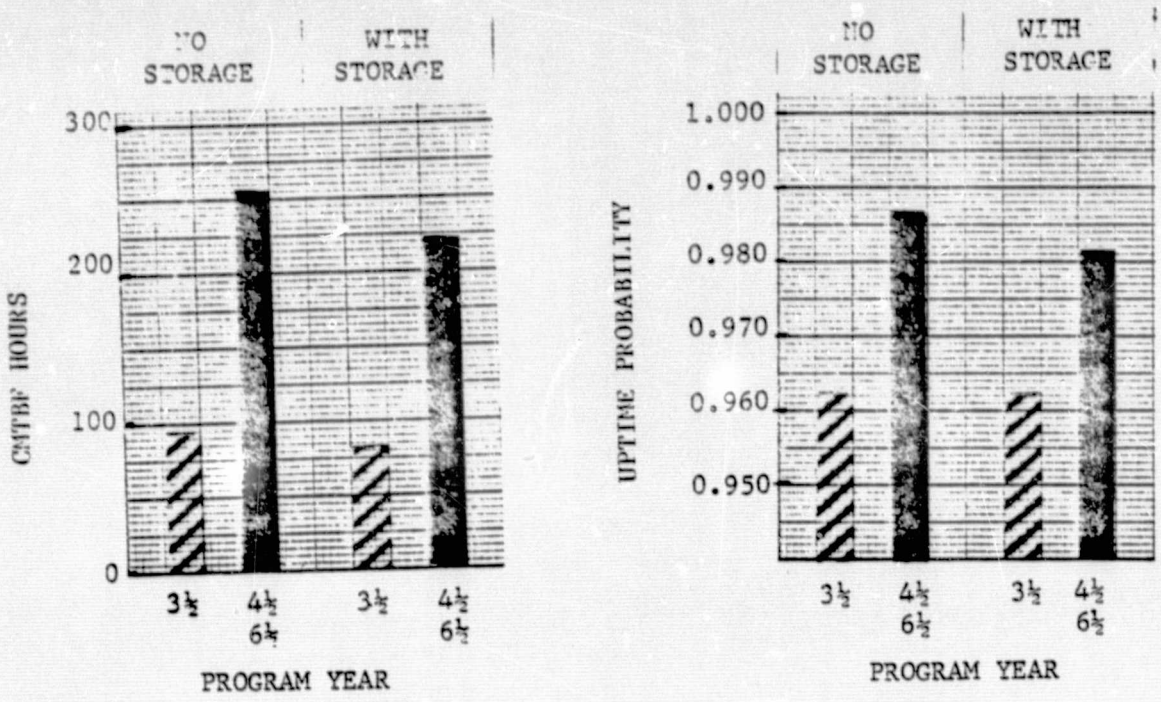

FIGURE 3-51. CMTBF AND P(UP) COMPARISONS FOR PROGRAMS CONSIDERED

TABLE 3.14 CORRECTIVE MAINTENANCE CONCEPT

LEVEL	ACTION	CRITERION	PARTS
1	*REPAIR IN PLACE	REPAIR TIME ≤ REPLACE TIME	ON-SITE
2	REMOVE, REPLACE, REPAIR* ON-SITE	REPAIR TIME > REPLACE TIME LOW LABOR SKILLS INEXPENSIVE PARTS	ON-SITE
3	REMOVE, REPLACE REPAIR* AT CENTRAL MAINTENANCE FACILITY	REPAIR TIME >> REPLACE TIME MODERATE LABOR SKILL EXPENSIVE PARTS/TOOLS	CENTRAL
4	REMOVE, REPLACE REPAIR* AT FACTORY	REPAIR TIME >> REPLACE TIME HIGH LABOR SKILL INFREQUENT FAILURES SPECIAL DIAGNOSTICS HIGH VALUE COMPONENT	AT FACTORY

*Repair/Throw Away/Scrap Decision Required

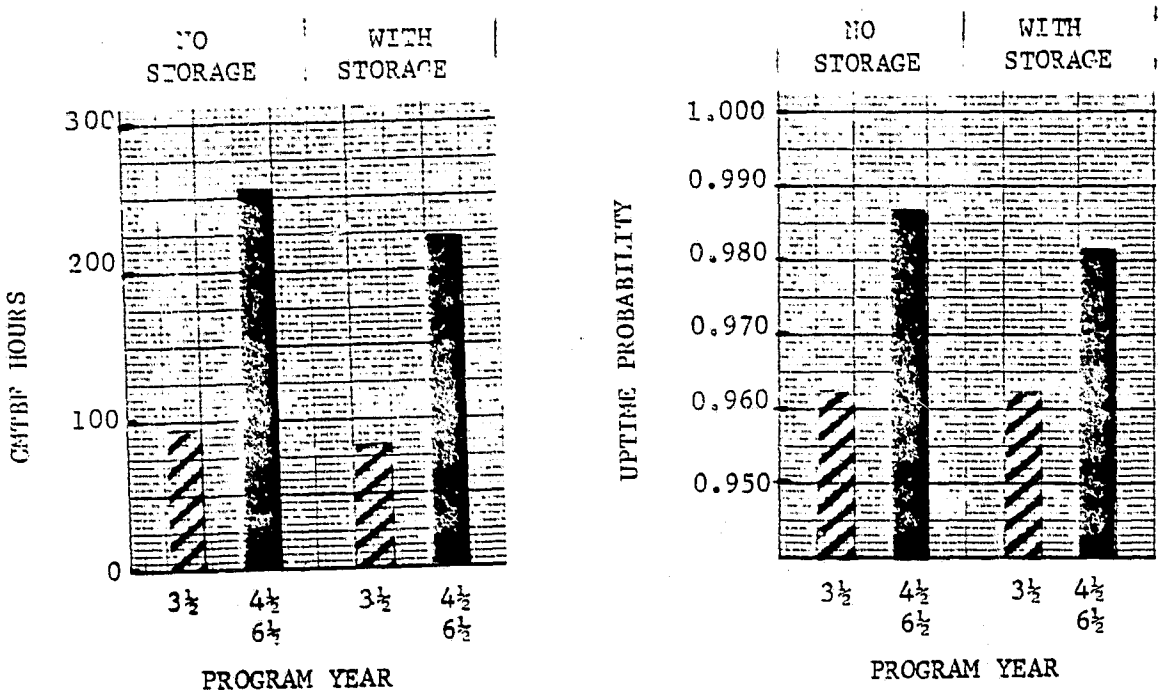

FIGURE 3-51. CMTBF AND P(UP) COMPARISONS FOR PROGRAMS CONSIDERED

TABLE 3.14 CORRECTIVE MAINTENANCE CONCEPT

LEVEL	ACTION	CRITERION	PARTS
1	*REPAIR IN PLACE	REPAIR TIME ≤ REPLACE TIME	ON-SITE
2	REMOVE, REPLACE, REPAIR* ON-SITE	REPAIR TIME > REPLACE TIME LOW LABOR SKILLS INEXPENSIVE PARTS	ON-SITE
3	REMOVE, REPLACE REPAIR* AT CENTRAL MAINTENANCE FACILITY	REPAIR TIME >> REPLACE TIME MODERATE LABOR SKILL EXPENSIVE PARTS/TOOLS	CENTRAL
4	REMOVE, REPLACE REPAIR* AT FACTORY	REPAIR TIME >> REPLACE TIME HIGH LABOR SKILL INFREQUENT FAILURES SPECIAL DIAGNOSTICS HIGH VALUE COMPONENT	AT FACTORY

*Repair/Throw Away/Scrap Decision Required

3.1.1.7 Safety/Environmental Factors. The Phase I study effort has included consideration of safety of personnel and equipment together with environmental factors in the selection of design approaches. Emphasis has been placed on the Stirling engine with sodium thermal transport system since it is the baseline concept; however, the Brayton and organic Rankine alternate engines have been studied.

a. Safety. A hazards evalution was prepared by FACC and documented in Reference 3-8.

The objective of the evaluation was to identify critical safety aspects and inherent system hazards so that the necessary design criteria, design features, safety devices, warning devices, and operational precautions could be defined during the conceptual design. Hazard severity levels based on MIL-STD-882A were defined based on a deductive or "top down" approach which starts with major system hazards or "undesired events" and traces them downward to where they originate. All known potential hazards were identified whether or not they were expected to present an actual problem during system design (Phase II). The results of this study are summarized on Table 3.15. As might be expected, the most significant potential hazard involves sodium and the requirement to isolate it from moisture sources -- which is equivalent to keeping it within the proper container.

The baseline sodium receiver/Stirling engine concept is unique in that the pressure of the sodium heat transfer fluid is very low -- less than one atmosphere at the nominal receiver temperature of 830 degrees Centigrade (1526 degrees Fahrenheit). This has important implications on the structural design of the receiver, and if a break should occur in the wall, the material will not be blown out by high internal pressure. Other advantages of sodium include its unique heat transfer properties which minimize receiver burn-out. The recognized hazard of using sodium is its very reactive nature especially with materials which contain water. Aeronutronic is convinced, however, that the sodium can be maintained within its container and used in the SPS program without undue hazards. This is based on the following background information on actual use of sodium:

- 25 years of experience using sodium in liquid metal nuclear reactors. Sodium safety procedures are very well known, and are part of the Sodium Technology Course given by Atomics International (References 3-11 and 3-12).

- Many thousands of hours of using a sodium heat pipe to transport energy to the heater head of Stirling engines. This work was done at both N. V. Philips in Eindhoven, Netherlands United Stirling in Malmo, Sweden (References 3-13, 3-14 and 3-15.

- Tens of thousands of hours of successful use of ordinary sodium heat pipes (for example, Reference 3-16).

TABLE 3.15 SUMMARY OF SAFETY CONSIDERATIONS

Concept/Component	Potential Hazards	Design Approach to Minimize Hazards	Conclusions/Comments
ENGINE TYPE	General; Overall hazards judged to be low due to modular, remote operation and safety procedures to be used.	General: Continuous monitoring of vital performance data via computer. Automatic shut-down of units if problems occur.	General: Remote operation minimizes personnel hazards. Alarms to identify type of problem. Fenced enclosure to minimize vandalism.
I. STIRLING			
• Sodium System	• Sodium very reactive if released from containment vessel, particularly with water.	(1) Adequate margin on material thickness for structural and corrosion effects.	Adequate design can be implemented. Alarm/shutdown system will minimize damage.
		(2) Assure material and impurity compatibility.	Valves (mostly bellows), lines, and connections have caused a great majority of leaks in nuclear industry. Minimize use of these components, and test rigorously.
	• High toxic hazard rating, especially if ingested or inhaled.	(3) Use all-welded, sealed system. Use double walls where practical.	
		(4) Define detailed plan for sensors, alarms, safety equipment and procedures.	Receiver door insulates cavity and minimizes range of thermal cycles.
		(5) Detailed handling/filling procedures for sodium based on prior work.	Subatmospheric pressure in receiver.
• Stirling Engine	• Rupture of heater tubes (Note: could pressurize sodium system).	• Proven design, tested for long life. Emergency shutdown if pressure loss.	Adequate sensors should protect engine. Preventive maintenance plan will minimize failures.
	• Failure of accessories.	• Sense overheat, low oil level, etc., and defocus (shutdown).	
II. BRAYTON	• High temperature, high pressure gas if released.	• Same as (1) and (2) above.	Use the computer-monitored alarm/shutdown system proposed for the Stirling System. Adequate design features available. Preventative maintenance will minimize failures.
	• Blade/component/ accessories failure.	• Sense failure condition and shutdown.	
III. RANKINE			
• Organic (Toluene)	• High temperature, high pressure, toxic and explosive if released (low to moderate toxic hazard).	• Same as (1) and (2) above.	Same as for Brayton System.
• Water	• High temperature and high pressure if released.	• Same as (1) and (2) above.	
• Both Systems	• Blade/component/ accessories failure.	• Sense failure condition and shutdown.	
CONCENTRATOR	• Overtravel conditions.	• Provide brakes, locks, limit switches, etc.	Adequate design procedures exist based upon microwave technology.
	• Excessive wind, hail, etc.	• Rapid movement to stow condition. Lighting protection provided.	
	• Concentrated beam impingment.	• Thermal protection for receiver lip, door, etc. Fast movement during emergency defocus.	Receiver lip and door will likely require ablative material which must be replaced periodically.
EMERGENCY TRANSPORT/STORAGE	• Electrical shocks.	• Provide standard electrical grounding, shielding and protective devices.	Standard procedures/ equipment available.
• Lead Acid Batteries	• Hydrogen/heat generation.	• Provide air conditioning and adequate ventilation. Use drip pans to contain leaks.	

These studies have been more than adequate to fully characterize the performance of sodium, define material compatibility, and establish safety procedures.

FACC is aware of the latest safety procedures because of a current contract on the development of a sodium-sulfur battery (DE-AM02-79CH10012). Safety personnel have attended the Atomics International course on sodium and have implemented a system to store, fill, remove, and dispose of sodium from the battery cells.

Fast reaction to onsite problems will be possible through the use of the central control computer. The computer will be programmed to continuously monitor key functions throughout the system -- including safety-related sensors -- and to initiate an automatic shutdown sequence if defined limits are exceeded. For example, if an over-temperature condition occurred on the receiver of Unit No. 6, an automatic emergency defocus procedure would be started to rapidly move the concentrated beam away from the aperture. An alarm would be sounded, a print-out would be made to identify the source and type of problem, and all systems on Unit 6 related to power conversion shut down. A restart would not be attempted until the unit had been inspected and found to be in operating condition and the reason for the over-temperature condition determined. Results of the detailed hazard evaluation (Reference 3-8) show that the baseline Stirling system presents no hazards which cannot be effectively controlled by well-known design techniques. Means of designing in system safety to assure adequate hazard control have been identified and will be implemented during detailed design.

b. Environmental Factors. An important environmental factor which was considered was the appearance (aesthetics) of a typical field of dish concentrators. The baseline parabolic concentrators will be quite visible due to their size. Designs with lower profiles were investigated, but were not selected because of increased design risk, more cost, or other factors such as problems in receiver design.

The baseline SPS design has a unique capability for siting flexibility which allows the concentrators to be located up the side of a hill, on uneven terrain in a random pattern, or in conventional rows and columns with close packing fractions (~25 percent or more) or spread apart. This flexibility could be used to improve the appearance of the system and tailor it to any location. This capability is due to the fact that electricity is generated at the focal point of each dish and the only penalty in locating the dishes far apart is increased electrical cable costs and increased costs for perimeter fencing (if required) and land. These are generally small factors in the cost of a complete system, particularly for the sites anticipated for the SPS.

Noise is also a factor in urban areas. This is no problem for Stirling engines since they are noted for their low operating noise (the accessories are generally noisier than the basic engines). The noise of a Brayton system is expected to be more severe due to the high speed of the engine/

gearbox. Noise suppression can be supplied, but this degrades system performance.

Requirements for large amounts of water can be a problem in high solar insolation (desert) environments. Mirror cleaning will require deionized water, and procedures will be developed to keep the usage to a minimum. The engines will not require significant amounts of water unless small quantities are needed for Rankine system make-up. Large amounts of water are required if evaporative cooling is used, but this has been ruled out as not being desirable for SPS applications because of the uncertain availability of water in desert climates.

Disposal of materials such as sodium or toluene will require special procedures and the use of an authorized disposal site. These requirements are well known and will be developed during Phase II.

3.1.2 RECEIVER DESIGN/ANALYSIS (COLLECTOR SUBSYSTEM)

The receiver is a key component and pacing item of the SPS; a comprehensive thermal/structural analysis was made to ascertain the viability of the baseline receiver in accordance with the method of approach formulated in paragraph 1.2. This section presents the results of the analyses for the baseline receiver; receivers for the alternate engines are also discussed.

The results of the design/analysis study show that a high temperature cavity receiver, employing pool-boiling sodium, is an excellent choice for use in dish-Stirling PFDR systems. The concept is technically feasible at the present time, employing state-of-the-art materials and technology, and will be a cost effective subsystem when put into production.

A sketch of the baseline receiver configuration is presented in Figure 3-52. The receiver is a simple structure consisting of two cylindrical shells, one cantilevered inside the other from a connecting toroidal shell. The two ends are capped with spherical heads forming a double-walled annular cavity. The cavity core is constructed of Type 316 Stainless Steel with boiling liquid sodium occupying the annulus. A short pipe connects the boiler to the engine and serves the dual function of vapor transport and condensate return. Operation is entirely passive, without pumps, and operates equally well at all solar-related attitudes. The extremely high heat transfer rates associated with sodium pool boiling minimize the required surface area and the associated size and weight of the complete receiver package. The possibility of surface burn-through is virtually eliminated, since peak boiling heat transfer rates are at least an order of magnitude greater than maximum solar flux deposition. An additional safety factor is associated with the low vapor pressure (~latm) of sodium at the high operating temperatures (~800°C) necessary for operating the Stirling engine at high efficiency. The dynamic performance of the subsystem is stable, well behaved, and has long time constants which facilitate engine control. The inherent buffer storage capability of the receiver permits continuous engine operation during moderately long (<30 minutes) cloud passages. If additional buffer storage is needed for a particular site location, it can be readily incorporated into the present design with minimal modifications. For the baseline system, the fully insulated receiver (20.3 cm of insulation) can accommodate the maximum 230 kW_t energy within a 1 x 1 x 1.2 m envelope at a gross weight of 310 kg including 33 kg of sodium. In production, the complete receiver/thermal transport package can be manufactured for under $2500. The operational life of the optimized, lowest life cycle cost receiver is selected at 15 years, based on design tradeoffs between material corrosion rate and creep relaxation cycle limitations.

Details of the design selection, associated analyses, thermal performance, and structural design are presented in the following paragraphs.

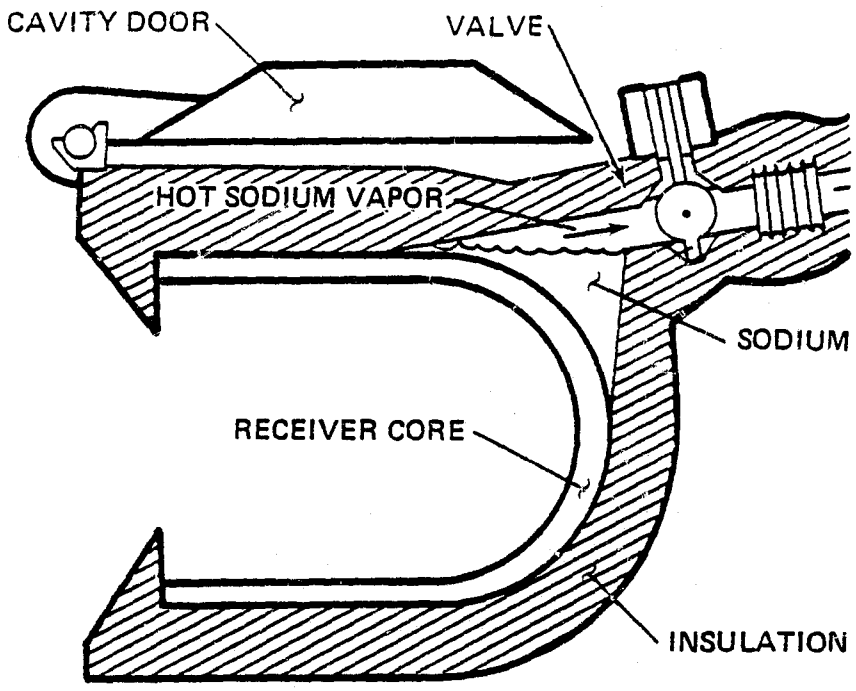

FIGURE 3-52. SKETCH OF THE BASELINE RECEIVER/BOILER

3.1.2.1 Thermal Design. The receiver configurations for the baseline Stirling system were modified and improved until a configuration was obtained which best meets the following thermal design criteria:

Performance

- The overall efficiency of the receiver must be as high as possible.
- The operating temperature should be low to reduce thermal losses and stresses.
- The temperature and pressure gradients should be low.
- The dynamic behavior of the subsystem must be stable.

Safety

- The subsystem should operate at low temperatures and pressures.
- The subsystem must survive all failure modes without catastrophic results and without damage to other subsystems.

Cost

- The design of the receiver should be simple and easy to fabricate.
- The materials should be readily available and inexpensive.
- The receiver should have a reasonably long life (>10 years minimum; 30 years preferred).

Flexibility

- The design should scale for various power levels.
- The receiver should accommodate buffer storage with minimal modifications.

Interface

- The subsystem design should avoid modifications to other subsystems (for example, the Stirling engine).
- The subsystem should ideally be small and lightweight to minimize solar blockage, and to reduce the load on the concentrator structure.

a. Cavity Analysis. Studies of both cavity and external types of receivers show several important advantages for the cavity configuration. The two principal advantages for state-of-the-art systems are high thermal efficiencies and considerable freedom of design for the heat transfer surface area.

The cavity design is influenced by the optical performance of the concentrator, the cavity geometry, the heat transfer surface properties and the radiation interchange factor from the cavity interior to the aperture. Key trade-off results are as follows:

(1) Geometric Configuration. The shape selected for the baseline cavity receiver is a cylinder with a cavity length of 0.718m and a cavity diameter of 0.584m. This results in a length-to-diameter ratio of 1.23 and a cavity-to-aperture area ratio (A_{cav}/A_{apt}) of 13.5. The cavity length was selected to obtain the required heat transfer surface area, increase the effective solar absorptivity, and to reduce receiver cost. The aperture area was determined by the optical/thermal performance trades presented in Paragraph 3.1.1.1. The interior cavity diameter was sized to preclude peak wall flux burnout. Based upon the aforementioned cavity optical analyses, a peak wall flux less than 400 kW/m^2 is predicted for the baseline receiver. As will be shown later, a safety factor of approximately 12 for peak flux burnout is obtained at rated operating conditions.

A spherical cavity was also investigated; it has about the same thermal performance as the cylinder, but with a more uniform flux distribution. However it is more difficult to fabricate and the configuration makes it more difficult to preclude bubble entrapment if a pool boiling heat transport system is to be used.

Cavity receivers are generally more efficient than external receivers. However, the latter configurations will yield higher collection efficiencies if operated with highly selective absorber surface coatings. At the present time, however, no such coatings are available for the temperature of interest (~830°C).

(2) Cavity Performance. The cavity performance of the receiver has a direct effect upon the collection efficiency of the entire system. The effective solar absorptivity (α_{eff}) and effective emissivity (ϵ_{eff}) terms, which characterize the cavity performance, are both strong functions of the interior surface radiation properties and the cavity geometry. The following relationship is derived in Reference 3-17 and has been used to approximate the effective solar absorptivity and infrared emissivity of cavities.

$$\alpha_{eff} \text{ or } \epsilon_{eff} = \frac{\epsilon_{cav}}{1 - \left(1 - \frac{1}{A_{cav}/A_{apt}}\right) \cdot \left(1 - \epsilon_{cav}\right)}$$

Where:

ε_{cav} = ε_s or α_s (the interior cavity surface absorptivity or emissivity)

A_{cav} = Interior cavity surface area

A_{apt} = Cross-sectional area of the aperture

The following conditions were assumed for this relationship:

- Reflection and reradiation are diffuse and obey Lambert's law. (This is a reasonably good assumption for the baseline receiver, since a fairly rough, oxidized surface is expected within the cavity.)
- Uniform flux distribution on the internal surface of the cavity. (This is not a very good assumption for cylindrical cavities without highly reflective surfaces. However, the uniform flux requirement is relatively unimportant since virtually all of the incident flux is absorbed.)
- The inner cavity surface is isothermal. (With sodium pool boiling taking place within the receiver annulus, this is a very good assumption.)

Figure 3-53 presents the effective cavity absorptivity and emissivity as a function of the interior cavity surface absorptivity and emissivity for various cavity-to-aperture area ratios. The surface absorptivity and emissivity for oxidized stainless steel at 700 - 800°C are approximately 0.85 (Reference 3-18). For the 13.5 cavity-to-aperture area ratio of the baseline receiver, the effective cavity absorptivity and emissivity values are 0.987.

Figure 3-54 shows the collection efficiency of the baseline system as a function of the cavity-to-aperture area ratio. The collection efficiency increases with increasing area ratio due to the increase in the effective solar absorptivity of the cavity. For the baseline area ratio of 13.5, the collection efficiency for the system is 0.740.

A cavity receiver also benefits from the use of a selective absorber surface. For example, Figure 3-54 shows cavity performance for a selective coating with an $\alpha_s = 0.90$ and $\varepsilon_s = 0.10$. As shown, the maximum collection efficiency for this system is 0.769 and occurs at an area ratio of six. The decrease in collection efficiency for area ratios greater than six is due to the continuing increase of ε_{eff} whereas α_{eff} is nearly unity. The optimum area ratio will vary with receiver temperature and radiative coating properties. As stated earlier, the major problem is to achieve a stable coating at these very high temperatures.

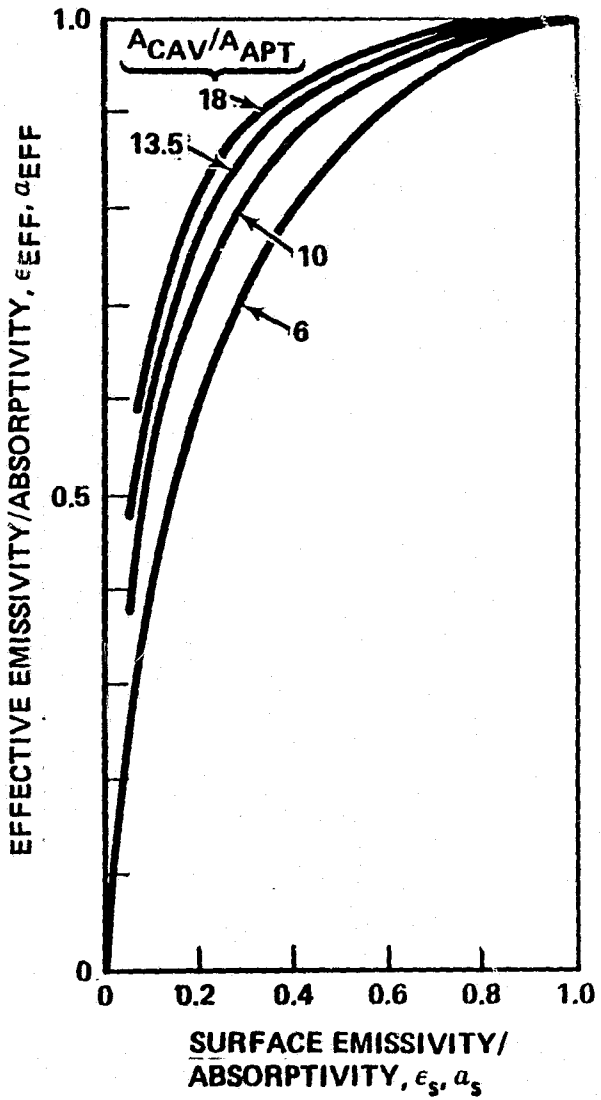

FIGURE 3-53. EFFECTIVE CAVITY ABSORPTIVITY/EMISSIVITY

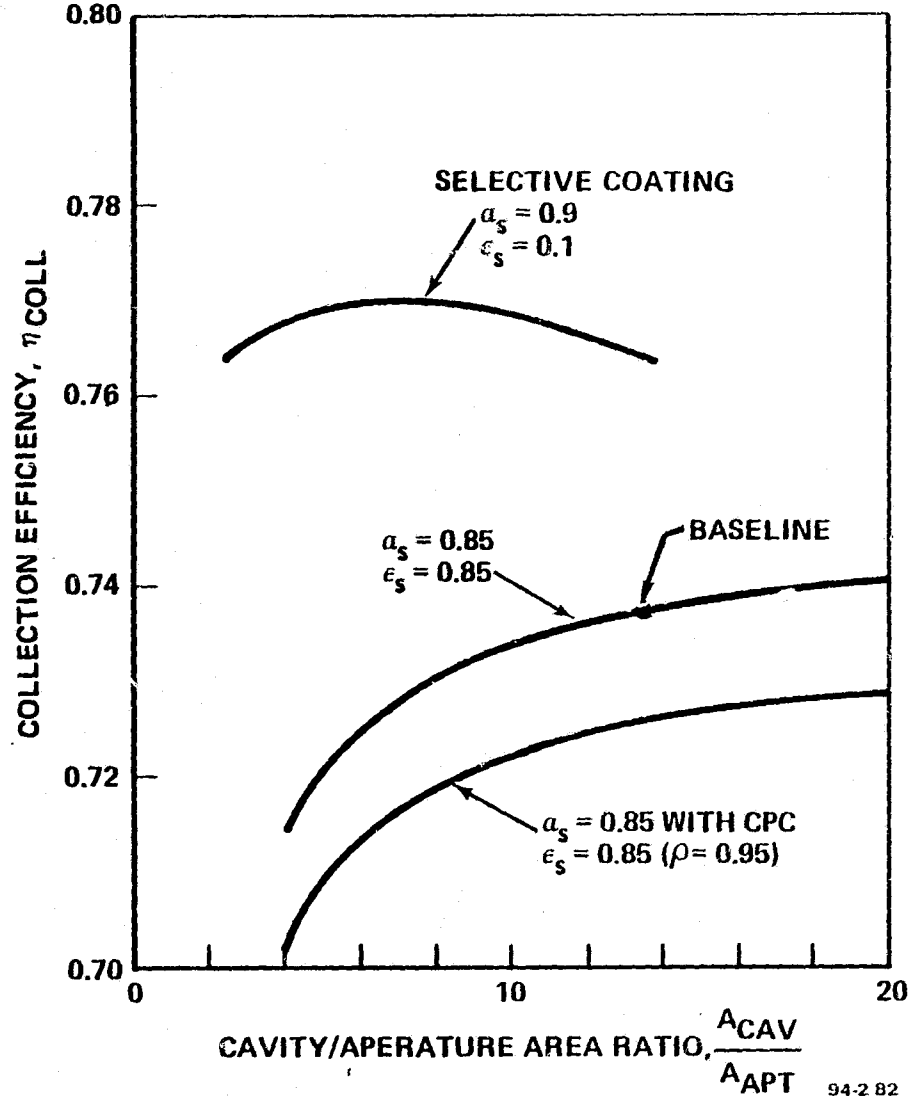

FIGURE 3-54. CAVITY PERFORMANCE

The use of a Compound Parabolic Concentrator (CPC) with the baseline cavity receiver was also investigated. The collection efficiency for the baseline system using a CPC as a second-stage "amplifier" was determined using the analyses presented in Reference 3-19. The results are shown in Figure 3.54 and demonstrate that a CPC is not of benefit to the baseline system since it actually reduced collection efficiency. The large rim angle of the primary parabolic dish results in a very short, large acceptance-angle CPC with a concentration ratio only slightly greater than unity. For CPC reflectivity ≤ 0.95, the slight gain in performance due to increased overall concentration is overcome by the thermal losses to the CPC surfaces.

b. Heat Transfer Fluid Selection. Sodium was selected for the heat transfer fluid of the baseline receiver/thermal transport subsystem. As shown in the following paragraphs, the use of a secondary heat transfer fluid (pool boiling sodium) in lieu of direct heating of the engine working fluid has many advantages. Both United Stirling and N. V. Philips (Holland) have successfully operated Stirling engines with sodium-heated heads for extended periods of time. Philips employed both pool-boiling natural convection heating and wicked heat pipes; USS has employed wicked heat pipes in a variety of attitudes. Both companies have recommended that we employ sodium for the solar-Stirling application.

(1) Direct Versus Indirect Heating. Figure 3-55 presents a comparison of typical boiling and gas-in-tube heat transfer rates. As shown, the boiling systems have much higher heat transfer rates than those of forced gas convection; less heat transfer surface area is required and lower temperature differentials between the surface and the working fluid are experienced. This is clearly shown in Figure 3-56, which compares various receivers on an equal power basis. Smaller heat transfer areas generally mean smaller, lighter and less expensive receivers. Lower temperature differentials mean that the receiver temperatures are closer to the engine temperatures, and overall system efficiency is increased.

(2) Sodium as Heat Transfer Fluid. An additional benefit of sodium is its low vapor pressure at high temperature. A low vapor pressure is desirable to minimize the structural loads on the receiver at the high steady-state operating temperatures (830°C). Figure 3-57 shows the vapor pressures of various heat transfer fluids as a function of temperature. Note that the vapor pressures of sodium and potassium are only about one atmosphere at steady-state conditions. The net pressure loading on the receiver is thus very low, with obvious safety advantages. Sodium was selected over potassium because there is much less corrosion of stainless steel and better heat transfer properties.

The peak heat flux (or burnout flux) capability of sodium operating in a pool boiling heat transfer mode is shown in Figure 3-58. The peak heat flux level is a function of saturation temperature (and pressure), a characteristic of most phase change fluids. For the baseline receiver

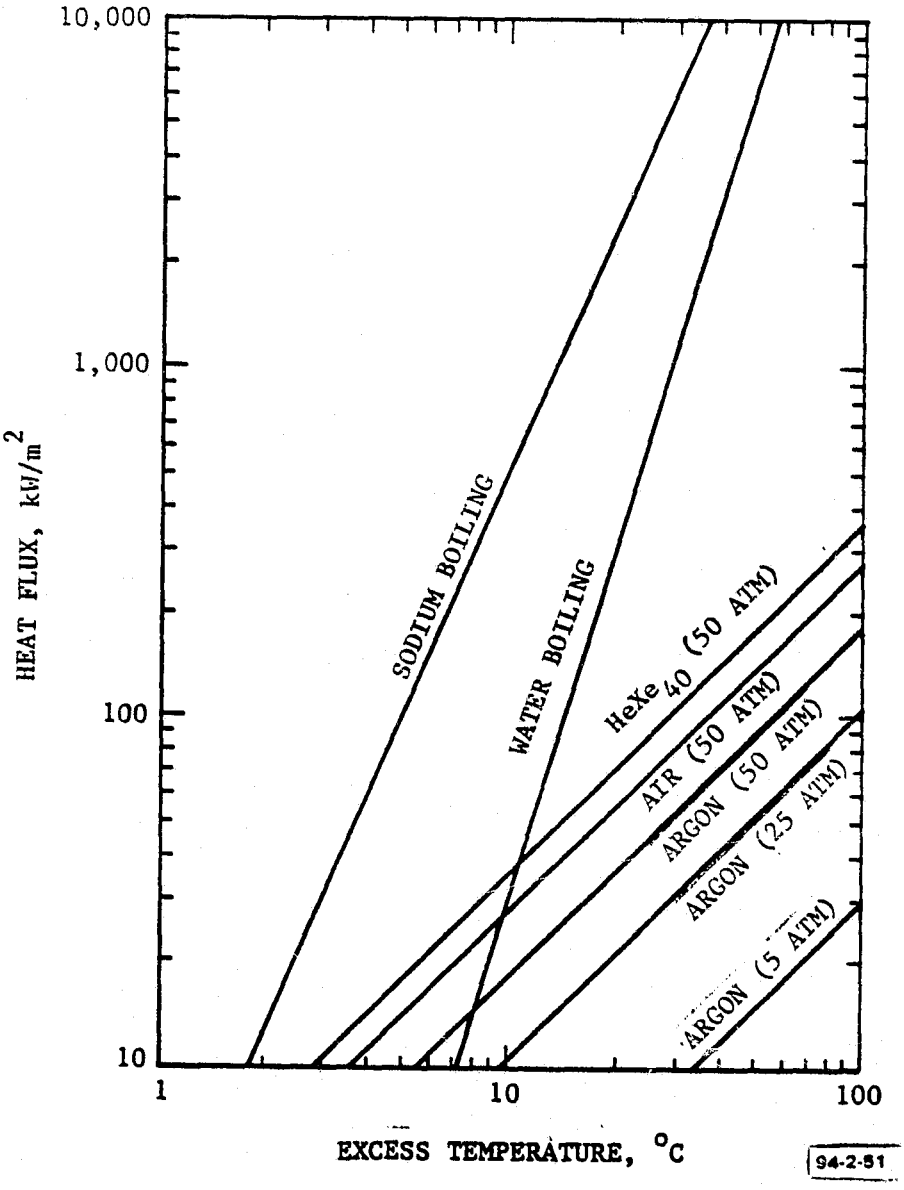

FIGURE 3-55. BOILING AND GAS-IN-TUBE HEAT TRANSFER

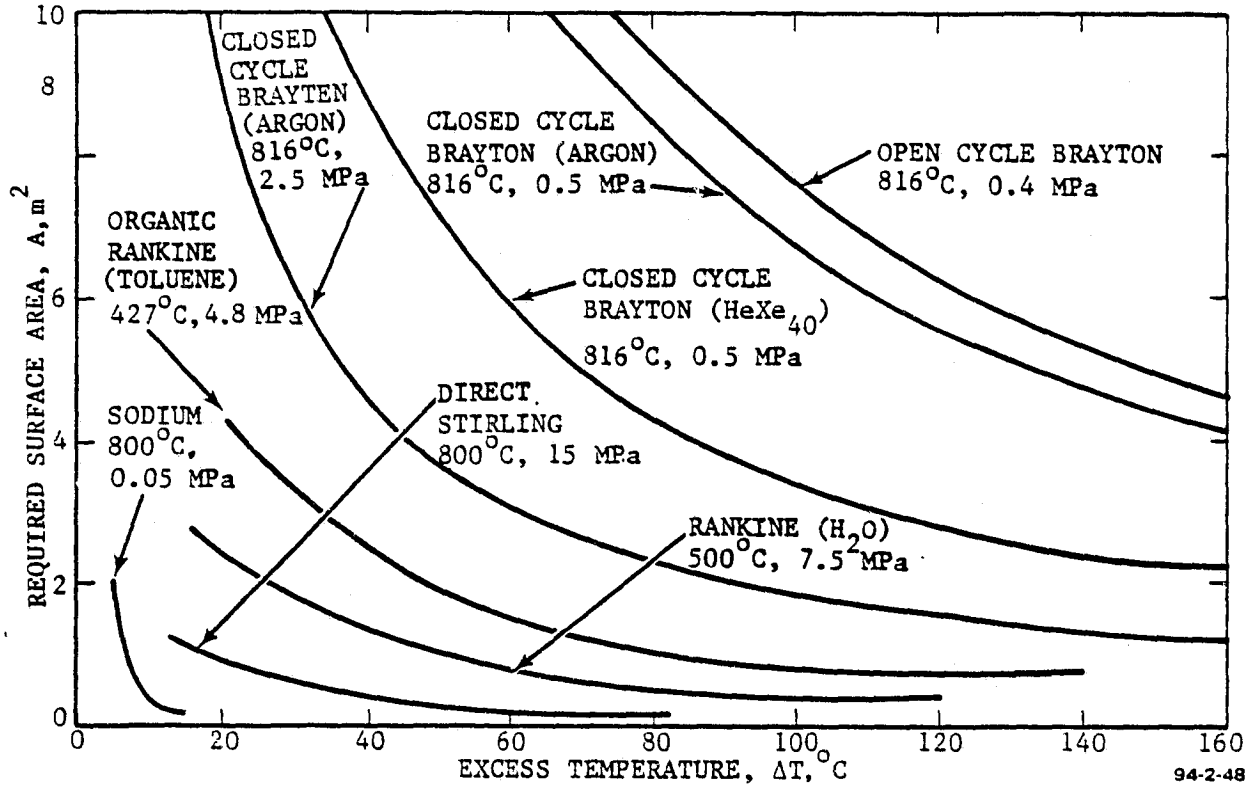

FIGURE 3-56. COMPARISON OF VARIOUS RECEIVERS FOR BRAYTON, RANKINE AND STIRLING ENGINES

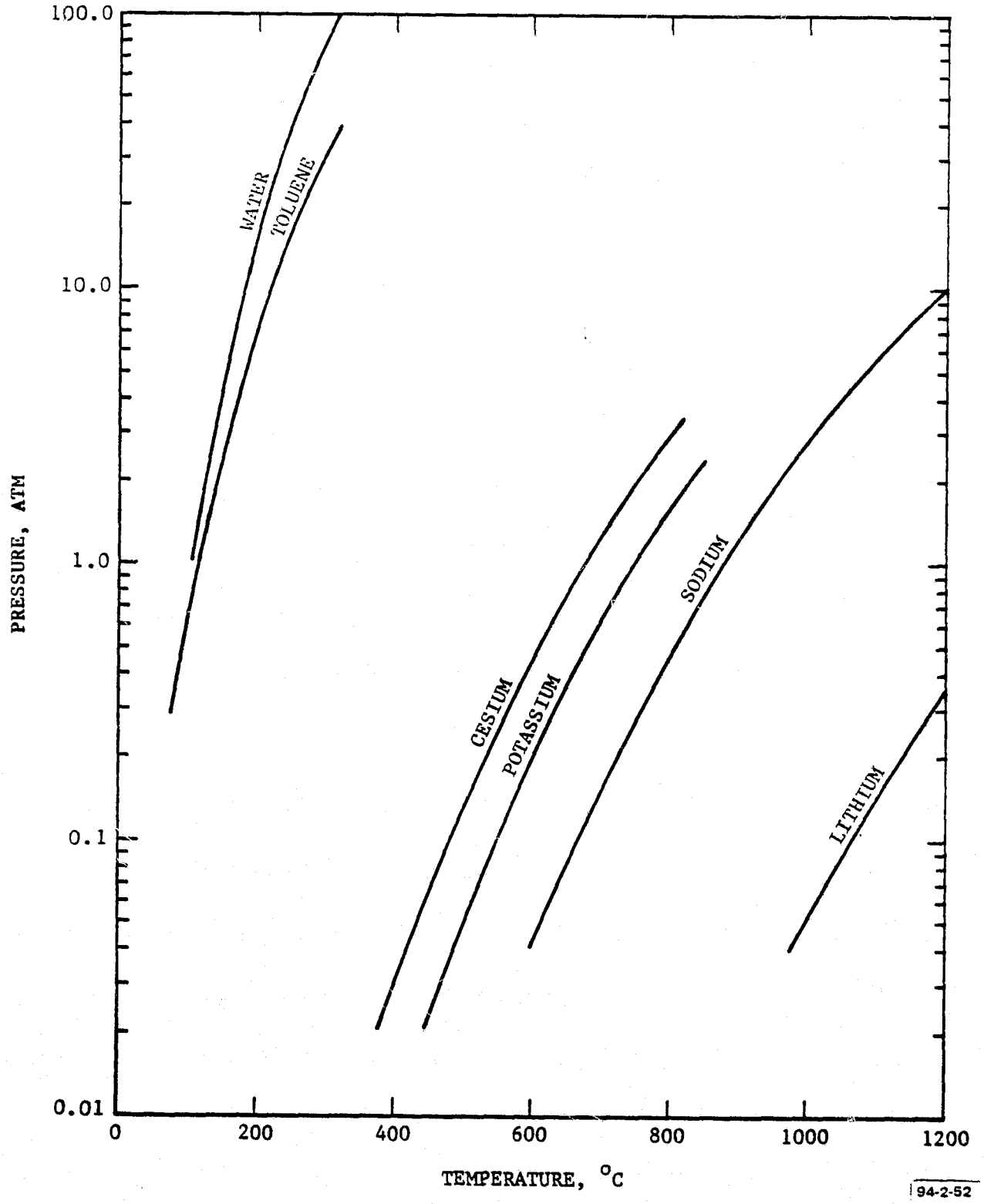

FIGURE 3-57. VAPOR PRESSURES FOR SEVERAL HEAT TRANSFER FLUIDS

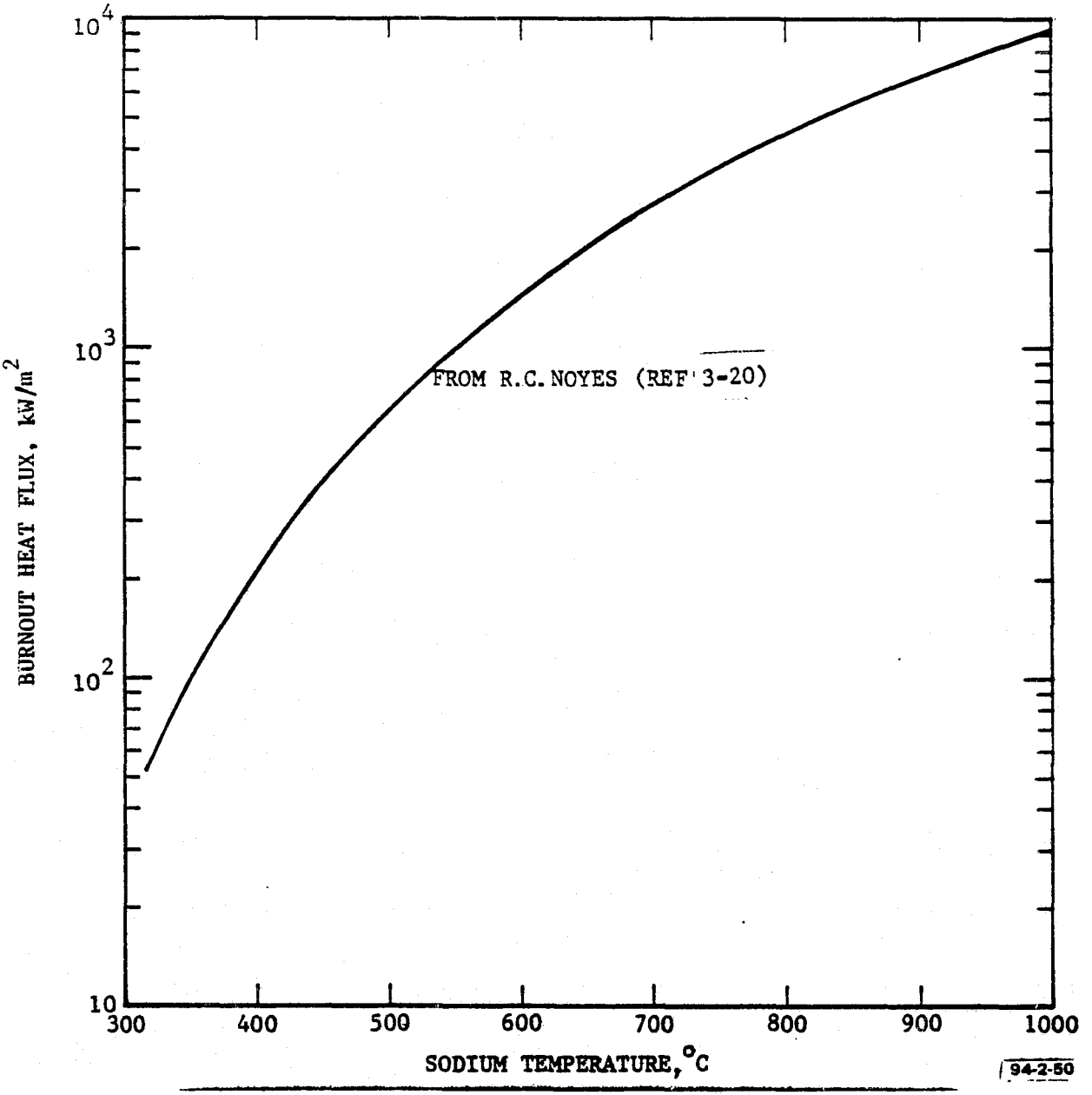

FIGURE 3-58. BURNOUT HEAT FLUX FOR SODIUM POOL BOILING

operating at steady-state conditions ($T_{POOL} \approx 800^{\circ}C$), the peak heat flux capability of sodium is approximately 4700 kW/m^2. This is about a factor of 12 greater than the worst case peak flux level of 400 kW/m^2 predicted for the cavity inner wall. The lowest operating temperature for the subsystem (during normal operating conditions) occurs during morning start-up. As presented later in this paragraph, the receiver pool is predicted to reach a minimum temperature of about $525^{\circ}C$ (after nightime cooldown). This corresponds to a peak heat flux capability of about 800 kW/m^2 or a safety factor greater than two. The receiver pool temperature, and thus the burnout safety factor quickly increase during the short start-up period. The start-up safety factor will actually be somewhat greater than presented above since the direct normal solar flux level is expected to be much less than the 1000 W/m^2 assumed here.

The use of sodium as a heat transport fluid has additional advantages. The high heat transfer rate of condensing sodium permits a substantial reduction in the number (and length) of the engine heater head tubes. This gives a gain in engine performance by reducing the dead volume of the heater head. In contrast, direct heating would require an increase in the surface area of the heater head tubes and requires careful cavity design to minimize the risk of tube wall burnout.

A pool boiling sodium heat transfer system was preferred to a heat pipe system for several reasons. Since the boiler is always below the condenser, gravity return can be used. In addition, vendor data indicates that the fabrication cost of a single two-shell boiler would be considerably less than a multitube heat pipe system. The boiling system is entirely passive as it does not require pumps or controls for operation. This also adds to the overall system reliability. The pool boiling system is flexible in the sense that additional buffer storage can be added to the receiver subsystem with minimal changes in configuration. For example, stainless steel cylinders containing a phase change salt can be added to the sodium pool by simply increasing the outer receiver wall diameter. An alternative is to simply increase the amount of sodium in the system.

c. Steady-State Operating Characteristics. This section presents the steady-state operating characteristics of the baseline receiver/thermal transport subsystem.

1. Heat Transfer Surface Area and Heating Rates. The required heat transfer surface area is determined primarily by the heat transfer capability of the fluid. For this study, the heat transfer rates of a pool boiling system were utilized since the heated walls are submerged below the free surface of the liquid. The baseline subsystem with a liquid sodium pool is expected to operate within the nucleate boiling regime. One widely-used correlation for sodium nucleate boiling is based upon the results of Noyes (Reference 3-20) and has the form:

$$(q/A)_{BOIL} = 2.259\ (\Delta T_{SAT})^{2.35}$$

where:

$(q/A)_{BOIL}$ = boiling heat flux, kW/m^2

$\Delta T_{SAT} = T_{WALL} - T_{FLUID}$ at saturated temperature, °C

This correlation indicates that the heat flux transferred to the fluid rises very rapidly with temperature, as shown in Figure 3-59. At rated conditions (P_{G_E} = 55.56 kW_e, $I_{d,n}$ = 800 W/m^2, T_∞ = 44.6°C), the USS P-75 Stirling engine operating at the baseline temperature (800°C) and speed (1800 rpm) requires 161.3 kW of thermal input. The baseline receiver has an internal surface area of approximately 1.33m^2 (14.31 ft^2). Thus, the average net flux level for the receiver is about 121.3 kW/m^2. From the nucleate boiling equations, the average temperature differential required between the receiver backface and sodium pool (film ΔT) is 5.4° C. For the worst-case peak wall flux of about 400 kW/m^2 the required temperature differential is only 9.1°C, ignoring the effects of lateral conduction. The nucleate boiling equation can also be expressed in terms of a boiling heat transfer coefficient and is simply

$$h_{BOILING} = 2.259\ (\Delta T_{SAT})^{1.35} \quad kW/m^2{}^\circ C$$

The average and maximum boiling heat transfer coefficients for the baseline receiver are therefore 22. $kW/m^2{}^\circ C$ and 44.5 $kW/m^2{}^\circ C$, respectively.

Much larger heat transfer rates are possible up to the "burnout point." However, this does not occur until $(q/A)_{max} \cong 4700\ kW/m^2$ for the steady-state conditions of the receiver. The possibility of burnout is very unlikely since the cavity diameter was sized to maintain the peak wall flux below a safe value (~400 kW/m^2). Both the boiling heat transfer coefficient and the burnout flux can be increased significantly by the use of a wick or grooved surfaces (as used in heat pipes). According to

Reference 3-16, the burnout flux can be increased by almost a factor of ten by this simple technique. However, the present safety factor of ~12 is more than sufficient for the present baseline subsystem. Thus, the added cost of wicking the boiler is not required.

Due to the exceptional heat transfer capability of pool-boiling sodium, the limiting resistance within the baseline receiver is the conduction through the receiver wall rather than the film resistance. The effective heat transfer "coefficient" for conduction can be written as

$$h_{COND} = \frac{(q/A)_{COND}}{\Delta T} = \frac{\bar{k}_{WALL}}{\Delta X} \quad ,kW/m^2\text{-}°C$$

where:

$\bar{k}_{WALL}$ = thermal conductivity of the wall at T_{WALL}, kW/m^2

ΔX = wall thickness, m

The baseline receiver has a 4.24 mm (0.167 inch) thick 316 stainless steel wall with a thermal conductivity of 0.0234 kW/m-°C (at 800°C). Thus, the average effective conduction heat transfer coefficient is 5.52 $kW/m^2°C$. This is one-quarter of the boiling heat transfer coefficient given above. The temperature gradients through the stainless steel wall for the average and worst peak flux cases are 22.0°C and 72.5°C, respectively. The gradient for the peak value is expected to be somewhat lower due to lateral conduction and reradiation effects.

The selected cavity surface area represents a careful balance between thermodynamic and structural requirements. Lowered surface area would result in a smaller receiver but cavity flux levels would increase together with wall temperature gradients and thermal stresses. Increased cost would result through necessary use of higher-strength steel.

Increased surface area would encounter increased membrane stresses and associated higher wall gradients despite lowered flux levels. Increased cost and weight would result.

2. Subsystem Temperature and Pressure Gradients. Figure 3-60 presents the temperature gradients throughout the receiver/thermal transport subsystem. The largest temperature drop (22°C) occurs through the stainless steel receiver wall. The backface wall-to-sodium pool temperature differential was previously shown to be about 5°C. The temperature drop through the vapor pipe is approximately 3 to 4°C, due to a pressure difference between the receiver pool and engine heater head. A 5°C temperature drop is also predicted for the condensation heat transfer to the Stirling engine heater tubes. The receiver surface-to-engine heater head temperature drop is thus approximately 30°C.

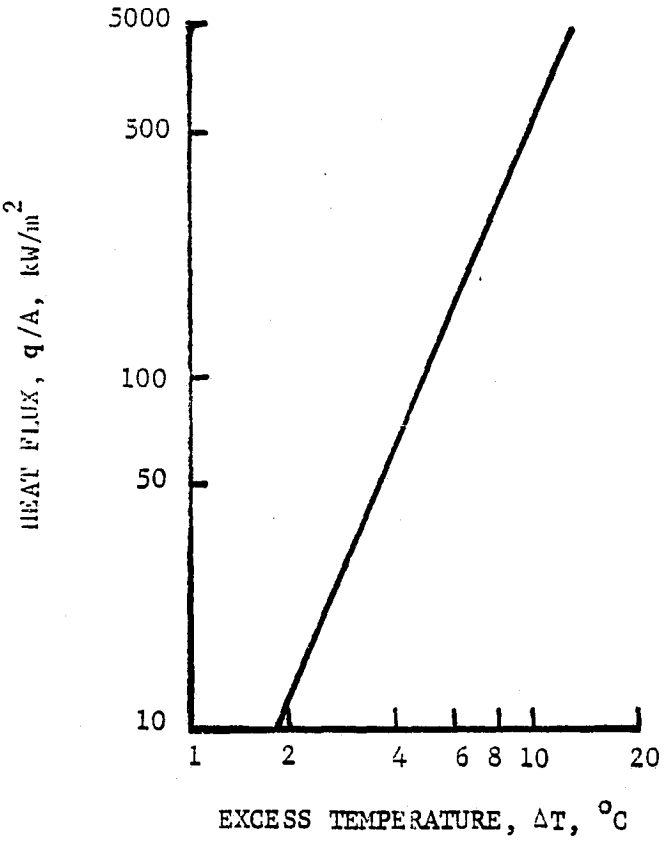

FIGURE 3-59. SODIUM BOILING HEAT FLUX

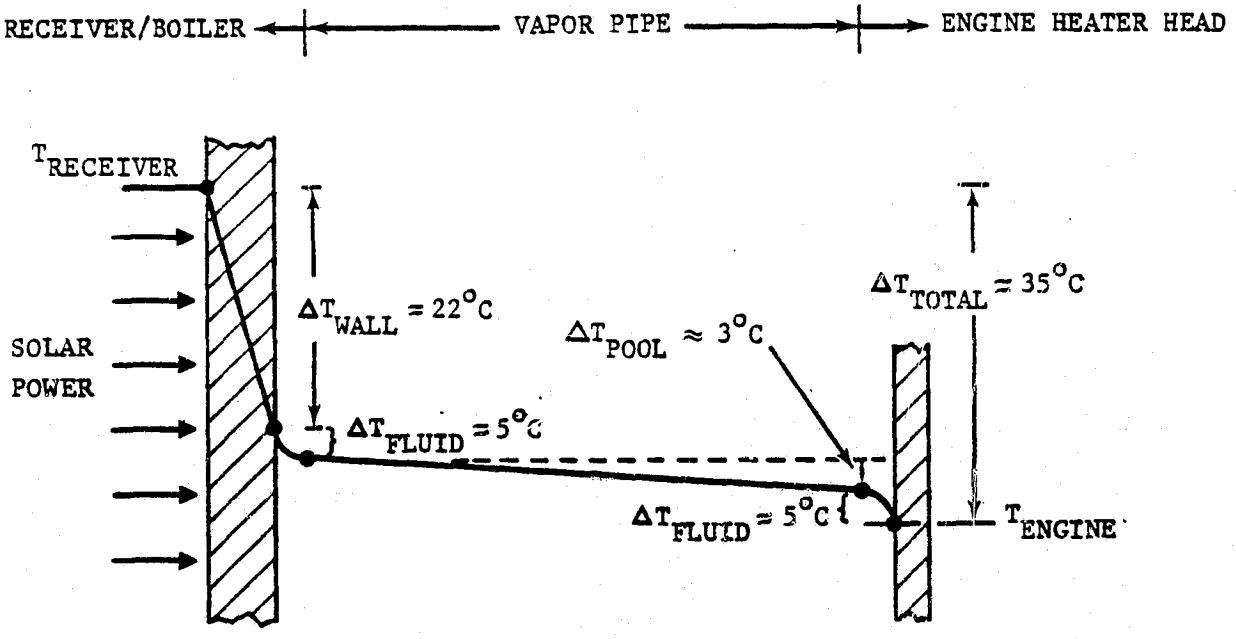

FIGURE 3-60. RECEIVER/THERMAL TRANSPORT SUBSYSTEM TEMPERATURE GRADIENTS

94-2-47

The temperature gradients throughout the rest of the receiver/thermal transport subsystem, including the outer receiver wall, are negligible. This is a result of very little heat transfer occurring elsewhere within the subsystem, and because the subsystem is operating in a saturated state. For example, the latent heat of vaporization of sodium is quite high (for instance, at 800°C, ΔH_v = 3873 J/g); thus, any small amount of heat loss results in a small amount of sodium condensation rather than in a temperature differential. The receiver/thermal transport subsystem is thus virtually isothermal. The thermal stresses and therefore structural requirements of the subsystem are maintained at low levels with this design.

The short pipe which connects the receiver pool to the engine heater head has the dual function of vapor transport and condensate return. The subsystem operates equally well at all operating conditions (i.e., from start-up to high noon to shutdown). The vapor pipe was sized to prevent choked flow from occurring at steady-state conditions in addition to minimizing the temperature and pressure drops. The sodium vapor flow Mach number for several vapor pipe diameters is presented as a function of engine head temperature at rated power operation in Figure 3- 61. For a given pipe diameter, the vapor Mach number quickly increases as the engine head temperature decreases. This is a result of the rapid vapor pressure reduction with temperature (See Figure 3-57) and the associated rapid reduction in vapor density. The Mach number of the sodium vapor can be reduced by increasing the vapor pipe diameter. For the baseline 7.62 mm (3 inch) vapor pipe the Mach number is approximately 0.10 at rated conditions. Since the system control scheme precludes engine rated power operation below 800°C, there is no danger of choked flow occurring in the vapor pipe.

The minimum elevation angle during system operation is approximately 10°, and occurs during morning start-up and evening shutdown. The vapor pipe has been inclined an additional 10° to assist the gravity return of the sodium condensate. The condensate return will form a 0.13 mm (0.005 inch) liquid film on the vapor pipe wall at rated power operation. The shear forces from the vapor to the liquid are small due to the relatively low vapor velocities, so the vapor flow is not expected to impede the condensate return to the boiler.

Figure 3-62 presents the operating pressures and pressure drops for the receiver/thermal transport subsystem as a function of engine head temperature. The pressure drops through the subsystem increase as the engine head temperature decreases. This is a result of the vapor velocity within the subsystem increasing as previously shown in Figure 3- 61. The pressure drop terms are defined as follows.

ΔP_{VISC} = viscous (or friction) losses through vapor pipe.

ΔP_{EXP} = expansion loss at vapor pipe-heater head interface.

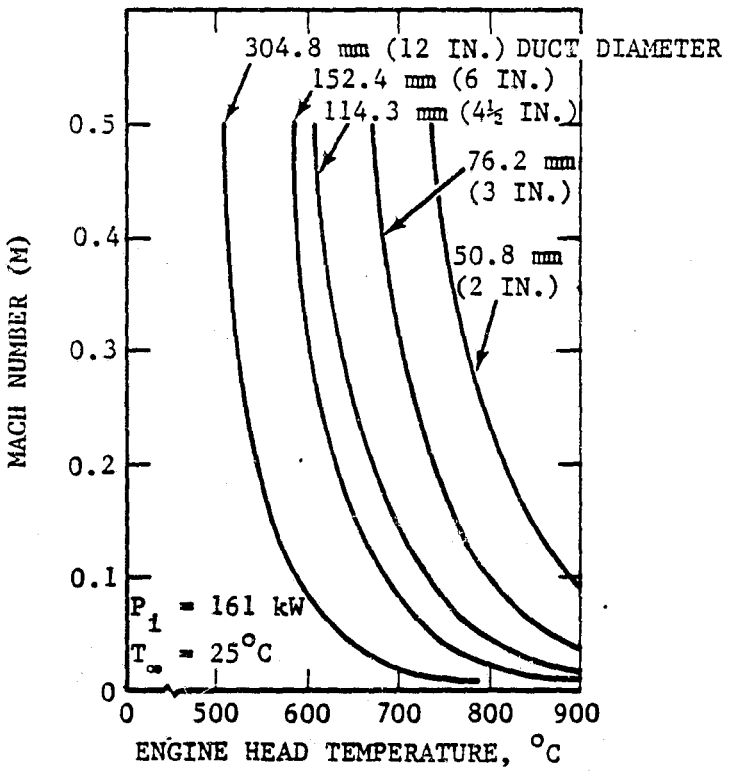

3-61. SODIUM VAPOR MACH NUMBER AT RATED POWER

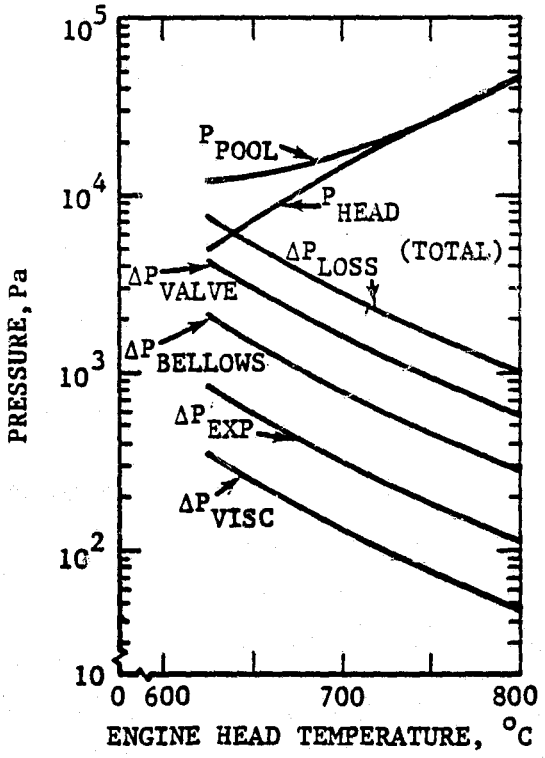

FIGURE 3-62. RECEIVER/THERMAL TRANSPORT SUBSYSTEM OPERATING PRESSURES AND PRESSURE DROPS

ΔP_{VALVE} = dynamic loss through the valve.

$\Delta P_{BELLOWS}$ = dynamic loss through the bellows.

The pressure difference between the receiver pool and the engine heater head increases as the subsystem temperature decreases. This is a result of the absolute pressure of the saturated subsystem decreasing with temperature, while the pressure losses increase. This pool-to-head pressure differential also causes a large temperature differential to occur between the pool and engine heater head.

The receiver pool-to-engine head temperature differentials are presented in Figure 3-63 as a function of head temperature and engine input power. For a given receiver output power (engine input power) the temperature differential increases with decreasing engine head temperature. Alternately, for a constant engine head temperature, the pool-to-head temperature differential will increase with increasing subsystem output power. The effect of increasing the vapor pipe diameter is to shift the power curves to the left, decreasing the pool-to-head temperature differential. The temperature differential for the baseline system is approximately 3 to 4°C.

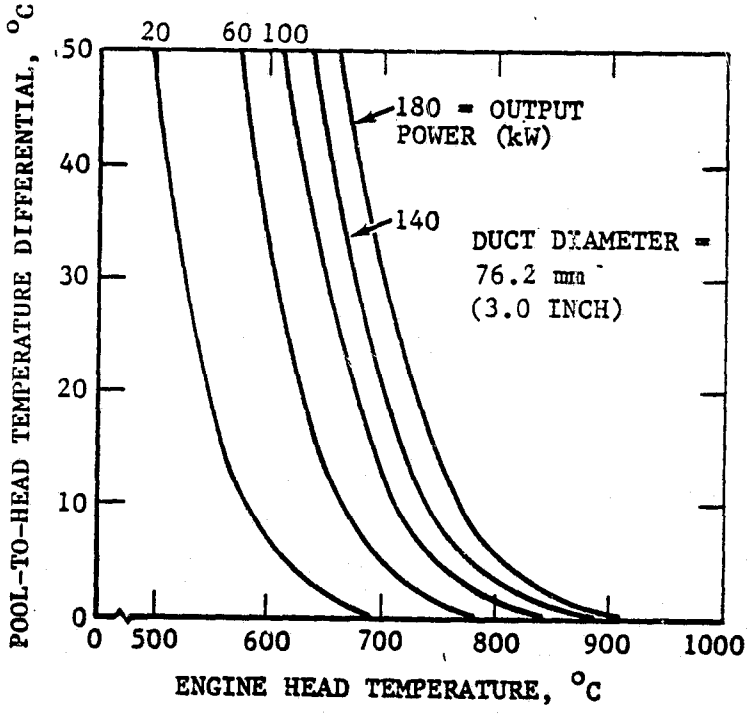

94-2-105

FIGURE 3-63. RECEIVER POOL-TO-ENGINE HEAD TEMPERATURE DIFFERENTIALS

3. Receiver Efficiency. The efficiency of the baseline receiver at rated power conditions is 89.2 percent. The receiver efficiency can be expressed as

$$\eta_{RCVR} = (Q_{SOLAR} - Q_{ENG})/Q_{SOLAR}$$

where:

Q_{SOLAR} = Total solar power leaving the concentrator at rated conditions ($I_{d,n}$ = 800 W/m^2).

Q_{ENG} = Net thermal power delivered to the engine (Q_{SOLAR} - Q_{LOSSES}).

Q_{LOSSES} = Total thermal losses from the receiver (including spillage).

For the baseline system, the Q_{SOLAR} delivered to the receiver is approximately 181 kW, Q_{ENG} = 161.3 kW, and Q_{LOSSES} = 19.7 kW.

4. Thermal Losses. Table 3.16 summarizes the calculated heat losses for the receiver/thermal transport subsystem.

TABLE 3.16: THERMAL LOSSES FROM THE BASELINE RECEIVER

Loss Due To:	Equation	kW	Btu/HR	Percent of Incoming Flux
Reflection	$Q_{Ref} = (1 - \alpha_{EFF})Q_{Solar}$	3.37	11500.	1.86
Spillage	$Q_{Spill} = (1 - \gamma)\ Q_{Solar}$	2.20	7510.	1.22
Reradiation	$Q_{RR} = \varepsilon_{EFF}\sigma A_{APT}(T_R^4 - T_\infty^4)$	11.51	39270.	6.36
Convection	$Q_{Conv} = h_c A_{APT}\ (T_R - T_\infty)$	1.76	6010.	0.97
Conduction	$Q_{Cond} = kA(T_P - T_\infty)/\Delta X$	0.82	2800.	0.45
Total		19.66	67090.	10.86%

where:

α_{EFF} = Effective absorptivity of the receiver cavity. (0.987)

γ = Intercept factor. (0.981)

ε_{EFF} = Effective emissivity of the receiver cavity. (0.987)

σ = Stefan-Boltzmann constant.

A_{APT} = $(\pi/4)D^2_{APT}$ = Area of the aperature. (0.1399m^2)

h_c = Effective cavity heat transfer coefficient. (0.016 kW/m^2-°C) (Average of values from the correlations of References 3-21 and 3-22 for a mean external wind velocity of 4.6 m/sec over the face of the cavity.*)

k = Mean thermal conductivity of the insulation**. (7×10^{-5} to 8×10^{-5} kW/m-°C)

A = Characteristic area for the various portions of the receiver/thermal transport; i.e., disc, cylinder, hemi-sphere and frustum.

ΔX = Insulation thickness. (20.3 cm)

T_R = Receiver cavity temperature.

T_P = Receiver pool temperature.

T_∞ = Ambient temperature.

5. Receiver Face Protection. A maximum equilibrium surface temperature of approximately 900°C is predicted for the inner radius of graphite protective ring located on the receiver face. This corresponds to the peak flux spillage that occurs just outside of the receiver aperture. The largest single loss in the subsystem is reradiation as it accounts for 60 percent of the total thermal losses at rated conditions. Reradiation accounts for 82 percent of the total non-operating thermal losses for an open receiver aperture during nighttime or inclement weather conditions. The baseline system incorporates a movable lid to reduce these losses. The use of an insulated lid (or door) is very effective in reducing reradiation and convective losses to negligible levels. The conduction loss through the closed lid is approximately 0.10 kW at the 830°C steady-state operating temperature. The use of a lid reduces the losses during nighttime or inclement periods by approximately 13.17 kW or 95.5 percent. Closing the receiver lid will therefore permit greatly extended on-line operation at idle power. This precludes the necessity of re-synchronizing to the grid with the passage of each cloud. The use of the receiver lid will obviously lengthen the cooldown period and therefore reduce the associated warm-up period when solar power returns.

*The mean wind velocity of 4.6 m/sec (10.3 mph) is based on the 15 minute Barstow data of 1976, and on extensive British measurements (Reference 3-23).
**See Appendix J for thermal and cost data for insulation.

d. Transient Operating Characteristics of Baseline System. An in-depth transient analysis of the receiver/thermal transport subsystem was necessary in view of the inherent non-steady nature of the solar flux. The objective was to characterize the behavior of the subsystem for all operational modes encountered in a solar application. The results demonstrate that the transient performance of the subsystem is stable, well behaved, and has long thermal time constants.

1. Transient Thermal Model. The transient thermal model was developed from the basic equations for conservation of mass, conservation of energy, the equation of state for vapor, and the vapor pressure equation. It is assumed that the sodium vapor is saturated (vapor and liquid in quasiequilibrium), the vapor volume is approximately constant and that the receiver orientation effects are negligible. The energy balance considered the incoming solar power, the thermal power to the engine, and the thermal losses from the subsystem. Pressure drops throughout the entire transport subsystem were also included. The basic equations listed above were reformulated into the following two differential equations.

$$\frac{dT_{POOL}}{dt} = \frac{(Q_{SOLAR} - Q_{RR} - Q_{CONV} - Q_{CONDP} - Q_{TRANS})}{C_{SODIUM} + C_{STRUCTURE} + C_{SALT}}$$

$$\frac{dT_{HEAD}}{dt} = \frac{(Q_{TRANS} - Q_{CONDH} - Q_{ENG})}{C_{HEAD}}$$

These equations were solved in a computer code developed for this program (RCVRTRNS), using a Runge-Kutta technique for numerical solution of simultaneous first-order differential equations with variable time steps. The model also incorporated variable thermal properties and accounted for various engine, receiver lid, and vapor valve control options. A detailed description of the transient thermal model is given in Appendix L.

2. Results. Transient results are presented in this section for the baseline receiver/thermal transport subsystem with the Stirling engine operating at the baseline 1800 rpm condition. Both normal and inclement operating conditions have been analyzed. Detailed results are presented for the normal start-up condition, while only the salient results are provided for all other conditions. Appendix L presents detailed results for all operating conditions.

The terminology used in this section is defined as follows: "Idle", "rated" and "equilibrium" power refer to the Stirling engine shaft output power level.

"Idle" power is the low power necessary to stay "on-line".

"Rated" power refers to the power required per engine for the system to generate rated electrical power (1 MW_e) at rated solar conditions ($I_{d,n}$ = 800W/m^2, T_∞ = 44.6°C).

"Equilibrium" power is the power level required by the engine controller to maintain the steady-state head temperature.

"Buffer storage" refers to thermal storage added to the subsystem, and therefore adds to the inherent thermal capacitance of the subsystem.

• NORMAL START-UP. Figure 3-64 presents the subsystem temperature response and engine output power during a normal start-up condition. The solar input power profile is based on the 15 minute Barstow Solar insolation data for a typical uncloudy day and includes the effects of both concentrator size and efficiency, thus representing the total power entering the receiver. This solar profile has been used for all start-up cases to facilitate direct comparison between them. In the morning, after normal operation from the previous day and nighttime cool down, the receiver sodium pool temperature is predicted to be approximately 525°C with the engine head at approximately ambient temperature. The receiver lid and vapor valve are opened prior to focusing on the sun. Once the sun is "on", the pool and head temperatures rapidly increase towards the steady-state operating level. The receiver wall temperature is an average of 22°C higher than the pool temperature during the start-up period. The pool and head pressures correspond to the saturated sodium vapor pressure at the respective temperatures. The temperatures, pressures, and vapor mass flow rate increase as the solar energy continues to enter the system. After about 3 minutes the engine head temperature has reached the predetermined start temperature of 450°C. The engine is then started and operated at a low or "idle" power level consistent with a previously selected helium mean working pressure ($\overline{P}$) for idle conditions (2.5 MPa for the present analysis). After approximately 8 minutes the engine head reaches the steady-state operating temperature (800°C) and the engine head temperature control mode is activated. At this point the temperature contoller moves the power valve to bring the engine $\overline{P}$ up (and hence the torque level) to an "equilibrium" power level. The power valve is then modulated to maintain the engine head temperature within the control band as the solar flux varies during the day. Appendix E presents a detailed discussion of the solar-Stirling engine control scheme.

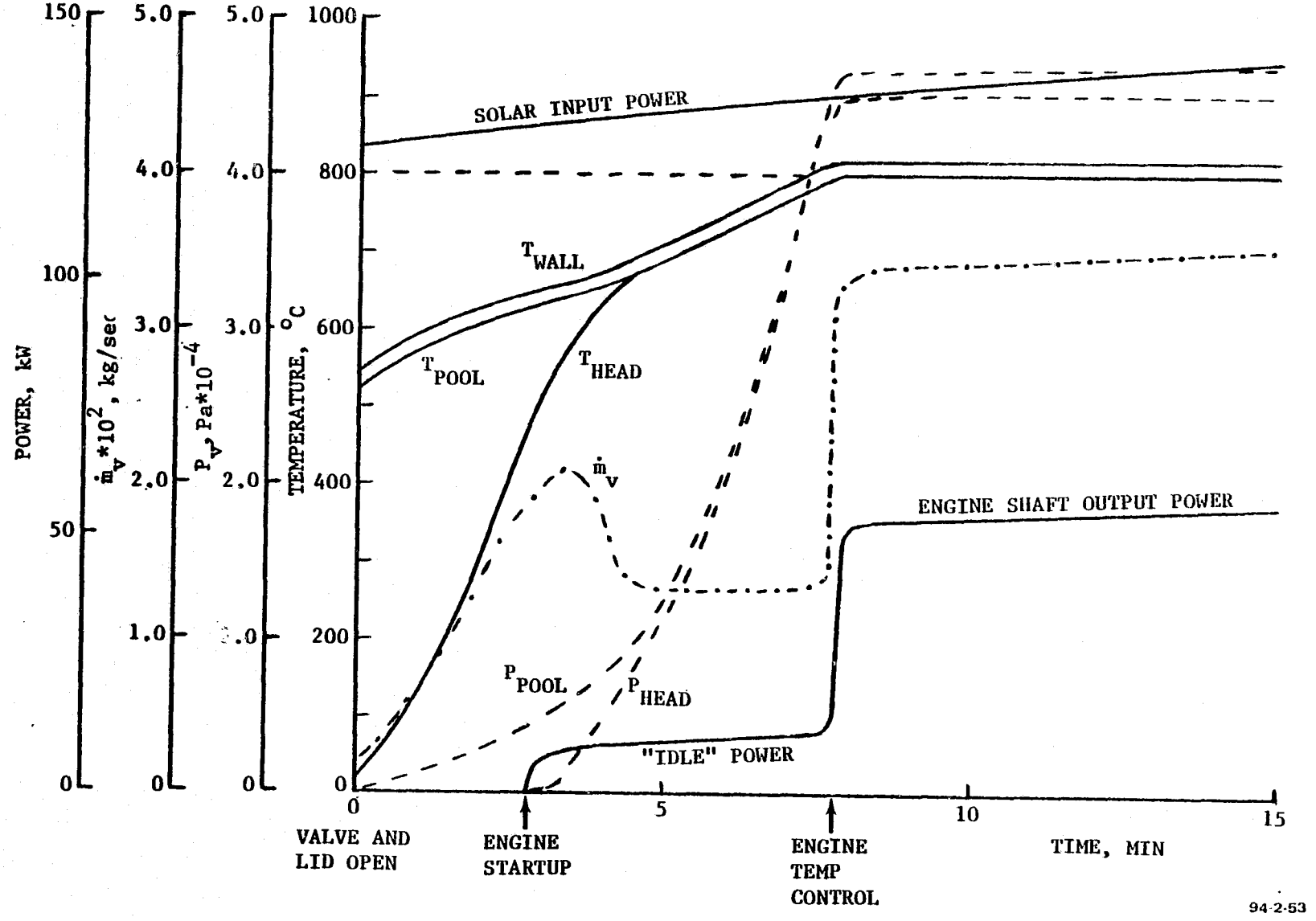

FIGURE 3-64. SUBSYSTEM RESPONSE DURING NORMAL START UP

• START-UP WITH FROZEN POOL. Start-up with a frozen sodium pool can occur after extended "bad" weather conditions or during the initial start-up. No problems are expected during the melt period based upon the extensive work by N. V. Phillips (Reference 3-24). However, at temperatures below approximately 450°C, the peak flux capability of sodium may be below the peak level within the receiver as shown previously. Thus, direct heating with the sun for warm-up below this level is not recommended. Nichrome heater wires can be placed between the outer receiver wall and the insulation, and current passed through the wires to slowly melt and heat the entire sodium pool before the receiver is exposed to the sun. This method requires approximately 15 kW-hours of electrical energy to raise the receiver temperature from ambient to a level above the recommended lower operating temperature. From this point on the start-up procedure is identical to that of a normal start-up.

• NORMAL START-UP WITH BUFFER STORAGE. Normal start-up to "idle" power requires approximately four minutes for the subsystem with 100 kg of buffer storage. The additional time required to reach "equilibrium" power (and to melt all of the salt) is a function of the salt melt temperature and mass.

• NORMAL SHUTDOWN. The engine was assumed to operate at the steady-state temperature and at any "equilibrium" power level above "idle" until the incoming solar power drops to zero. At this time the receiver lid and vapor valve are closed to maintain subsystem temperature. The pool will drop to 590°C during a 12 hour nighttime period and 550°C during a long 16 hour night. (To account for cold nights, all normal start-up temperatures were assumed to be 525°C.) The engine could also have been operated for approximately 15 minutes in the evening at "idle" power from the inherent thermal capacitance of the subsystem. However, no significant power is obtained and the pool temperature is quickly lowered to approximately 540°C. The receiver pool temperature would slowly reduce to 430°C during the subsequent 12 hours of non-operation. This low pool temperature would then require a short electrical warm-up period in the morning to preclude peak flux limitations. Thus, the former operating sequence is preferred. If the receiver lid remains closed during extended "bad" weather conditions, the pool temperature is predicted to stay above freezing in excess of three days. With the receiver lid open the pool temperature drops to the sodium freeze temperature in about sixteen hours.

• CLOUD PASSAGE. The same solar input power profile (based upon the Barstow insolation data) has been used for all cloud passage cases to facilitate direct comparison between the various cases. Steady-state temperatures and "equilibrium" power conditions are assumed to exist prior to the onset of cloud passage. Cloud passage was assumed to start at 11:00 A.M. for all cases investigated. Figure 3-65 presents the baseline subsystem temperature response to a

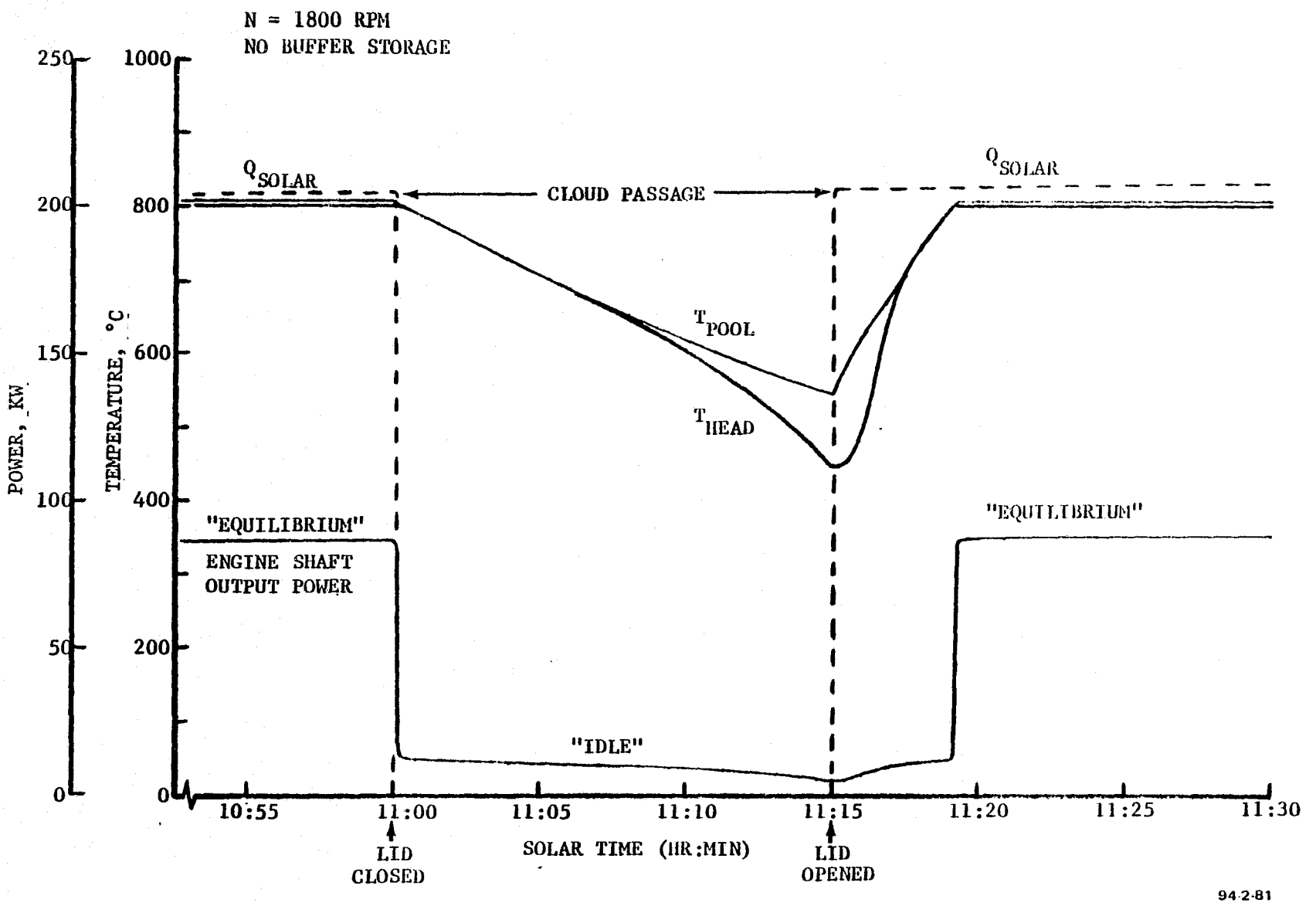

FIGURE 3-65. SUBSYSTEM TEMPERATURE RESPONSE TO A 15-MINUTE CLOUD PASSAGE

fifteen minute cloud passage. As the cloud starts its passage, the solar input power goes to zero, the receiver lid closes and the subsystem temperatures start to decrease. The helium working fluid pressure ($\bar{P}$) will decrease until the preselected minimum value is reached resulting in engine operation at a low or "idle" power level. During cloud passage the receiver pool and engine head temperatures decrease while the engine "idle" power remains relatively constant. When the cloud has passed, the solar power returns and the receiver lid is opened allowing the pool and head temperatures to increase. Approximately four minutes is required to heat the subsystem back up to the steady-state operating temperature and return to the "equilibrium" power level. The reheat time in this case is one minute less than for the previously presented normal start-up time because the solar input power is greater for this mid-day case. Thus, a fifteen minute cloud passage causes the baseline system to operate at "idle" (and minimum "on-line") conditions for only nineteen minutes before normal conditions are resumed.

Operating during longer periods of cloud passage was also investigated. Since the baseline system will stay "on-line" during a fifteen minute cloud passage without adding buffer storage, shorter inclement periods were not of concern. As shown later, the addition of a phase change eutectic salt, such as $75NaF/25MgF_2$, is an excellent method for adding buffer storage. For example, adding 100 kg of eutectic salt to the sodium pool will permit approximately one hour of operation at the "idle" output power ($\sim$1 kW shaft) required to stay "on-line". Operating at "rated" power conditions is also possible. By adding 250 kg of eutectic salt to the system, approximately 15 minutes of "rated" power operation can be obtained from the latent heat of fusion.

• EMERGENCY OPERATION. The receiver wall temperature increases approximately 65°C per minute for the baseline subsystem during an emergency operation in which the engine load suddenly drops to zero. This temperature rate is sufficiently slow to permit defocusing before damage to the receiver can occur. The emergency slew rate of 5 degrees per minute requires approximately 37 seconds to defocus from the redeiver aperture and just over one minute to completely defocus from the receiver lip. The aperture flux profile used to determine the transient lip heating is presented in Figure 3-66. The predicted peak flux level of approximately 10,000 kW/m^2 (10,000 suns) requires the use of a material with a farily high thermal conductivity that can operate at high temperature, and has a good resistance to thermal shock. The surface temperatures of low thermal conductivity materials (for example, many ceramics) would rise very rapidly to the melt values in this environment. An inexpensive, grade of graphite material will work well for this application since the receiver lip is used only for protection (it has no applied loading). The surface of a 25.4mm (1.0 inch) thick slab of graphite will reach a worst case maximum temperature of approximately 2230°C about three seconds after the peak portion of the flux

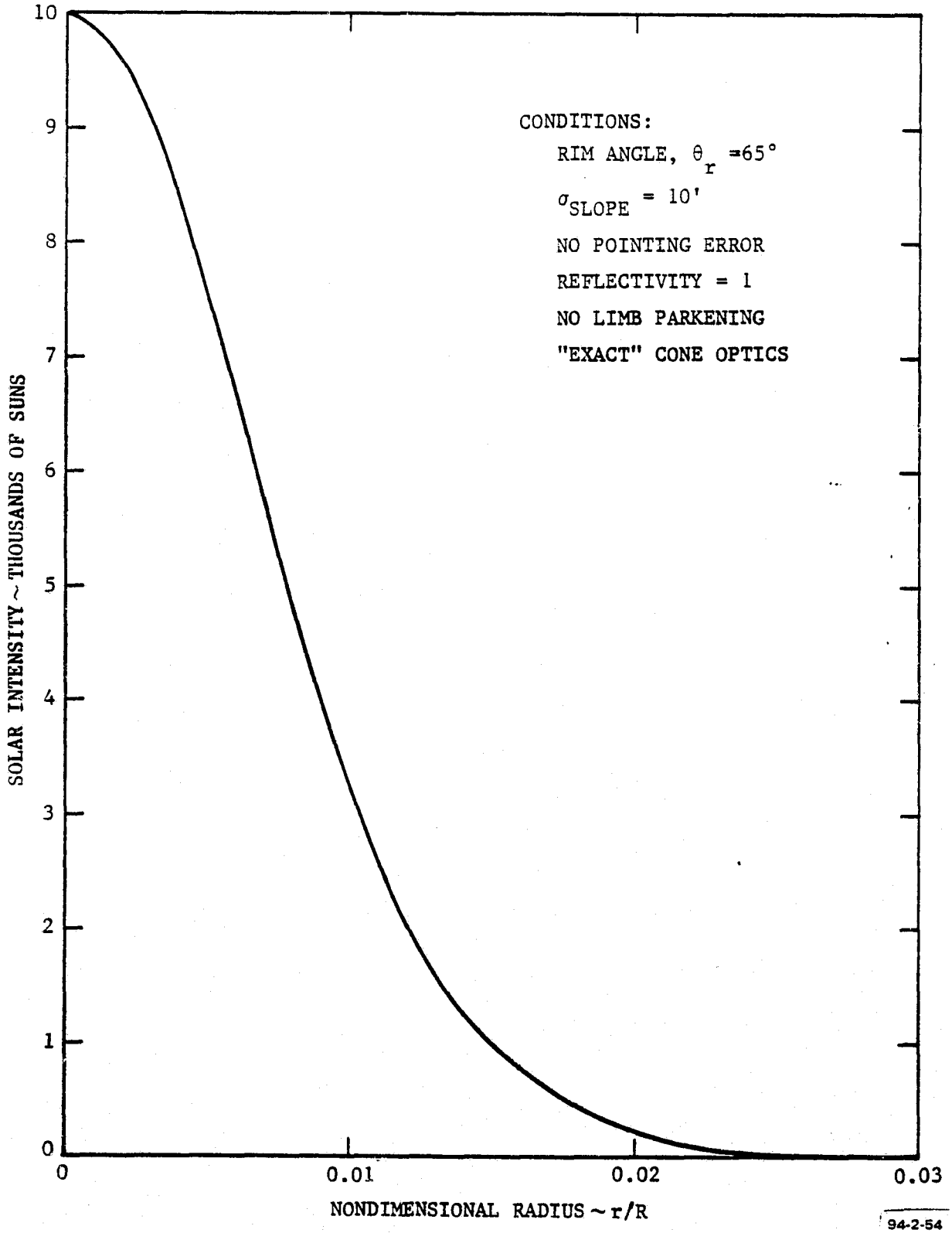

FIGURE 3-66. TYPICAL FLUX PROFILE AT THE FOCAL PLANE

distribution has passed. The backface temperature of the protective ring reaches a maximum of approximately 950°C as a result of conduction. If required, the lip temperatures can be restricted to lower values by using a thicker graphite slab.

e. Buffer Storage. The term "buffer storage" refers to thermal storage added to the receiver/thermal transport subsystem, and is therefore in addition to the inherent thermal capacitance of the subsystem. The primary purpose of buffer storage is to maintain "rated" power during moderate cloud passages. In addition, buffer storage may be used to produce minimal power to stay "on-line". This avoids having to re-synchronize a multi-engine system every time a solar dropout occurs. It is our understanding that buffer storage is not required for power leveling in a grid-connected system since the power utility companies will accept any amount of power delivered from a small solar plant. Also it is not required for engine life since the present USS Stirling engines are designed for automotive applications in which much more frequent (and rapid) transient cases are encountered.

1. Available Materials and Comparison. It is desirable to maintain a temperature near the steady-state operating temperature since the Stirling engine operates less efficiently at lower head temperatures (Reference 3-25). In addition, engine operation cannot continue at a "rated" output power level for temperatures below about 500-600°C because choked flow conditions will occur in the vapor pipe. Thus, thermal storage materials with a phase change near the steady-state operating temperature are preferred to sensible heat store materials. Appendix K presents a comparison of various eutectic salt materials for use as buffer storage. These materials can effectively maintain efficient engine operation during moderate solar drop-out periods by giving up their stored heat during a constant temperature liquid to solid phase change. The eutectic salt would be encapsulated within long, slender, thin-wall stainless steel containers which are placed within the sodium-filled annulus of the receiver. (A high surface area to volume ratio is desirable for the salt containers to minimize temperature drops within the salt.) The salts are melted ("charged") during normal insolation conditions. During inclement periods, the salt freezes, releasing the latent heat of fusion to the sodium pool. This heat would then become the source to continue the boiling process and vapor transport to the engine heater head.

2. Buffer Storage Performance. The analyses of Appendix K and Reference 3-26 suggests NaF/MgF_2 eutectic salt as being an excellent candidate for thermal storage. A $75NaF/25MgF_2$ eutectic salt has been used for the present performance analyses. The effects of adding the eutectic salt thermal buffer storage are presented in Figure 3-67 and 3-68. These two figures are based upon the analyses of Appendix L.

Figure 3-67 presents the sodium temperature response during engine operation at "rated" and "idle" conditions. Operation was for a subsystem with and without buffer storage as well as for an open and closed receiver lid. The effect of closing the lid is negligible during "rated" power operation since heat lost by radiation and convection out the receiver aperture is small compared to the energy removed by the engine. However, with the engine operating at "idle" power, the re-radiation and convection losses are very significant. For example, by simply closing the receiver lid during "idle" conditions, engine operation at 800°C with 100 kg of buffer storage can be extended from 33 minutes to 60 minutes.

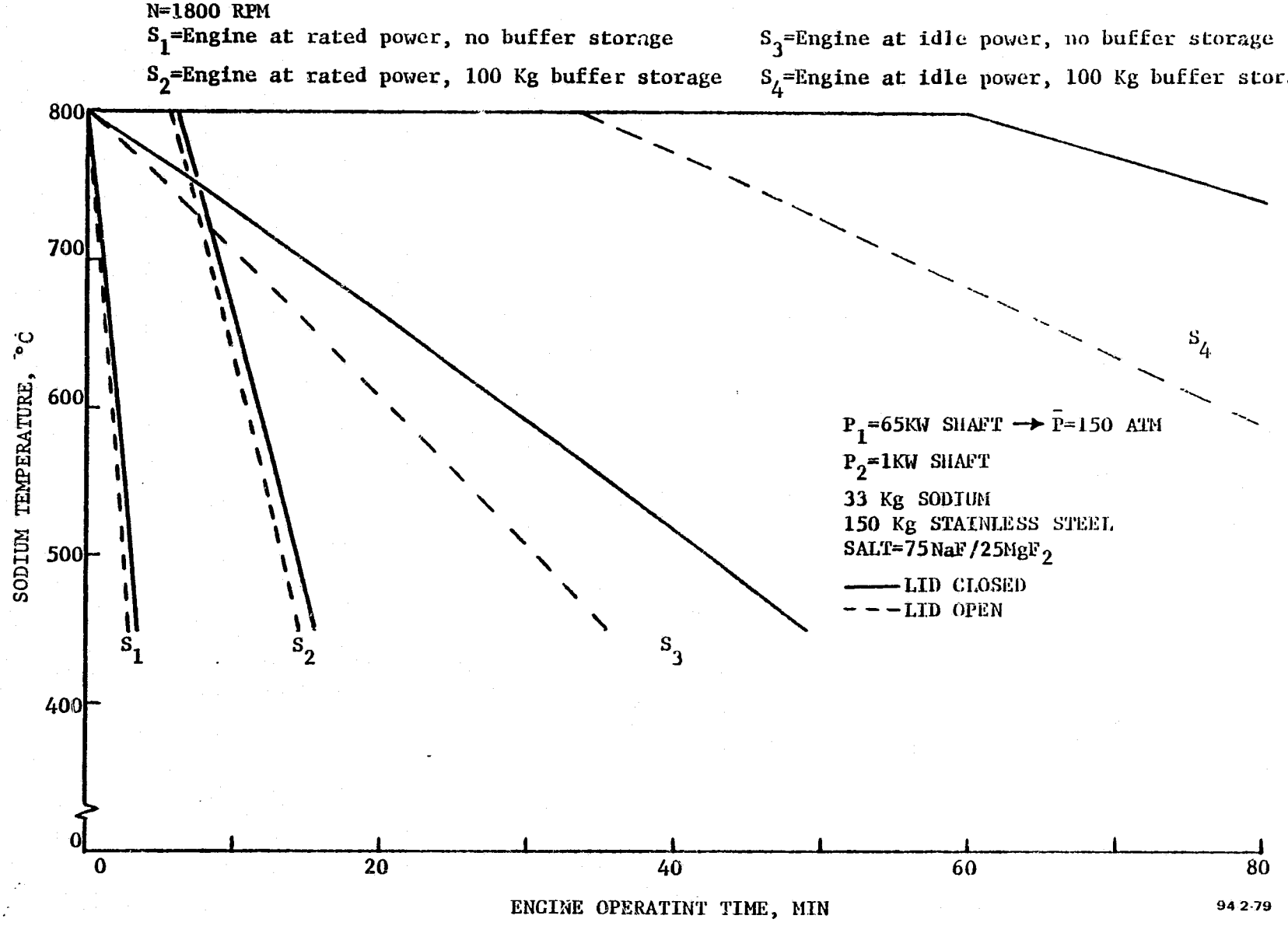

FIGURE 3-67. SODIUM TEMPERATURE RESPONSE AT RATED AND IDLE ENGINE POWER

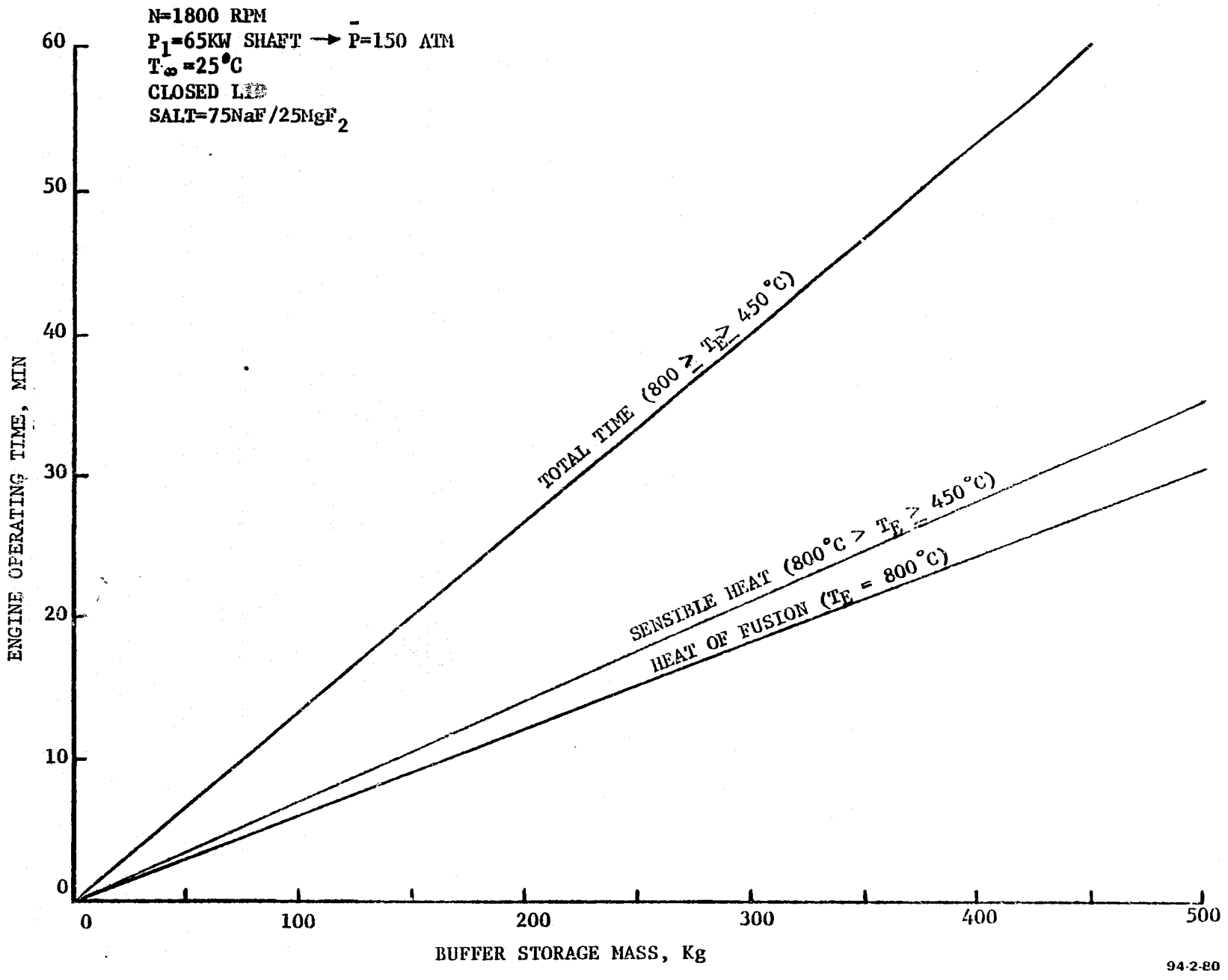

FIGURE 3-68. ENGINE OPERATING TIME WITH BUFFER STORAGE

Figure 3-68 presents the engine operating time with a closed receiver lid as a function of buffer storage mass. As shown, engine operating time during the salt phase change can be increased by 6.0 minutes for each 100 kg of 75 $NaF/25MgF_2$ eutectic salt added to the subsystem. An additional 7.0 minutes of engine operation can be obtained from the entire subsystem sensible heat. However, it may not be desirable to operate at "rated" power below the steady-state head temperature. This is due to the fact that engine efficiency will decrease and warm-up time will increase as the engine head temperature decreases.

Engine operating time is thus gained at the expense of subsystem weight. For example, 250 kg of eutectic salt is required to maintain "rated" output power for a 15 minute solar drop-out period. Although not considered in the present analysis, the weight of encapsulation must also be added to that of the salt. It is desirable to use thin wall containers to minimize structural weight, cost and temperature drops to and from the salt. By incorporating the following two techniques, additional wall thickness for corrosion allowance and pressure differentials is not required: (1) By purifying the salt and using a "getter", e.g., aluminum, the corrosion of 316 stainless steel can be virtually eliminated. (References 3-24, 3-27 and 3-28). (2) By adding a small amount of sodium to the evacuated salt container, the sodium vapor pressure inside and outside the container are (automatically) nearly equal all the time (Reference 3-24).

"On-line" operating time at "idle" power can be extended by two other methods. The first method is by simply increasing the mass of sodium within the receiver. The second is by reducing the "idle" shaft output power level from the present 10 kW level to the minimum level of approximately 1 kW. This would increase "idle" operating time by a factor of three or four.

3. Is Buffer Storage Required? The use of thermal buffer storage (sensible or phase change) is site-dependent. A cursory investigation of both the Barstow and Lancaster insolation data indicate, as shown in Figure 3-69, that short cloud passages (less than 3 minutes) occurred more than a thousand times at these locations during 1976. Cloud passages on the order of 15 and 30 minutes in length occurred much less frequently (less than 100 times). There were eighteen days in which the total available energy was between 50 percent and 10 percent of the annual mean level. Only eleven days had a total energy level less than 10 percent of the annual mean level. Although it is very difficult to determine the frequency and length of cloud cover from 15 minute insolation data, the above figures indicate that the duration of a "typical" cloud passage is less than 15 minutes. Adding buffer storage for a longer period of time is therefore unnecessary. Thus, buffer storage for the baseline system is not required for this site. This is because the inherent thermal capacitance of the subsystem is sufficient to maintain "on-line" engine operation at "idle" power for periods greater than 15 minutes as shown in Appendix L. Subsequent analyses show that "on-line" engine operation at a reduced "idle" power can be maintained for well over 30 minutes from the inherent buffer storage of the subsystem.

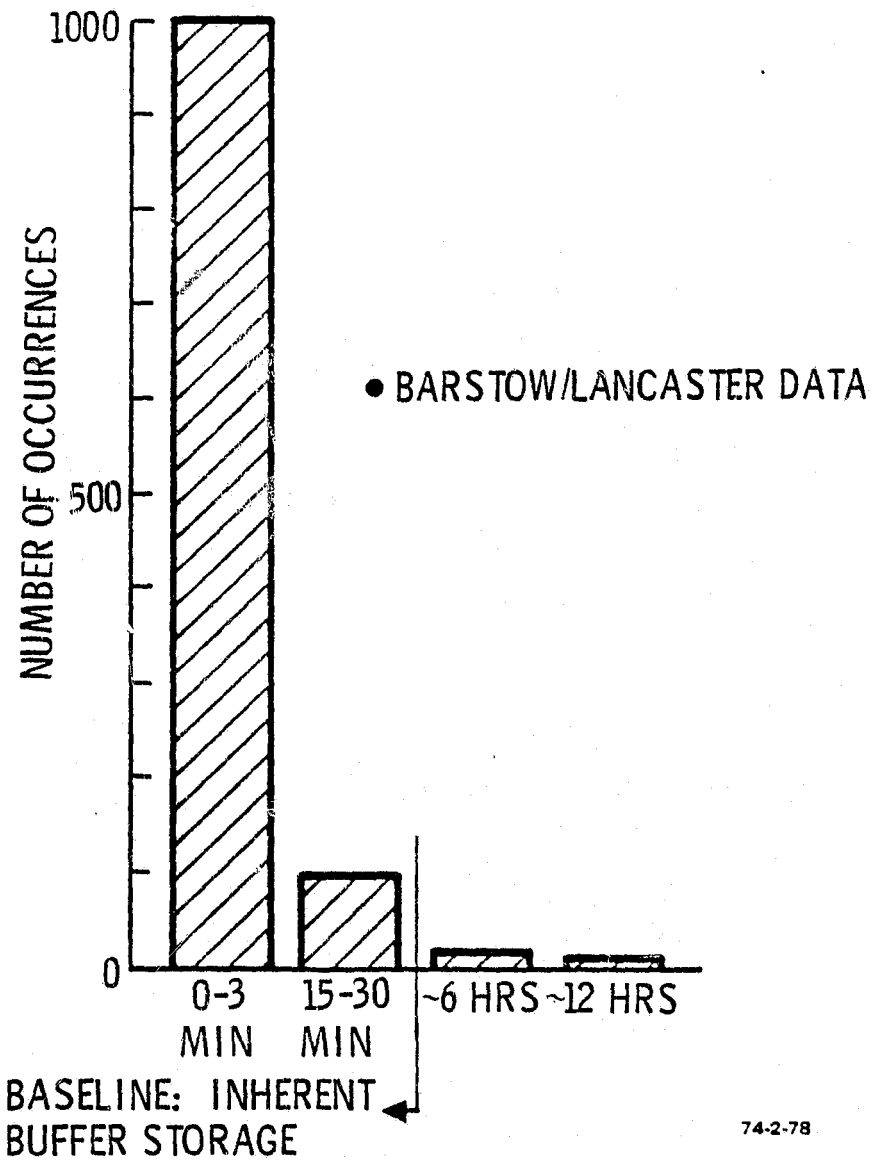

FIGURE 3-69. CLOUD PASSAGE FREQUENCY AND DURATION

f. Alternate Receivers. Brayton Engine parametric thermal analyses were performed for the Brayton receiver to obtain realistic size, performance and cost data for the systems analysis comparisons. A sketch of the receiver configuration for the Brayton system is presented in Figure 3-70. The receiver consists of tubes enclosed within a cylindrical cavity using argon as the working fluid. Direct sun-to-tube impingement is used in order to minimize the size of the receiver. The tubes are located at a position in the cavity to preclude burn-through, and spaced to permit energy reflection and reradiation to the backside of the tubes. This minimizes the thermal stresses caused by differential heating and reduces the required number of tubes. In addition, the tube spacing facilitates welding during fabrication. A high temperature refractory insulation must be used as a backing material since direct energy passes between the tubes. The alumina-silica fiber blankets are ideal for this application. The insulation surface has a solar reflectance of approximately 0.7 and is mostly diffuse, with only a slight peak in the direction of the specular reflection angle. The surface emissivity is approximately 0.85. An aperture lid and vapor valve are not needed for this design. Table 3.17 presents the thermal characteristics of the receiver.

TABLE 3.17. THERMAL CHARACTERISTICS OF THE BRAYTON RECEIVER

Gas = Argon

D_{APT} = 0.375m (aperture diameter)

D_{CAV} = 1.50m (diameter at the centerline of the tubes)

L_{CAV} = 1.65m (cavity length)

$A_{CAV}/A_{APT} \approx 100$

$\alpha_{EFF} = \epsilon_{EFF} = 0.998$

Effective cavity temperature = 910°C (1670°F)

Fluid exit temperature = 816°C (1500°F)

Fluid inlet temperature = 576°C (1068°F)

Maximum tube wall temperature = 871°C (1600°F)

Compressor exit pressure = 0.5 MPa (72 psia) } For use with Garrett CCPS 40-1 closed cycle Brayton (30 kW output).

Mass flow rate = 1 kg/sec (2.205 lbm/sec) }

Tube I.D. = 0.0127m (0.5 inch)

Tube length = 3.45m (11.32 ft)

Number of tubes = 54 (U-tube configuration)

Gas velocity = 65m/sec (213 ft/sec)

Average heat transfer coefficient = 301 W/m^2-°C (53 $Btu/hr\text{-}ft^2$-°F)

Pressure drop/compressor exit pressure = 0.05

Peak wall flux ≈ 35 kW/m^2

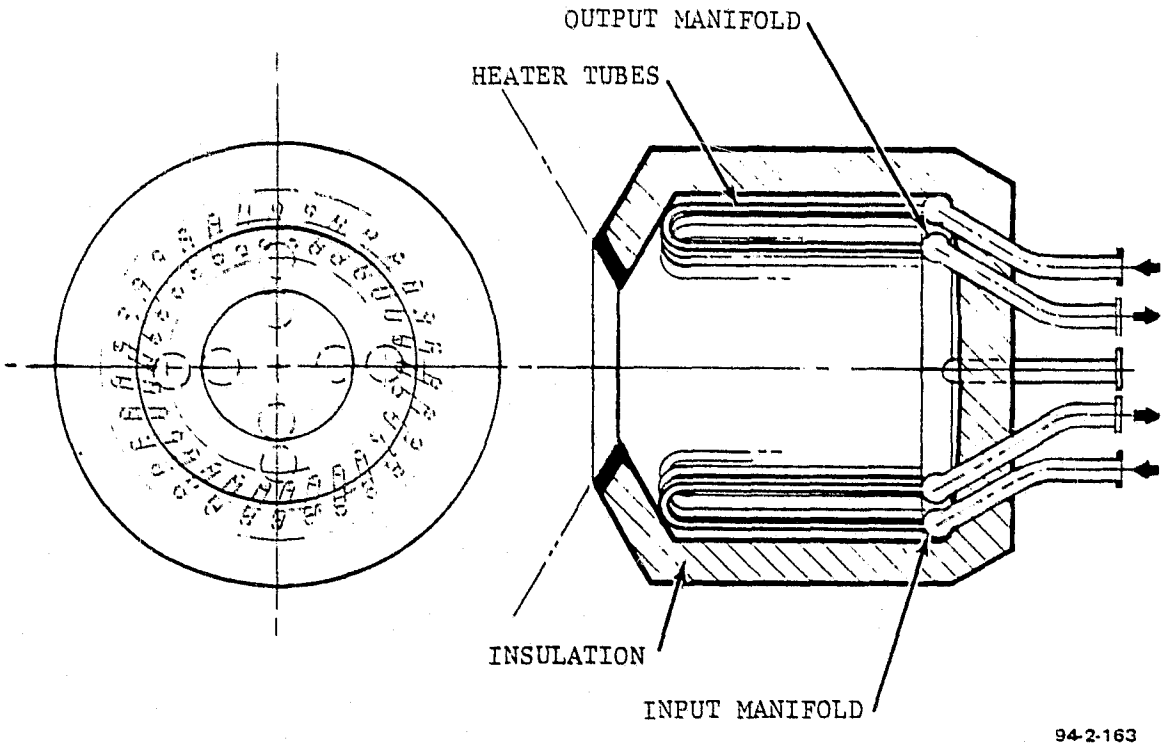

FIGURE 3-70. SKETCH OF THE BRAYTON CYCLE RECEIVER

The calculated thermal losses from the Brayton receiver during steady-state operation are approximately the same as for the baseline sodium/Stirling receiver except for conduction losses, which are about 3.5 times larger (3kW for the Brayton receiver vs. 0.82 kW for the Stirling). This difference is due to the considerably larger size required for the Brayton receiver. The insulation thickness was increased to 35.5 cm (14 inches) to minimize conduction losses. The average thermal conductivity of the alumina-silica insulation blanket used for this application was 9.3×10^{-5} kW/m-°C.

As previously shown in Figures 3-55 and 3-56 the capabilities of gas-in-tube heat transfer are quite low when compared with that of sodium pool boiling. Thus, the Brayton receiver is large by comparison to the baseline receiver. The size and cost of the present receiver can be reduced by increasing the heat transfer coefficient. One method of increasing heat transfer coefficient is to increase the gas velocity as shown in Figure 3-71. However, the pressure drop through the receiver becomes excessive for gas velocities above the present 65 m/sec. The average heat transfer coefficient is presented as a function of gas pressure in Figure 3-72. The heat transfer coefficient increases significantly with gas pressure. However, the present CCPS 40-1 engine has a recommended pressure range of about 0.20 to 0.40 MPa. Thus, the advantages of a high pressure subsystem cannot be obtained. Air, helium, xenon and helium-xenon gases were also investigated to determine a preferred heat transfer fluid. Helium was selected for its high thermal conductivity and xenon for its high molecular weight. For good heat transfer it is desirable to have low Prandtl numbers. Thus, a helium-xenon mixture with a molecular weight of about 40 ($HeXe_{40}$) would be optimum. A comparison of the average heat transfer coefficients for air, $HeXe_{40}$ and argon are presented in Figure 3-73. The heat transfer coefficients for air and the $HeXe_{40}$ mixture are 50 percent and twice as large as that for argon, respectively. However, one significant drawback to the $HeXe_{40}$ mixture is that it may be prohibitively expensive due to the very high cost of xenon. Augmentation of the tube flow heat transfer coefficient with the addition of internal finned surfaces was not considered a viable method since the pressure drop increases more rapidly than the heat transfer coefficient. The additional cost of finned tubes would also tend to offset any performance benefits.

1. Organic Rankine Engine. Thermal analyses were performed for the Rankine receiver to obtain realistic size, performance and cost data for the systems analysis comparisons. A sketch of the receiver configuration for the Rankine system is presented in Figure 3-74. The receiver consists of coiled tubes enclosed within a cylindrical cavity using supercritical toluene as the working fluid. Direct sun-to-tube impingement with some tube spacing is used to obtain a small receiver. The tube spacing permits energy reflection and reradiation to the backside of the tubes. An alumina-silica refractory insolation is used as backing material for the tubes. An aperture lid is used for this receiver to maintain temperature during inclement or nighttime periods. Table 3.18 presents the thermal characteristics of the receiver.

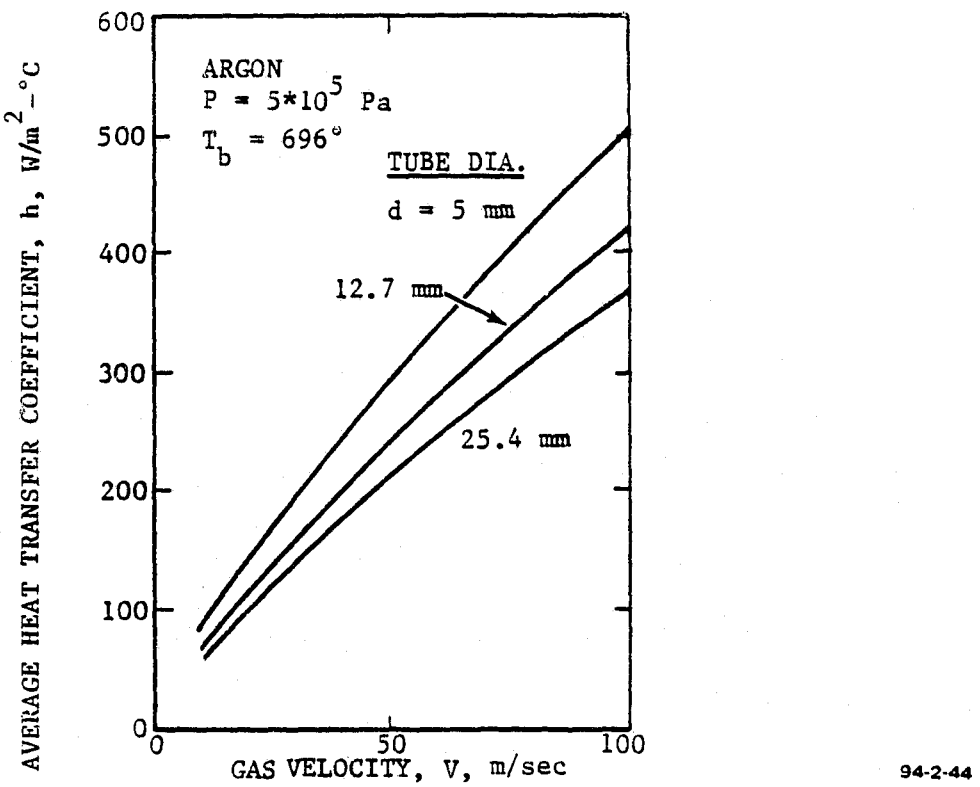

FIGURE 3-71. EFFECT OF GAS VELOCITY ON HEAT TRANSFER COEFFICIENT

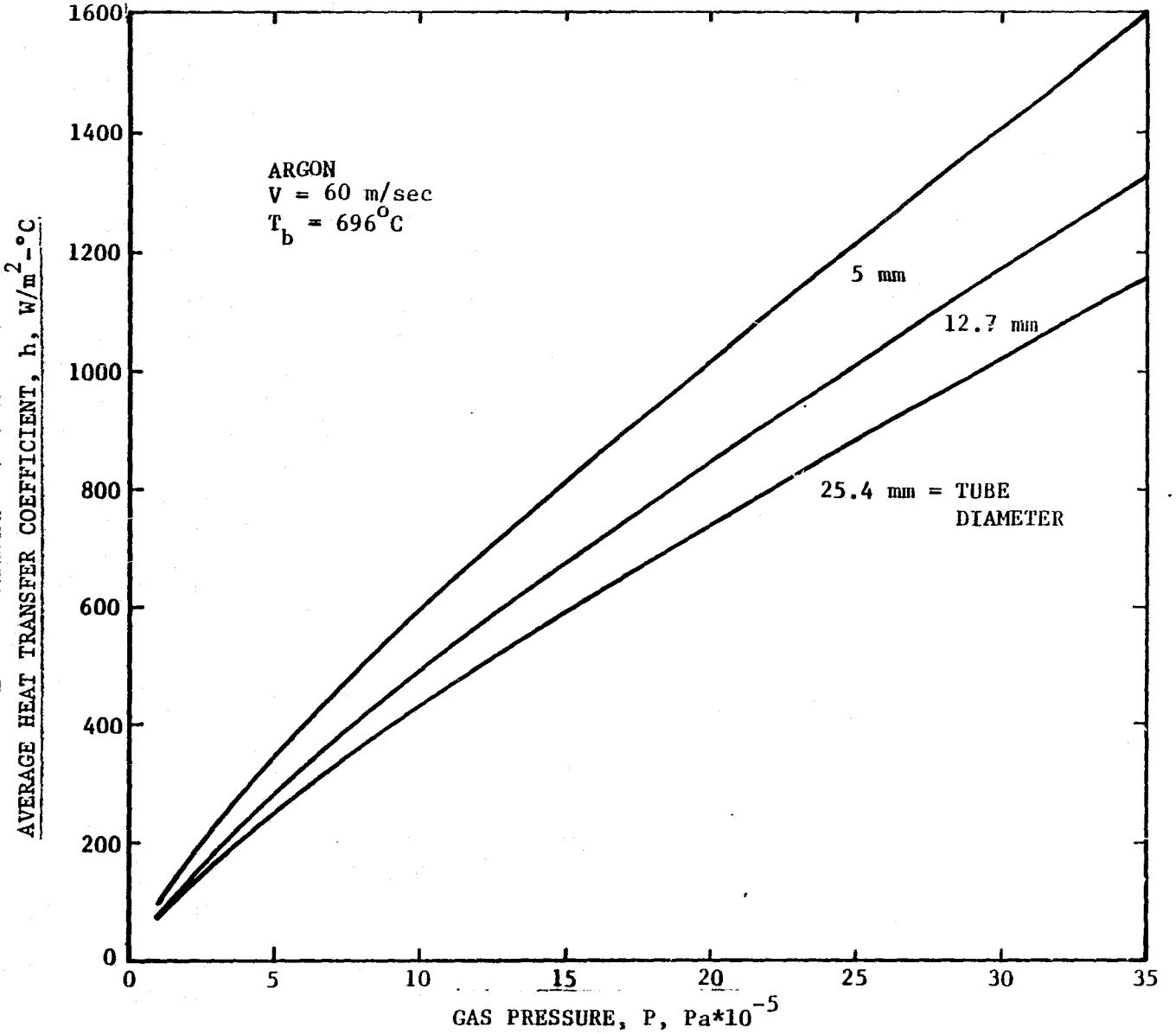

94 2-46

FIGURE 3-72. EFFECT OF GAS PRESSURE OF HEAT TRANSFER COEFFICIENT

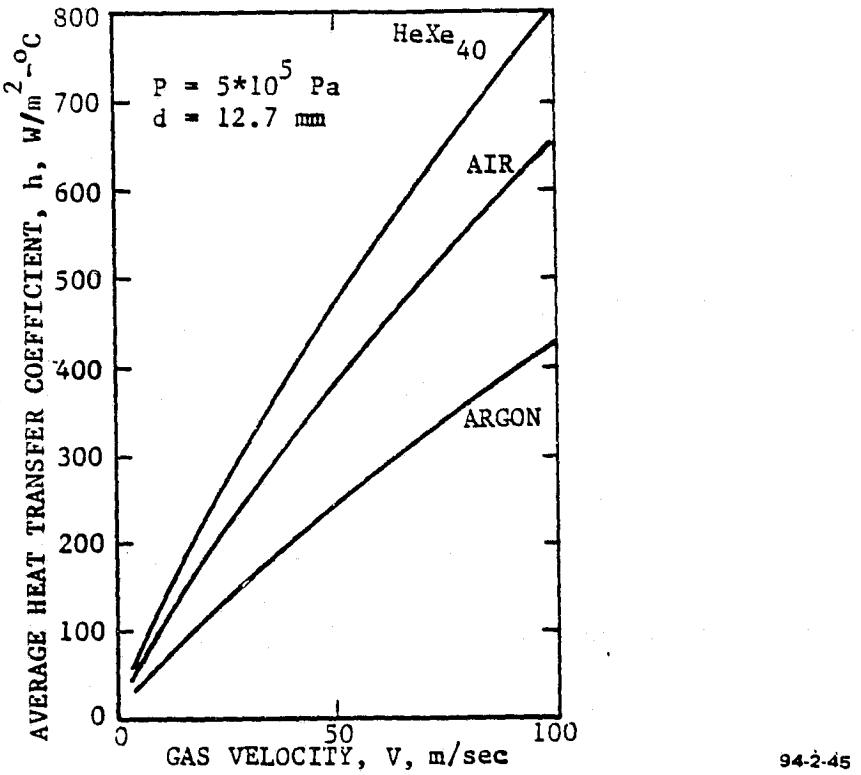

FIGURE 3-73. HEAT TRANSFER COEFFICIENTS FOR TYPICAL GASSES

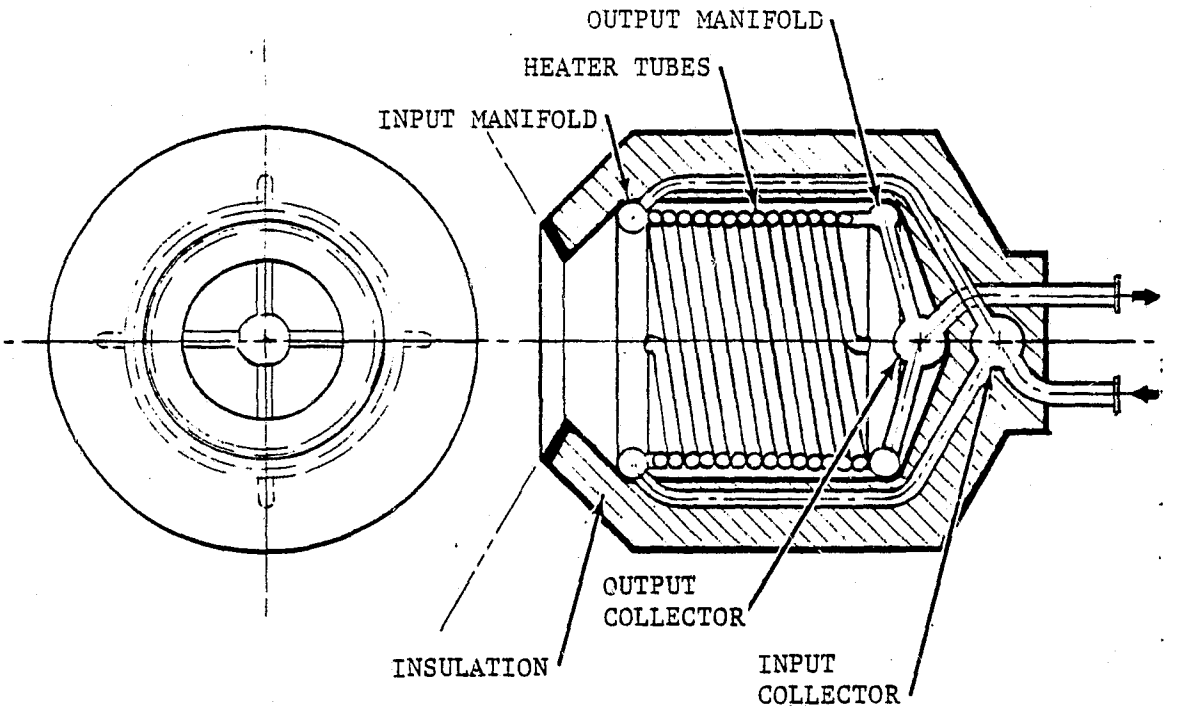

FIGURE 3-74. SKETCH OF THE ORGANIC RANKINE CYCLE RECEIVER

TABLE 3.18. THERMAL CHARACTERISTICS OF THE RANKINE RECEIVER

Fluid = Toluene

D_{APT} = 0.629m (aperture diameter)

D_{CAV} = 1.0m (diameter at the centerline of the tubes)

L_{CAV} = 1.2m (cavity length)

$A_{CAV}/A_{APT} \approx 13.5$

$\alpha_{EFF} = \varepsilon_{EFF} = 0.987$

Effective cavity temperature = 477°C (891°F)

Fluid exit temperature = 427°C (800°F)

Fluid inlet temperature = 241°C (465°F)

Maximum tube wall temperature = 454°C (850°F)

Receiver inlet pressure = 4.84 MPa (702 psia)

Mass flow rate = 0.438 kg/sec (0.967 lbm/sec)

Tube I.D. = 12.7mm (0.5 inch)

Tube length = 20.25m (66.4 ft)

Number of tubes = 8 (coil configuration)

Gas velocity = 6.9 m/sec (22.6 ft/sec)

Average heat transfer coefficient = 2.06 kW/m^2-°C (363 $Btu/hr-ft^2$-°F)

Receiver pressure drop/inlet pressure = 0.046

Peak wall flux ≈ 300 kW/m^2

Heat transfer to the toluene working fluid was determined using a correlation given by Reference 3-29 for turbulent flow of supercritical fluids. The calculated reradiation loss for the Rankine receiver is 5.33 kW. This is about one-half that of the baseline sodium/Stirling receiver and is a result of the low effective receiver temperature. The convection and conduction losses are approximately 2.15 kW and 0.90 kW, respectively. These two losses are slightly higher than the baseline receiver since the aperture and overall size of the Rankine receiver are larger.

2. Comparison of Receivers for Brayton, Rankine and Stirling Engines. Figure 3-56 presents a comparison of the required heat transfer area and excess surface temperatures for various types of receivers, all sized for a receiver outlet power of 200 kW. Here the term "excess temperature" is defined as the difference between the heat transfer surface (wall) back face temperature and the mean temperature of the fluid. Both factors are important in receiver design; minimum area is desired for a compact and efficient design, whereas low excess temperature minimizes the possibility of burnout.

The results plotted in the figure show that receivers for the Brayton engines require large surface areas and high excess temperatures. This is a result of the relatively low heat transfer coefficients associated with forced convection heat transfer from the wall to the gas. Higher heat transfer coefficients and thus smaller surface areas can be obtained by increasing the working fluid pressure and/or by using a better heat transfer fluid such as a helium-xenon mixture with a molecular weight of 40 (denoted by $HeXe_{40}$ on the figure).

The use of a liquid instead of a gas is even a more important effect in reducing the area and excess temperature. This is demonstrated by the curve labeled "Rankine" on the figure, which is based on the use of water as the working fluid.

Two types of Stirling engine receivers have been shown in Figure 3-56; "direct", where the concentrated solar energy falls directly on the tubes which contain the engine working fluid (a gas), and a sodium receiver concept which heats the engine working fluid via condensing sodium. A direct-heated receiver requires a relatively small area compared to a Brayton or even Rankine receiver due to the high heat transfer coefficients obtained from the very high gas pressure. However, the use of a sodium pool boiling receiver results in an even more favorable design, and is the baseline approach taken by Aeronutronic. The required surface area is minimal, combined with low excess wall temperatures. Other advantages include a low vapor pressure (subatmospheric) and peak solar flux at least an order of magnitude below the burnout conditions. Additional advantages of a small receiver are, in general, lower cost, lighter weight, reduced thermal losses, and minimum solar blocking.

3.1.2.2 Structural Design/Analysis. Preliminary and detailed structural analyses have been performed for various receiver concepts. Preliminary structural design calculations have been made for the baseline receivers associated with each power conversion system, i.e. Stirling, Brayton, and Rankine. The detail of the preliminary calculations was adequate to establish feasible receiver geometries, materials, and component thicknesses based on stress and corrosion considerations. The analysis of the baseline sodium receiver was extended to include a computerized shell stress analysis combined with an extensive assessment of the creep damage to allow a comprehensive receiver life prediction.

For the baseline sodium receiver, an extremely simple annular design (Figure 3-33) was selected from possible receiver geometries - tubular, cylindrical, spherical, etc. The resulting baseline annular receiver is a simple structure consisting of two cylindrical shells, one cantilevered inside the other from a connecting toroidal shell. The two ends are capped with spherical heads forming a double-walled annular cavity. Metallic sodium, which is contained within the annulus, is utilized as the heat transfer medium. The low vapor pressure (< 1 atm) and excellent heat transfer characteristics of the sodium enables the use of the simple annular structure to withstand the resulting low thermal and pressure induced stresses. The cavity is constructed of Type 316 Stainless Steel. The corrosion behavior of stainless steel alloys in hot sodium has been well studied and is very predictable. The low corrosion rates of austenitic stainless steel (such as Type 316) make it an excellent material for a long life solar receiver. In addition, austenitic stainless steel materials are relatively inexpensive and readily available.

Based on a predicted total material corrosion rate of 0.0876 mm/yr. and an allowable secondary stress limit (thermal and shell discontinuity bending stresses) of 48.3 MPa (7000 psi) at 816°C for the Type 316 Stainless Steel, a life of 15 years was established for the annular sodium receiver. Corrosion rate predictions were made with data developed from existing sodium heat transport systems (References 3-30 and 3-31). The limiting allowable secondary stress of 48.3 MPa results from a detailed analysis of the creep damage accumulated during creep relaxation cycles produced by the daily changes in incident heat flux and attendant sodium vapor pressure variations. The primary shell membrane stresses induced by the external pressure loading were limited to a low 5.10 MPa (740 psi) resulting in a large margin for a 15 year life. Possible material and configuration changes to improve the life are not warranted as the low cost of the simple annular design ($1700 in quantities of 100K units) allows for the cost effective replacement of the receiver after 15 years.

Preliminary analyses of alternate receiver designs for Brayton and Rankine cycle systems have also been completed. To contain the high pressure gases of the Brayton and Rankine Systems with reasonable wall thicknesses, conceptural tubular receiver designs have been developed.

The Brayton cycle receiver design, which operates with an internal pressure of 0.5 MPa (72 psi), consists of a large diameter cavity with 54 individual "U" shaped tubes 15.9 mm in diameter connected to input and output toroidal

manifolds (Figure 3-40). The working fluid in the receiver is argon gas. The component parts of the design are constructed of nickel base Inconel 625 alloy to withstand the high operating temperature of 871°C (1600°F). Based on an allowable secondary stress limit of 138 MPA (20 Ksi) at 871°C for the Inconel 625, a life of 15 years was predicted. The far-term cost (quantities of 100K units) of the Brayton receiver core is approximately $8000.

The Rankine cycle receiver design, which operates with an internal pressure of 4.84 MPa (702 psi), consists of helical-shaped tubular cavity with eight individual tubes 25.4 mm (1 inch) in diameter connected at each end with toroidal manifolds (Figure 3-42). The working fluid in the receiver tubes is toluene. The receiver component parts are constructed of Type 316 Stainless Steel to withstand the mild operating temperature of 427°C (800°F). Based on an allowable stress limit of 138 MPa (20 Ksi) for the Type 316 Stainless Steel at 427°C, a life of 15 years was predicted. The far-term cost of the Rankine receiver core shown in Figure 3-42 is approximately $4500.

Brayton and Rankine cycle receivers most likely could be optimized beyond the preliminary designs presented here to give 30 year lives. However, the cost data presented here is probably representative and likely conservative.

a. Material Selection for Baseline Receiver. To maintain structural integrity over the desired life expectancy (30 years) for the baseline system, the major considerations of material selection are high strength (stress-rupture properties) at elevated temperatures and good material corrosion resistance in a boiling sodium environment. Additional requirements, of equal importance, for a suitable receiver materials are: low material costs, material availability in desired forms (sheet, plate, tubing, etc.), formability, and weldability.

An indepth materials search which focused primarily on material stress-rupture properties at elevated temperatures has resulted in a wide variety of candidate materials. Applicable materials with this temperature capability include the following: iron, nickel, and cobalt base alloys:

- Austenitic Stainless Steel Type 304 and 316 (iron base)
- Incoloy 800 (iron base)
- Inconel 617 and 625 (nickel base)
- Hastelloy X (nickel base)
- Haynes 25 and 188 (cobalt base)

A comparison of relevant short-time mechanical properties of these materials are given in Table 3.19. Figure 3-75 presents stress-rupture data for the candidate materials at the receiver temperature of 816°C (1500°F).

TABLE 3.19 MECHANICAL PROPERTIES OF CANDIDATE MATERIALS

Material	Relative Cost	Room Temperature Properties			816°C Properties			
		Modulus of Elasticity (10^3 MPa)	Yield Strength	Ultimate Strength	Coeff. of Thermal Expansion (Microns/m -°C)	Modulus of Elasticity (10^3 MPa)	Yield Strength (MPa)	Ultimate Strength (MPa)
Stainless Steels								
304	1.0	200	248.2	586.1	18.8	131	82.7	158.6
316	1.0	195.1	255.1	579.2	18.5	131.7	137.9	206.9
Heat-Resistant Alloys					816°C/871°C Properties			
Incoloy 800	2.0	195.8	289.6	593	$18/_{18.2}$	$142/_{137.9}$	$103/_{93.1}$	$165.5/_{110.3}$
Inconel 625	4.5	205.5	517.1	965.3	$15.4/_{15.7}$	$152.7/_{148.2}$	$410.3/_{275.8}$	$434.4/_{284.1}$
Hastelloy X	5.0	206.9	448.2	758.5	$16/_{16.3}$	$144.8/_{131}$	$218.9/_{177.2}$	$343.4/_{251.7}$
Haynes 25	12	235.8	496.4	965.3	$16/_{16.2}$	$165.5/_{151.7}$	$239.9/_{237.9}$	$452/_{321.3}$
Haynes 188	12	231.7	466.1	943.2	$16.6/_{17}$	$167.2/_{162.7}$	$282.7/_{278.6}$	$547.1/_{435.8}$

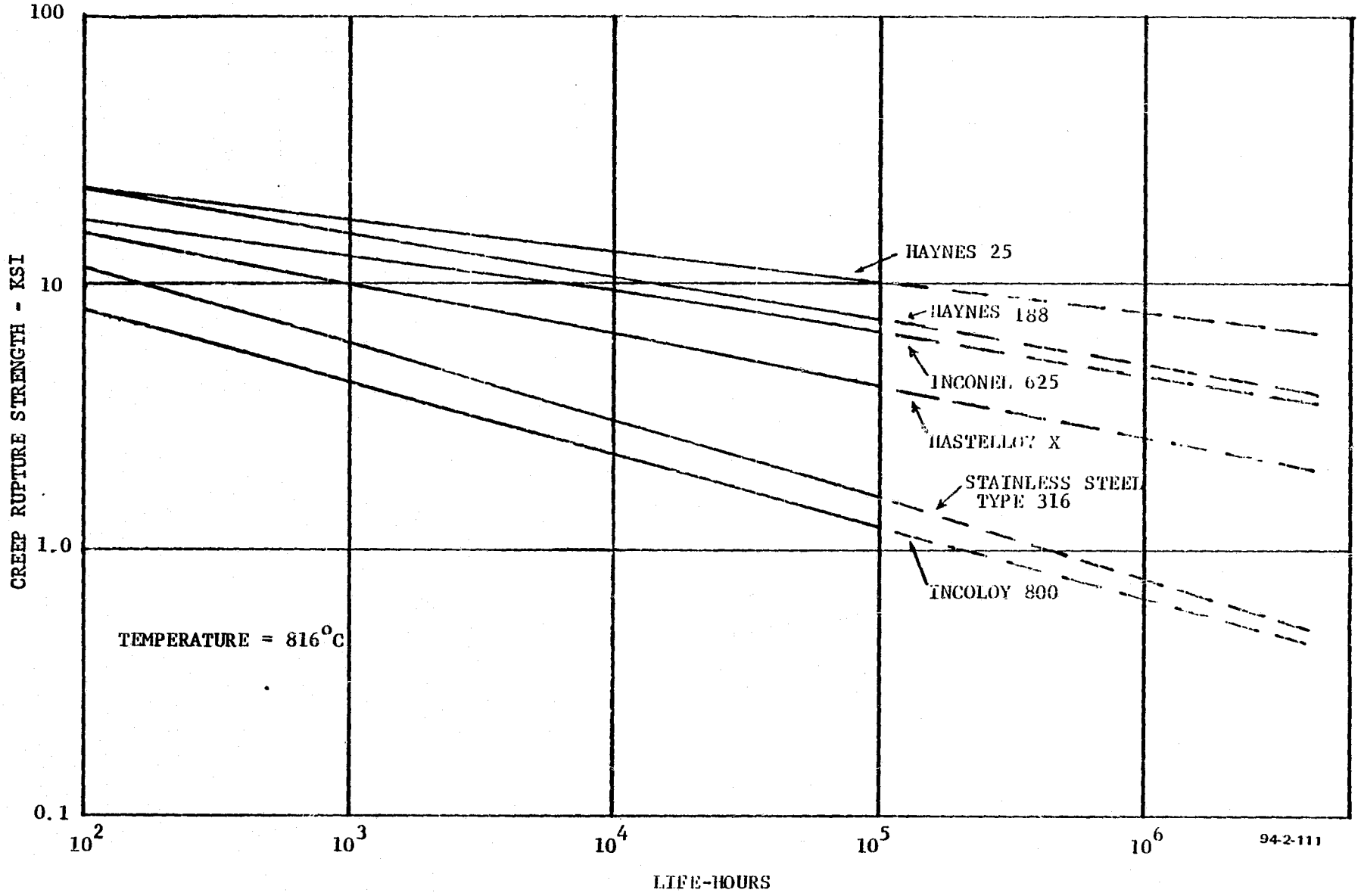

FIGURE 3-75. TYPICAL CREEP RUPTURE DATA OF CANDIDATE MATERIALS

From the above candidates, the Type 316 Stainless Steel was selected for the baseline sodium receiver core. This material presents the compromise of strength, cost and ease of fabrication. Secondly, stainless steel (300 series) has excellent corrosion resistance in boiling sodium. Recent surveys of material availability indicate that the high strength cobalt-base alloys are in very limited supply, if available at all. Black market prices as high as 40 dollars per pound for cobalt have been quoted. The problems associated with the nickel base alloys are somewhat different. Although there is a sizable lead time involved in obtaining the material, the real problem is the high corrosion and mass transport rates of nickel when exposed to boiling sodium.

b. Compatibility of Metallic Sodium with the Baseline Receiver Design. Pertinent facts relative to the design and operation of a sodium-filled heat transport system are presented here. The information was derived from data collected by operators of existing sodium systems designed to meet requirements comparable to those for the current solar energy application. Prior sodium system experience are given in available literature demonstrates that, with proper design allowances, predictable long-life sodium systems can be practically and economically constructed. Most of the usual design complications associated with sodium systems are avoided by the simple FACC receiver system. Examples of the successful prior commercial applications of sodium for high temperature heat transfer are given in Appendix N.

Special design allowances and features required for the SPS Baseline Sodium Heat Transfer system are presented in the following paragraphs. Valve design, corrosion allowance, and receiver filling requirements are discussed. The baseline design, utilizing boiling sodium, is much simpler than many sodium heat transfer loop designs which typically require relatively sophisticated liquid metal pumps, filters, and cold traps as integral parts of the loop.

1. Blocking Valve. To minimize heat loss to the engine overnight, the baseline design incorporates a single blocking valve. Typical valves found in sodium systems are blocking valves, throttle-type valves and ball-type check valves. These valves are designed to perform specific tasks and meet requirements to provide safe and efficient operation.

The general requirements for valves for liquid sodium systems are:

- Zero valve stem leakage to prevent impurities from entering the system
- Corrosion resistance for long and reliable life
- Thermal shock resistance for proper operation and long life

The FACC baseline receiver will utilize a plug-type blocking valve (see Figure 3-37). The valve plug will be actuated by a long shaft driven by an electromagnetic rotary actuator. Frozen sodium on the driving shaft will seal and prevent sodium vapor from entering the motor housing. The materials used in the valve construction are readily available and relatively inexpensive.

2. Corrosion of Materials in Sodium Environment. The corrosive effects of sodium on the materials of the receiver and associated ducting is significant. These effects have been studied and quantified, and have been carefully accounted for in the baseline design. The various parameters which affect the rate of mass transfer, rates of material loss, and carbonization of stainless steels, have been considered. These parameters include the effect of temperature in the range 600°C to 900°C, the effect of impurity content of the liquid metal (oxygen and carbon) and the effect of alloying content such as high percentages of nickel. The effect of fluid flow rate can be considerable but is not relevant to the FACC baseline sodium receiver design. Each of the above parameters are separately discussed below and comparisons, where appropriate, are made between various sources of information.

(a) Mass Transfer. A common mechanism of corrosion in liquid-metal systems is mass transport. Mass transport results from a coexistence of a temperature differential and an appreciable thermal coefficient of solubility. Corrosion deposits from the structure materials will tend to dissolve in regions of high chemical activity (hot areas) and will tend to deposit from solution in regions of low chemical activity (cold areas). This continued transfer of material in the system can accelerate corrosion attack in the areas of high activity. The precipitated material will accumulate in colder regions of the system and may eventually cause plugging of flow passages. At present most pumped sodium systems utilize "cold trapping" as a means of continually filtering the flowing sodium. These cold traps, which are maintained at a temperature of approximately 170°C, provide a cold area for safe material deposit.

Mass transport of impurity substances virtually will not exist in the FACC baseline sodium receiver design. The temperature differential within the sodium boiler is not sufficient to cause the impurities held in suspension to precipitate out of the sodium. The rate of material loss and corrosion of receiver material are therefore minimized.

(b) Effects of Temperature and Oxygen Content. Corrosion experiments involving high-temperature sodium have been conducted using electromagnetically pumped sodium loops (see References 3-30, 3-31 and 3-32. These loops employed flowmeters to monitor fluid velocity through hot-and-cold-leg sections. Heat was supplied to the system by wound heaters placed around the hot-leg section. The cold-leg consisted of a cold trap which collects material deposits during the time of system operation. Measurements of mass transfer rates were determined by gravimetric and metallographic analysis of the cold trap deposits.

Measured mass transfer rates (from Reference 3-32) of 300 series stainless steel as well as nickel-base materials are presented in Figure 3-76 as a function of temperature. The experimental mass transport results shown in the Figure 3-76 are based on a system oxygen content of approximately 10 parts per million (ppm). From a corrosion standpoint, the advantages of stainless steel over higher-strength nickel alloys is evident by inspection. A marked temperature dependence of mass transfer in Inconel and Hastelloy materials between 648° and 816°C is evident from the results. The mass transfer rate of the nickel-base alloys is very much higher at 816°C compared to 300 series stainless steel under comparable conditions. Similar findings were noted by

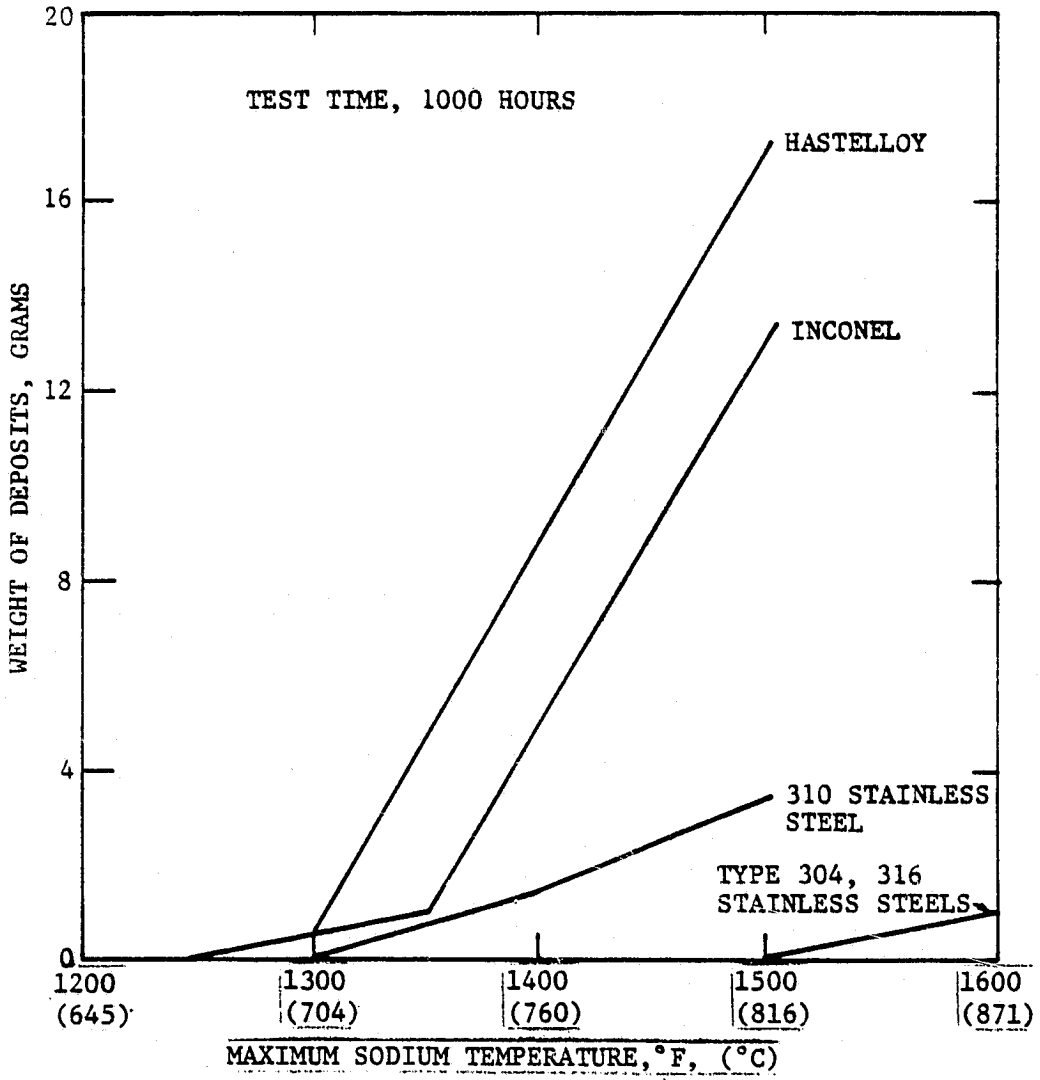

FIGURE 3-76. MASS TRANSFER RATES OF STAINLESS STEELS AND NICKEL-BASE ALLOYS

94-2-93

Russian investigators (Reference 3-32) in comparable high temperature evaluations. The cold-leg deposits in both the Inconel and Hastelloy systems were composed primarily of nickel with small amounts of chromium and virtually no iron. The deposits found in the stainless steel systems were composed predominantly of chromium with small equal amounts of iron and nickel. The steels containing 18 percent chromium and 10 percent nickel (Types 304 and 316) were the most corrosion resistant of the various types tested. Reference 3-32 indicated intergranular penetration rates of approximately 0.165 mm/yr for the Hastelloy and Inconel materials between 704 and 816°C; whereas test results from Reference 3-30 and 3-31 indicate a lower corrosion rate at 816°C of approximately 0.074 mm/yr for Types 304 and 316 stainless steel.

Another parameter, in addition to the nickel content of the alloy, of importance when selecting materials for sodium service concerns the effect of oxygen contamination on corrosion. Contrary to the high mass transfer rates of nickel-base alloys resulting from high temperature levels (816°C), increase in oxygen content levels up to 500 ppm has no measurable affect on the material corrosion rates. However, for stainless steel the oxygen content of the sodium is one of the most important parameters. Test results (Reference 3-31 indicate that if the oxygen level is reduced from 25 to 10 ppm the corrosion rate is reduced by 50 percent at 650°C. With proper filling procedures (See Section 3.1.2.2 an oxygen concentration of 10 ppm is achievable, a material loss rate of 0.074 mm/yr at 816°C has been applied to the baseline stainless steel receiver. Figure 3-77 presents a comparison of corrosion rates (mm/yr) for 300 series stainless steel from References 3-30 and 3-31. For an oxygen content of 10 ppm and a temperature range from 700°C to 816°C, good data correlation can be seen for the 0.074 mm/yr.

(c) Carburization of Stainless Steel. Research studies indicate that a reduction of room temperature ductility of Types 304 and 316 stainless steel is likely with increases in carbon content when the materials are exposed to liquid sodium. This carbon increase can be attributed to the following:

- Carbon dioxide (CO_2) impurities in the system are reduced by the molten sodium to form carbon and oxides
- Higher than normal carbon percentages present in the material following manufacture
- Small amounts of carbon present in the sodium

Long term sodium loop tests (Reference 3-31) at 650°C show that the average carbon levels in both stainless steel materials (304 and 316) increased approximately 0.25 percent. Both material specimens contained carbon gradients through their cross-section. However, the carbon levels that resulted did not materially affect the high temperature ductility of the materials. The type of carbide resulting from the carburization of the steel surface was identified as Fe_4Mo_2C, which is dispersed in the steel matrix.

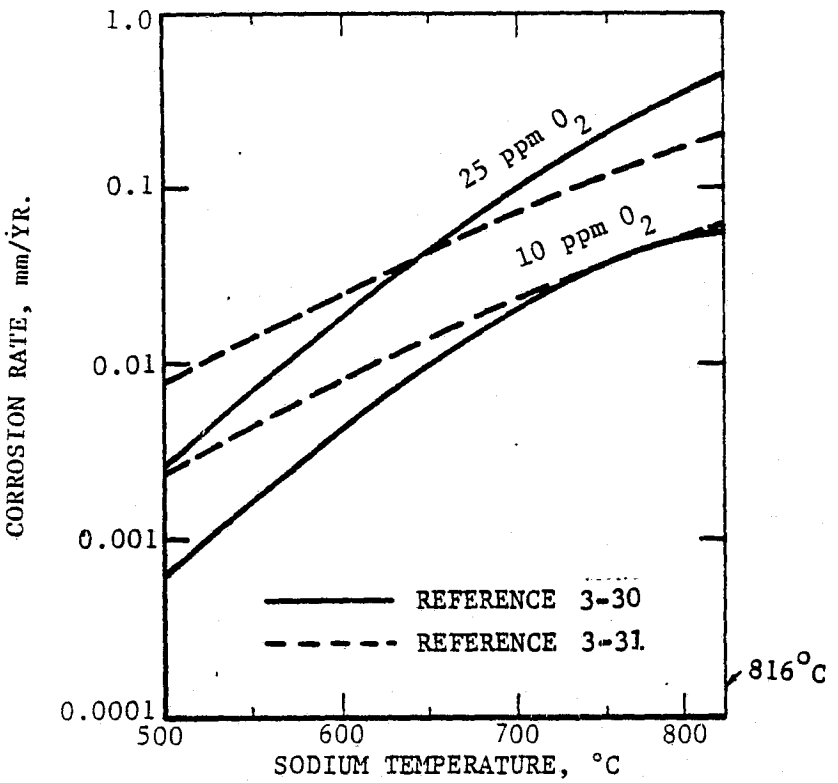

FIGURE 3-77. COMPARISON OF SODIUM CORROSION DATA - 300 SERIES STAINLESS STEELS

By contrast, data presented in Reference 3-32 showed only small increases in the carbon content. For long-term exposure (1300 hours) the samples indicated that the carbon content increased slightly to approximately 0.036 percent. Further testing (Reference 3-33) was conducted to evaluate the room temperature mechanical properties of the stainless steel specimens. These test results indicated that the tensile strength of the exposed sample was above the minimum value specified by the ASTM for Type 304 stainless steel pipe, whereas the yield strength was at the minimum value specified.

The filling procedure for the baseline sodium receiver is outlined in a later section of this report titled "Sodium Handling". The handling, cleaning, and filling procedure described therein will ensure very low levels of impurities trapped within the system after filling. Therefore, no carburization (decrease in ductility) of the stainless steel receiver material is expected.

3. Corrosion Allowance. Material corrosion rates due to boiling sodium have been estimated for 15 years of receiver life. The rate of material loss was computed from curves (References 3-30 and 3-31) showing sodium temperature as a function of material loss (mm/year). Calculated material corrosion rates were based on the amount of time spent at each temperature for both day and night exposure. Table 3.20 presents a data breakdown of the material loss rate for each portion of the thermal cycle. The material loss rate was estimated to be 0.0559 mm/yr. The additional approximated material loss rate due to atmospheric oxidation corrosion was 0.0318 mm/yr. The total material corrosion rate was equal to 0.0876 mm/yr.

Table 3.20. SUMMARY OF MATERIAL LOSS

Operating Temp. (°C)	Operating Time (Hrs.)	% of 24 Hr. Cycle	Corrosion Rate (mm/year)	Material Loss (mm/year)
649	3	12.5	0.0097	0.00121
704	3	12.5	0.0211	0.00264
760	3	12.5	0.0410	0.00513
816	15	62.5	0.0742	0.0469
			Total =	0.0559 mm/year

c. Allowable Stresses. Allowable operating stresses (primary and secondary) based on the high temperature mechanical properties of Type 316 stainless steel have been established. Based on a primary stress allowable, pressure-induced shell membrane stress levels - away from shell geometric discontinuities - will be limited by the material creep-rupture strength. In the case of the secondary allowable stresses, i.e. shell discontinuity bending stresses and thermal stresses, levels are governed by the creep damage accumulated during stress relaxation cycles induced by the temperature and pressure cycling during a 24-hour day.

1. Primary Allowable Stress. Primary stresses are low level stress conditions (stress controlled) as illustrated by the stress-strain history shown in Figure 3-78(a). For primary stress conditions - i.e. shell membrane stresses due to gravity or pressure loads - stress levels are limited by the material creep-rupture strength. Because of the receiver temperature (816°C max), material creep limits the primary stresses to well below the yield and ultimate strengths of the material. Figure 3-79 shows the receiver temperatures throughout a 24-hour day.

The primary stress allowable used in the present analysis is based on creep-rupture data for Type 316 stainless steel as shown in Figure 3-75. It was necessary to extrapolate the rupture data at each temperature to 10^7 hours in order to estimate the primary allowable stresses. To allow for extrapolation and data uncertainties, the primary allowable was based on the creep-rupture strength for the Type 316 stainless steel at 10 times the design life of 15 years. The resulting primary allowable is approximately 5.10 MPa (740 psi).

2. Secondary Allowable Stress. The stress-strain history for a secondary stress condition is illustrated in Figure 3-78. The secondary stress condition is a high stress, strain-limited situation as shown in Figure 3-78. A much higher stress allowable is permitted (compared to the primary stress condition) because the creep damage occurs only during the initial phases of each day and night period. Material creep rates and stress levels establish the amount of stress relaxation per daily cycle, and creep damage accumulated as a function of the stress levels during each relaxation period is evaluated from the "Linear Damage Rule" formulated by D. Spera (Reference 3-34). Fatigue damage to the material virtually does not exist because of the small magnitude of working strain.

Thermal and pressure cycle data used to determine the secondary allowable working stress are shown in Figure 3-79. The daytime portion of the cycle was assumed to consist of 15 hours of isothermal operation followed by three steps (idealized) for nighttime cool down at three hours each. The stress relaxation during each assumed isothermal segment of a 24-hour day was predicted with the following equation from Reference 3-35:

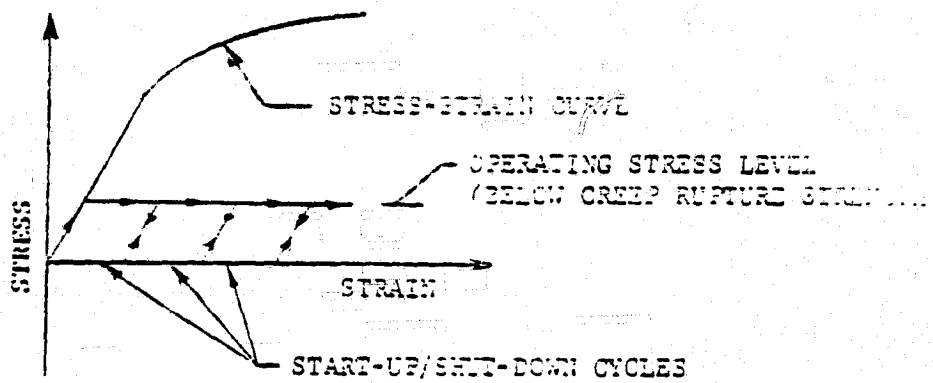

(a) CASE 1 - LOW STRESS REGIONS (PRIMARY STRESSES)

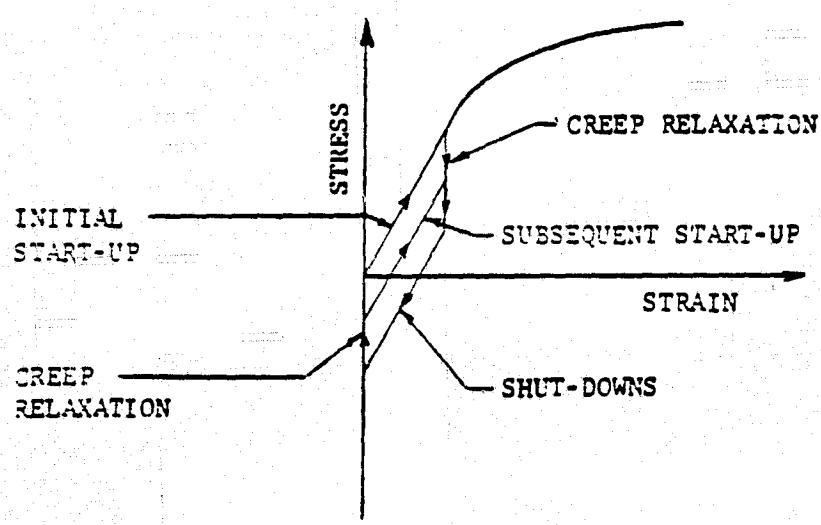

ORIGINAL PAGE IS
OF POOR QUALITY

(b) CASE 2 - MODERATE STRESS REGIONS (SECONDARY STRESSES)

94-2-113

FIGURE 3-78. SIMPLIFIED STRESS-STRAIN HISTORIES

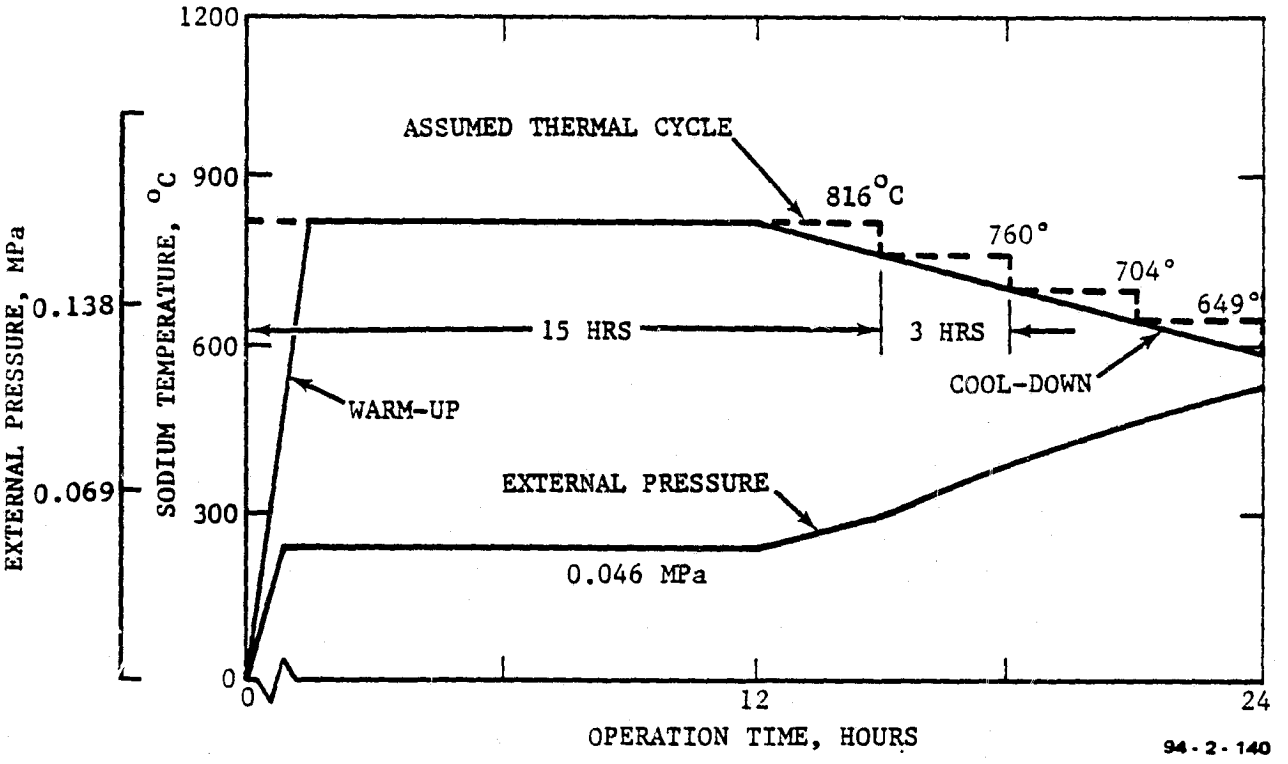

FIGURE 3-79. SODIUM PRESSURE AND TEMPERATURE RESPONSE

$$\sigma_F = \left[\frac{t + \frac{\lambda^N \sigma_o}{(N-1)E}^{-N+1}}{\frac{\lambda^N}{(N-1)E}} \right]^{-\frac{1}{N+1}}$$

where:

σ_F = Final stress after time t, MPa
t = Time of operation at a constant temperature, hrs.
N, λ = Creep rate constants for the material.
E = Young's Modulus at working temperature, MPa.
σ_o = Initial working stress at the start of relaxation period, MPa.

Figure 3-80 presents a typical stress-strain history for secondary stresses initially at 48.3 MPa (7000 psi). A stabilized hysteresis loop where the majority of the damage accumulates, results after approximately three months (90 cycles) of operation and continues with little change throughout the remaining life of the receiver. As shown in Figure 3-80, during the morning or initial warm-up and daytime operation, the working stresses are compressive; however, the cool-down and nighttime period results in tensile stresses.

The cyclic creep life was calculated from the stress-relaxation equation (above) and combined with a "Linear Damage Rule". For a given initial stress level, the life of the structure has been determined using a hypothetical quantity "creep damage" as defined by Spera (Reference 3-34). The "creep damage" is zero at the start of cycling and equals one at failure. The accumulation of "creep damage" is calculated from the following equations:

$$\Delta \phi_c = \sum_{0}^{t_1} \frac{\Delta t}{t_R}$$

and $\Sigma \Delta \phi_c = 1$ @ failure

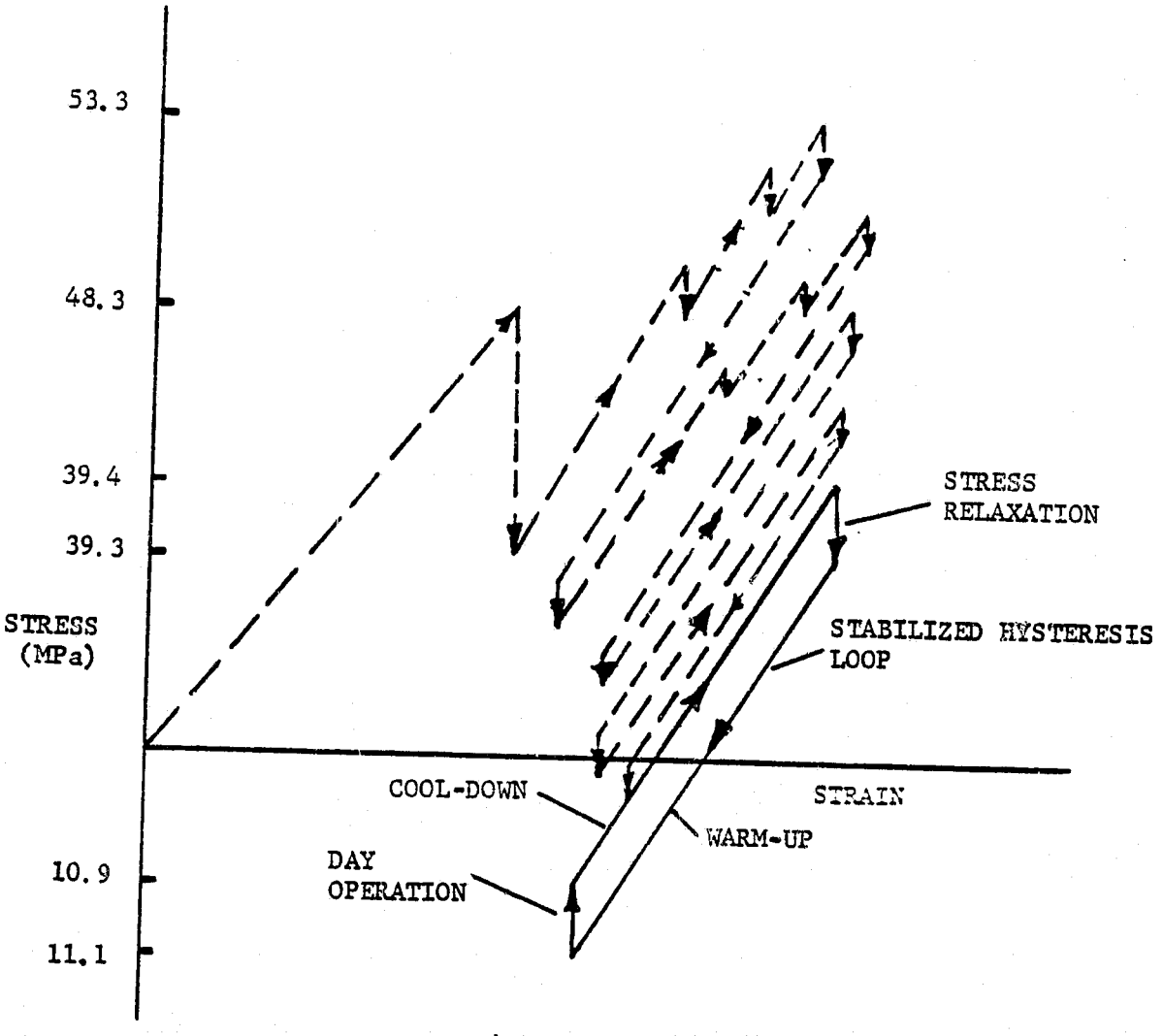

FIGURE 3-80. STRESS STRAIN CYCLE

94-2-110

where:

$\Delta\phi_c$ = Creep damage per relaxation period

Δt = Increment of time (hold time), hours

t_1 = Duration of one cycle, hours

t_R = Creep-rupture time at S and T

S = Absolute value of average stress during t, MPa

T = Average temperature during t, ^{o}C

For Type 316 stainless steel at a temperature of 816°C (1500°F), this equation predicts an operating life of approximately 15 years for the stress-strain history of Figure 3-80 that results from an initial stress of 48.3 MPa (7000 psi).

d. Structural Analysis. A detailed elastic structural analysis of the baseline (sodium) receiver operating at 816°C (1500°F) has been completed. Structural loads accounted for include an external pressure ranging of 0.5 to 1.0 atmospheres and the thermal gradients shown in Figure 3-81. Initial sizing of receiver shell components for Type 316 stainless steel was based on the primary allowable stress of 5.10 MPa (740 psi - See Section c) and the external pressure condition. The sizing calculations were performed using simplified equations taken from the current ASME Boiler and Pressure Vessel Code (Reference 3-36). Figure 3-82 presents a cross-section of the receiver configuration analyzed. Secondary stress considerations accounting for local discontinuity bending stresses, and stresses caused by thermal gradients were then computed based on the initial material sizes. Final stress calculations were made using the "BOSOR4" computer program for the analysis of shells of revolution. Simplified calculations have been made to demonstrate that the receiver structure is not susceptible to buckling.

1. Structural Design. Initial sizing of receiver component parts was performed using equations from Reference 3-36 based on allowable membrane stresses. The cylindrical and spherical portions of the receiver design were sized using the following equations:

$$t_{cyl} = \frac{PR}{SE_o - 0.6P} \qquad (3\text{-}25)$$

and

$$t_{sph} = \frac{PR}{2SE_o - 0.2P} \qquad (3\text{-}26)$$

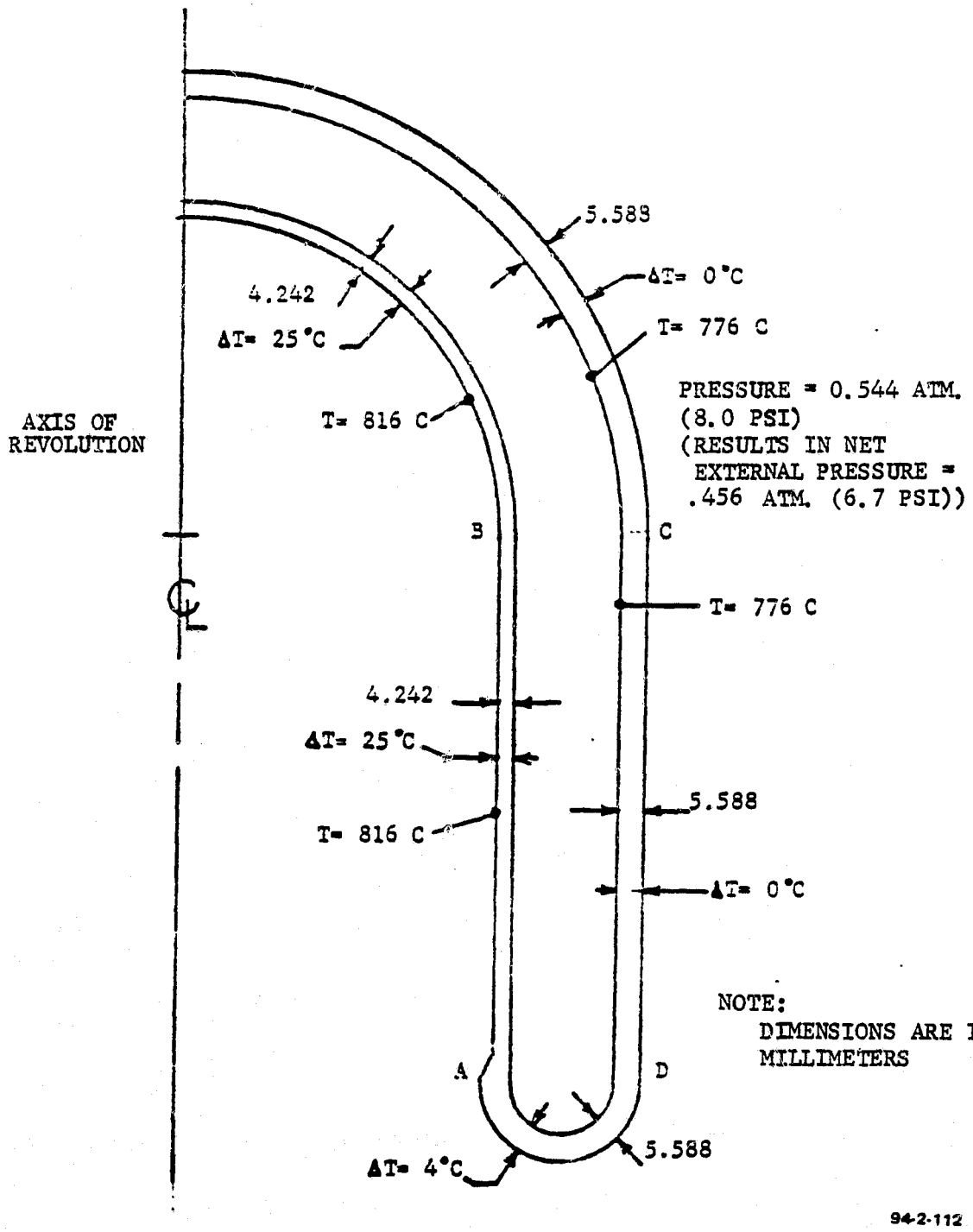

FIGURE 3-81. "BOSOR4" RECEIVER MODEL

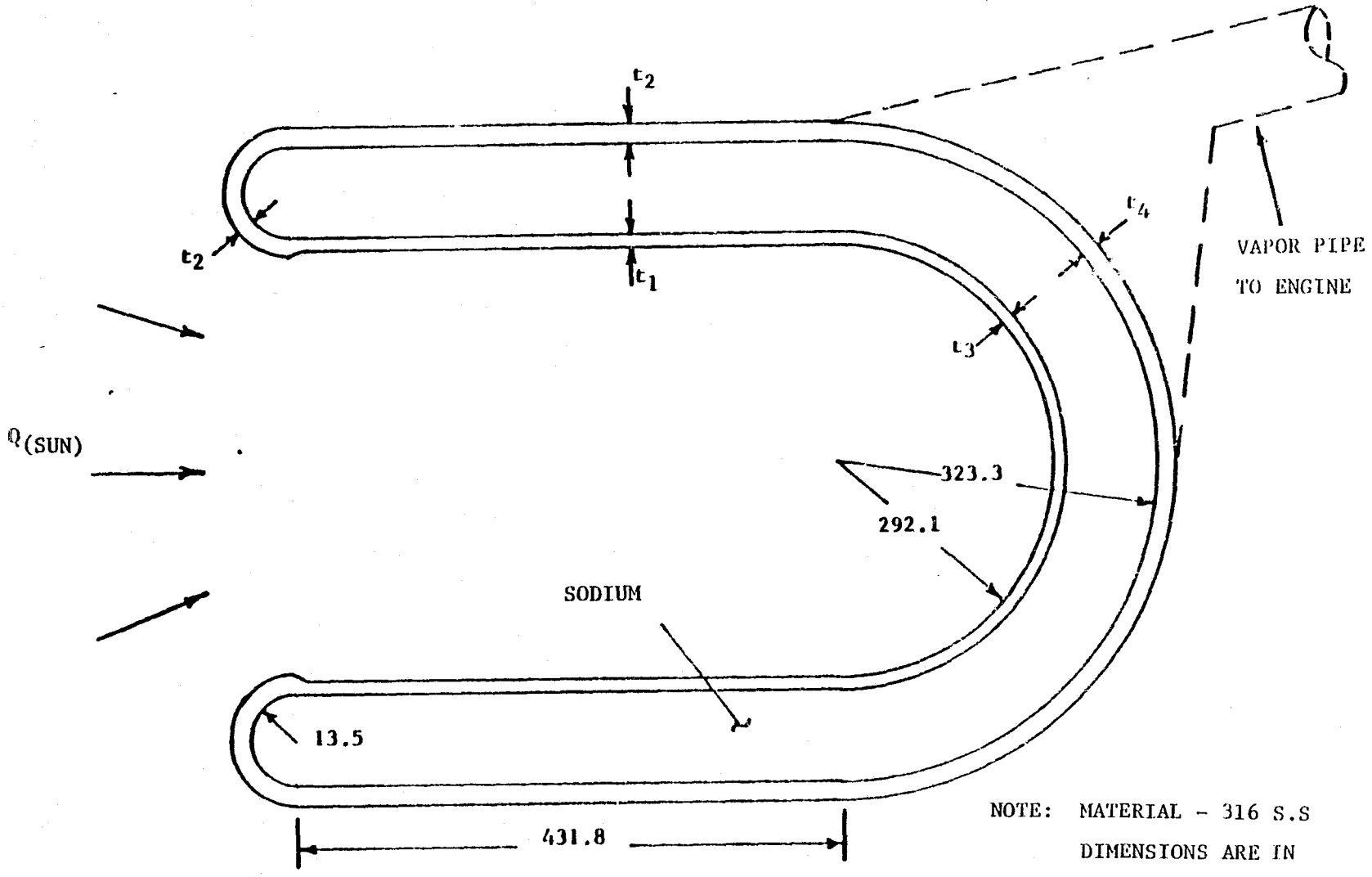

FIGURE 3-82. RECEIVER STRUCTURAL MODEL

where:

t = Thickness of the cylindrical or spherical area, mm

P = External pressure at working temperature, MPa

R = Inner or outer cylinder radius, mm

S = Primary stress allowable, MPa

E_o = Welded joint efficiency = 0.9

The critical external pressure (buckling pressure) of outer cylindrical shell and the critical pressure (pressure to cause dimple) of outer spherical head, were estimated from the following equations:

$$P_{c_{cyl}} = 0.807 \frac{Et^2}{LR} \left[\left(\frac{1}{1-\upsilon^2} \right)^3 \left(\frac{t}{R} \right)^2 \right] \quad (3\text{-}27)$$

and

$$P_{c_{sph}} = 0.365E \left(\frac{t}{R} \right)^2 \quad (3\text{-}28)$$

These equations were obtained from References 3-37 and 3-38, respectively. The terms are:

P_c = Critical external pressure of cylindrical shell or spherical head, MPa

E = Young's Modulus at temperature, MPa

t = Wall thickness, mm

L = Cylinder length, mm

R = Cylinder outside radius, mm

υ = Poisson's ratio, = 0.3

The preliminary sizing calculations of the receiver component parts, using Equations (3-25) through (3-28) with a working external pressure of 0.05 MPa (7.0 psi) and primary allowable stress of 5.10 MPa (740 psi from Subsection (d) at 816°C), resulted with the following thicknesses and critical pressures:

- Inner cylinder: $t_1^* = 2.95$ mm (0.116 inches)
- Outer cylinder: $t_2^* = 3.33$ mm (0.131 inches)

  $P_c = 0.986$ MPa (143 psi)

  Margin of Safety = (0.986/.101**) - 1 = 8.7 (For Buckling)
- Inner spherical head: $t_3^* = 1.47$ mm (0.058 inches)
- Outer spherical head: $t_4^* = 1.65$ mm (0.065 inches)

  $P_c = 1.34$ MPa (194.3 psi)

  Margin of Safety = (1.34/.101) - 1 = 12.3 (For Buckling)

*These values do not include a corrosion allowance.

**At maximum external pressure = 0.101 MPa (14.7 psi)

2. Detailed Stress Analysis. The structural integrity of the receiver model shown in Figure 3-81 has been evaluated in detail using the "BOSOR4" computer program (Reference 3-39). The external loads applied to the model consists of a net external pressure*, and temperature gradients through the shell walls and between shell segments. The simplified receiver design allows for unrestrained overall thermal growth due to the high operating temperatures; and therefore, thermal strains are minimized. The critical stress points on the structural model are indicated by the letters A, B, C, and D on Figure 3-81. The stress predictions were based on the following conditions:

- Meridional and circumferential pressure stresses
- Temperature gradients across shell walls
- Differential radial expansion of shell components due to high operating temperatures

The above conditions were evaluated using the net external pressure load and temperature gradients shown in Figure 3-81. The shell wall thicknesses which appear in the Figure 3-81 are maximum values which include additional thickness to account for subsequent material loss due to sodium corrosion**. However,

*Net external pressure = atmospheric pressure less the internal (vapor) pressure of the heat transfer fluid.

**Total corrosion rate = 0.0876 mm/yr; thickness increase = (0.0876 mm/yr) (15 year) = 1.314 mm.

the minimum skin thicknesses (predicted thicknesses near the end of the receiver life) were used in the stress calculations and resulted in the largest combined stresses (pressure stresses superimposed with thermal stresses). The outer cylindrical shell and outer spherical head thicknesses (t_2 and t_4 shown in Figure 3-81) were both increased to 5.89 mm from the values required by the analysis of Subsection 3.1.2.2 to provide continuity at shell intersection points.

The "BOSOR4" computer model calculated stresses are presented in Table 3.21 shown on the following page. The maximum stress computed occurred at Point A in Figure 3.81 and was equal to 48.3 MPa (7000 psi). Since the stresses at Point A are mostly local discontinuity stresses due to differential pressure and thermal induced expansions of the receiver shell segments, the resulting 48.3 MPa (7000 psi) stress will allow for a receiver life of at least 15 years as predicted in Section 3.1.2.2 (c).

e. Brayton Cycle Receiver Configuration. The Brayton cycle receiver core consists of "U"-shaped tubes extending longitudinally and arranged circumferentially inside the cavity. The "U"-shaped tubes are connected to input and output toroidal manifolds located at the closed end of the cavity. The goal was to establish a design which allows direct sun-to-tube impingement in order to minimize cavity size and secondly, permit sun energy reflection and reradiation to the backside of the tubes. In addition, an optimized design should be light in weight and economically feasible. Specific requirements and conditions assumed for the Brayton cycle receiver subsystem design are listed in Section 3.1.2.1

1. Material Selection. The primary requirement for material selection of the Brayton Cycle engine receiver is high strength (stress-rupture properties) at an operating temperature of approximately 871°C (1600°F) for a desired life expectancy of 30 years. Secondly, material cost and material availability in various forms are important considerations. Of the list of potential candidate high temperature materials, (Inconel 617, Hastelloy X, Haynes 25 and 188), Inconel 625 was the leading candidate material because of its high strength at elevated temperatures and also because it contains only one percent cobalt (a scarce and high cost material). Inconel 617 was also a potential material, but contains approximately 13 percent cobalt; and therefore, is not considered desirable at this time.

2. Allowable Stresses. The allowable operating stresses (primary and secondary) are based on the high temperature mechanical properties of Inconel 625. Primary stresses, pressure-induced tube membrane stress levels away from connection points to the toroidal manifolds, will be limited by the material creep-rupture strength. In the case of the secondary allowable stresses, the same approach presented in Subsection c for the baseline receiver has been applied.

TABLE 3.21 "BOSOR4" STRESSES

Stress Location	External Pressure, MPa (Inner fiber / Outer fiber)		Thermal, MPa (Inner fiber / Outer fiber)		Effective* (Combined) Stress, MPa		Margin of Safety
	Circumferential	Meridional	Circumferential	Meridional	(Inner fiber)	(Outer fiber)	
A	14.51/4.90	15.47/-13.82	30.12/-4178	35.76/-35.89	48.3	44.70	0.0/.08
B	3.35/3.35	2.23/2.23	35.90/-36.11	35.90/-36.14	38.70	33.40	.25/.45
C	-2.02/-2.02	-1.35/-1.35	0.0/0.0	0.0/0.0	1.78	1.78	26./26.
D	-7.56/3.54	-19.89/17.09	15.47/11.40	6.81/-6.76	18.40	13.30	1.63/2.64

*Von Mises combined stress.

TABLE 3.21 "BOSOR4" STRESSES

Stress Location	External Pressure, MPa (Inner fiber / Outer fiber)		Thermal, MPa (Inner fiber / Outer fiber)		Effective* (Combined) Stress, MPa (Inner fiber / Outer fiber)	Margin of Safety
	Circum-ferential	Merid-ional	Circum-ferential	Merid-ional		
A	14.51/4.90	15.47/-13.82	30.12/-4178	35.76/-35.89	48.3/44.70	0.0/.08
B	3.35/3.35	2.23/2.23	35.90/-36.11	35.90/-36.14	38.70/33.40	.25/.45
C	-2.02/-2.02	-1.35/-1.35	0.0/0.0	0.0/0.0	1.78/1.78	26./26.
D	-7.56/3.54	-19.89/17.09	15.47/11.40	6.81/-6.76	18.40/13.30	1.63/2.64

*Von Mises combined stress.

Primary Allowable Stress. The primary stress allowable used in the present analysis is based on creep-rupture data for Inconel 625 as shown in Figure 3-75. To allow for extrapolation and data uncertainties, the primary allowable was based on the creep-rupture strength for the Inconel 625 at 10 times the design life of 30 years. The resulting primary allowable is approximately 9.31 MPa (1350 psi).

Secondary Allowable Stress. The procedure followed to determine the secondary stress allowable for the baseline system will be utilized in the present analysis. Again, material creep rates and stress levels establish the amount of stress relaxation per daily cycle, and creep damage accumulates as a function of the stress levels during each relaxation period.

Thermal and pressure cycle data used to determine the secondary allowable working stress are shown in Figure 3-83. The daytime portion of the cycle was assumed to consist of 12 hours of isothermal operation followed by three steps (idealized) for nighttime cool down at one hour each. The remaining cool down time (9 hours) is assumed to happen rapidly until ambient temperature is reached. The stress relaxation during each assumed isothermal segment of a 24 hour day was predicted with methods used for the Stirling receiver. For the Inconel 625 at a temperature of 871°C (1600°F an operating life expectancy of approximately 15 years for the stress-strain history of Figure 3-84 results for an initial stress of 138 MPa (20 Ksi).

3. Structural Analysis. A preliminary structural analysis of the Brayton Cycle Engine receiver core operating at 871°C (1600°F) has been completed. Applied loads on the receiver consisted of an internal pressure ranging from 1 to 5 atmosphere and the thermal gradients shown in Figure 3-85. Initial sizing calculations of the receiver heater tubes and toroidal manifold components for Inconel 625 was performed using equations from References 3-36 and 3-37. Secondary stress considerations, which account for local discontinuity pressure induced bending stresses and stresses caused by thermal gradients, were computed based on the initial material sizes. Figure 3-86 presents a detailed sketch of a portion of the receiver core showing the heater tube interface with the toroidal manifold. The estimated thermal gradients and internal pressure are also shown in Figure 3-86. Final stress calculations were made from appropriate equations from Reference 3-37.

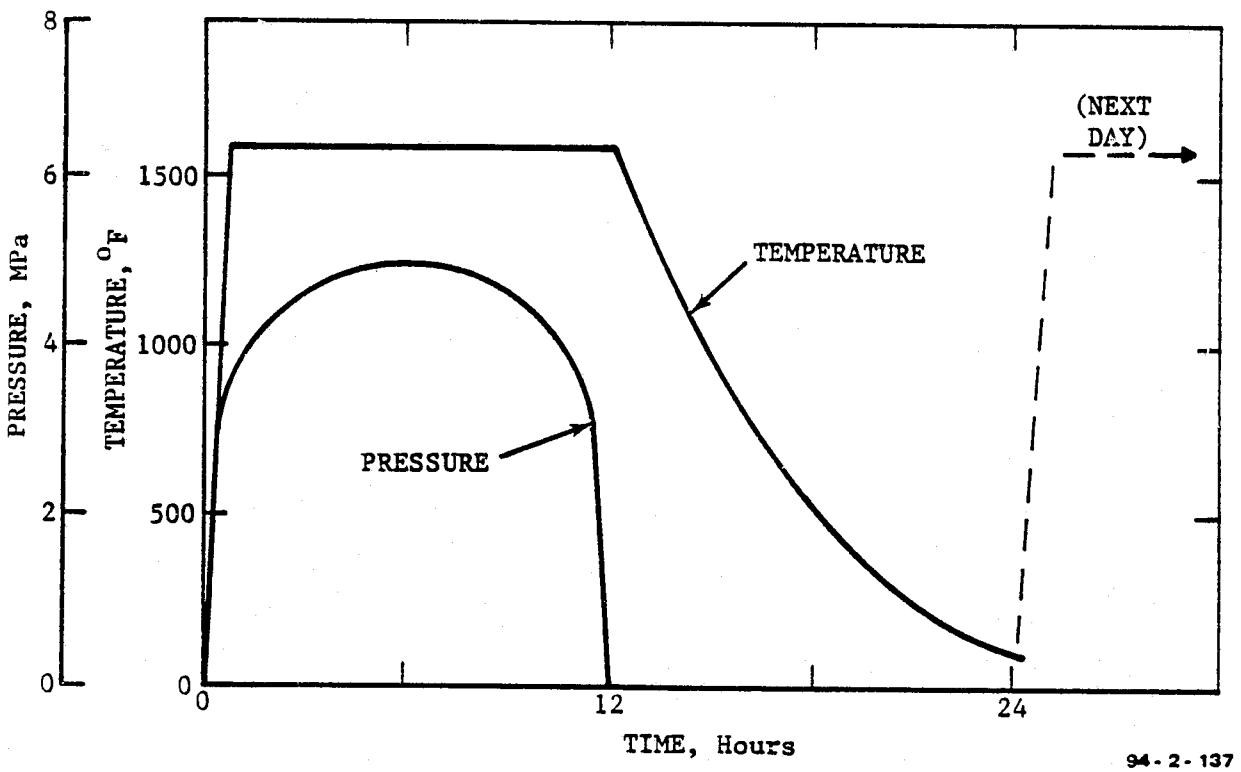

FIGURE 3-83. TYPICAL DAILY PRESSURE/TEMPERATURE PROFILES

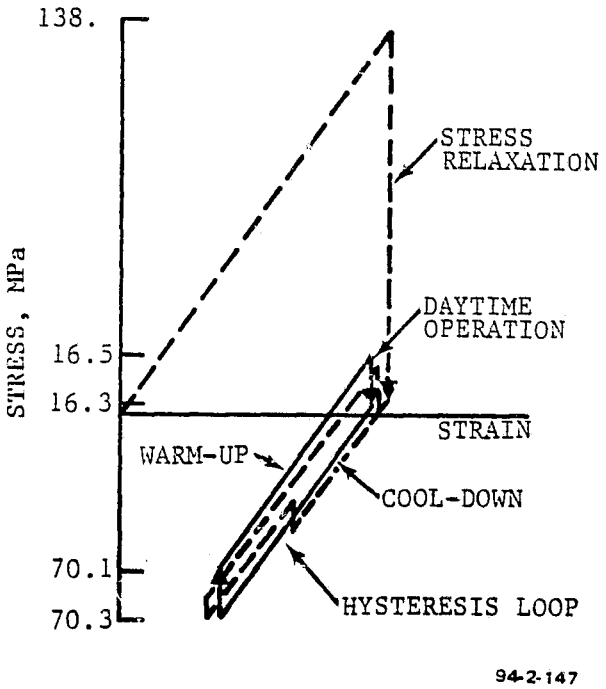

FIGURE 3-84. STRESS-STRAIN CYCLE

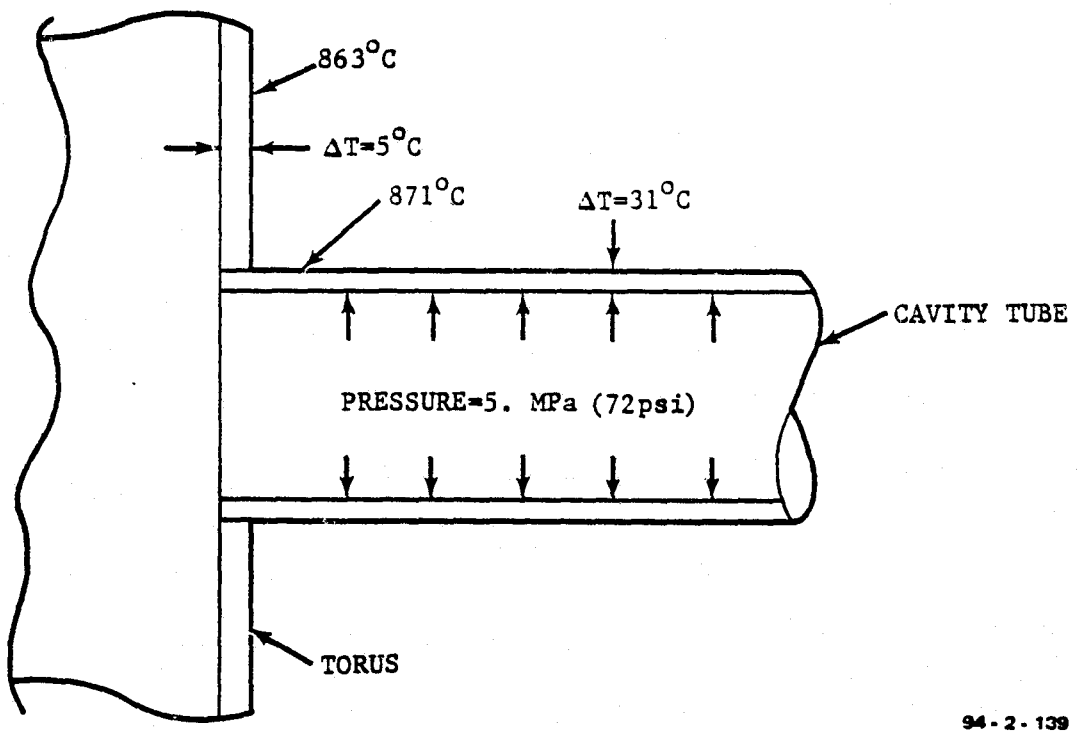

FIGURE 3-85. PRESSURE/TEMPERATURE OPERATING CONDITIONS

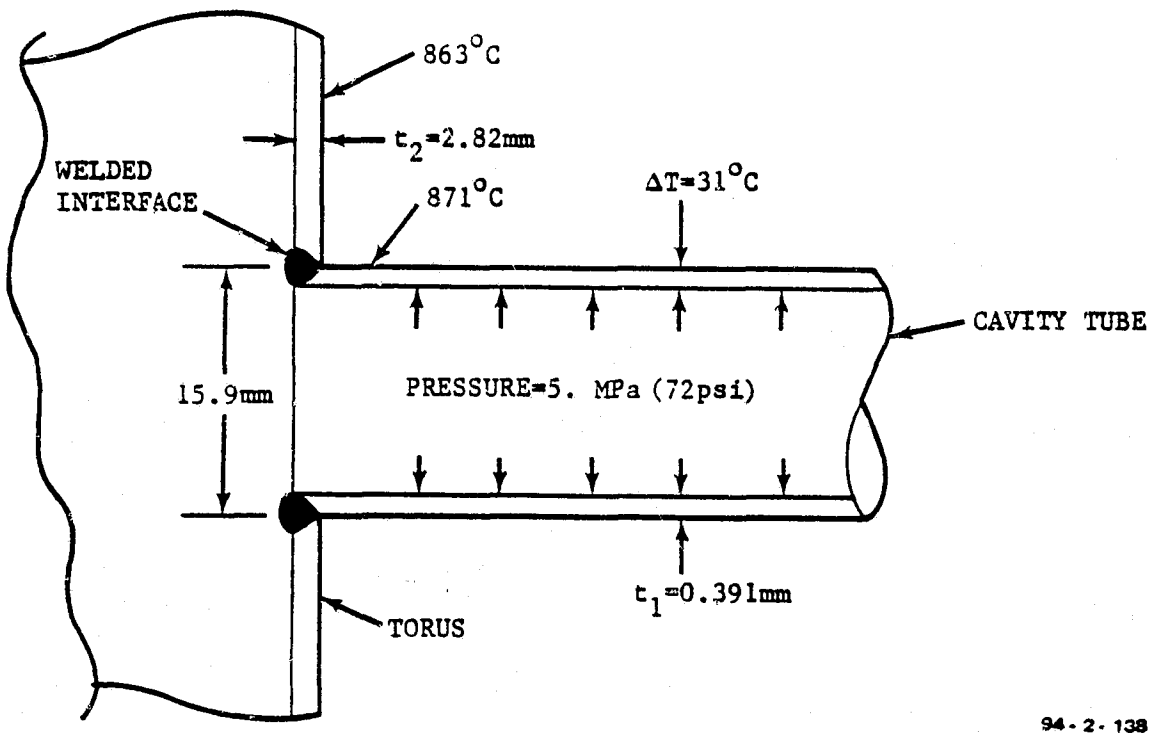

FIGURE 3-86. DETAILS OF TUBE/MANIFOLD INTERFACE

(a) Structural Design. Initial sizing of receiver component parts was performed using equations from References 3-36 and 3-37 based on allowable membrane stresses. The tubular and toroidal shaped portions of the receiver design were sized using equations (3-29) and (3-30):

$$t_{cyl} = \frac{PR}{SE_o - .6P} \quad \text{(mm)} \qquad (3\text{-}29)$$

and

$$t_{sph} = \frac{1}{2}\frac{PR}{S}\left[\frac{2R_1 - R}{R_1 - R}\right] \quad \text{(mm)} \qquad (3\text{-}30)$$

where:

t = Thickness, mm

P = Internal Pressure at working temperature, MPa

R_1 = Outer Toroidal Radius, mm

S = Primary stress allowable, MPa

t_o = Welded joint efficiency = 0.9

The preliminary sizing calculations of the receiver component parts, using Equation(3-29)and(3-30)with a working internal pressure of 0.5 MPa (72 psi) and primary allowable stress of 9.31 MPa (1350 psi), resulted with the following thicknesses:

- Heater tubes ("U"-shaped cavity tubes) $t_1^* = 0.391$ mm (0.0154 inches)
- Supply manifold (Input torus) $t_2^* = 2.81$ mm (0.111 inches)
- Return manifold (Output torus) $t_3^* = 2.90$ mm (0.114 inches)

*These values do not include a corrosion allowance.

(b) Corrosion Allowance. Material corrosion rates due to atmospheric oxidation have been estimated for 15 years of receiver life. The rate of material loss was assumed to be approximately 0.0318 mm/yr. This rate of corrosion would account for approximately 0.477 mm of material loss over the entire life (15 years) of the receiver core. This allowance for material loss would therefore be superimposed with the initial heater tube thickness and result with a final tube thickness of approximately 0.868 mm (0.034 inches).

(c) Stress Analysis. The structural integrity of the typical heater tube/manifold interface shown in Figure 3-86 has been evaluated in detail. The external loads, as shown in Figure 3-86, consists of an internal pressure of 0.5 MPa and temperature gradients through the tube walls and between tube and torus components. The "U"-shaped heater tubes, which are cantilevered

from the torodial manifolds, are unrestrained and allow thermal growth due to the high operating temperatures. The critical stress point predicted by the model is the tube/manifold intersection.

The detailed stress evaluation of the structure interface shown in Figure 3-86 was based on the following conditions:

- Meridional and circumferential pressure stresses.
- Temperature gradients across tube walls.
- Differential radial expansion of tube/toroidal components due to high operating temperatures.

The above conditions were evaluated using the internal pressure load and temperature gradients shown in Figure 3-86. The tube and manifold thicknesses are minimum skin thicknesses and resulted in the largest combined stresses. The effective stress computed was approximately 138 MPa (ksi). This stress level will allow for a receiver life of at least 15 years.

f. Rankine Cycle Receiver Configuration. The Rankine cycle receiver design consists of helical shaped tubular cavity with 8 individual tubes 25.4 mm (1 inch) in diameter connected at each end to toroidal manifolds. The tubular (helical) configuration proves a reasonably large cavity surface area with a relatively small cavity diameter. This allows sufficient heat transfer capability and reduces thermal gradients through the tube walls. The low operating temperatures allow the use of relatively low cost stainless steel. Specific design requirements and conditions assumed for the Rankine cycle receiver subsystem core are listed in Section 3.1.2.1.

1. Allowable Stresses. The allowable operating stresses (primary and secondary) are based on the mechanical properties of Type 316 Stainless Steel. Primary stresses, pressure induced tube membrane stress levels, will be limited by the material creep-rupture strength. The mild operating temperature of 427°C (800°F) of the receiver allows a high primary stress allowable of 444.7 MPa (64.5 Ksi) for 30 years of operation. The amount of stress relaxation occurring during the receiver life will be very limited because of the mild operating temperatures. Most likely the dominant amount of damage will result from low cycle fatigue. Based on low cycle fatigue damage, the secondary stress level is anticipated to approach the yield strength (~ 138 MPa) of the material at operating conditions.

2. Structural Analysis. A preliminary study concerning the structural integrity of the Rankine Cycle Engine receiver core operating at 427°C (800°F) has been completed. The study was aimed at estimating the receiver operating life-time based on a limited amount of current pressure and thermal information. Initial sizing calculations of the receiver helical tubes and toroidal manifold com-

ponents for Type 316 Stainless Steel was performed using equations from References 3-37 and 3-39. These preliminary sizing calculations were increased by an amount equal to the material corrosion rate (~ 0.102 mm/year) times the predicted life expectancy (~ 15 years) of the receiver core. The resulting tube thickness is 1.65mm (0.065 inches). Secondary stress considerations, which account for local geometric discontinuities, were estimated based on the initial material size.

The results of this conservative, preliminary study indicate a receiver life of at least 15 years; perhaps as long as 30 years.

3.1.2.3 Receiver Cost Analysis

1. Sodium Receivers. The manufacturing cost quotations for two sodium receiver subsystem configurations are presented in this paragraph. A drawing of the baseline receiver is shown in Figure 3-33 (Paragraph 3.1.1.4). Figure 3-36 presents the same type of receiver but with added buffer storage. This storage is obtained from a eutectic salt (typically 75 NaF/25 MgF_2) encapsulated in the tubes contained within the walls of the receiver.

The cost quotes that were obtained for fabricating the two sodium receiver cores are presented in Table 3.22.

TABLE 3.22. RECEIVER CORE
(Sodium "Reflux" Boiler for P-75 Stirling Engine)

Vendor	Configuration	Cost Per Unit, Dollars	
		2 units(1)	100K units(2)
B&B Precision, Inc. 15506 Minnesota Ave Paramount, Ca. 90723	Baseline Buffer Storage	14305 21410	950 1800
In-House Manufacturing FACC, Newport Beach	Baseline Buffer Storage	8178 19262	1618 4109
Fansteel Precision Sheetmetal 5235 West 104th St. Los Angeles, Ca. 90045	Baseline Buffer Storage	26800 41693	2201 4596

(1) Near term (2) Far term

The estimated costs of the receiver components which includes cost for limited quantity (2 units) and large production runs (100K units) are shown in Table 3.23 for the baseline receiver design.

TABLE 3.23. RECEIVER COMPONENTS

Item	Cost Per Unit, Dollars	
	2 Units	100K Units
Vapor Pipe	40	15
Receiver Door	65	25
Sodium	215	40
Bellows	1500	72
Insulation	600	180
Drive Motor & Mechanism	570	196
Valve	4000	238
Total Materials & Labor	$6990	$766

The far term (100K units) manufacturing costs for the receiver subsystem without buffer storage is divided into labor and materials cost in Table 3.24.

TABLE 3.24. LABOR/MATERIAL COSTS

Vendor	Labor Cost, $		Material Cost, $	
	Receiver Core	Receiver Components	Receiver Core	Receiver Components
B-B Precision	467	365	483*	401
FACC	1135	365	483*	401
Fansteel	1718	365	483*	401

* Material cost from each vendor is constant.

An equation was derived to determine the cost of receivers of arbitrary size based upon the information presented above. The relationship between receiver subsystem cost, labor, and materials is:

$$\text{Cost } (\$) = \text{Labor} + \text{Material} \left(D_r^2 \Big/ D_{r_o}^2 \right)$$

Where

Cost = Total subsystem cost, Dollars
Labor = Receiver core labor plus receiver components labor costs, Dollars.
Material = Receiver core material plus receiver components material costs, Dollars.

D_r = Receiver cavity aperture diameter, meters.

D_{r_o} = Baseline receiver cavity aperture diameter, meters

The cost figures from the three sources can be written:

B-B Precision $\quad \text{Cost } (\$) = 832. + 4960 \left(D_r^2 \right)$

FACC $\quad \text{Cost } (\$) = 1500. + 4960 \left(D_r^2 \right)$

Fansteel $\quad \text{Cost } (\$) = 2083. + 4960 \left(D_r^2 \right)$

Figure 3-87 presents plots of these equations for cavity aperture diameters of 0.1 to 0.6 meters. The results indicate the nominal cost for the complete baseline receiver subsystem (D_r = 0.422m) as approximately $2400. The high and low bids were $2950 and $1700, respectively.

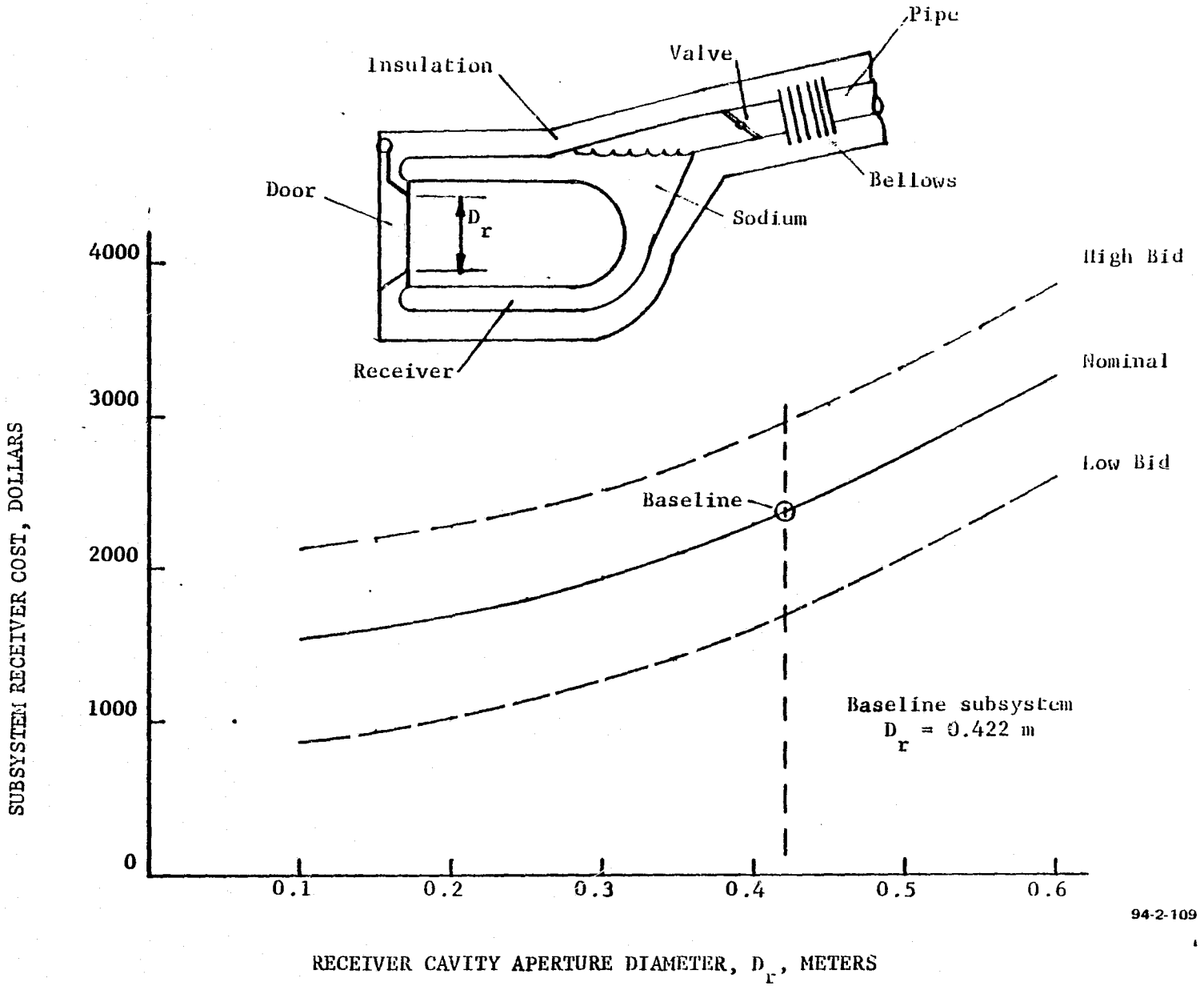

FIGURE 3-87. FAR TERM COST OF COMPLETE RECEIVER SUBSYSTEM

2. Brayton Receiver Cost Analysis. The cost quotes for the Brayton receiver configuration shown in Figure 3-40 (Paragraph 3.1.1.4) were:

Brayton Receiver

Quantity	Cost, Dollars
Near Term (1 or 2 units)	100,000
Far Term (100K units)	10,455

These values include the thermal insulation.

The Brayton receiver cost equation for the far term cost data is:

$$\text{Cost (\$)} = 6000 + 37641\left(D_r^2\right)$$

which relates receiver cost, labor, and materials as a function of cavity aperture diameter.

Figure 3-88 shows a plot of the cost curves for the Brayton receiver together with the baseline Stirling receiver and the Rankine receiver. The results of the Brayton cycle receiver cost analysis indicates a receiver subsystem cost, including insulation, with a cavity aperture diameter of 0.344 meters to be approximately $10,455.

3. Rankine Receiver Cost Analysis. Updated Rankine receiver costs have been obtained based on the receiver design shown in Figure 3-42 (Paragraph 3.1.1.4). Thermal insulation and other miscellaneous hardware were also included in the following estimate.

Rankine Receiver

Quantity	Cost, Dollars
Near Term (1 or 2 units)	50,000
Far Term (100K units)	4,500

The cost equation of the Rankine receiver based on the far term cost data is:

$$\text{Cost (\$)} = 1500 + 7300\left(D_r^2\right)$$

Figure 3-88 shows a plot of this equation. A cavity aperture diameter of 0.64 meters results in a receiver cost of approximately $4500.

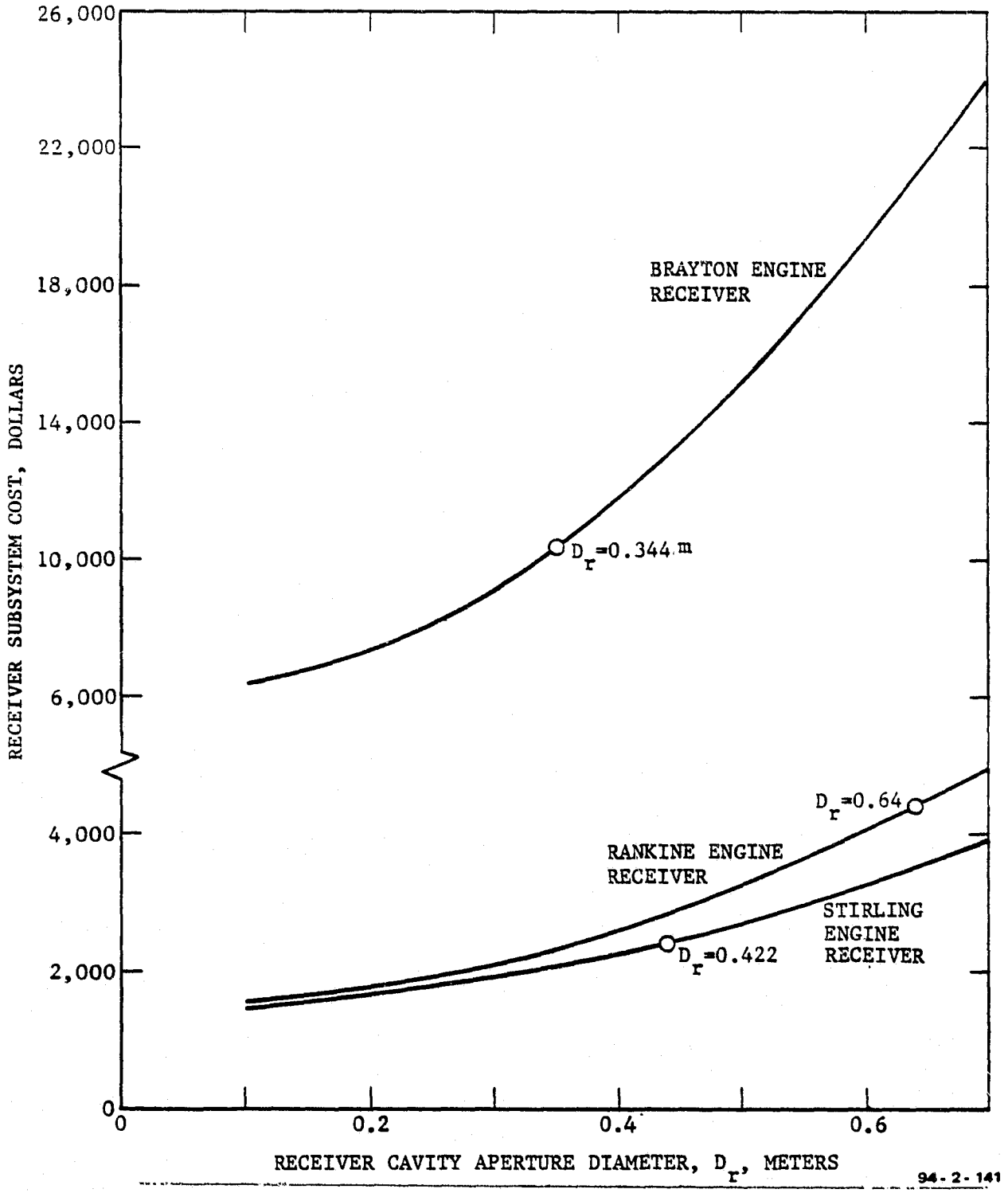

FIGURE 3-88. GENERALIZED RECEIVER COST IN MASS PRODUCTION, CA 1990

3.1.3 CONCENTRATOR DESIGN AND INSTALLATION

3.1.3.1 Design. The concentrator design is based on mature microwave dish technology, modified to fit the particular requirements for solar applications. The major difference with microwave technology was to find ways to cut the cost of the concentrator, since current microwave dishes are prohibitively expensive for solar applications. A significant cost reduction was obtained by two techniques: (1) relaxing the requirements, since the values of the surface errors, tracking errors, etc. are not as restrictive for solar concentrators (although the cost of the reflective surface is greater), and (2) the development of innovative approaches to the design and fabrication. The second technique is the major factor in concentrator cost reduction.

The analyses that were performed to select the baseline concentrator were too extensive to publish in the body of this report, therefore, the material is contained in Appendix A, along with other information on costs, construction techniques and cleaning. Only a summary of the concentrator design is contained in this section.

Figure 3-89 is an artist's conception of the baseline concentrator concept. The interesting and innovative feature of the design is that the structure to support the 18.6 m reflector or mirror (11.2 m for the 3-1/2 year system) is in front of the parabolic surface. Trade studies documented in Appendix A demonstrate that this is a cost-effective approach. Actually, the design in a direct development of conventional microwave structures in which the usual back structure is moved to the front. This significantly enhances the structural stiffness and improves the load paths, resulting in a lighter and less costly design. The primary disadvantage is the solar blockage/shadowing caused by the radial and circumferential elements. These must be carefully sized and located to minimize the loss of solar energy. In actual practice, the diameter of the concentrator (dish) is increased slightly to offset this effect.

Figure 3-90 shows a side view of the complete unit. The dish drive is a conventional azimuth-elevation configuration (Az-El). A tripod is used to support the power module (receiver/engine/AC generator) behind the focal plane. The optimum rim angle determined from system studies is 65°.

A summary description of key components follows:

- Reflector Panels. Glass has been chosen for the panels, specifically Corning draw fusion process, Code 7806 modified glass. Chemical silvering will be applied to make a second-surface reflective coating which will be protected with copper cladding. The glass will be shaped by pressing (or sagging) while heated to form the proper two-dimensional shape. The details of a typical panel construction are shown in Figure 3-91. The glass is supported by a sandwich structure of 5 cm (2 in.) of structural foam enclosed by galvanized steel sheets. The attachment of the glass to the steel is by means of a layer of silicone rubber adhesive. The panels are pie-shaped; five

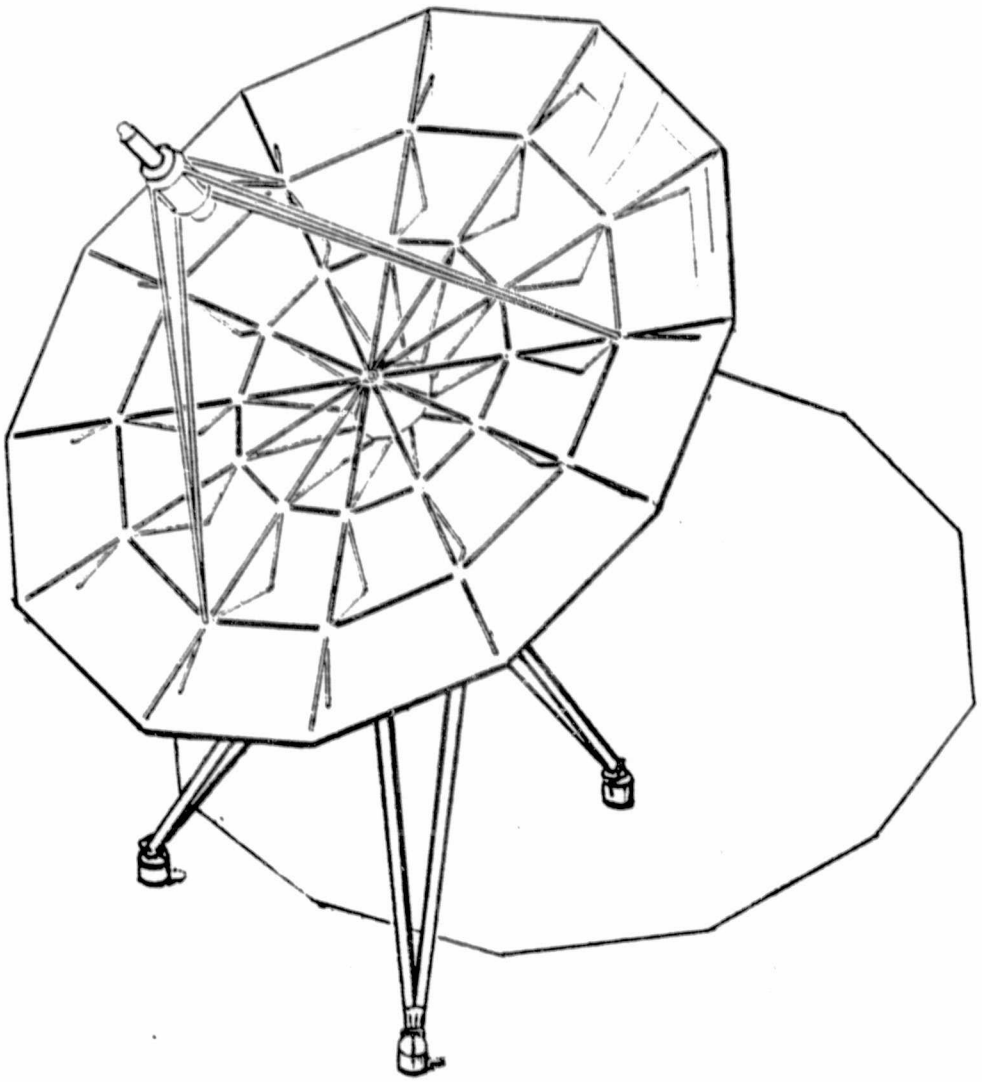

94-2-119

FIGURE 3-89. PROPOSED FRONT-BRACED CONCENTRATOR DESIGN.

ORIGINAL PAGE IS
OF POOR QUALITY

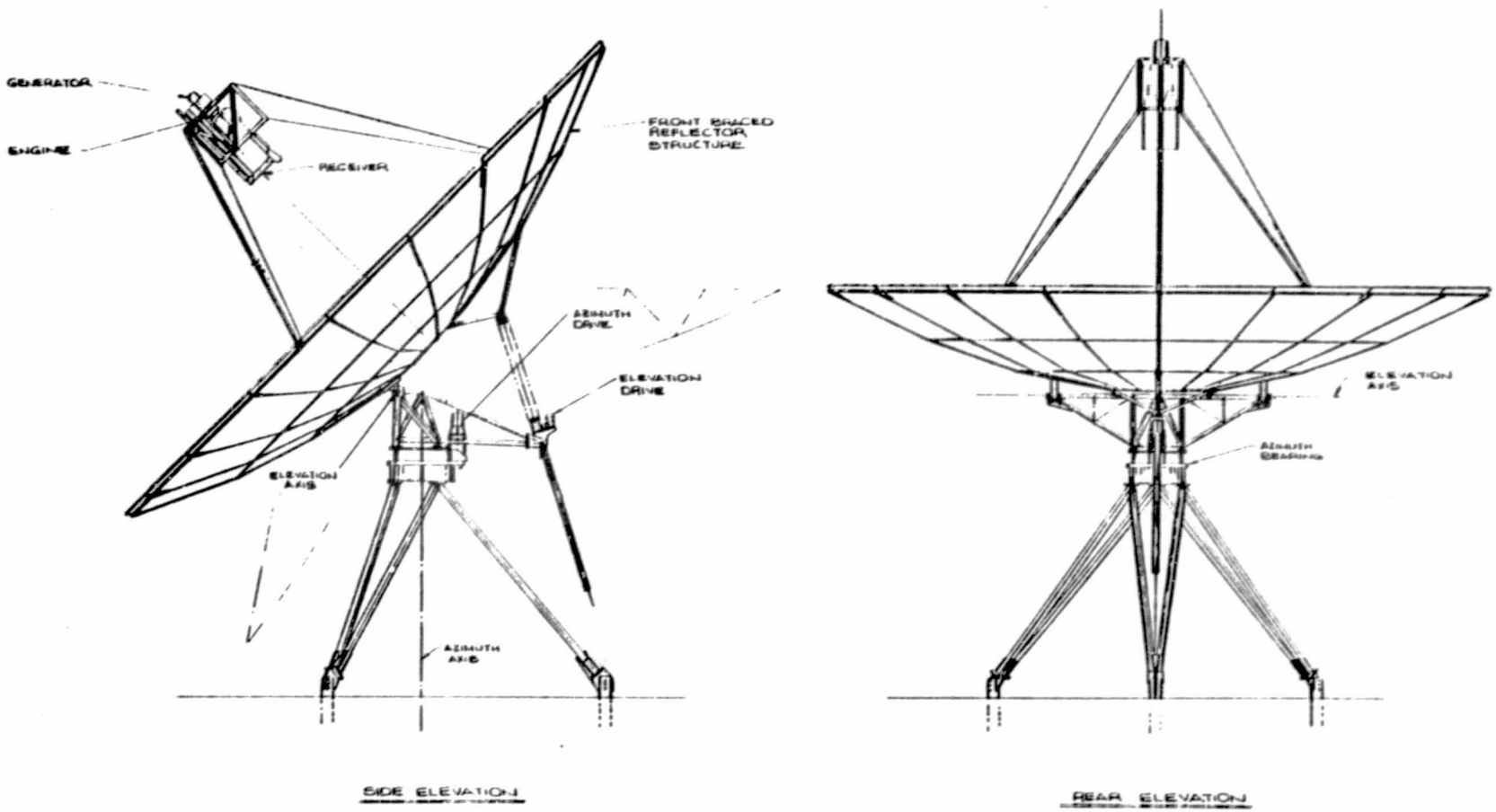

FIGURE 3-90. PROFILE VIEWS OF 18.6m FRONT BRACED CONCENTRATOR WITH Az-El FIXED LEG MOUNT

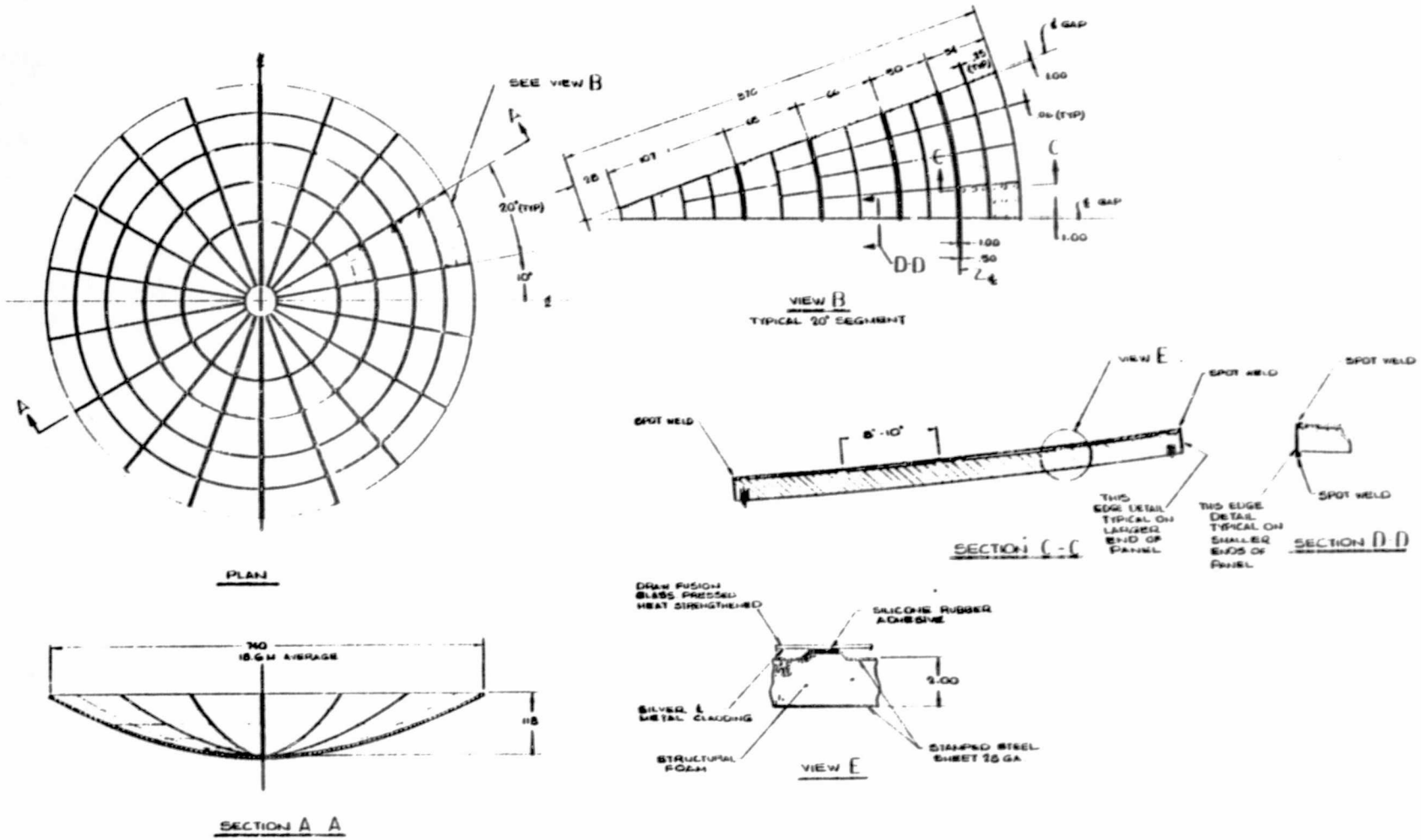

FIGURE 3-91. DETAILS OF REFLECTIVE SURFACE PANELS

rows are used in the radial direction for the 18.6 m dish, and there are 18 panels in each row. The average panel length is 2.3 m (7.7 ft) and the average width is 1.3 m (4.4 ft). Panel attachment is made using steel clips which are mounted to the sandwich and bolted to the truss structure.

- Reflector Structure. The reflector structure is a space truss composed of 18 radial trusses radiating from the center of the structure (See Figure 3-92). These are connected in the circumferential direction to form hoop members (two circumferential hoops on the front structure, 6 on the structure behind the mirrors). Torsional bracing is provided in the structure behind the mirror for additional stiffness and stability. Typical cross-section of the front structure members is about 4.6 cm (1.8 inches), and they are made from readily available square steel tubing.

- Pedestal. The Az-El mount was selected as a result of a trade study. The features and advantages are detailed in Appendix A. The base support (fixed pedestal) shown in Figure 3-90 consists of six members transferring loads from three points on the underside of the azimuth bearing housing to three foundation piles. All members are made of steel and were primarily designed on the basis of gravity plus survival wind loads. Other components are:

  - Azimuth Bearing (Ball Bearing)
  - Elevation Bearings (Two Spherical Roller Bearings)
  - Azimuth Drive (Bull Gear and Pinion)
  - Elevation Drive (Machine Screw Actuator)

- Drive Control. Each axis will be equipped with an electric motor, gear reducer and drive unit. These single-speed AC induction motors will be driven in steps based upon commands from the central microprocessor.

- Tracking System. Solar tracking consists of a combined (hybrid) system of coarse programmed tracker with a fine optical step-track. The central microprocessor will generate the coarse solar ephemeris data and convert it to the appropriate signals for the concentrators. The optical tracker will consist of a narrow field of view photo-cell sensor which will be used to provide a calibration of the ephemeris inputs.

3.1.3.2 Installation. The installation and check-out of large concentrators require careful planning to minimize costs and assure the required performance. A summary of the details presented in Appendix A is given below.

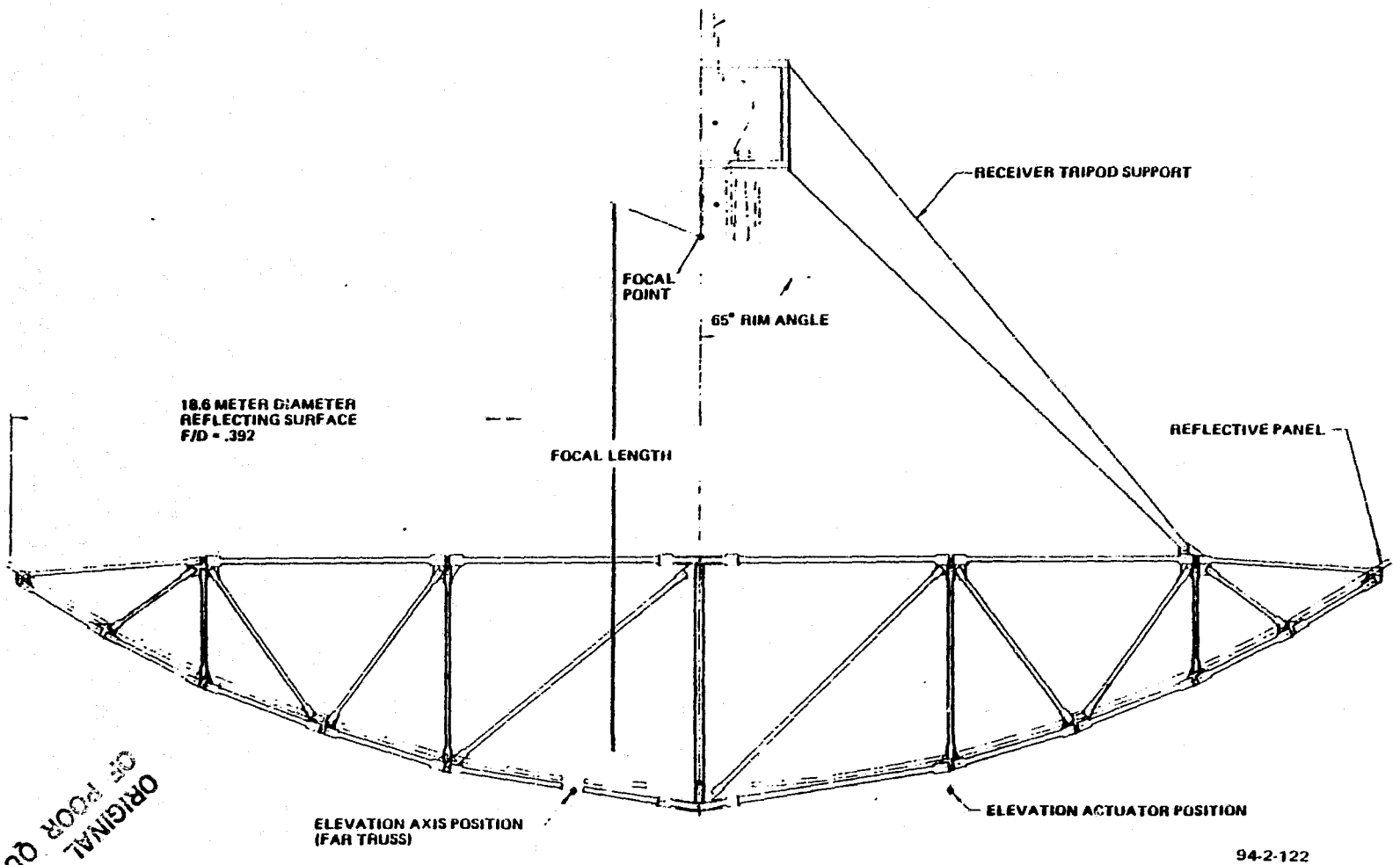

FIGURE 3-92. RADIAL TRUSS FOR FRONT BRACED CONCENTRATOR

ORIGINAL PAGE IS OF POOR QUALITY

- Site Layout. This consists of surveys, clearing, access roads, etc.

- Foundation Construction. Inexpensive pile foundations are used, three per concentrator. Wooden piles are the most cost-effective and will be driven by a conventional pile driver (see Step (1A) of Figure 3-93.)

- Initial Set-Up. After delivery to the site all components will be positioned according to a staging plan. The necessary alignment fixtures, jigs, cribbing, supports, cranes, etc. will be available.

- Reflector Radial Truss/Assembly. The tubular members are assembled into two horizontal assembly jigs (a single jig is shown in Step (1B). These assure precise alignment and rapid assembly.

- Reflector Structure and Panel Assembly. The radial trusses are mounted into a reflector assembly jig (Step (2B), Figure 3-93). The fixture will position each truss in its proper location. Circumferential and diagonal members are added and attached. When all the structure has been connected, the reflector panels are installed (Step (3B)). Since all trusses are automatically aligned in the jig, reflector panels are simply bolted in place -- no further adjustments are needed.

- Pedestal Assembly and Concentrator Erection. The first action is to mount the azimuth bearing/gear housing portion of the turret into a support fixture (Step (2A)). The six support tubes are connected and the elevation actuator attached. The tripod assembly is made on the ground (see Step (3A)). Next, the base/turret/actuator assembly is raised (Step (4)), positioned, and bolted (Step (5)). The crane rotates and lifts the reflector assembly (Step (6)), and positions it so the connections can be made with the elevation actuator clevis and the vertical link bar (Step (7)). The reflector is then raised until the elevation bearing connections can be made and other two links connected (Step (8)). Finally, the tripod structure is added (Step (9)), completing the major assembly of the concentrator.

Maintenance techniques for the concentrator are described in Appendix A.

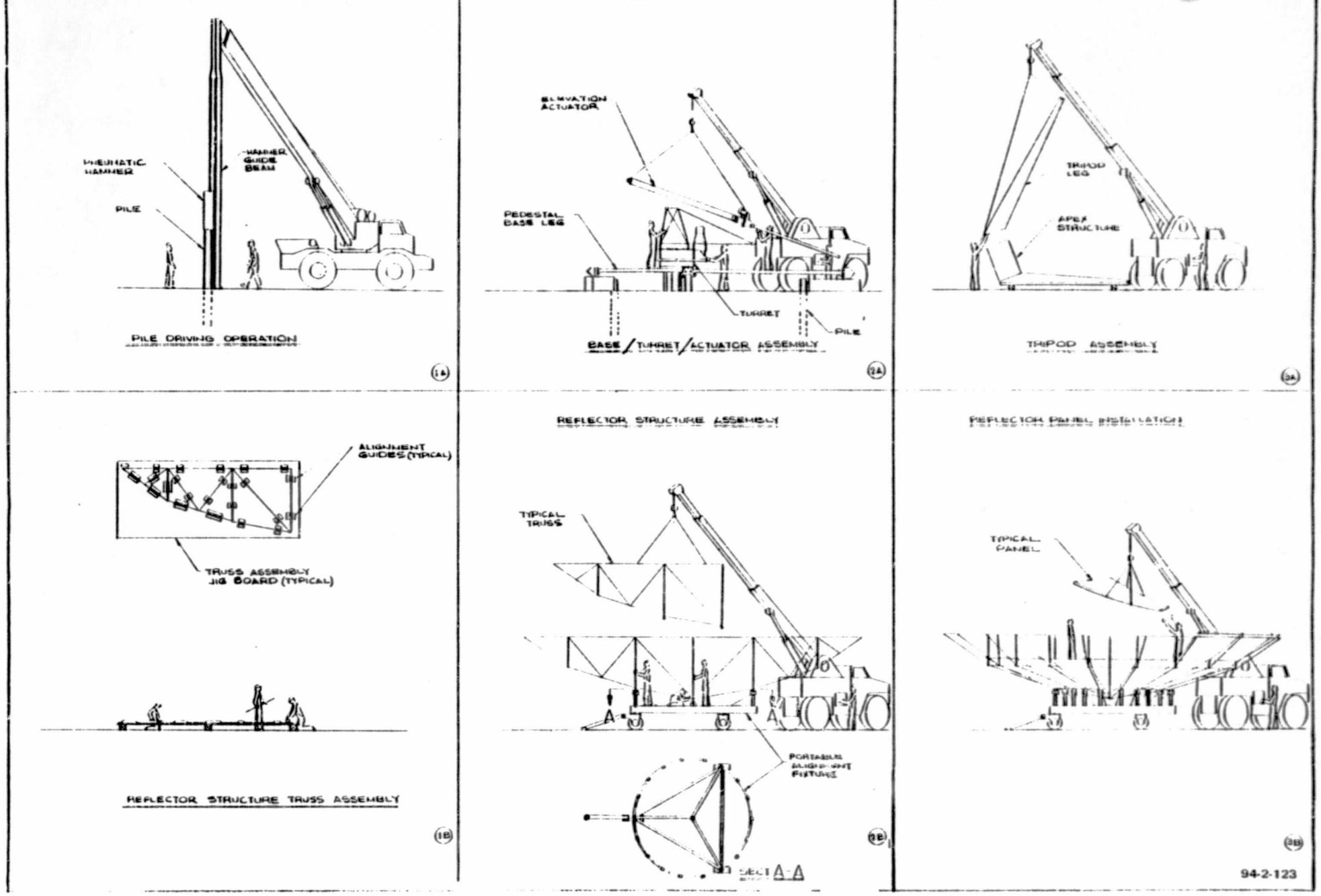

FIGURE 3-93. TYPICAL CONCENTRATOR INSTALLATION SEQUENCE (SHEET 1 of 2)

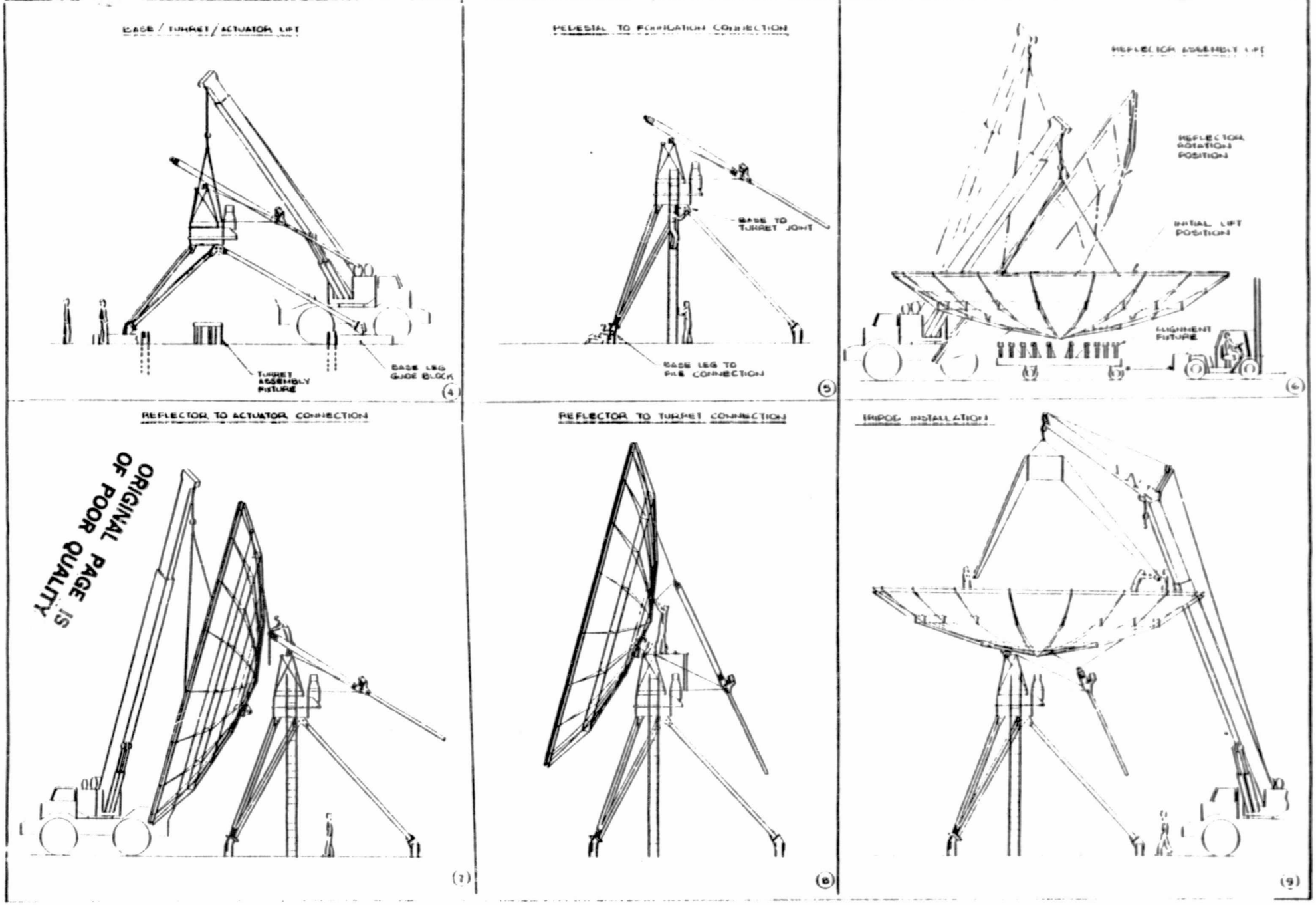

ORIGINAL PAGE IS OF POOR QUALITY

FIGURE 3-93. TYPICAL CONCENTRATOR INSTALLATION SEQUENCE (SHEET 2 of 2)

3.1.4 POWER CONVERSION SUBSYSTEM

The power conversion subsystem is comprised of the Stirling cycle heat engine, its associated power control equipment and the direct-coupled 1800 rpm synchronous AC generator (alternator) and interconnected voltage regulator/sensing circuitry. This equipment is detailed in the following paragraphs. Data on Brayton and organic Rankine cycle engines as received from several engine manufacturers are also presented. These data cover currently available engines and projected future developments in the size range of interest.

3.1.4.1 Baseline Stirling Engines. The United Stirling P-40 engine (Figure 3-94) is the selected power plant for the 3-1/2 year SPS program; the P-75 engine (Figure 3-95) is the selected power plant for the 4-1/2 and 6-1/2 year programs. These engines are the culmination of over 10 years of development by United Stirling of Sweden which is described in detail in Appendix C. Both engines are constructed in the U-crank configuration which is shown in cross-section in Figure 3-96. Although earlier developmental engines have employed a V-crank configuration, USS has determined that the U-crank engines can be manufactured more easily (and cheaper) with the general purpose tooling appropriate to the relatively low production rates anticipated, that is 10,000-15,000 per year. This configuration also offers benefits regarding servicing and ease of maintenance. Comparative physical characteristics of the two power plants are given in Table 3.25. Note that the Stirling cycle features very high specific output; the burner head version produces about 100 kW per liter of displacement (swept volume). This permits very effective power control by displacing only a very small amount of the working fluid. By contrast, the gas turbine is a low specific output power plant, albeit with high power/weight ratio, and a large amount of working fluid must be displaced in the closed-cycle system to achieve a comparable power change.

TABLE 3.25. STIRLING ENGINE PARAMETERS
(@ 1800 RPM WITH SODIUM HEAT PIPE)

PARAMETER	P-40	P-75
DRY WEIGHT (kg)	225	350
DISPLACEMENT (cm^3)	380	1100
WIDTH (mm)	655	800
HEIGHT (mm)	705	920
LENGTH (mm)	580	750
$\bar{P}$(MAX) (Atm)	150	150
MAX. POWER* (kW)	27.3	81.9
RATED POWER* (kW)	21.8	63.4
EFFICIENCY AT RATED POWER	0.373	0.393

* @ T_E = 800°C, T_∞ = 44.6°C

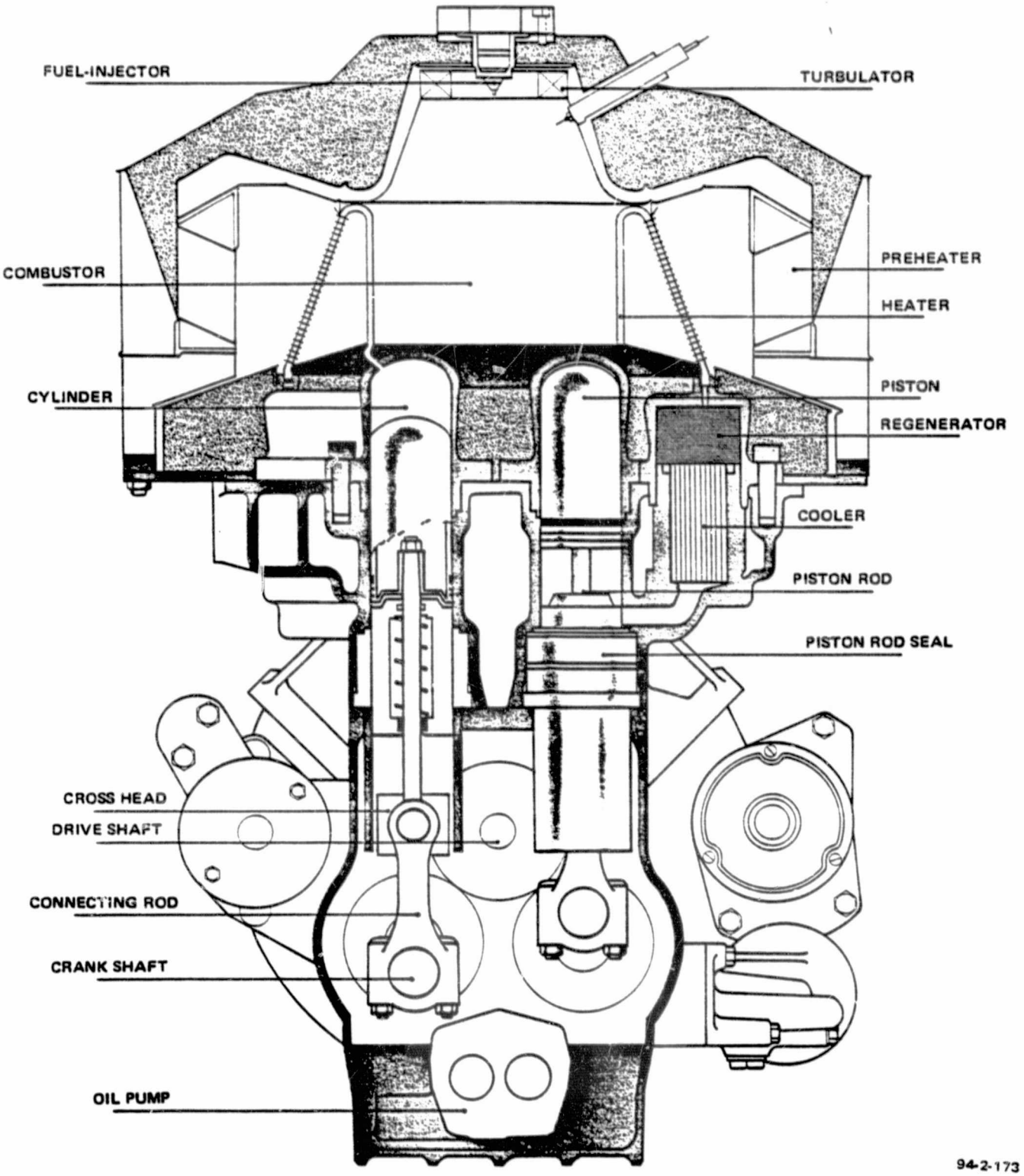

FIGURE 3-96. SCHEMATIC OF USS P-75 STIRLING ENGINES - U-CRANK CONFIGURATION

PRECEDING PAGE BLANK NOT FILMED 3 - 181
3-182

a. Performance - P-40 and P-75 engine performance provided by USS is shown in Figures 3-97 and 3-98, respectively. The data are for engines converted for remote heating operation, that is using a sodium heat pipe (or vapor pipe) to transport thermal energy to the heater tubes. The working fluid is helium rather than hydrogen which avoids contaminating the sodium system. The existing external combustion components (preheater, turbulator, blower, A/F controls, etc.) are removed and the amount of heater tube area is substantially reduced to accommodate the very high heat transfer rates associated with condensing sodium. The net result of these changes is a significant increase in shaft power and efficiency compared with the burner head version. Note that the data of Figures 3-97 and 3-98 have been generated for the rated, hot-day conditions (44.6°C) at Barstow, California.

For input to the annualized performance computations described in Paragraph 3.1.1.2, the performance data have been generalized into the form: $P_o = f(P_i, T_\infty)$. Specific equations for 1800 rpm operation are given below:

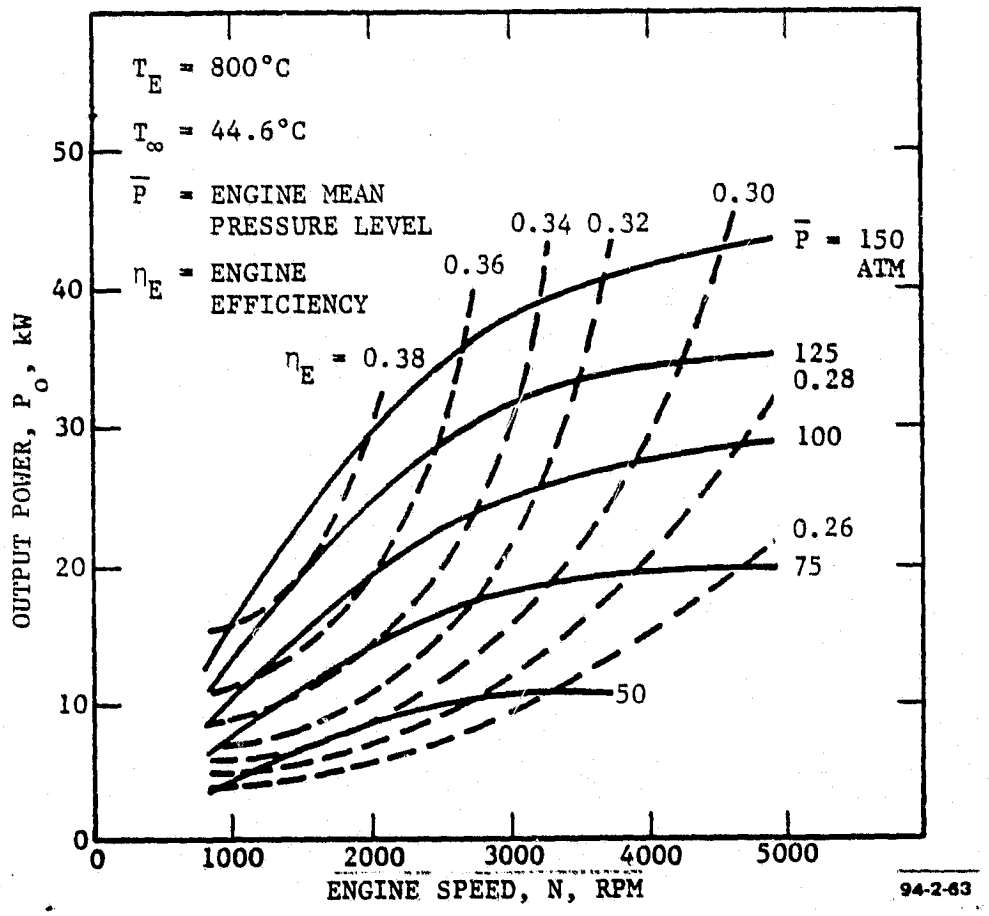

FIGURE 3-97. SODIUM-HEATED USS P-40 ENGINE PERFORMANCE MAP FOR HOT DAY CONDITIONS

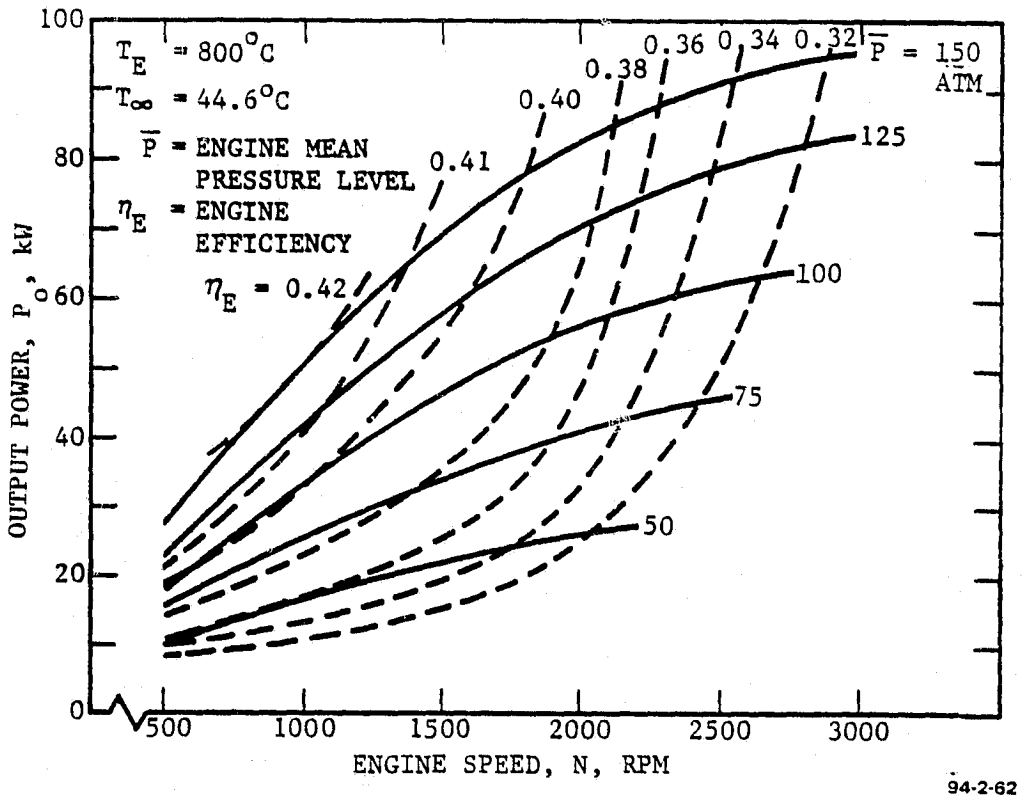

FIGURE 3-98. PERFORMANCE MAP FOR SODIUM-HEATED USS P-75 ENGINE AT HOT DAY CONDITIONS

P-40 Engine:

$$P_o = (0.4083\ P_i - 3.319)\ F_1(T_E)F_1(T_\infty)$$

where

P_o = Shaft (output) power, kW

P_i = Input power, kW

T_E = Engine heater head temperature, °C

T_∞ = Ambient temperature, °C

and $F_1(T_E) = 1.25(10)^{-9}T_E^3 - 4.28(10)^{-6}T_E^2 + 5.155(10)^{-3}T_E - 0.9594$

$F_1(T_\infty) = 1.136 - 3.16(10)^{-3}(T_\infty + 7.0)$

P-75 Engine:

$$P_o = \left[(T_E^{0.1529} - 2.29)\ P_i - 8\right](1.0532 - 0.00355\ T_\infty)$$

Figures 3-99 and 3-100 show the input/output power behavior for the two engines for a range of ambient temperatures.

Note that the above engine data are computer-generated, based on USS fully-verified burner head engine correlations, modified by experimental data on a test engine driven by sodium heat pipes (see Appendix C). All accessories are included in the data, with the exception of the water pump and heat exchanger (radiator) fan which are remotely located and driven by an electric motor.

b. Method of Control. Paragraph 3.1.1.5 describes a simple method of control to accommodate start-up/shut-down and operation under varying solar insolation. The existing engine-located power control subsystem is employed to vary engine output by valving helium into or out of the engine from the integrated compressor/storage bottle assembly. Start-up and synchronization to the utility grid are accomplished under command from the central microprocessor, after which the power control system is slaved to heater head temperature; constant temperature and near-constant efficiency are thus achieved despite substantial solar insolation variation. Engine dynamic response is very good -- much faster than the combined receiver/boiler/heat transport subsystem, which acts as a thermal "choke" to smooth out the small-scale variations in solar insolation. USS reports that the engine can be brought from idle to full power in approximately 1/3 second.

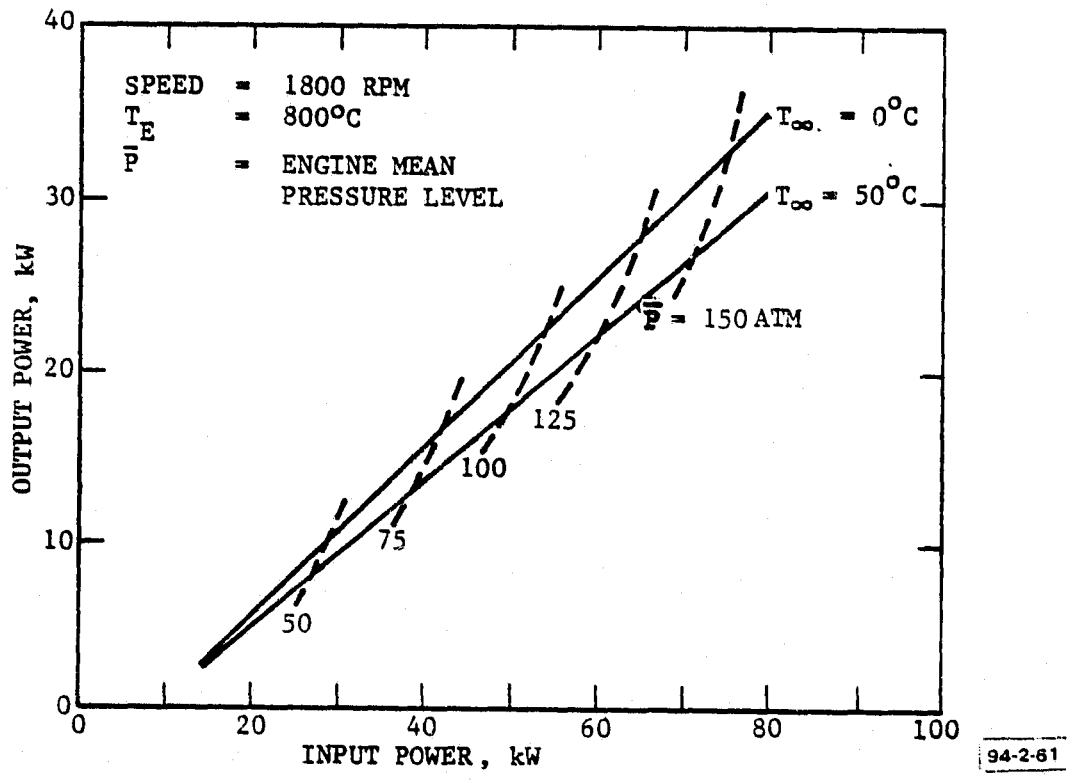

FIGURE 3-99. CONSTANT SPEED OUTPUT/INPUT POWER CHARACTERISTICS FOR USS P-40 STIRLING ENGINE

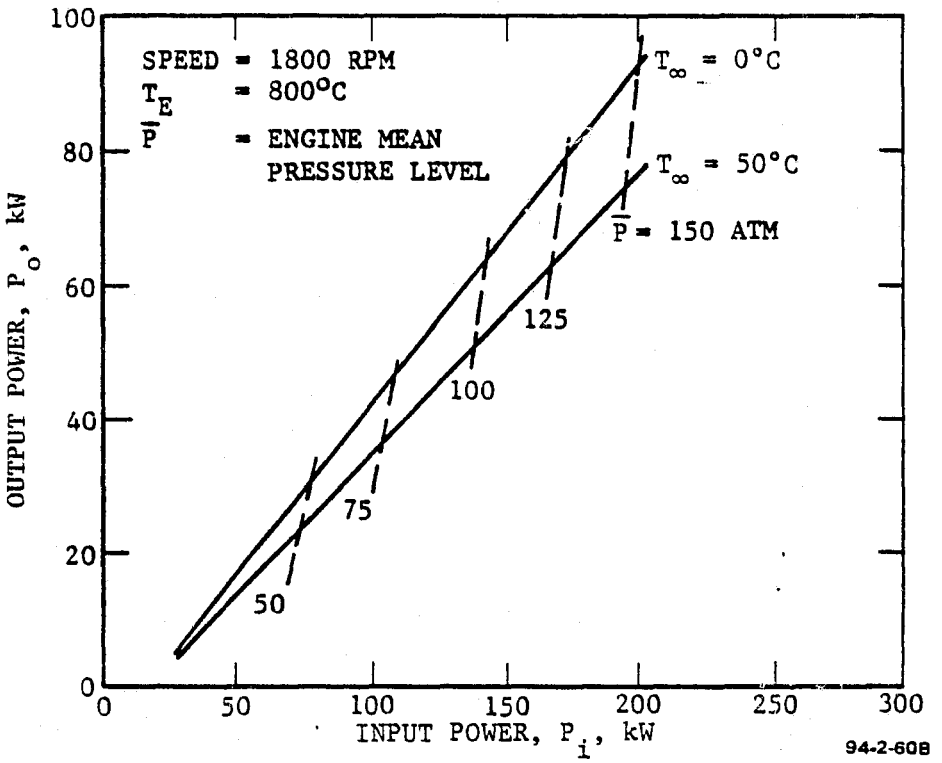

FIGURE 3-100. CONSTANT SPEED OUTPUT/INPUT POWER CHARACTERISTICS FOR USS P-75 STIRLING ENGINE

c. Cost. Figure 3-101 shows engine cost over the power range encompassing the P-40, P-75 and P-150 power plants. The USS data reflect the projected cost (selling price) of the engine, as presently designed, for two different production rates, that is, 10,000/15,000 per year and 100,000 per year. The FACC data are projections based on data supplied by Ford Motor Company personnel for high-volume automotive production, with allowance for retention of high-reliability, long life components. To achieve the lower figures, that is, $2500 for the P-75 engine (~$39/kW rated power), some engine re-design would be necessary and special-purpose tooling would be employed. The capital investment required for this re-design effort has not been estimated; work is currently underway at both USS and MTI, however, to generate such data for the DOE-sponsored automotive Stirling program. It is not clear from the present cost analyses (Paragraph 3.1.1.3) that large capital investment for engine redesign is warranted, since the switch from a $4500 to a $2500 P-75 engine results in a decrease in system energy cost (BBEC) of about 3 mills kWh (~6% reduction).

Figure 3-102 shows projected maintenance costs over the power range of interest. Annaul maintenance costs include (1) quarterly inspection of engine oil supply, helium gas supply components and other externally-located engine equipment and (2) annual replacement of piston-rod seals and piston rings. This latter schedule is somewhat conservative, since current test data show ring/seal life in excess of 4000 hours whereas the engine is actually operated less than 3000 hours per year (except for the integral hybrid concept described in Paragraph 3.1.6.2). USS projects overall engine life at 75,000 hours (~27 years) with replacement of the heater head, regenerator bearings and the sodium inventory at 25,000 hours (~9-year) intervals. A breakdown of these costs, included estimated parts and labor cost, is given in Table 3.26. Levelized maintenance costs, based on life cycle cost projections, are also shown.

TABLE 3.26. STIRLING ENGINE COSTS

COST FACTOR	ENGINE		
	P-40	P-75	P-150
• SALE PRICE ($) (FACC, ca 1990)	1800	2500	4500
• SPECIFIC COST ($/kW RATED POWER)	82	39	36
• ANNUAL MAINT. ($)	135	195	330
(Parts)	(35)	(50)	(90)
(Labor)	(100)	(145)	(240)
• 25,000 HR MAINT ($)	1498	1968	3220
(Parts)	(648)	(900)	(1620)
(Labor)	(850)	(1068)	(1600)
• LEVELIZED MAINT COST ($/kW/YR)	24	11	9.80

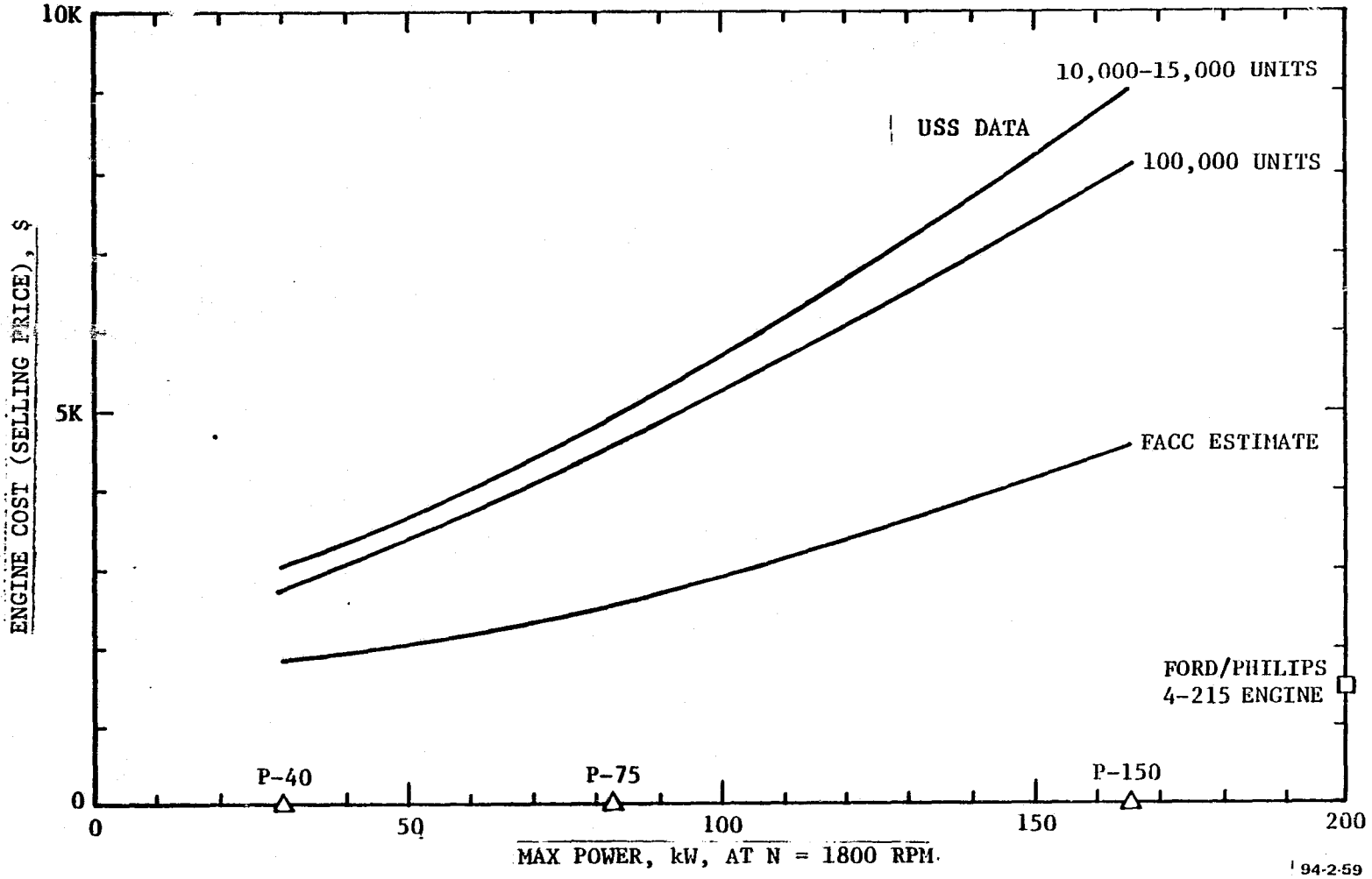

FIGURE 3-101. COST PROJECTIONS FOR PRODUCTION STIRLING ENGINES (SOLAR VERSION)

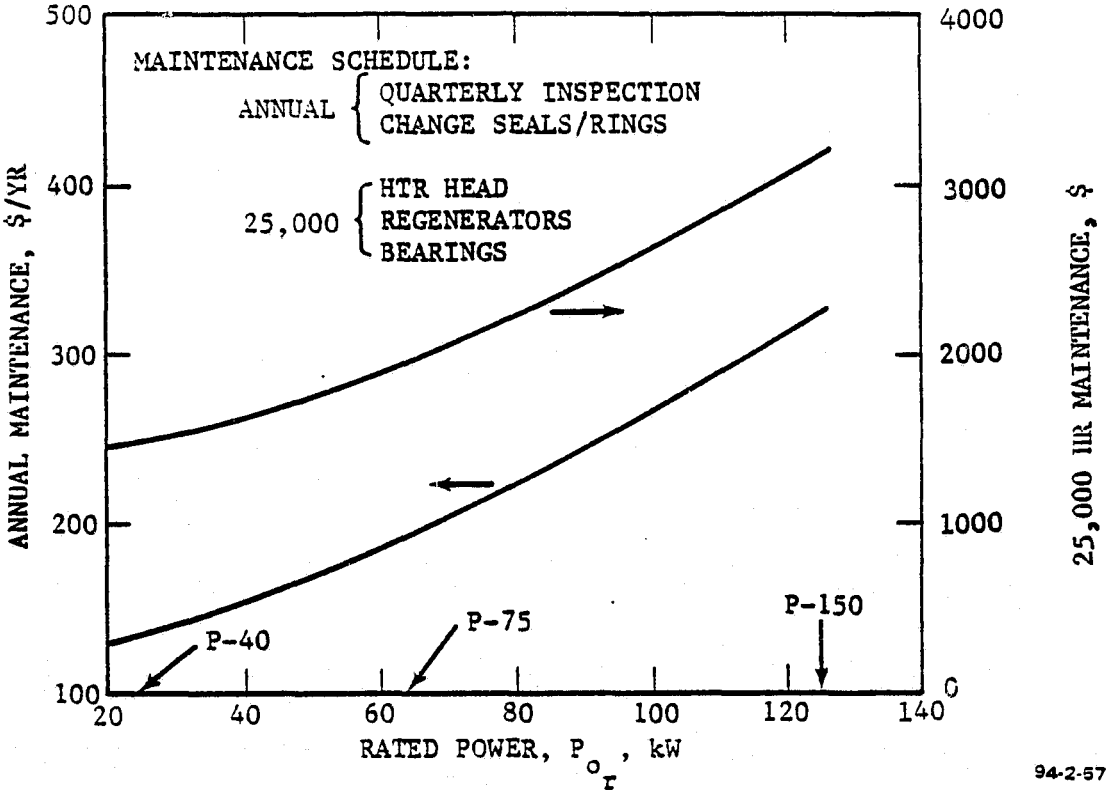

FIGURE 3-102. PROJECTED MAINTENANCE COSTS FOR PRODUCTION STIRLING ENGINES (SOLAR VERSION)

3.1.4.2 Alternator. The AC generator (alternator) for the 4-1/2 and 6-1/2 year program will be a 75 kW/93.5 kVA, 480 volt, 3 phase, 60 Hertz, 1800 rpm machine. A standard commercial unit will be used having a single ball bearing constructed. It will be drip-proof and brushless, and connected directly to the P-75 Stirling engine shaft. It will have Class F insulation suitable for a 50°C rise above ambient and is fan cooled. The maximum voltage imbalance between phases will be 1%; a 5% maximum waveform deviation from pure sinewave; and a maximum harmonic content of 5%. The same type of unit will be used for the 3-1/2 year program except the rating will be 40 kW to correspond to the P-40 engine.

Voltage will be regulated by a built-in SCR-type electronic voltage regulator to 480 V ± 0.5% at any load between 0 and 100%. The regulator will be able to absorb any transient caused by a 50% load change (or less) and restore normal line voltage within 0.1 sec (6 Hz). The unit will be in an all-weather resistant metal enclosure mounted on the alternator.

Selection of an alternator was made on the basis of electrical subsystem trade studies documented in Appendix B. The subsystem configuration shown in Figure 3-103 was determined to be optimum for the SPS application. Note that the alternator efficiency is rated at 90% today; however, 94% has been projected for ca. 1990 systems.

Additional characteristics of the (typical) alternator are:

- Make: Triclad Type SJ (or equivalent)
- Weight 499 kg (1100 lb)
- Dimensions: 51 cm dia. x 89 cm long (20 x 35 inches)
- Cost: $2689 in quantity production, ca. 1990 (including voltage regulator)

Specific features of the alternator have been chosen for minimum maintenance and reliability (i.e. single-bearing, brushless design). The bearing is permanently sealed with a rated life of 5 years for continuous service of a life of 15 years for solar applications. Bearing replacement will be scheduled to coincide with engine overhaul or other maintenance functions. The voltage regulator has no moving parts and requires no maintenance. With bearing replacement, the life of the alternators will exceed 30 years.

The alternator is a part of the power module package (receiver/engine/alternator). Details of the installation of the unit have been described in Paragraph 3.1.1.4.

3.1.4.3 Alternate Engines. Brayton and Rankine cycle engines were studied as possible alternates to the Stirling heat engine. Although complete in-depth analysis of these engines was not possible within the schedule and cost constraints of the program, substantial input data were received from several engine manufacturers relating both to currently available engines in the size range of interest as well as to projected future developments. This information was used in system-level analysis of alternate engines.

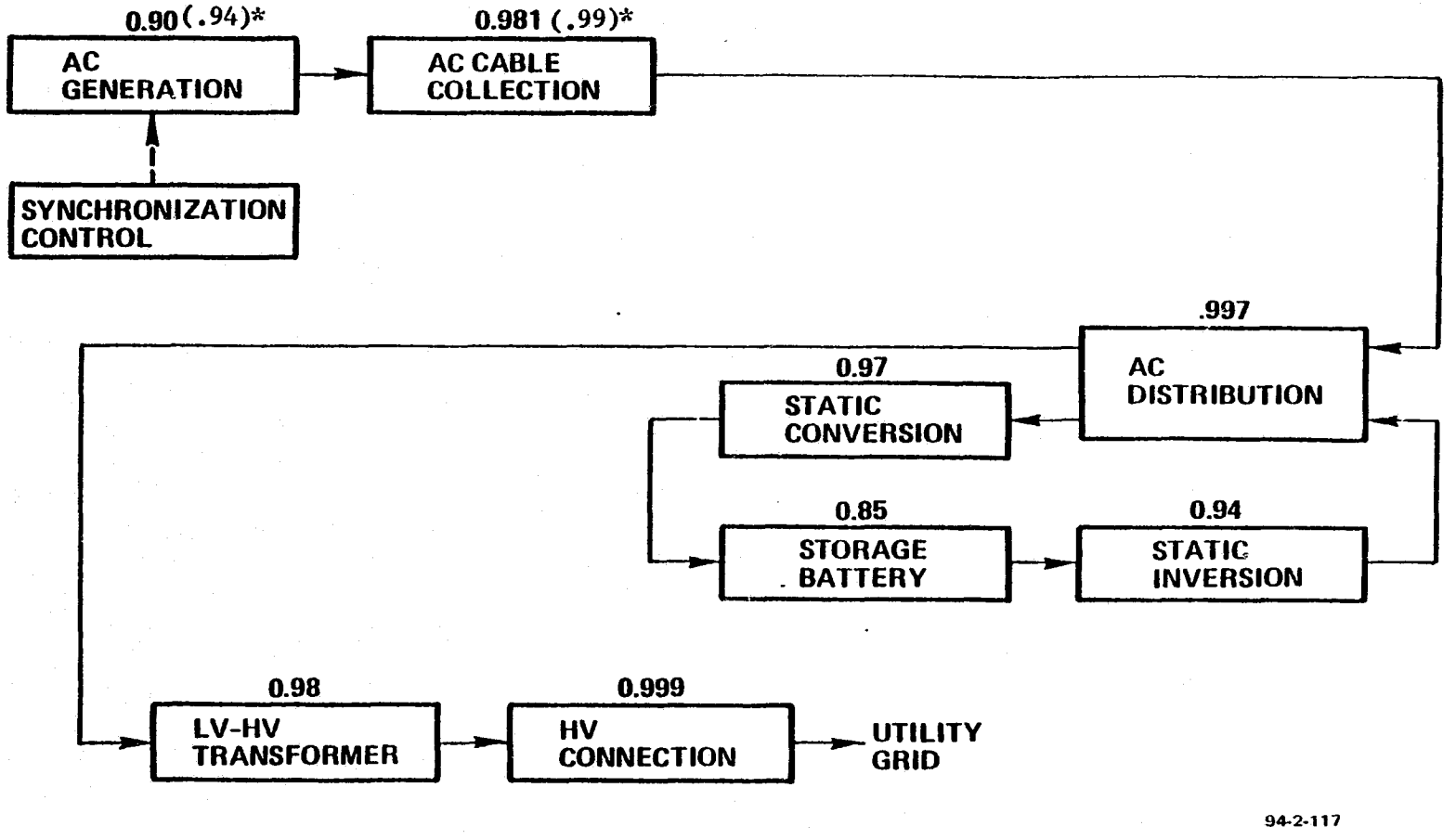

*ca. 1990 PERFORMANCE

FIGURE 3-103. BASELINE ELECTRICAL SYSTEM BLOCK DIAGRAM

The Sundstrand Corporation was given a small contract to study the Rankine cycle for their application and they chose an organic (toluene) Rankine cycle engine design operating at TIT = 427°C (800 F).

Extensive discussions were held regarding the Brayton cycle engines with personnel from the following firms:

(1) Garrett Air Research Manufacturing Co., (Phoenix, Arizona)
(2) Williams Research (Walled Lake, Michigan)
(3) Solar Turbines Instl. (San Diego, California)
(4) Ford Motor Co., Scientific Research Lab.

Garrett provided several general data packages dealing with both open and closed cycle engines; they also provided a performance map for their 30 kW, CCPS-40-1 engine which was used in the FACC computations of annualized performance based upon the Barstow 15 minute environmental data tapes. These data verified our earlier in-house performance estimates made for the CCPS-40-1 engine (Appendix F). Garrett has also provided B & P cost/schedule data pertaining to the Phase II/III development effort as well as to the ultimate (ca. 1990) operational system. Solar Turbines Intl. provided preliminary data regarding their existing Gemini and Titan series of small open cycle (non/-recuperative) gas turbines; they also made available earlier work with Honeywell on a similar point-focusing concept studies for the Sandia/DOE sponsored irrigation program. Williams Research provided performance data on their WR-34 engines modified to accommodate a recuperator. Ford Motor provided data on their automotive turbine work, particularly with regard to their efforts in the area of ceramic materials. On the basis of these contracts and prior to initiating computational work, the following conclusions were reached, regarding Brayton engines:

- Turbine Inlet Temperature (TIT). This is clearly the major performance variable when high efficiency is the goal. The general consensus of all firms contacted was that TIT should by held to maximum of about 816°C (1500°F) to permit use of metal engines. Ceramic components have the potential to raise this value but practical ceramic components on a large scale and at reasonable cost are one to two decades away. The problem is largely money -- millions of dollars for the very extensive materials development required. Barring some substantial military interest in small recuperated high temperature engines, such power plants will not be available for the solar application addressed by Engineering Experiment No. 1. For the near future, therefore, the realistic efficiency of small Brayton engines is on the order of 25% to 30%. (Note that the high temperature material problem also applies to the receiver, which must of necessity operate at temperatures higher than TIT.)

- Component Efficiencies. The above comments on TIT bear most directly on small engines (~100 kW) since it is very difficult (and very costly) to achieve high compressor and turbine

efficiencies in small, high-speed rotating machinery. Some gains can be achieved by reducing system pressure drop and resorting to very high effectiveness (also very large and costly) recuperators, i.e. $\varepsilon \sim 0.95$; once again, however, the development effort can be sizable.

- Power Control. The method of engine power control has a strong influence on system performance because of its effect on engine part-load efficiency. For closed-cycle powerplants, power level is controlled solely by varying the amount (~pressure) of working fluid in the system and both TIT and engine speed remain constant. Engine efficiency is thus virtually constant over a wide load range. Open-cycle powerplants present a problem, however, particularly with a grid-connected system. If the engine is direct-coupled (reduction gearing only) to the AC generator, its speed is fixed by the grid and TIT must be varied to vary power as the solar insolation changes. This introduced a substantial drop in efficiency as the load diminishes. If a variable-ratio transmission (VRT) is introduced between the engine and the AC generator, then speed control can be employed with constant TIT and part-load efficiency will be almost as good as that of the closed-cycle machine. The VRT, however, is a costly item, particularly in small sizes and would have to be developed for this application. Another approach is to resort to a DC system and provide electronic grid interfacing and frequency control. DC systems in the sizes of interest here, however, are heavy, less efficient and more expensive than AC systems. Garrett reports the use of direct-coupled permanent-magnet alternators (PMA) incorporating integral rectification, with the added benefit of avoiding the multi-engine synchronization problem. However, the PMA approach seems limited to very small size engines ($\leq$ 15 kW) which FACC studies show not to be cost effective (paragraph 3.1.1.3).

a. Closed-Cycle Brayton. The in-house analysis of the Garrett CCPS-40-1 engine is summarized in Appendix F; the analysis is based on the test data reported in Ref. 3-40. Figure 3-104 shows output power vs. input power for several different ambient temperatures at a TIT = 816°C (1500°F); the Garrett-supplied data are shown in the figure. An approximate curve fit to the data is:

$$P_o = [0.30375 - 0.001275\ (T_\infty)]\ (P_i + 6) - 1$$

where

T_∞ = Ambient temperature, °C

P_i = Input power, kW

P_o = Output power, kW

Note that the data of Figure 3-104 make use of component efficiencies which vary with engine power output. At a nominal power level of 25 kW these values are:

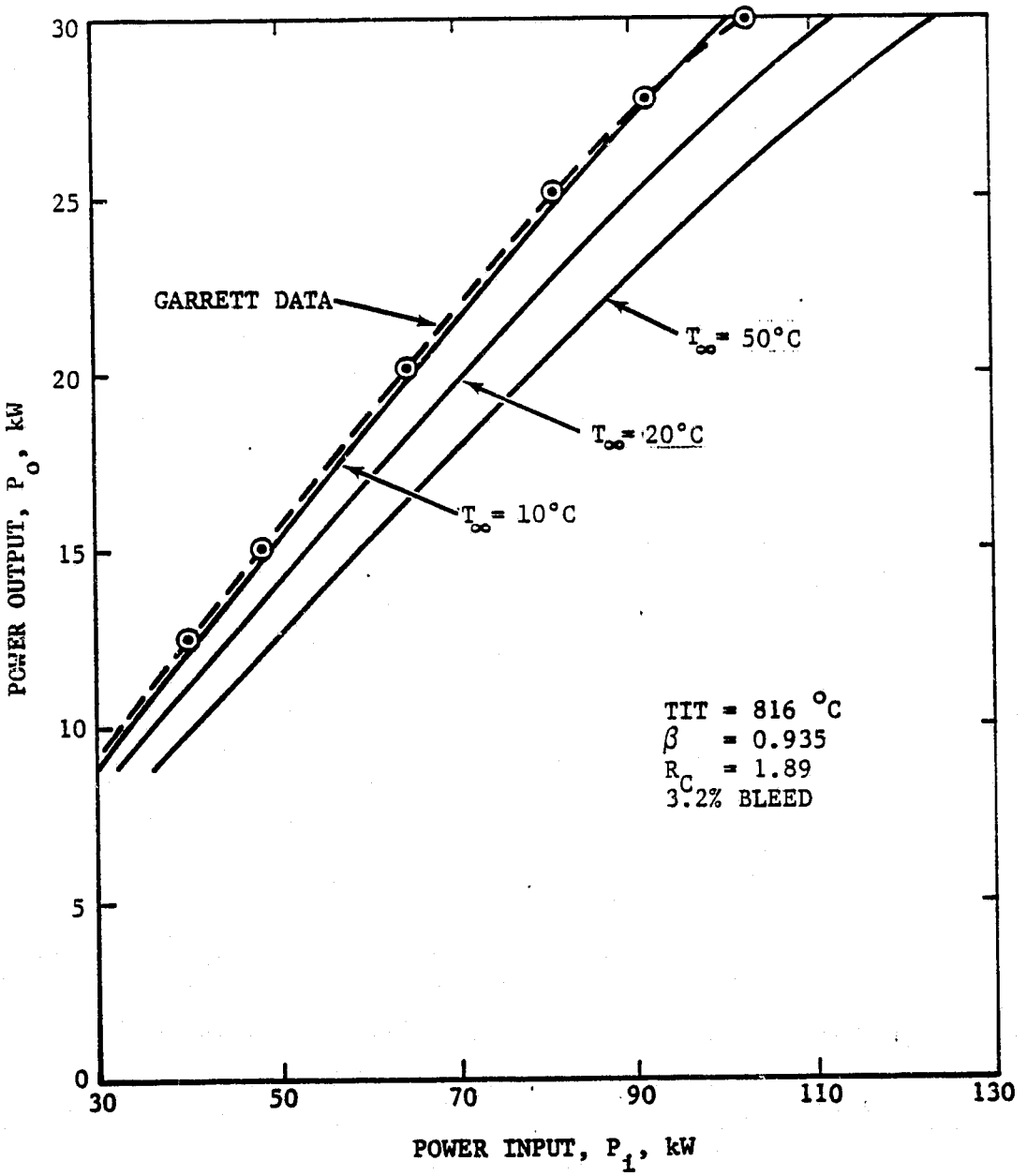

FIGURE 3-104. OUTPUT/INPUT POWER CHARACTERISTICS FOR CLOSED CYCLE BRAYTON ENGINE

94-2-49

- Compressor efficiency, η_C = 0.757
- Turbine Efficiency, η_t = 0.872
- Recuperator effectiveness, ε_R = 0.895
- Cooler Effectiveness, ε_C = 0.960
- Pressure Loss Parameter, δ = 0.935

The engine working fluid is argon and the compressor pressure ratio is 1.89. Engine efficiency at rated conditions is 0.251; rated power is ≈ 30 kW. Figure 3-105 is a plot of part-load efficiency and power, based on the Garrett data for the closed-cycle engine at TIT = 816°C and T_∞ = 44.6°C.

Garrett projects engine cost (selling price) with high volume production in the ca. 1990 period to be $5500, which corresponds to about $180/kW rated power. The engine could not be made available in time to support the 3.5 year program but one engine could be available in 19 months to support Phase II of the 4.5 year program and several engines could be available to support the 6.5 year program. B&P cost estimates for the development effort is as follows:

1) Phase II - One engine set in 19 mo. ARO - $4,000,000

2) Phase III - 20-30 engine sets in 24 mo. ARO -
   - Non-recurring $2,350,000
   - Hardware (per unit) $85,000

3) Phase IV - Further development between Phase III and 1990
   - Product improvement support 20-30 engines (per year) $1,000,000

Engine maintenance data were supplied by Solar Turbines International and compared with FACC in-house estimates. A levelized value of $5/kW per year was established for both closed and open-cycle Brayton engines.

Basic engine weight of the CCPS-40-1 engine is 124 kg, exclusive of the additional air/water heat exchanger required to interface with the existing water/argon cooler. (The engine was originally developed as a powerplant for a submersible vehicle). The additional heat exchanger, fan and electric motor drive assembly will weigh in the order of 150 Kg but would be mounted behind the dish.

b. Open-Cycle Brayton. The in-house analysis of the open-cycle engine is summarized in Appendix F. Since FACC was unable to identify an existing engine (with recuperator) in the desired size range, a paper engine was assumed,

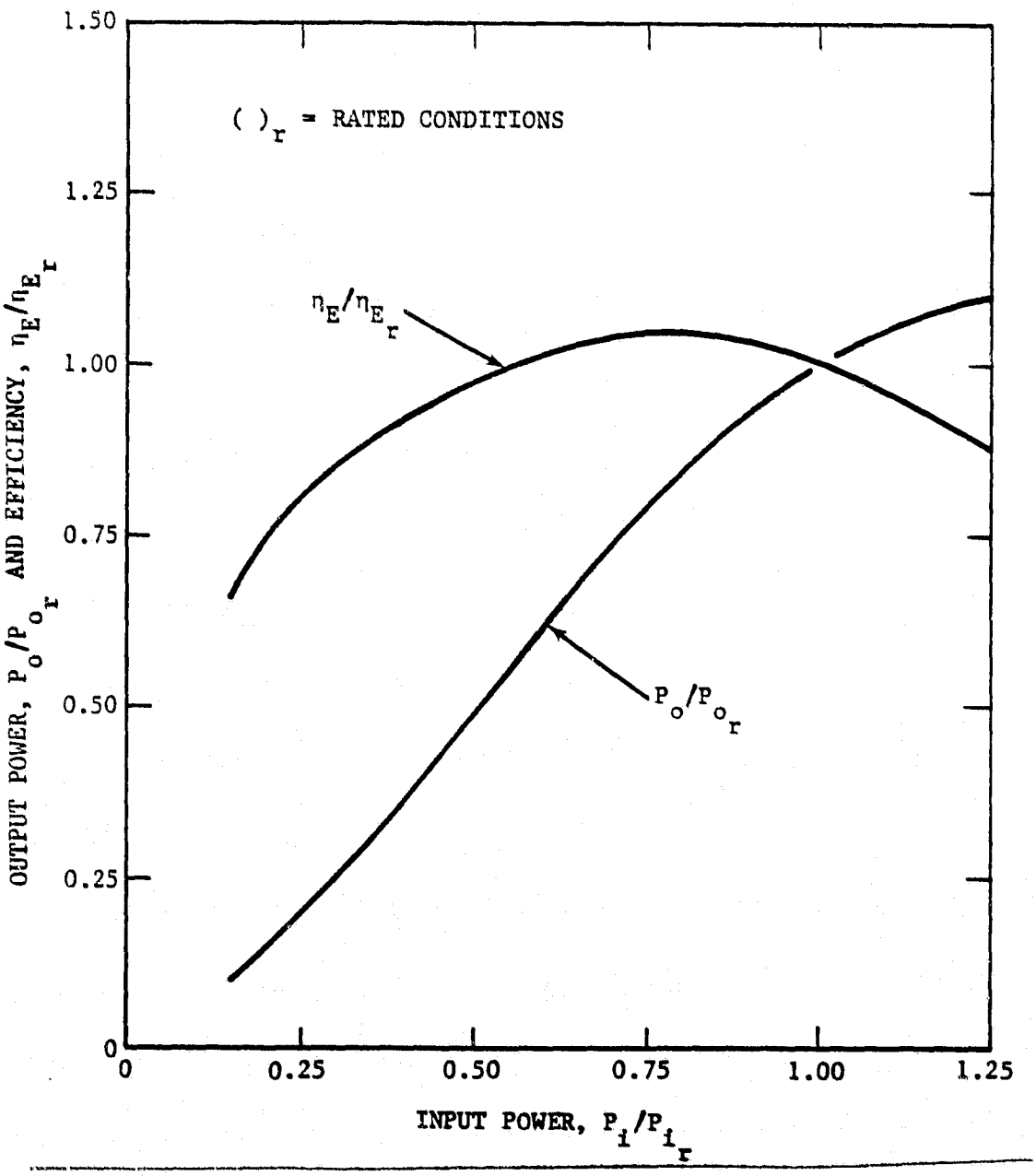

FIGURE 3-105. PART-LOAD PERFORMANCE OF CLOSED-CYCLE BRAYTON ENGINE AT TIT = 810°C

94-2-99

based on the rotating components of the CCPS-40-1 closed cycle engine*. Cycle analysis was carried out to define the input/output power relationship and to ascertain the influence of the selected power control mode. The analysis assumes TIT control and the following (constant) component efficiencies:

- Compressor efficiency, $\eta_C = 0.758$
- Turbine efficiency, $\eta_t = 0.873$
- Pressure drop parameter, $\beta = 0.935$
- Recuperator effectiveness, $\varepsilon_R = 0.90$

Note that these values are essentially the same as those used previously for the closed-cycle engine at rated power; engine efficiency at rated conditions is 0.281 and rated power level is also 30 kW. As shown in Appendix F, a recuperator bypass vlave is provided to prevent TIT from exceeding its maximum (design) value. Best overall system performance is achieved by setting the maximum TIT point at approximately the rated power point, i.e. when the insolation is $\approx$ 800 W/m^2. Figure 3-106 is a plot of output power vs. input power for a range of ambient temperatures. Curve fits to the data -- for input to program SPEE1 to ascertain annualized system performance -- are as follows:

for

$$\left(\frac{P_i}{P_{i_r}}\right) \leq \left(\frac{P_i}{P_{i_r}}\right)_x$$

$$\left(\frac{P_o}{P_{o_r}}\right) = 2.31\left(\frac{P_i}{P_{i_r}}\right) - (0.00412)T_\infty$$

where

T_∞ = Ambient temperature, ^oK

P_{i_r} = Input power at rated condition, kW

$$\left(= \frac{P_{o_r}}{\eta_{E_r}}, \quad \eta_{E_r} = 0.281\right)$$

*The Garrett GTP36-51 30 kW engine is a candidate but requires the addition of a recuperator for this application.

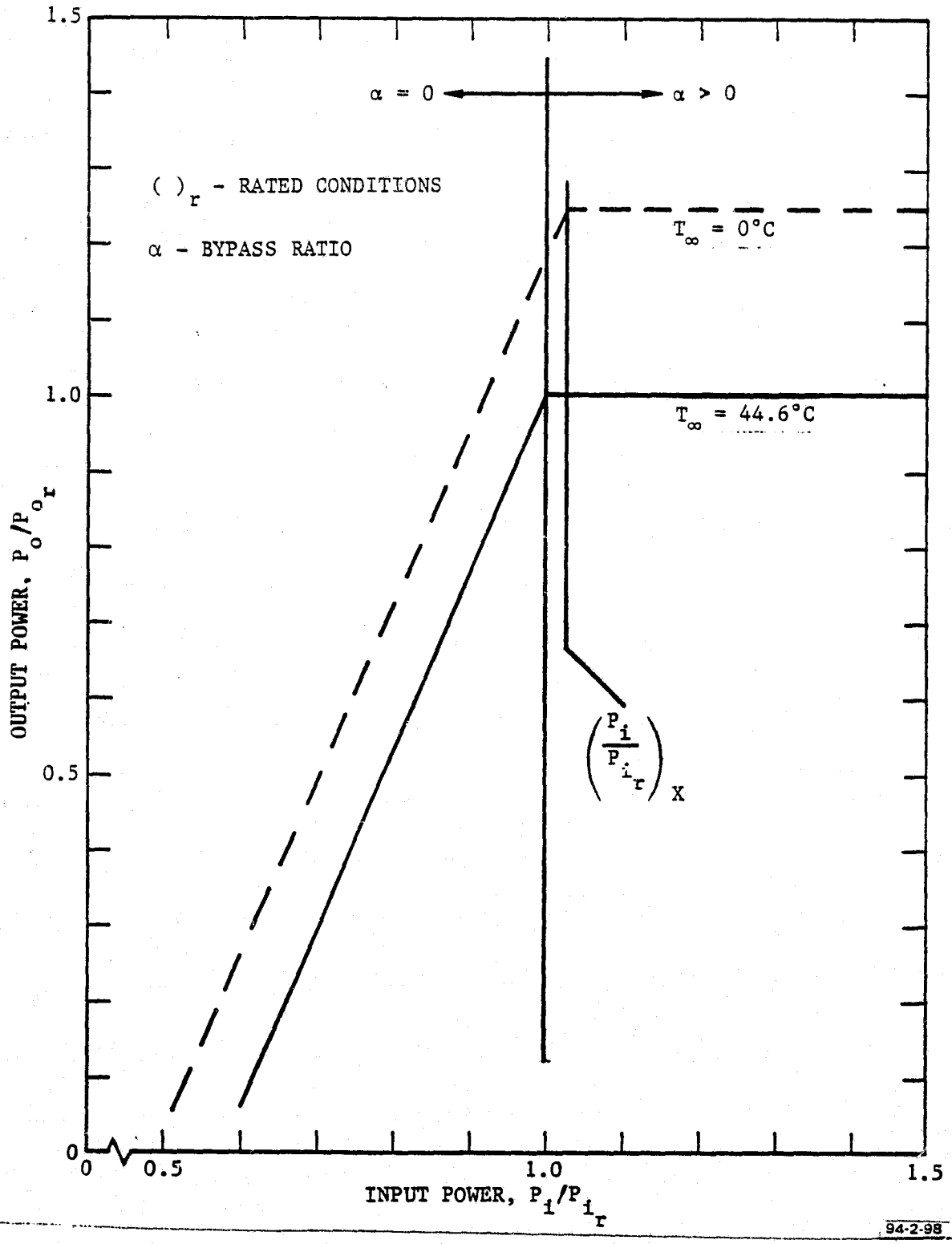

FIGURE 3-106. OUTPUT/INPUT POWER CHARACTERISTICS FOR OPEN-CYCLE BRAYTON ENGINE WITH BY-PASS CONTROL (VARIABLE TIT)

and

$$\left(\frac{P_i}{P_{i_r}}\right)_x = 1.1781 - (0.0005604)\, T_\infty$$

For

$$\left(\frac{P_i}{P_{i_r}}\right) > \left(\frac{P_i}{P_{i_r}}\right)_x$$

both output power and TIT are held constant (at P_{o_m} and 816°C, respectively) by opening the recuperator bypass valve, which reduces the engine efficiency as well. Maximum output power is given by

$$\left(\frac{P_{o_m}}{P_{o_r}}\right) = 2.7214 - 0.00054145\, T_\infty$$

Figure 3-107 shows engine efficiency variation experienced with this control mode. As discussed in para. 3.1.1.2 this large variation in efficiency contributes to a much reduced ACF compared with the closed-cycle powerplant despite a higher efficiency at rated conditions.

Detailed engine cost estimates were not available to FACC, primarily because of the non-availability of a recuperated engine in the desired size range. However, the engine should be cheaper than the same size of closed cycle engine discussed above; a cost of $150/kW rated power is projected.

The open-cycle machine is projected to weigh approximately 91 kg.

c. Organic Rankine Cycle (ORC) - Appendix D presents the data package prepared by Sunstrand for the toluene ORC engine at TIT = 427°C (800°F). The derived input/output power relationship for the constant turbine/fan speed arrangement is shown in Figure 3-108. Note that the Sundstrand design point has been shifted to the higher ambient temperature to correspond to specified rated power condition. The rated power values are:

- Alternator output, P'_{o_r} = 71.3 kW
- Engine shaft output, P_{o_r} = 77.5 kW
- Efficiency, η_{E_r} = 0.250

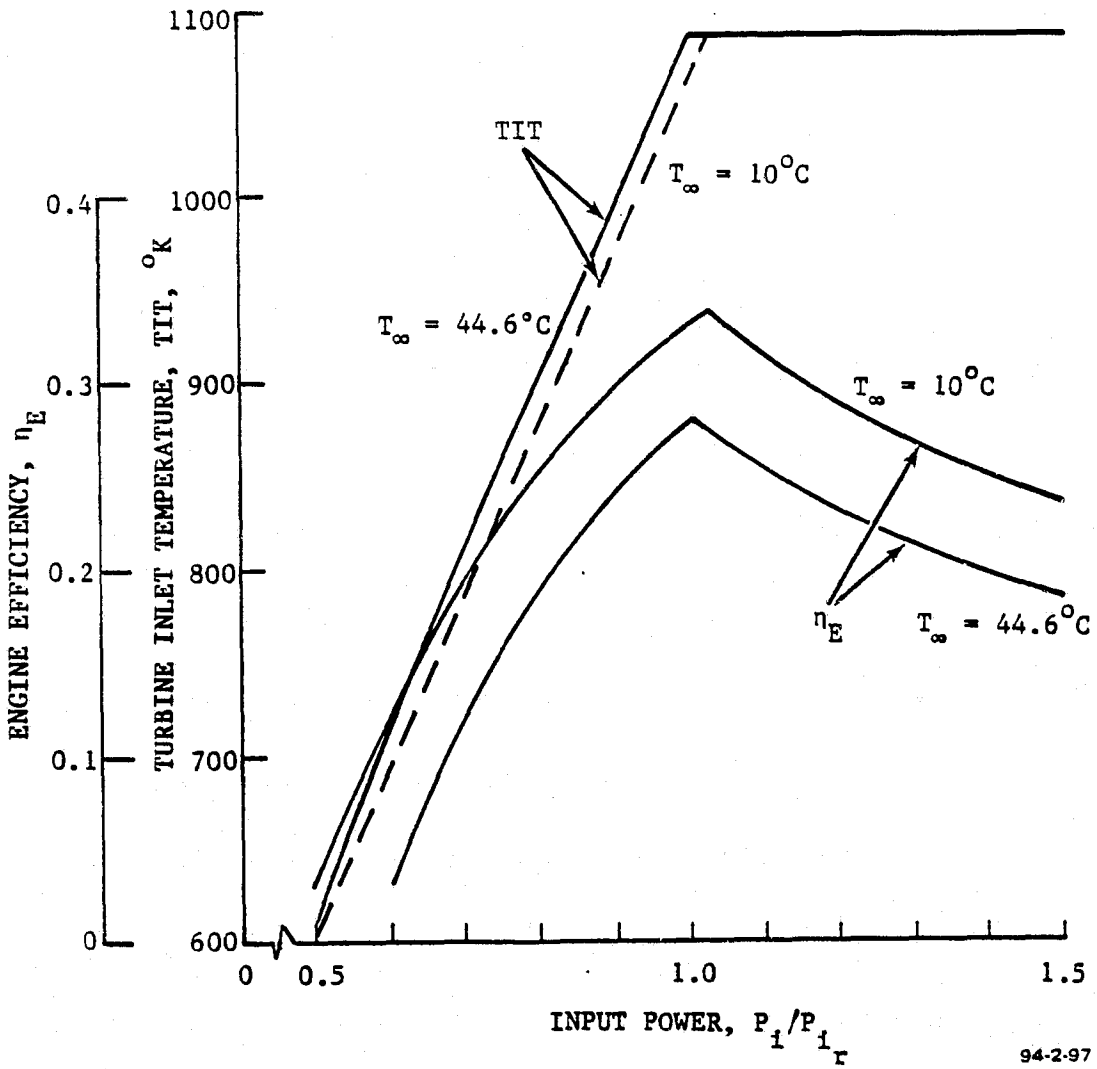

FIGURE 3-107. PART-LOAD PERFORMANCE OF OPEN-CYCLE BRAYTON ENGINE WITH BY-PASS CONTROL (CONSTANT SPEED, VARIABLE TIT)

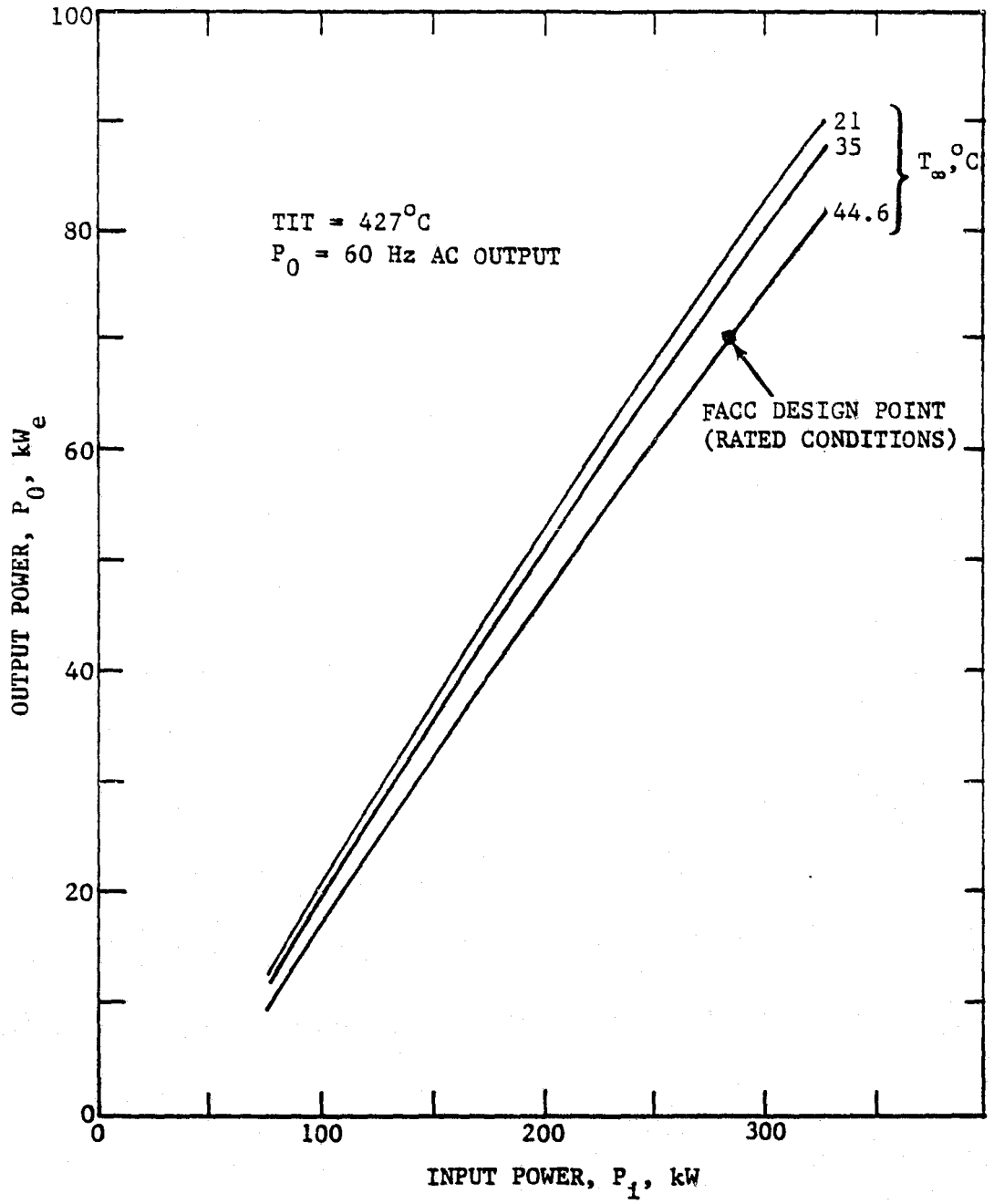

FIGURE 3-108. OUTPUT/INPUT POWER CHARACTERISTICS FOR ORGANIC RANKINE ENGINE

94-2-96

At the maximum expected insolation of ~1000 W/m^2, the engine will generate 89.1 kW. Figure 3-109 shows the part-load efficiency of the ORC engine for the two operating modes supplied by Sundstrand, i.e. constant turbine/fan speeds and variable turbine/fan speeds. In both cases, the part-load performance is excellent, which contributes to the high ACF for this concept.

Gross weight of the ORC engine is 537.2 kg (generator included). A detailed weight breakdown is given in Appendix D. Sundstrand projects engine cost (selling price) of ≈$400/kW of rated power for production rates of 400,000 units/year. For Phase II, the cost of one engine is $2,000,000; for Phase III, engine cost is $1200/kW. Estimated maintenance cost is $12,100 over the 30-year life of the engine, including parts, labor and inventory, which translates to $5.38/kW per year.

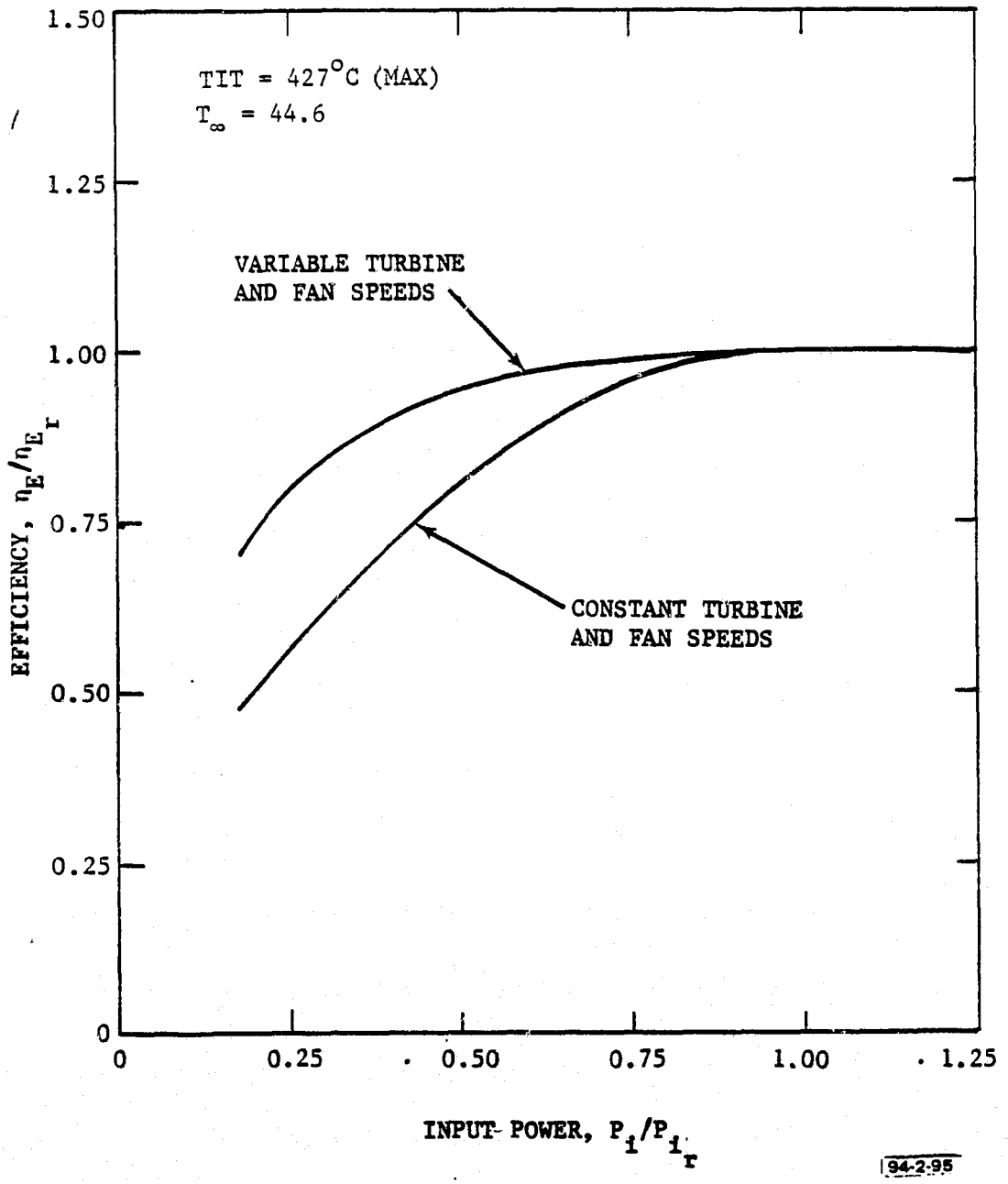

FIGURE 3-109. PART-LOAD PERFORMANCE OF ORGANIC RANKINE ENGINE

3.1.5 ENERGY TRANSPORT SUBSYSTEM

The energy transport subsystem consists of the following components:

- Electrical cables from each power module to the central switchboard
- Switchboard
- Transformer
- Switches/Contactors/Misc. Equipment

The major components are identified in the electrical system block diagram shown in Figure 3-110, and in the one-line electrical diagram shown in Figure 3-111. Both figures represent a 4-1/2 or 6-1/2 year Phase II system with battery storage (0.4 capacity factor). The same basic electrical equipment would be used for a 3-1/2 year program, but with more collectors and the equipment would be sized for the smaller P-40 Stirling engine (40 kW alternators, etc.). Specific requirements for most of the energy transport subsystem components are identified in these two figures. The trade studies that were conducted to arrive at these selections are described in Appendix B, along with other information concerning costs, detailed performance information, etc.

3.1.5.1 Subsystem Components. All components selected for the energy transport system (as well as the other parts of the electrical system) are off-the-shelf items; their performance is known and there is virtually no risk in their use. All conform to the applicable electrical code and are UL approved. A summary description of key components are:

- Electrical Power Cabling-Alternator-to-Ground. Flexible copper cables are used to carry the generated power across the rotational axis to the ground. This is done with weather-proof, 3-conductor power cables consisting of No. 2/0 extra flexible, stranded copper wires, insulated to withstand 600v AC and jacketed with sunlight-resistant, weatherproof neoprene. Okocord Brand, Type W is a typical cable of this type.

- Control Box. A weather-proof control box will be put at the base of each concentrator. This NEMA-12 enclosure will contain the following components:

  - AC Generator power contractor
  - AC Generator circuit breaker
  - Stirling engine pump/fan motor starter
  - Pump/fan motor circuit breaker
  - 1 kVA transformer (power for concentrator)
  - Circuit breaker for transformer
  - Circuit breaker for panelboard
  - Circuit breaker for concentrator drives
  - Utility outlets (for maintenance)

  These components are described further in Appendix B.

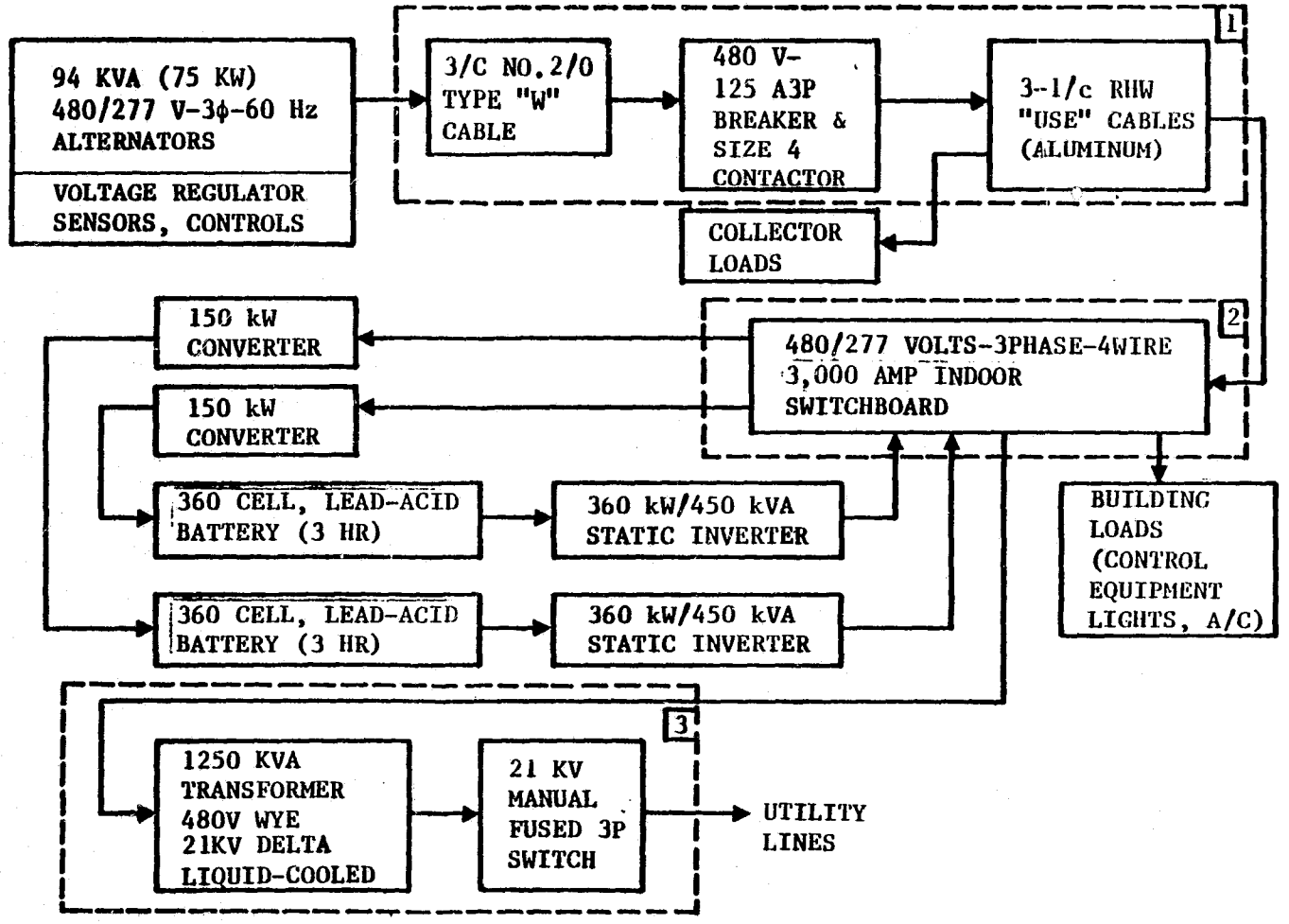

NOTE 1) ITEMS 1, 2 AND 3 ARE THE ENERGY TRANSPORT SUBSYSTEM

2) 4½ & 6½ YEAR SYSTEM

FIGURE 3-110. ELECTRICAL SYSTEM BLOCK DIAGRAM INCLUDING ENERGY TRANSPORT SUBSYSTEM

94-2-108

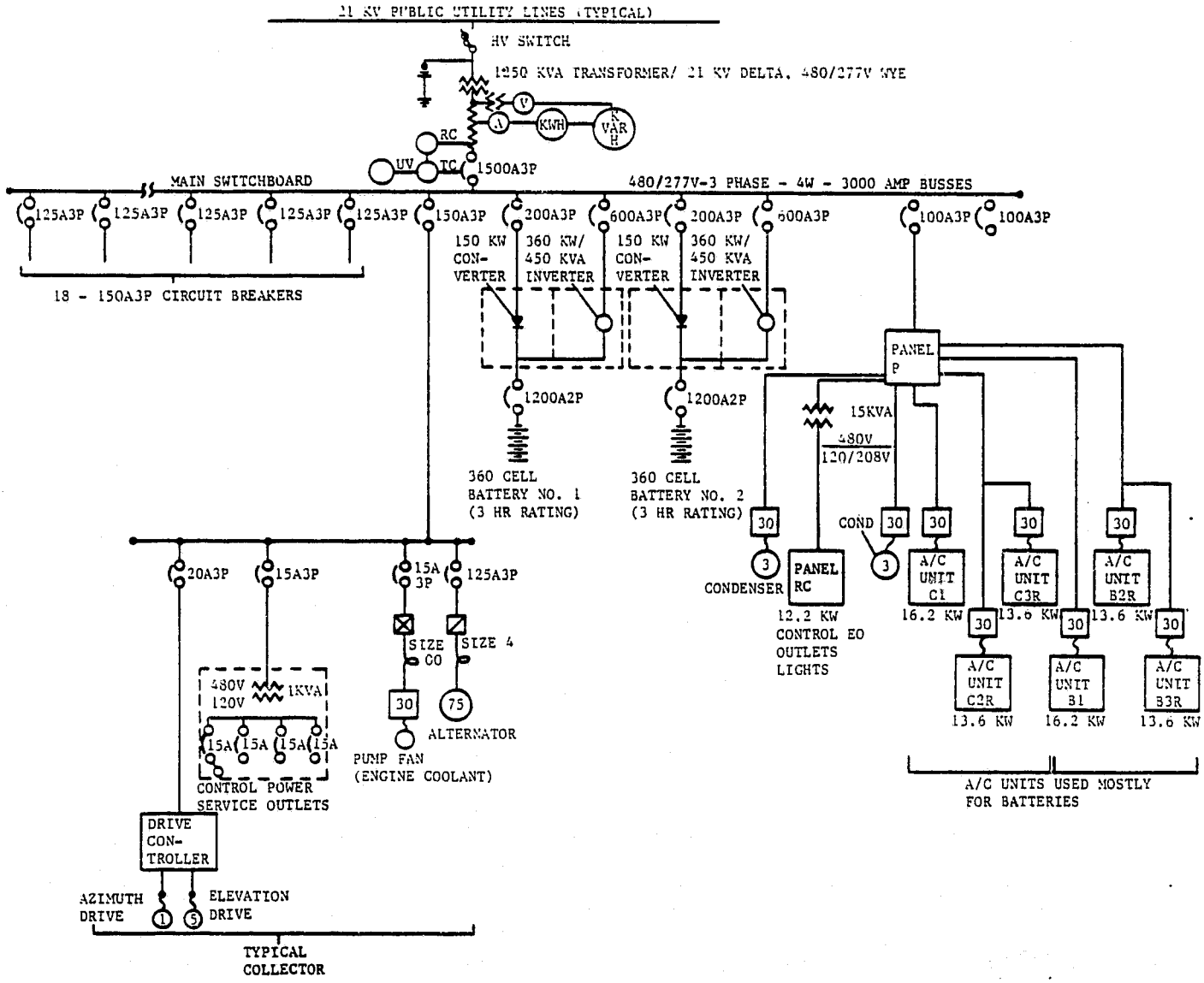

FIGURE 3-111. ONE-LINE DIAGRAM FOR SPS ELECTRICAL SYSTEM (INCLUDING BATTERY STORAGE)

- Power Cabling - Control Box to Switchboard. Trade studies have shown the power cables should be buried underground without ducts. (Installation procedure is outlined below.) The power lines should be single conductor stranded aluminum, typically No. 4/0 and No. 250 250 MCM sized, with 480 volt RHW-USE 600v insulation suitable for direct burial in earth. The exact cable size depends on the length of the line; a computer code was developed to calculate the optimum cable size based on a specified loss in the lines. X-Olene Brand Type RHH-RHW is a typical cable which meets these requirements.

- Switchboard. All power cables will terminate at circuit breakers in the main switchboard located in the control building. The switchboard will be metal enclosed, UL approved, 480 volt, 3000 ampere bussed, and indoor type. (See Figure 3-112) It will have tin-plated aluminum busses, with a neutral bus, a ground bus, main circuit breaker, branch breakers and instruments for voltage, current, frequency, kilowatts and kilovars. The latter two will also be recorded as a part of the routine data collection.

  The generator-branch breakers will be 125 ampere (A), 3-pole manually-operated devices with an interrupting capacity of 20,000A, symmetrical. The main breaker will be 1500 A, 3-pole, air-insulated and operate electrically, (i.e., remotely). A spring-powered drawout type breaker will be used having adjustable long-term and short-term current and time delay trip circuits. Interrupting capacity will be 25,000A at 480v, symmetrical. The switchboard will also contain breakers for the power to operate the concentrators and the equipment in the control building.

- Power Cabling - Switchboard to Transformer. The 1500 amperes capacity will require 6 parallel No. 500 MCM stranded aluminum cables with 600v polyethylene USE-type insulation and USE neoprene jacket for burial.

- Transformer. The transformer will be a 1250 kVA/1000 kW, 60 Hz, 3-phase, silicone liquid filled, air-cooled unit. It will be a metal enclosed, weather-proof, pad-mounted unit. The primary voltage will be 480v, the secondary will be 21,000v (or matched to the grid requirement). The maximum impedance is 5%, and overall efficiency is 98%. The unit will have liquid level and temperature indicators, and other items for maximum reliability. The high voltage side will have a 40A fused, 3-pole, 35,000v, mechanically operated switch and three lightning arrestors. McGraw-Edison has a commercial unit which fills all of the requirements for the system and conforms to AN Standard requirements.

- Power Cabling - Transformer to HV Switch. This cable will consist of 3-conductor, No. 4 stranded copper, shielded, 35 kV class butyl-rubber insulated cable. The cable will terminate in a 35 kV class "pothead", suitable for pole mounting.

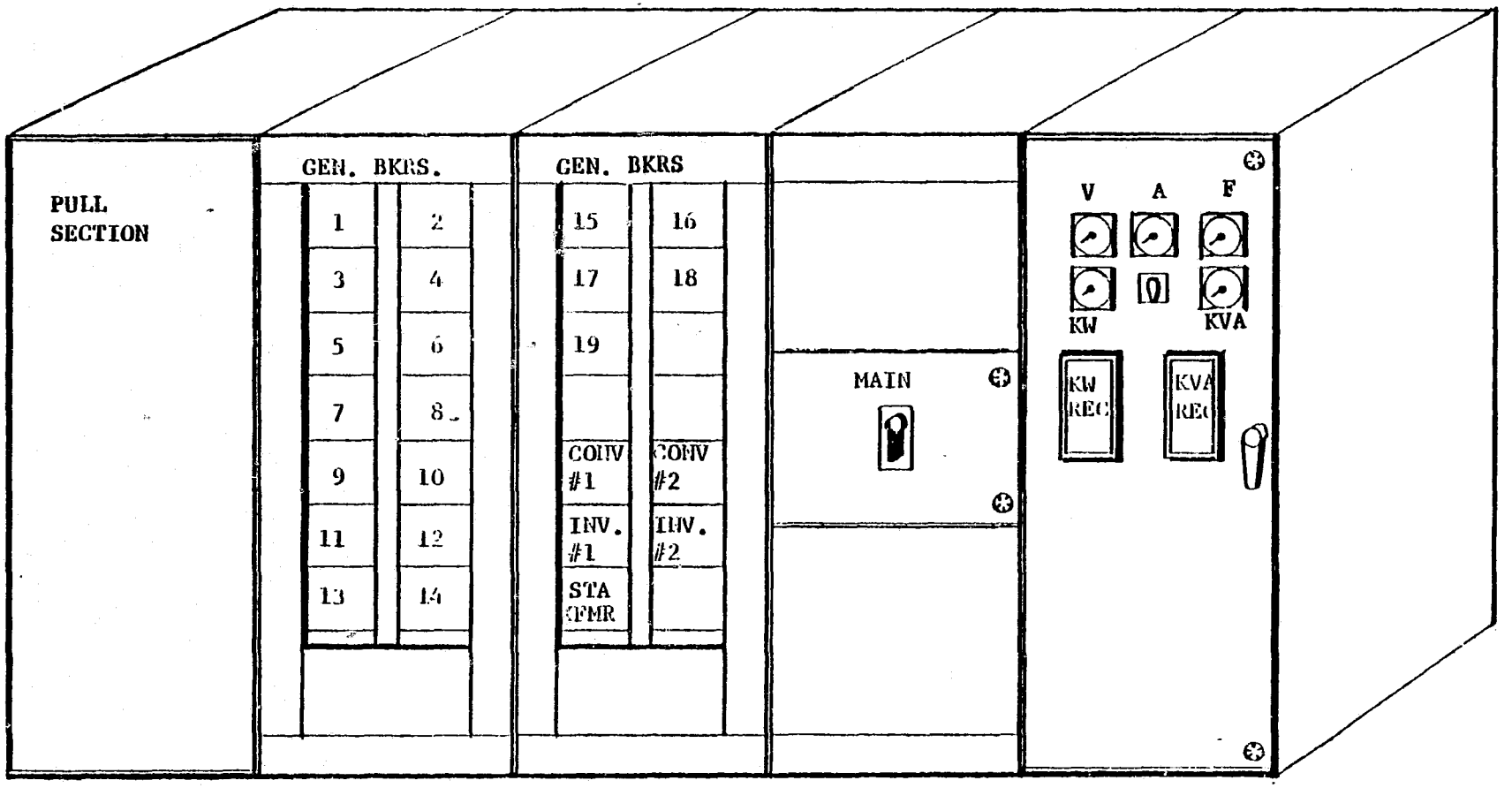

FIGURE 3-112. ILLUSTRATION OF MAIN POWER SWITCHBOARD

- HV Switch. A 3-pole switch will be located between the pothead and the utility lines. Requirements are 200A, non-fused, 35 kV, manually operated pole-top switch. A Westinghouse LCB switch is a typical device.

3.1.5.2 Installation. The location of the electrical power cables and the method of installation was based on a trade study described in Appendix B. The following summarizes the most costly item for the electrical transport subsystem --burial of the power cables between the concentrator control boxes and the switchboard. Steps to be taken are identified in Figure 3-113. A typical site trenching plan is shown in Step (1) of the figure, based on 19 concentrators in a (approximately) 6 x 3 matrix. Typical row and column spacings are 28 and 56m, respectively. The trenching operation shown in Step (2) is planned to go directly between concentrator centerlines, and the foundation piles will be positioned to avoid the trenches. A layer of sand 3 to 6 inches deep is deposited in all the trenches (Step (3)), followed by cable-laying using a special vehicle for laying the cables (Step (4)). After the cables have been cut to length, the ends will be protected (Step (5)). The final steps include another 3 to 6 inch sand layer (Step (6)), backfilling using a grader (Step (7)), and compacting the excavated areas between concentrators (Step (8)).

3.1.5.3 Station Size and Stand-Alone Options. The discussion above has been based on a grid-connected, 1 MW_e station for the 4-1/2 or 6-1/2 year start-up time. As stated elsewhere this entails the use of the P-75 Stirling engine, and a total of 18 concentrators plus an additional one if battery storage is used. The 3-1/2 year option uses the P-40 engine and many more smaller concentrators (55 without storage, 60 with storage). The station output does not change, therefore all components associated with the concentrators will be the same type, only smaller and more numerous. These factors have been accounted for in the system cost analysis summarized in paragraph 3.1.1.3.

Stand-alone operation will use the same components, except the transformer may not be needed (subject to detailed analysis of stand-alone loads). A discussion of the stand-alone electrical system requirements is given in Appendix B.

3.1.6 ENERGY STORAGE SUBSYSTEM

The purpose of the storage subsystem is to take part of the power generated by the station and temporarily retain it in a storage device of some type for later use. The power that is available for storage consists of two parts: the excess power generated when the solar insolation is greater than 800 W/m^2, (i.e., when the station produces greater than rated power), and any dedicated concentrators which are used exclusively for this purpose. In the baseline system, one concentrator is used for charging the store for the 4-1/2 and 6-1/2 program; approximately five concentrators are used for the purpose for the 3-1/2 program. Detailed survey of possible storage concepts has shown that a battery system is the only viable choice for the near term (including a 6-1/2 year Phase II program), but there are a number of alternate concepts which are attractive for the far term (ca. 1990) system, provided they perform as predicted. This section contains a discussion of both near term and far term concepts.

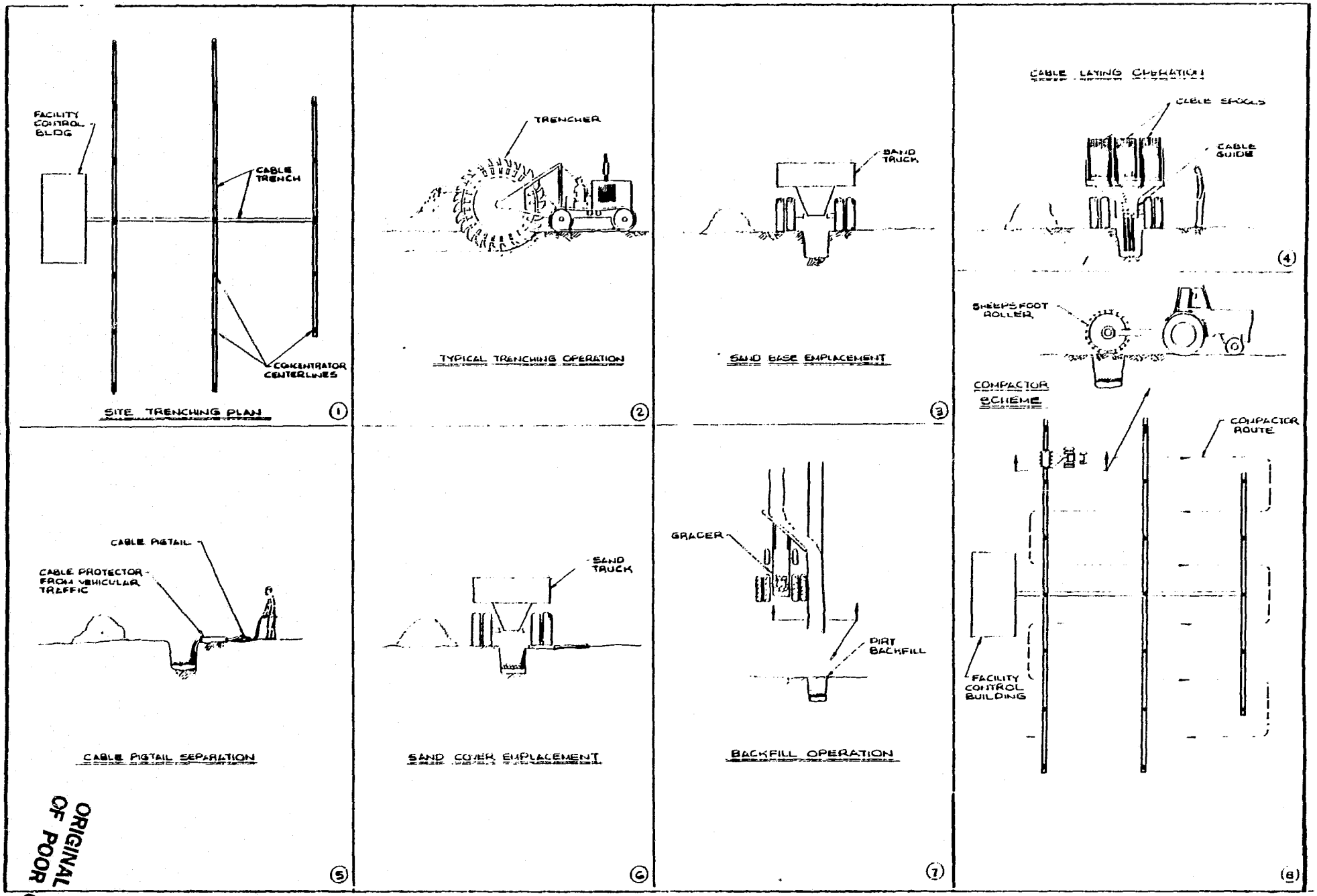

FIGURE 3-113. TYPICAL ELECTRICAL CABLE BURIAL SEQUENCE

94-2-116

ORIGINAL PAGE IS OF POOR QUALITY

3.1.6.1 Lead-Acid Battery Storage Subsystem. Off-the-shelf lead acid batteries were chosen for the baseline system because of current availability. Appendix B documents the trade studies made to select the components which comprise the battery storage subsystem.

These components are:

- Static converters
- Batteries
- Static inverters

The relationship of the storage subsystem to the overall electrical system is shown in Figures 3-110 and 3-111.

The primary requirements of the storage subsystem are:

- Energy storage: 2132 kWh (delivered to grid, P-75 system)
- Input/output: 480v, 3-phase, 60 Hz
- 3 hour discharge
- Rating 1815 amp-hour (per 180 cell string)

A summary of the components in the subsystem are given below:

- Converters - The converters are standard silicon-controlled rectifiers (SCRs) with current limiting to prevent overloads on initial charging of discharged batteries, and then current limiting at the 405 float voltage level. Two units will be used, each containing two full wave bridges composed of six SCRs each. The efficiency of the units is 97 percent.

- Batteries - The standard commercial lead-acid batteries will have lead-antimony plates immersed in a sulfuric acid/water electrolyte. The cells will have a nominal 2v output and 180 cells will be connected in series to give a nominal terminal voltage of 360v (405v at float voltage, 333v at the end of discharge). Strings of 180 cells (with the 360v terminal voltage) are connected in parallel to give the required storage capacity (2132 kwh). The batteries are about 85% efficient, and have a life of about 2000 cycles (i.e., 5-1/2 years for SPS). After 2000 cycles the batteries only have 80% of their capacity and are replaced. The batteries will be mounted on earthquake-resistant racks built of coated metal. Figure 3-114 shows a typical battery installation of the type proposed for SPS. A typical commercial battery which meets the requirements is the Electra Co. C & D type MT series 2000. Physical characteristics are:

  - Size: 438 x 432 x 712 mm (17.25 x 17 x 28 in.)
  - Weight per cell (filled): ~ 251 kg (550 lb)

  Therefore, the total weight of the 720 cells required for a 0.4 ACF is ~ 180,720 kg or 346,000 lbs.

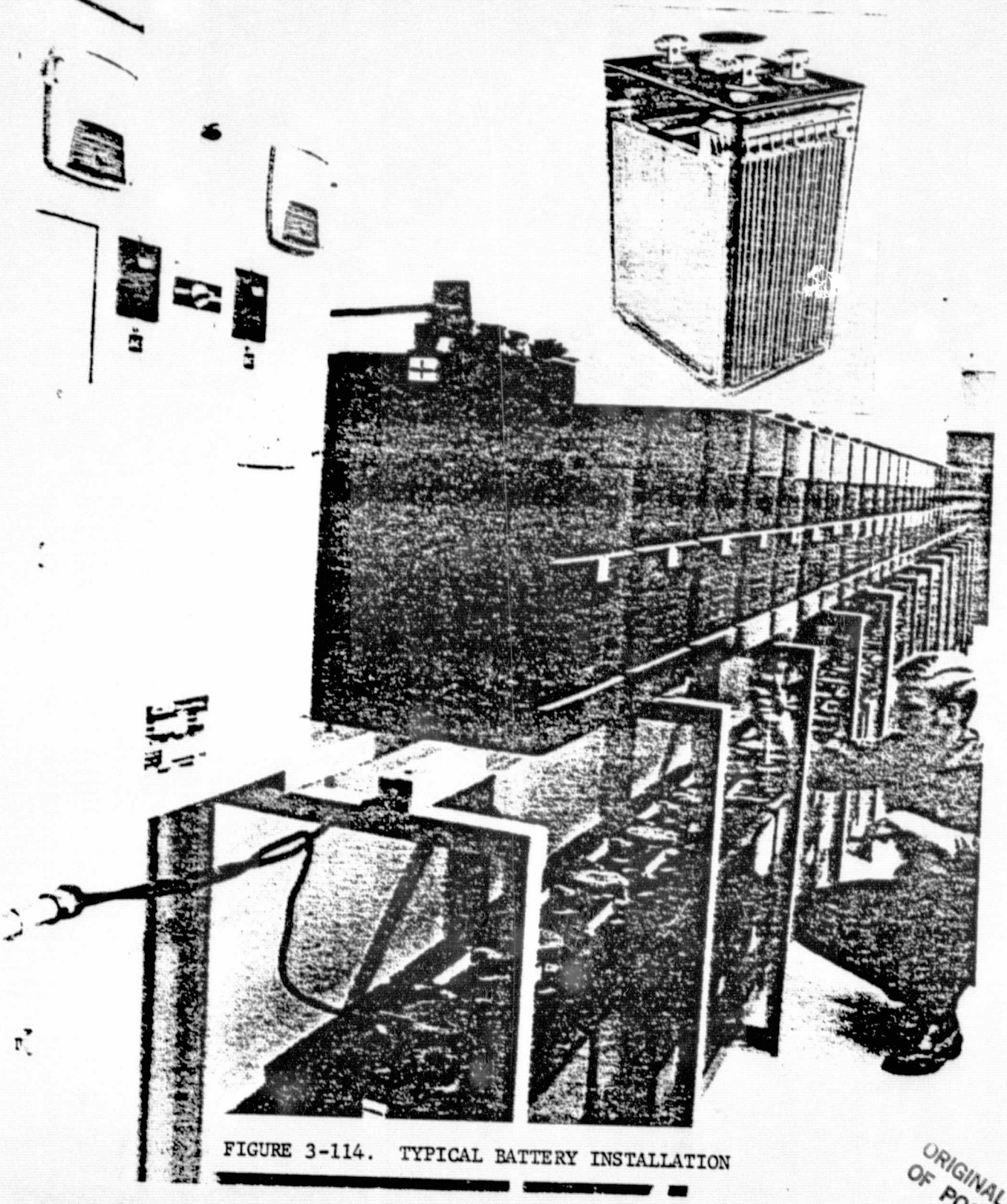

FIGURE 3-114. TYPICAL BATTERY INSTALLATION

ORIGINAL PAGE IS
OF POOR QUALITY

94-2-143

- Inverters - the SCR inverter has a maximum input voltage of 405v, therefore, the battery cells are arranged in the 180 cell series unit to supply this voltage. Two inverters are needed (as well as two converters and two batteries of 360 cells each, see Figure 3-111). The inverters convert the 405v DC to 480v, 3-phase 60 Hz with voltage regulated within 0.5% and with less than 5% harmonics. The efficiency is 94 percent. International Power Machines makes a combined converter/inverter unit which will meet the requirements.

Battery and battery storage subsystem costs are presented in the following paragraphs.

3.1.6.2 Alternate Storage Concepts - A number of alternate storage concepts were investigated as replacements for the interim lead-acid battery system. The following paragraphs briefly describe the results of these investigations.

A. Advanced Batteries - References 3-41, 3-42 and 3-43 present an overview of present research and cost projections for a number of advanced batteries currently under extensive research. These batteries include the sodium-sulfur, the sodium-antimony chloride, the lithium-iron sulfide and the zinc chlorine battery. Ref. 3-44 discusses recent research on the Redox battery concept and the authors of Ref. 3-45 argue for extending research on the lead-acid system. It is clear from the literature and from extensive discussion with the FACC sodium-sulfur battery personnel that none of these advanced batteries will be available to meet the schedules for the SPS program Engineering Experiment No. 1, although some basic decisions on proceeding with the sodium-sulfur battery development will have been made about the time of the 6-1/2 program schedule. For input to our systems analysis, however, two key data points were established, 1) the advanced battery will cost ≈ $45/kWh (possibly less) and 2) will be capable of 5000 cycle operation (possibly more). In addition, it is assumed that the batteries will require cooling on the order of present industrial lead-acid systems; it is further assumed that the replacement cost will be 80% of the original cost. The cost of battery electrical support equipment, i.e., inverters, converters, cabling, racks, shipping, etc., is correlated by:

$$C_{EL_B} \ (\$/kWh) = \frac{58000}{E_b} + \frac{2600}{\sqrt{E_b}} + 20.6$$

where

$$E_b = 1585 + (547.25)N_1, \ kWh/day$$

E_b = Maximum daily energy delivered to grid from storage (for batteries)

N_1 = Number of add-on collectors for charging the storage system.

The added cost of the building to house the batteries, C_{PL_B}, is

$$C_{PL_B}(\$) = 3111\ E_b^{0.3945}$$

The cost of lead-acid batteries, $C_{B_{LA}}$, is

$$C_{B_{LA}}(\$) = 230{,}644 - 4373\sqrt{E_b} + 155.2\ E_b,$$

The influence of these parameters on P-75 system performance is shown in Figure 3-115, which presents BBEC as a function of ACF for various battery options. Note that BBEC always increases with ACF even if the storage system is free. Also, the cost of battery-related electrical equipment is ≈ 20 mills/kWh at the high ACF value. Note further that battery life is a major cost driver.

B. Advanced Flywheels - Ref. 3-46 reports on an extensive study of flywheel energy storage using advanced composite materials. The end-to-end efficiency is projected at 0.82 and the total subsystem cost, including electrical equipment, is computed to be

$$C_{FLY}(\$) = 99{,}400 + 138.2\ E_b$$

where

$$E_b = 1677 + 579\ N_1,\ \text{kWh/day}$$

= Maximum daily energy delivered to grid from flywheel storage

If the projected performance of the advanced composite flywheel is verified in practice the flywheel will be a leading candicate for an SPS storage system.

C. Hybrid - For some applications, particularly the stand-alone case, the addition of fuel-burning capability (either in the form of extra Stirling engines or by integrating a fuel burner into the receivers) offers an attractive alternative, depending of course on the cost of fuel. Figure 3-116 compares the performance of the two hybrid approaches as a function of ACF for two different current (1978) fuel rates. Note that the fuel escalation rate built into the cost equations is 7%, which may not now be adequate.

D. Thermal - A substantial effort was devoted to the formulation of a viable thermal storage concept. The storage material selected was the same eutectic salt mixture (75 NaF/25MgF_2) defined in paragraph 3.1.2.1 for use as extra buffer storage. Unfortunately, none of the methods tried succeeded in achieving reasonable cost. In view of the sensitivity of the concentrator cost to

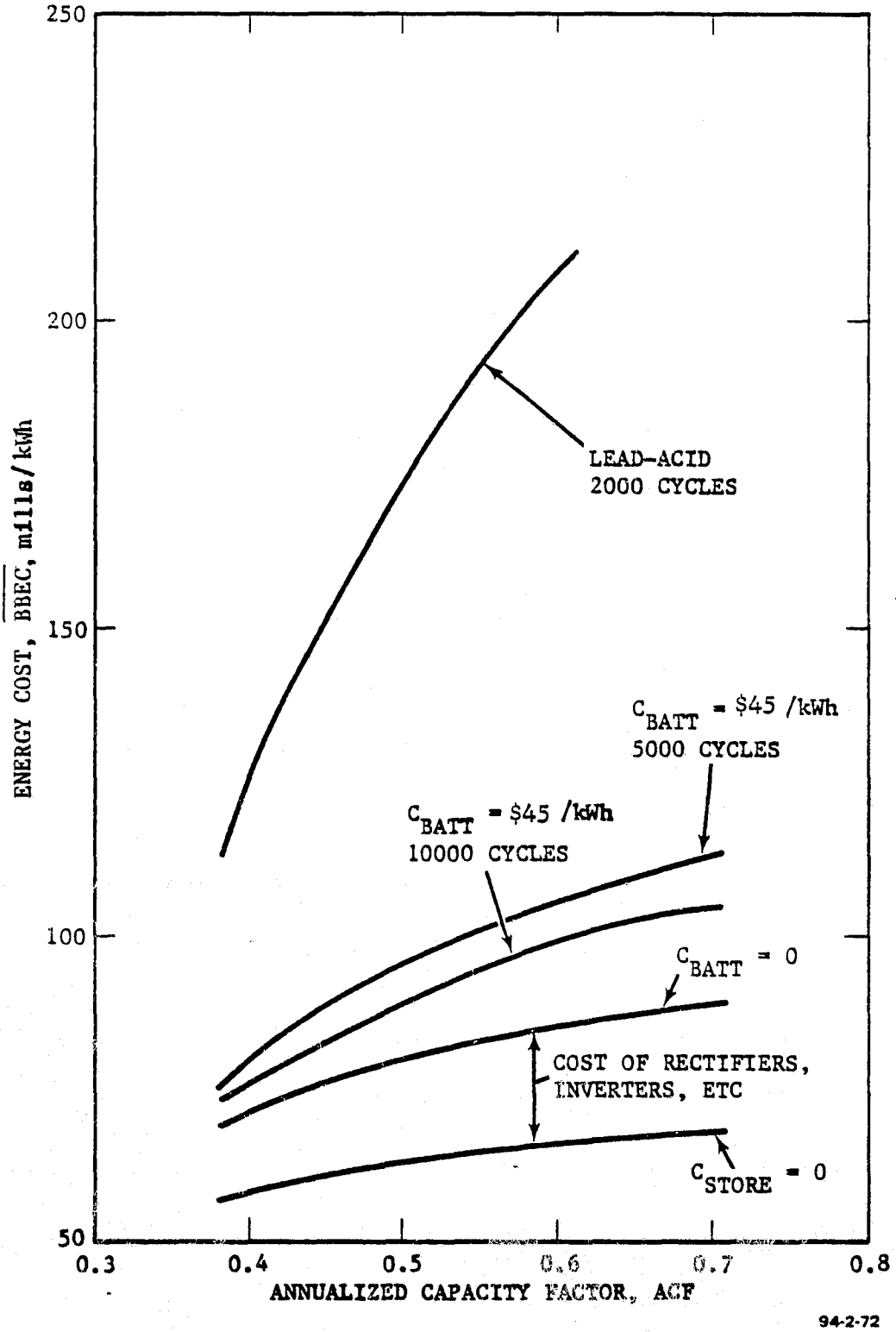

FIGURE 3-115. ENERGY COST BREAKDOWN FOR DISH-STIRLING SYSTEM WITH BATTERIES

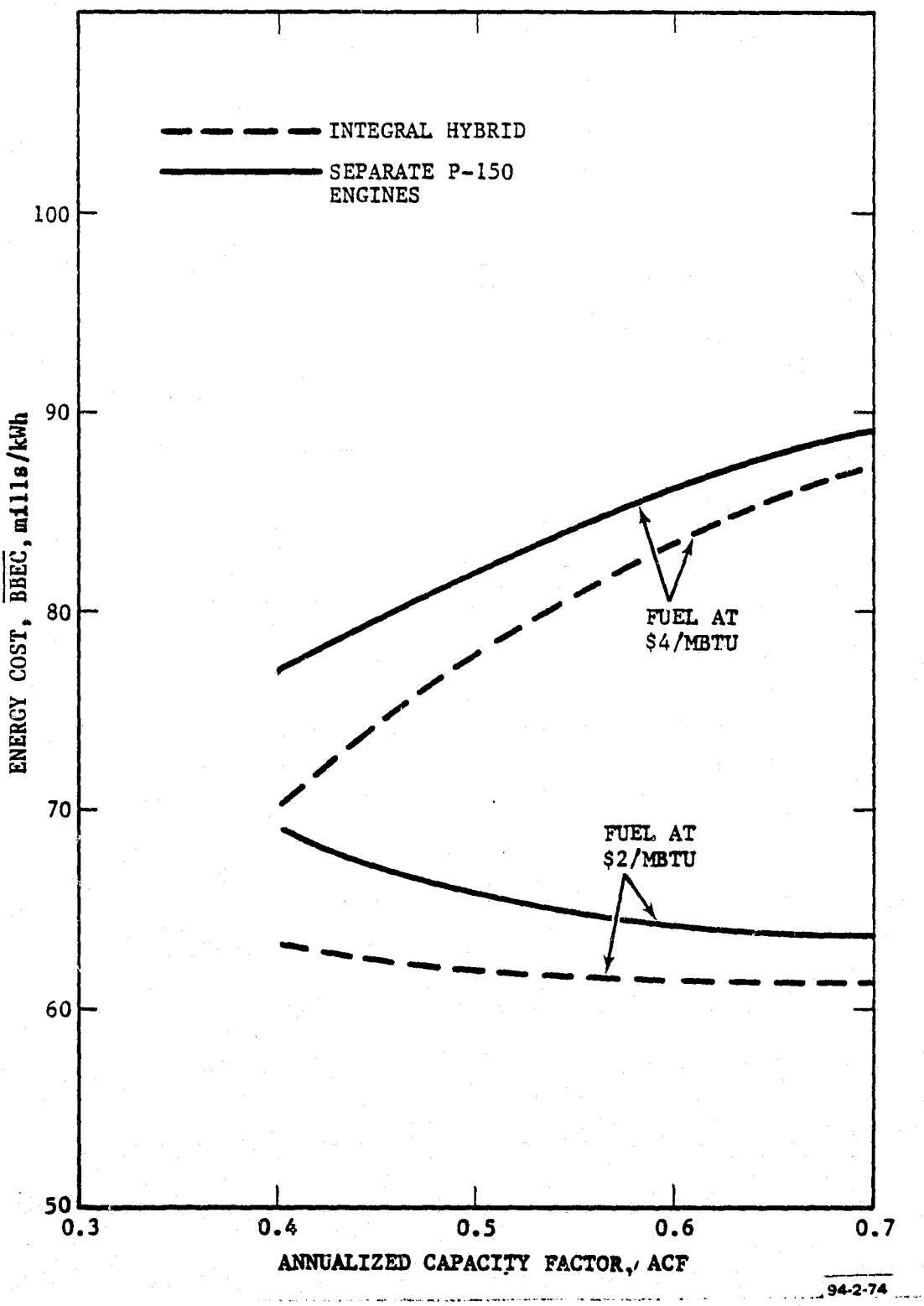

FIGURE 3-116. HYBRID SYSTEM ENERGY COST

weight at the focus, it is obvious that the thermal storage components must be on the ground. Since it is impractical to "pipe" the energy to the ground at the high temperatures of interest (~800°C), several multibounce collector geometries, e.g., the Cassegrain, were examined (Figure 3-117); an external system was also examined, as shown in Figure 3-118. In both cases, system performance was quite low and resultant energy costs exceed that of the lead-acid battery. No further work was then devoted to thermal storage.

E. Other Storage Concepts - There are a number of other storage concepts which may have applicability to the SPS program. Schedule and funding limitations prevented anything but a cursory examination:

1) Hydrogen Production - Potentially attractive since the Stirling engine can run quite well on hydrogen fuel; would be a "self-fueled" hybrid. Conversion efficiencies appear to be low (~50%) with present electrolysis techniques, however, and scarcity of water in the southwest U.S. would seem to preclude use of this concept.

2) Pumped Hydro - Lack of necessary topography; questionable cost effectivity in small plant size.

3) Compressed Air - Lack of necessary topography; uncertainty regarding interface of conversion equipment with Stirling engine.

3.1.7 CONTROL SUBSYSTEM

A summary of the control and operating sequence - primarily related to the key problem of engine/AC generator synchronism - is contained in paragraph 3.1.1.5. The entire 1MWe station is controlled by a microprocessor performing the role of master power controller (MPC). The equipment used in the subsystem and the functions performed are summarized in the following paragraphs. The trade studies made to define the hardware and additional details concerning the subsystem are contained in Appendix B.

3.1.7.1 Control Hardware. The subsystem consists of the following major elements:

- Master power controller (MPC)
- Central control interface assembly (CCIA)
- Remote control interface assemblies (RCIA)
- Control and status cables
- Control building

Figure 3-119 is a block diagram showing the basic hardware elements for the control subsystem and their interfaces. Note the system includes battery storage and was sized for the 4-1/2 or 6-1/2 year system. The 3-1/2 year system is basically the same except for almost three times as many collectors.

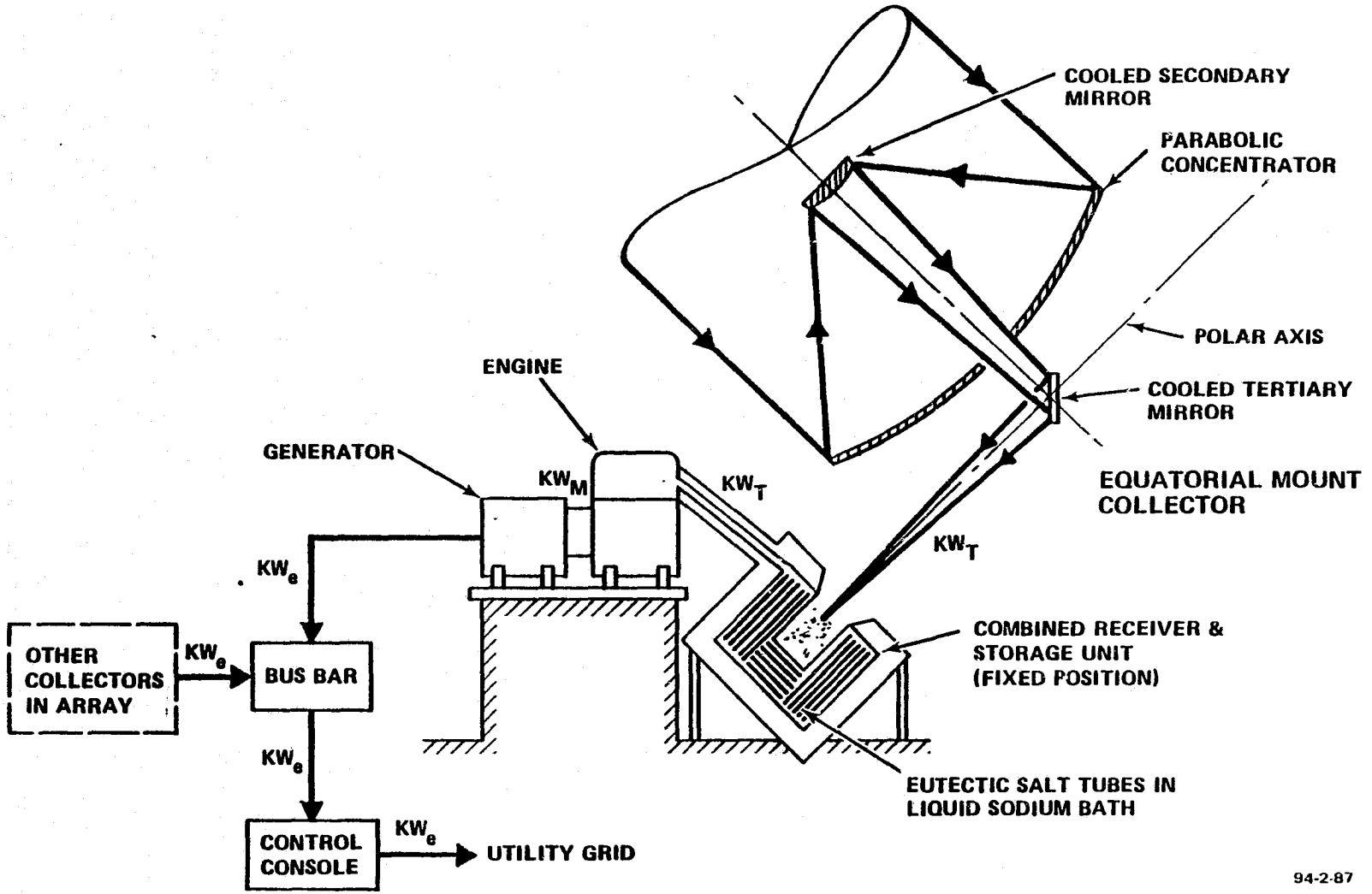

FIGURE 3-117. INTERNAL THERMAL STORAGE (COMBINED RECEIVER AND STORAGE TANK)

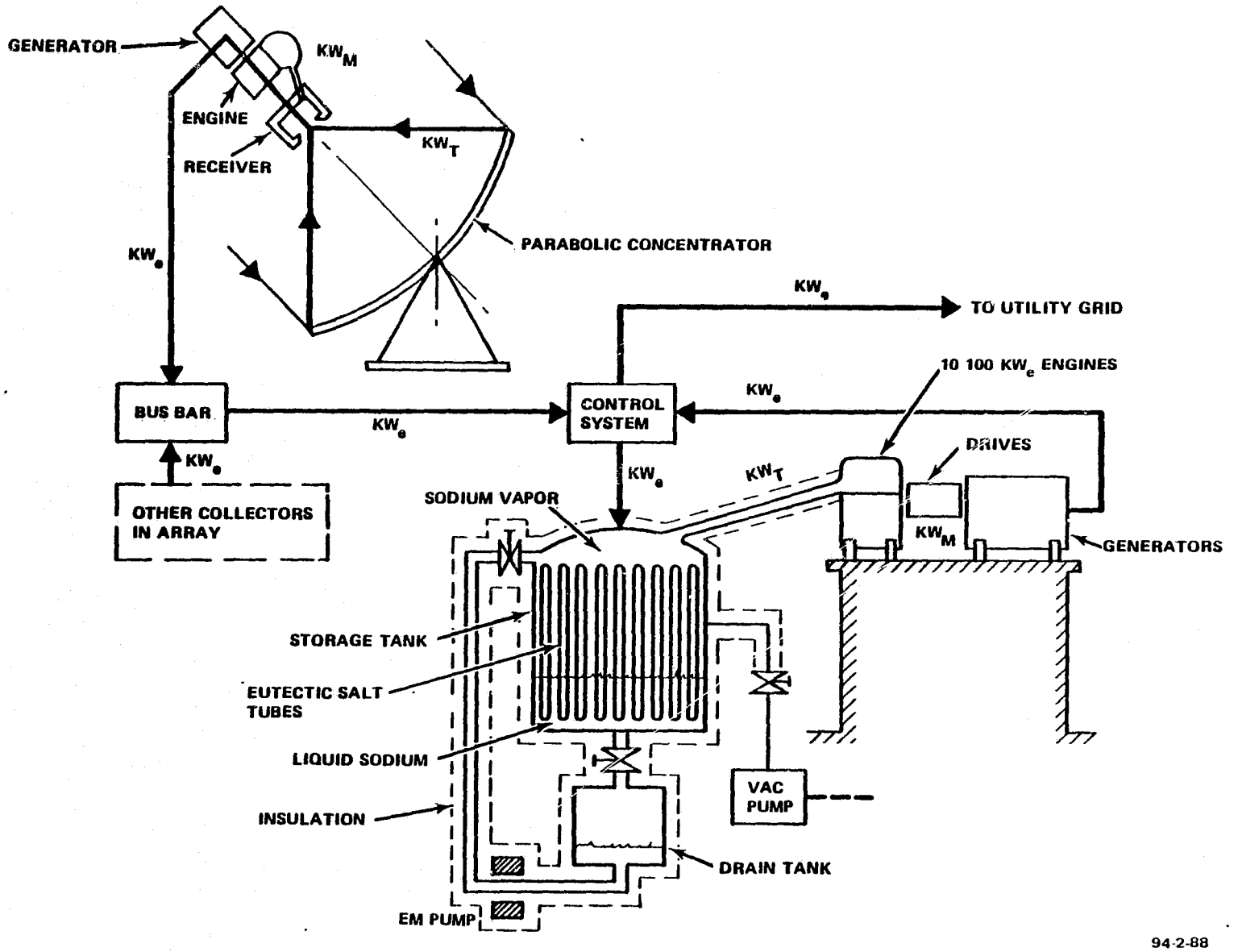

FIGURE 3-118. EXTERNAL THERMAL ENERGY SYSTEM

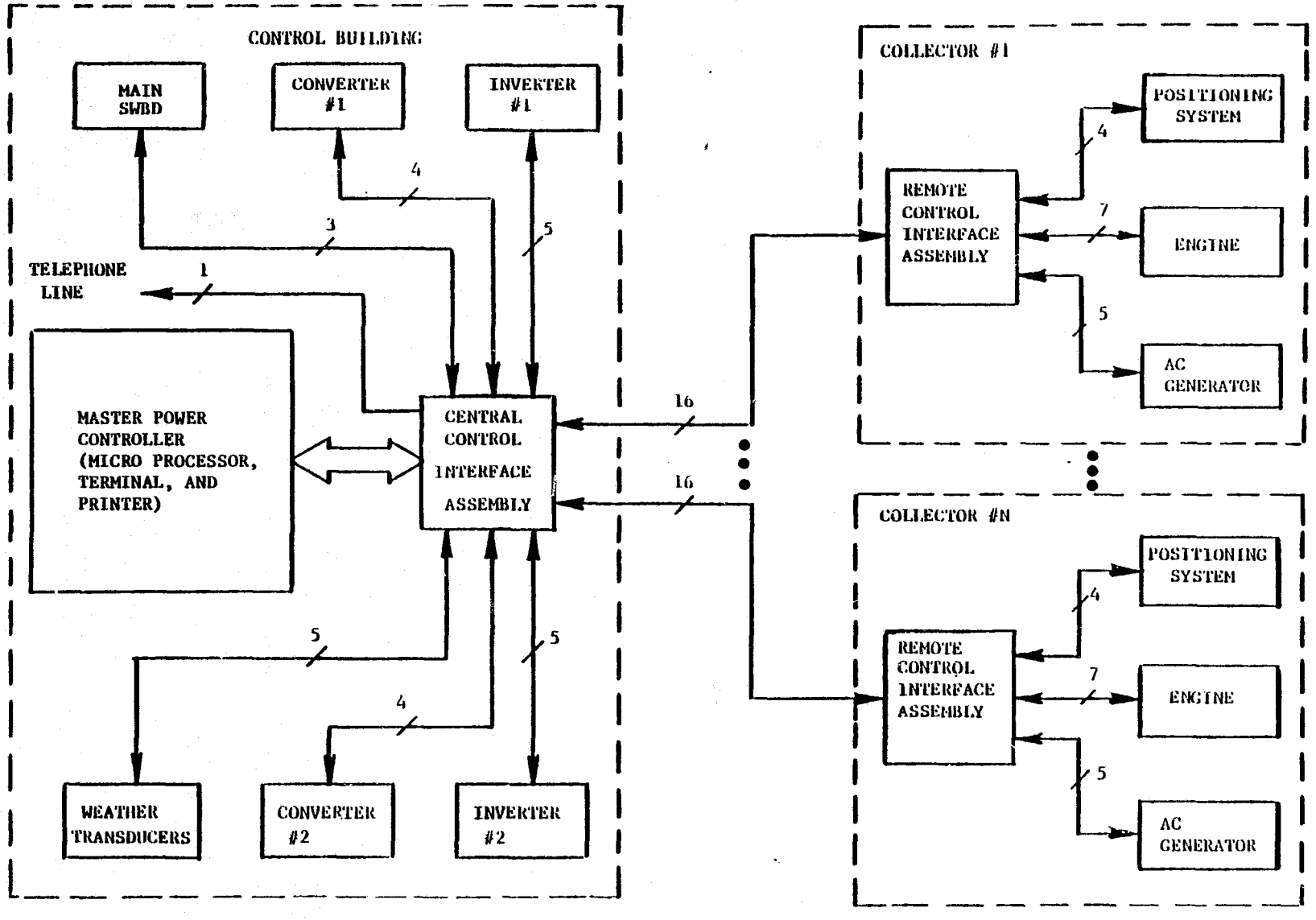

FIGURE 3-119. CONTROL SUBSYSTEM HARDWARE BLOCK DIAGRAM

94-2-151

- Master Power Controller. The MPC consists of a Cromemco CS-3 Microcomputer (microprocessor), a SOROC Technology IQ-120 CRT terminal, and a Texas Instruments Model 810 line printer. The microprocessor is an 8-bit machine operating in a S-100 bus configuration at a 4MHz clock rate. It will be equipped with two 8-inch "floppy" disks and a PROM programmer (used in first power station only). Figure 3-120 is a photograph of the CS-3 unit. Details of this commercially available computer, terminal and printer are given in Appendix B.

- Central Control Interface Assembly (CCIA). The CCIA will provide the interfacing between the microprocessor and the collectors and other equipment (see Figure 3-119). It performs all the conversions, suppression, multiplexing, and driving of the various signals (see Appendix B).

- Remote Control Interface Assembly (RCIA). A RCIA will be packaged in the MENA-12 enclosure located at the base of each concentrator. It will fan out the incoming signals on the 18-pair control/status cable to smaller cables to the power module and concentrator drive system. It will also provide signal level conversions and line-driving capability for analog signals.

- Control and Status Cables. The control cables from the CCIA in the control building to the RCIA's will consist of 18 individually shielded pairs of No. 20 AMC stranded conductors (similar to Belden No. 9886) with a high density polyethylene jacket suitable for direct burial installation. Cables on the concentrators will be 6-pair construction of the same type of cable used elsewhere.

- Control Building. The control building will house not only the control equipment, but also the main switchboard and work areas. Figure 3-121 is a floor plan with a station with no storage batteries; Figure 3-122 is a floor plan with the amount of battery storage necessary to achieve a 0.4 Annualized Capacity Factor (see paragraph 3.1.6.1). Note that the floor area increases by more than a factor of 5, and the number of air conditioners increases from one to five. Power requirements for operating the building are listed in Appendix G.

3.1.7.2 Control Functions and Inputs. The functions of and inputs to the control system are summarized below.

a. Resident Functions. The information generated by the CS-3 microprocessor is:

- Calendar time

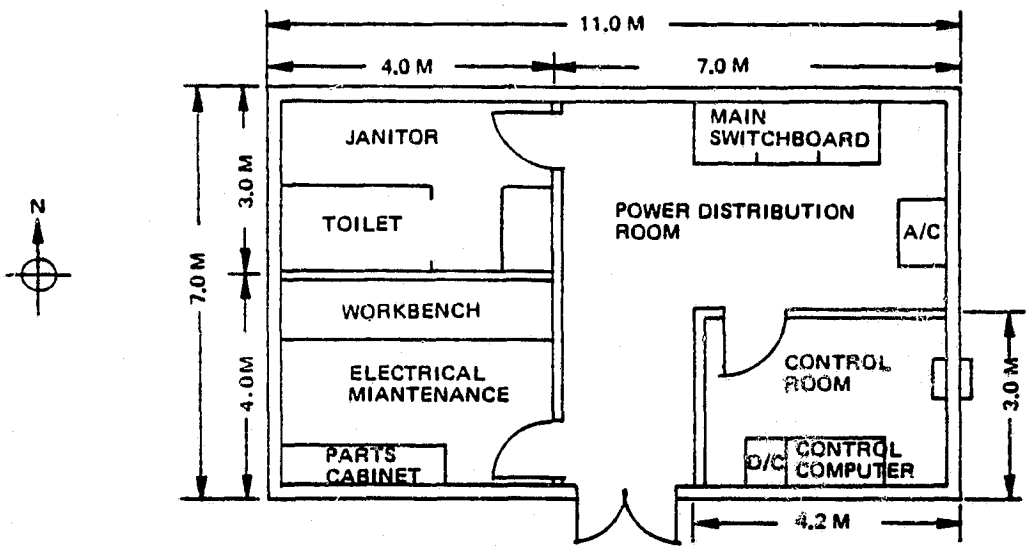

FIGURE 3-121. CONTROL BUIDING FLOOR PLAN (NO STORAGE)

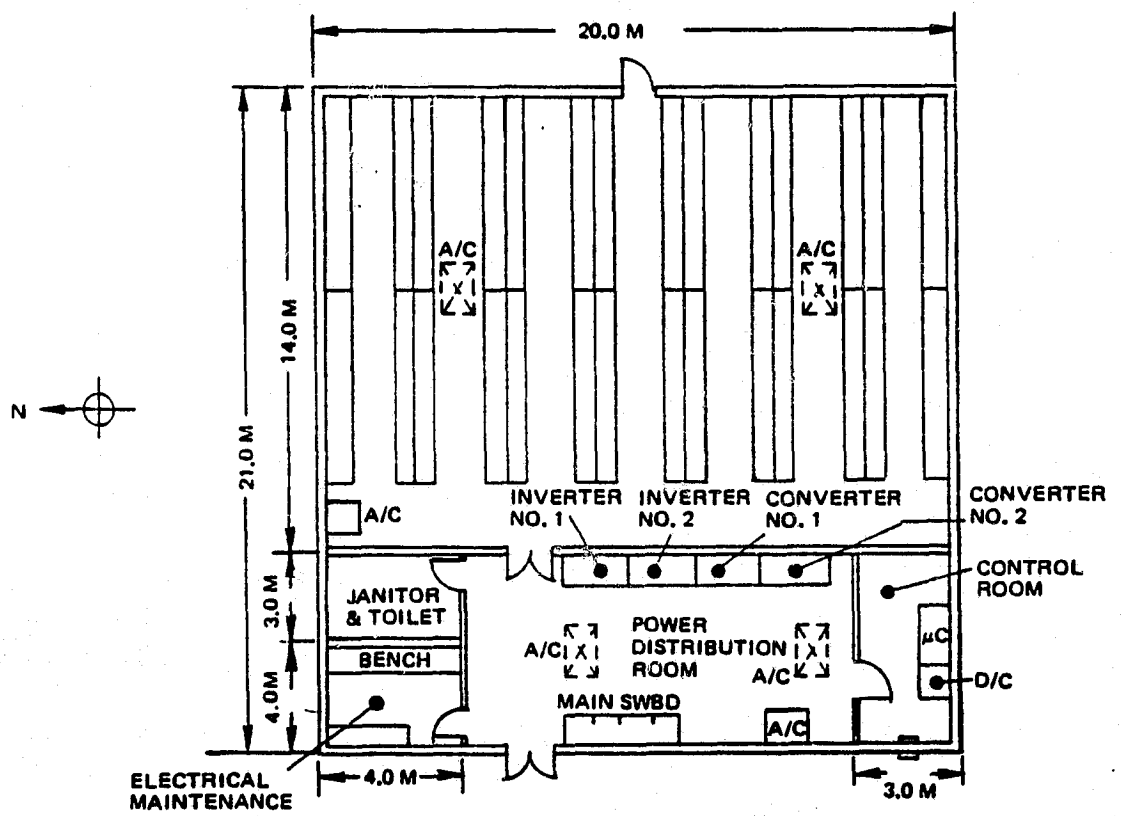

FIGURE 3-122. CONTROL BUILDING FLOOR PLAN INCLUDING BATTERY STORAGE (0.4 ACF)

PRECEDING PAGE BLANK NOT FILMED

- Clock time
- Solar ephemeris data

b. Input Signals. The MPC receives the following analog inputs from other components in the stations:

- Engine head temperature
- AC generator output voltage
- AC generator output current
- Converter output voltage*
- Converter output current*
- Battery bank voltage*
- Battery bank current*
- Inverter output voltage*
- Inverter output current*
- Main switchboard bus voltage
- Station output current
- Solar insolation level
- Wind speed
- Wind direction
- Temperature
- Relative humidity

*Used only for battery storage (also applies to converter, battery and inverter items in c. and d. below)

c. Status Signals. The following status and alarm signals are received:

- Engine summary failure alarm(s)
- Receiver temperature alarm
- Engine ready
- Concentrator summary failure alarm
- AC generator output contactor
- Converter summary failure alarm
- Inverter summary failure alarm
- Main circuit breaker
- Control room air conditioner alarm
- Station fire alarm
- Station intrusion alarm
- Sodium detector alarm**
- Door or receiver lip temperature status**

**Optional signals; selection to be made later

d. Output Control Signals. The microprocessor processes the resident and input signals and produces the following analog output signals:

- Synchronize signal to engine electronic control unit
- AC generator excitation offset
- Converter output current
- Inverter phase offset
- Inverter output voltage offset

The bi-state output control signals are:

- Engine start/stop
- Receiver door open/close
- Sodium blocking valve open/close
- Concentrator focus/defocus
- Concentrator operate/stow
- AC generator output contactor open/close
- Converter on/off
- Inverter on/off
- Battery contactor open/close
- Main circuit breaker open/close
- Station local alarm

A single serial-bit stream is sent to all collector drive controllers at ~15 second intervals throughout the day consisting of:

- Concentrator azimuth position | Details of the concentrator control
- Concentrator elevation position | strategy are contained in Appendix A.

Also, the control system originates an automatic telephone dialing signal when necessary to advise the power system control operator of abnormal operating conditions.

3.2 SUBSYSTEM DEVELOPMENT STATUS

The research and development (R&D) requirements to bring each subsystem to maturity are described in this section. Although the proposed SPS concept is different from any system that has been operated in the past, all the components have been demonstrated. Therefore, no technical break-throughs are required to translate this concept into real hardware.

3.2.1 RECEIVER AND RELATED COMPONENTS

3.2.1.1 Sodium/Stirling Systems. The solar-heated sodium receiver (reflux boiler)/vapor pipe/Stirling engine concept has not been demonstrated in the past; however, a very similar concept has. Figure 3-123 is a photograph of a Stirling engine operating basically the same as the SPS except the sodium is heated by electrical resistance heaters rather than from the sun. The original color photograph shows the boiler, vapor pipe, engine heater head glowing yellow-hot. (The insulation was partially cut away to show these components.) The test also had a separate return line for the liquid sodium, whereas the SPS does not in order to prevent the possibility of the line plugging up from solidified solium and to eliminate the need for a electromagnetic pump. This test was successfully run for many hours by N. V. Philips (Eindhoven, The Netherlands) in 1969-1970.

A similar set-up was used by United Stirling (Malmö, Sweden) in 1973 in which the Stirling engine was operated by a series of electrically heated sodium heat pipes (see Appendix C.)

Both the Philips and the USS tests were successful and many hours of Stirling engine operation were achieved using condensing sodium vapor as the heat source for the engine. The material used for the container and pipes is the same type of Stainless Steel proposed for SPS. Procedures were developed for minimizing the impurities in the system which is the key to controlling corrosion.

3.2.1.2 Sodium as a Heat Transfer Medium. The superiority of sodium for this application has been demonstrated in paragraph 3.1.2.1. The use of sodium is considered by some to be excessively hazardous, but the experience over the last 20 to 30 years does not bear this out. Atomics International is the recognized expert in sodium technology (including safety), and the thermostructural and safety aspects of the SPS sodium system have utilized the AI work. An in-depth study of applications and properties of high-temperature sodium was carried out as part of the program (Reference 3-47), and it was concluded that with proper procedures and design techniques sodium is a very safe and effective material.

3.2.1.3 Fabrication. The fabrication of the sodium receiver and vapor pipe uses ordinary manufacturing techniques. They are fabricated of readily available stainless steel using well established, closely controlled machine welding methods. All welds are accessible for inspection (including X-ray techniques) that will fully check the receiver for leak tightness and pressure integrity. The selection of materials and wall thicknesses were based upon structural analysis taking into consideration corrosion and the effects of long term temperature cycling.

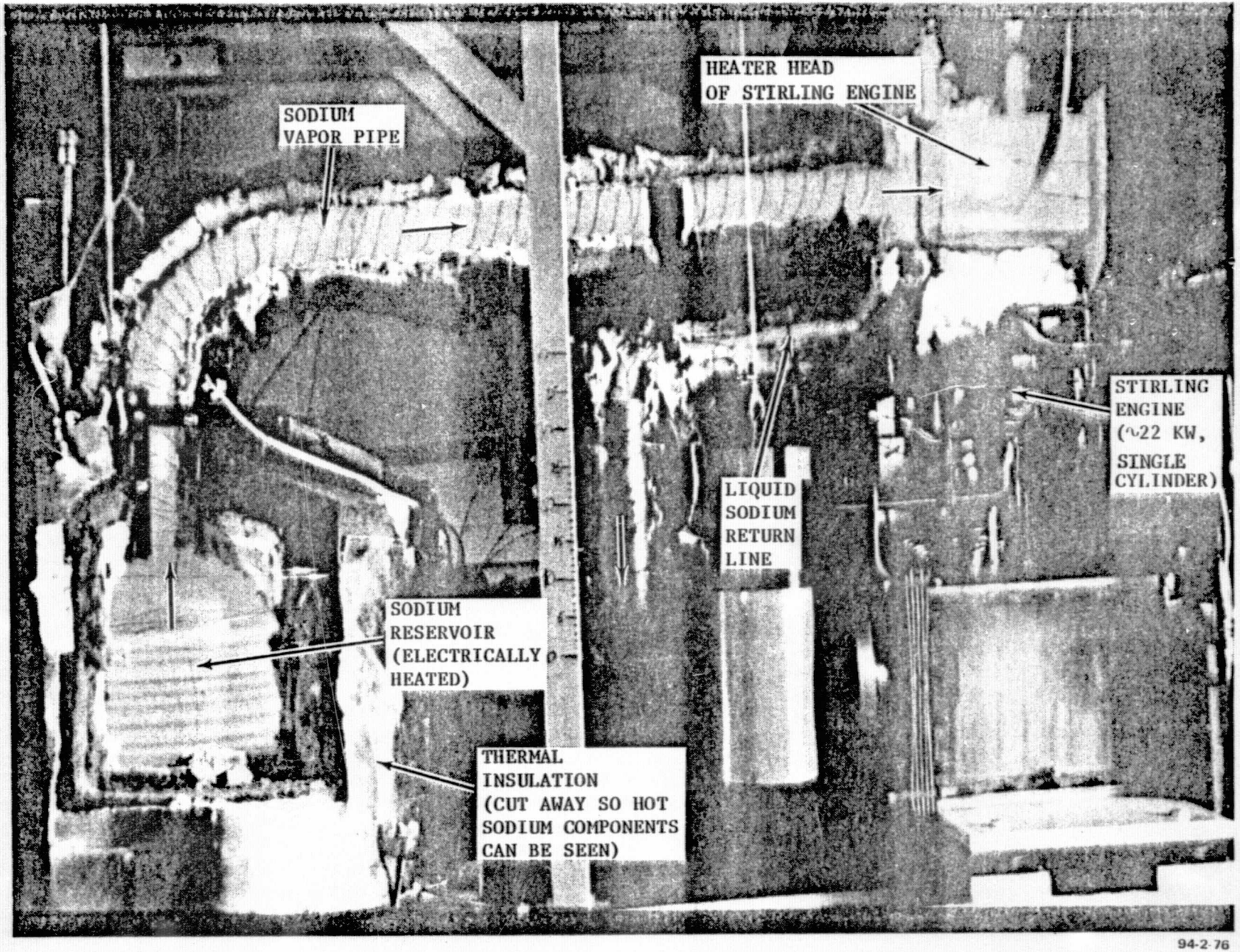

94-2-76

FIGURE 3-123. SODIUM BOILER/STIRLING ENGINE SYSTEM IN OPERATION (SOURCE: N.V. PHILLIPS)

ORIGINAL PAGE IS
OF POOR QUALITY

3.2.1.4 Blocking Valve. A special blocking valve will be fabricated but the design is based on fully-developed hardware. Valves have been used extensively in the nuclear industry for liquid sodium systems. Present day valves manufactured by Anderson-Greenwood or the Nupro Company operate successfully under high pressures and temperatures with large flow rates of liquid sodium. The blocking valve for the heat transport system is not subjected to high pressures or high flow rates, and acts only to prevent flow of sodium vapor to the engine. The proposed design is fully sealed from the outside environment and will be manufactured to loose tolerances from readily available materials. The electromagnetic actuator which operates the valve is a standard device similar to those manufactured by Kimco or Inland Motors Corporation.

3.2.1.5 Bellows. The expansion bellows design has been developed from existing units manufactured by the Robert-Shaw Company. The bellows are made from standard stainless steels using well-developed fabrication techniques for forming the finished bellows. Similar bellows designs are used extensively in sodium valves to provide an effective seal around the valve stem mechanism; these operate over many cycles at high pressures.

3.2.2 CONCENTRATOR

The majority of concentrator components utilize current state-of-the-art materials and techniques in their fabrication, as summarized in the following paragraphs. However, R&D activity should be devoted to those aspects of the concentrator design and manufacture which bear on cost, since the concentrator is the major cost item in the complete system. These costs need to be reduced in order for the proposed SPS concept to become commercially viable.

3.2.2.1 Panel Development Status. To a limited extent, most aspects of the panel design have been tested. However, full scale model testing of the baseline and alternate concepts will be required to verify the predicted performance.

Donnelly Mirrors, Inc., has pressed mirror facets for other solar applications and has successfully demonsrated this capability. The slope error and the specular beam spreading (specularity) must be measured for the proposed panel design (mirror plus back-up structure). No further development of metal stamping for the baseline steel/foam sandwich support structure is required, but several candidate organic foams must be evaluated for cost, adhesion to the metal surfaces, shear strength and creep stability. The low thermal distortion of the pressed facets on a steel structure must also be demonstrated.

JPL and others have demonstrated success with the fabrication of small elastically curved glass mirrors similar to that proposed for the alternate glass sandwich design. However, more testing is required to evaluate allowable elastic stress levels when these panels are subjected to high wind and hail load conditions. The tests will consist of loading test sandwich beams to "fast fracture" where the glass sheet is elastically curved to various radii.

In addition, various adhesives need to be evaluated for both panel concepts to identify adequate lifetime structural performance at lowest manufacturing cost. Accelerated weatherability tests are required to demonstrate the combined silver protection offered by the metal cladding and the dual layer, butyl/silicone rubber edge seal. Testing of the predicted surface reflectance will be part of these tests.

Large volume production techniques to measure and analyze the panel surface slope should be developed using automated computerized measurements and data reduction to minimize quality assurance costs.

3.2.2.2 Structural Components. Analysis and optimization techniques currently exist to design a cost-effective structure for the reflector structure, receiver support system and pedestal. This also applies to other components such as bearings and drives. Knowledge and experience with design details (which are quite important for high volume production) are available through the services of the Ford Motor Company Manufacturing Feasibility Department. High volume (i.e., low cost) manufacturing techniques are now available; the only development required is the design of the tooling and its implementation into a production line. Therefore, no further development work is required in this area.

3.2.2.3 Tracking System. Implementation of tracking system proposed for SPS is state-of-the-art. Solid-state electronic components, discrete elements, and microprocessors are regularly combined in similar applications, and the design has become routine. Although the optical tracking sensor is not off-the-shelf, the components and materials from which it is constructed are available and the design is similar to existing hardware.

3.2.2.4 Recommended Tests. The following tests are recommended in addition to the panel development tests outlined above.

a. Sand/Dust. Conduct sand/dust environmental tests to confirm sandstorm survival of outdoor mechanical and electrical components.

b. Wind Tunnel Tests/Analysis. It is desirable to perform wind tunnel tests on the selected concentrator configuration because this major cost item is directly affected by the wind loads on the structural and mechanical components. Structural analyses would be used to resize the structural elements of the aerodynamic coefficients show significant change compared to existing JPL data. Wind tunnel tests could also be used to determine the wind effects for a field of collectors, particularly to determine which collectors are subjected to the highest loads in a closely packed field.

3.2.3 POWER CONVERSION SUBSYSTEM

3.2.3.1 Stirling Engine. United Stirling (Sweden) has been engaged in intensive development of the Stirling cycle machine since 1968. Production of P-75 and P-150 engines in the previously-discussed U-crank configuration is scheduled to begin in 1982 with 200 units per year, increasing to 10,000 units per year by 1986. The P-40 engine is the developmental power plant for the U-crank concept. USS does not now plan to produce the P-40 engine because its power output is too low for the automotive/truck-type application of interest to USS. USS has indicated, however, that they could put the engine into production if there were "sufficient" demand for it. If the SPS were to reach operational status, of course, there would be ample demand. However, as discussed previously, the only benefit of the P-40 over the P-75 engine is its availability for the 3-1/2 year program. An in-depth presentation of the history/development status of the Stirling cycle engine at USS is contained in Appendix C.

The above comments apply to fuel-burning engines, which must be converted for the solar application. The required changes are:

(1) The existing combustion components must be removed; this includes the preheater, blower, turbulator and air/fuel control bandwave.

(2) The working fluid is changed from hydrogen to helium.

(3) The existing Electronic Control Unit (ECU) will be modified to provide an output signal denoting engine rpm.

(4) The existing heater head must be removed and replaced with a tubular system matched to the requirements for heating the working fluid with condensing sodium (see Appendix C).

Item (2) results in a drop in engine power and efficiency; the remaining items increase power and efficiency so that there is a net improvement in performance over the fuel burner configuration (see Appendix C). The major engine modification is item (4); this modification will be carried out by FACC under USS direction. Figure 3-124 is a sketch showing the existing heater head arrangement, The "envolute" assembly is a set of closely packed, partially finned tubes arranged in quadrants with each quadrant connecting the top of one cylinder with the tops of 2 regenerator housings as shown in Figure 3-125 For the solar application, there will be fewer tubes (all unfinned) arranged as shown in Figure 3-126 The tube ends will be brazed into "adaptors" configured into the cylinder/regenerator end housings as shown. Bellows are provided to permit thermal expansion of the adapters and the lower head enclosure plate relative to the colder cylinder/regenerator walls. A drawing of the complete heater head system is shown in Figure 3-127; all materials are 316 SS and ready access to the cylinder/regenerator cap bolts is provided for removal of the head as a single unit.

3.2.3.2 Alternators. The technology of small synchronous AC generators (alternators) appears to be mature. The efficiency of present-day machines of the 75 kW class is about 90%, however efficiency is becoming more important than initial capital costs. It is projected that the use of better magnetic materials and reduced stator-rotor air gaps will increase the efficiency to ~94% in about 1990. However, this will result in increased material and manufacturing costs.

3.2.4 ENERGY TRANSPORT SUBSYSTEM

The energy transport subsystem (electrical cables, switchboards, etc.) are mature, off-the-shelf technology and no development is required.

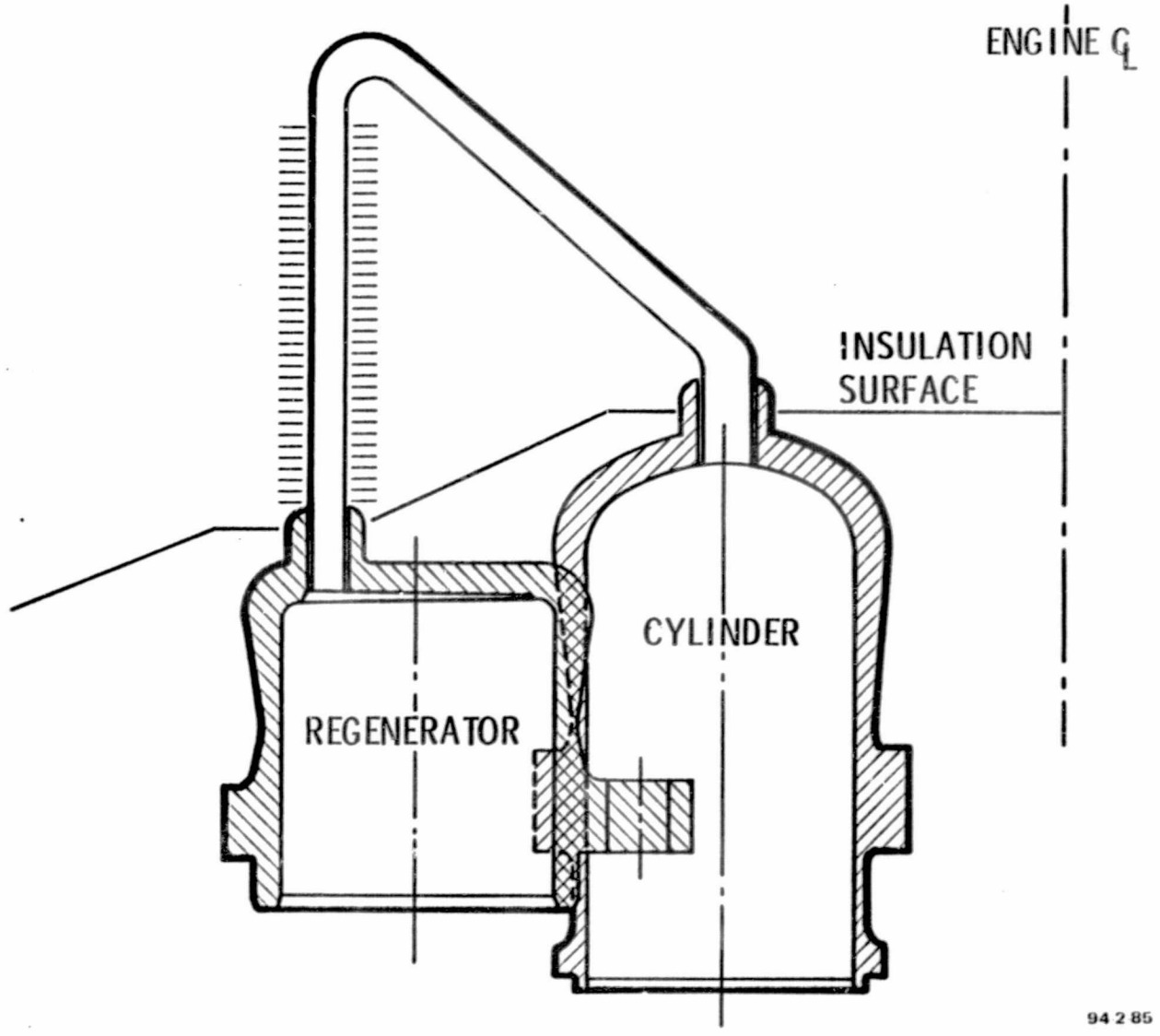

FIGURE 3-124. CURRENT ENVOLUTE HEAT HEAD LAYOUT FOR P-40/P-75 STIRLING ENGINES

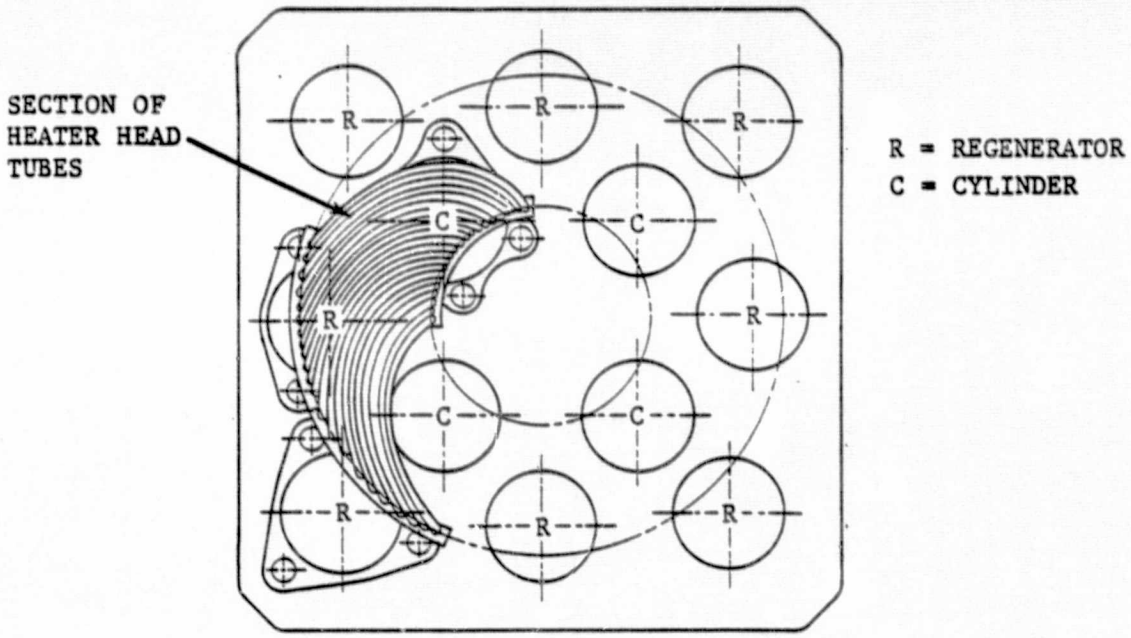

FIGURE 3-125. PLAN VIEW OF P-40/P-75 ENGINE BLOCK

94-2-60A

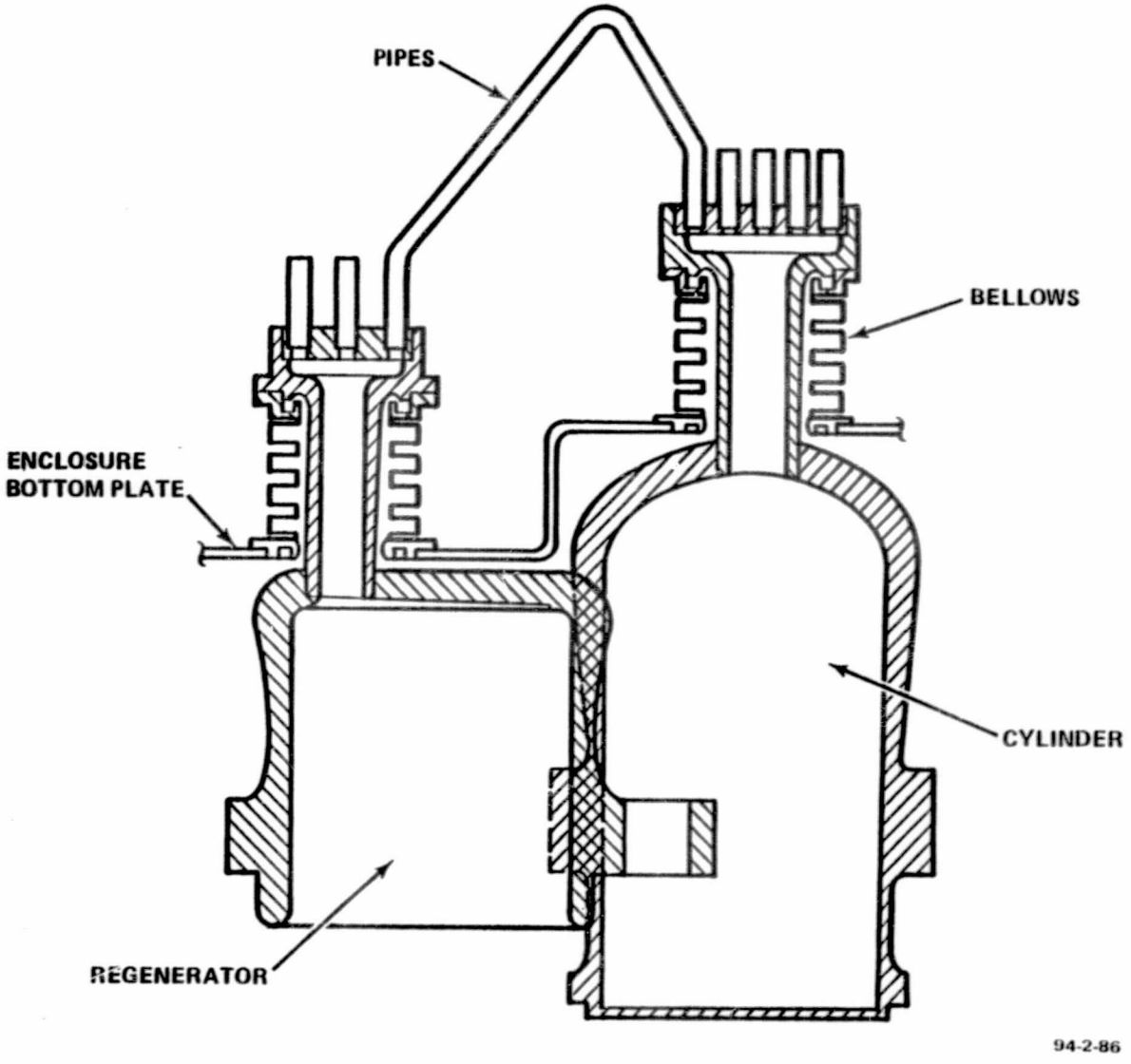

FIGURE 3-126. PROPOSED MODIFIED HEATER HEAD ARRANGEMENT FOR SOLAR STIRLING ENGINE (P-40, P-75)

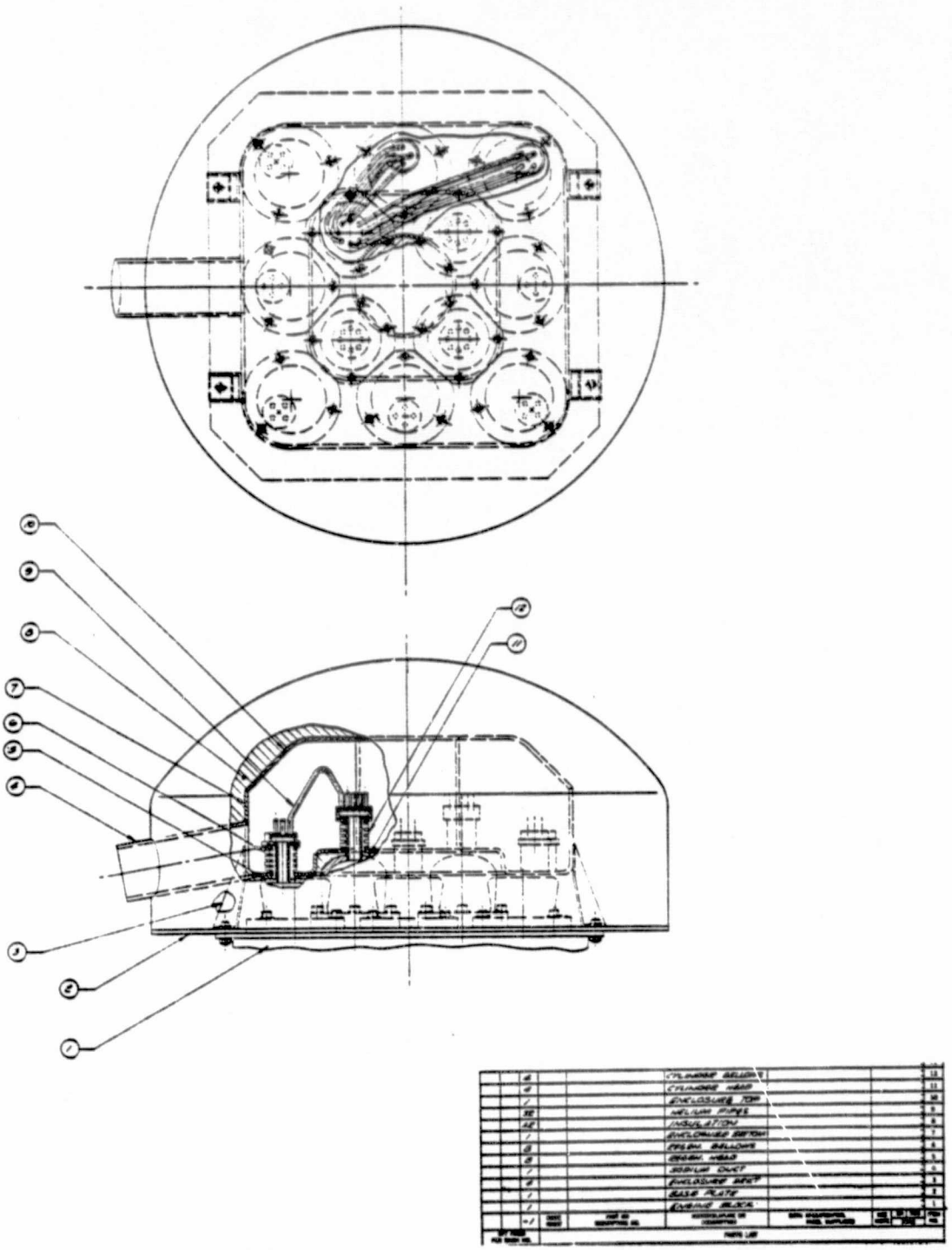

FIGURE 3-127. MODIFIED SODIUM-DRIVEN HEATER HEAD AND ENCLOSURE FOR P-75 STIRLING ENGINE

3.2.5 ENERGY STORAGE SUBSYSTEM

3.2.5.1 Lead-Acid Batteries and Ancillary Equipment. The converters and inverters selected for the storage subsystem are fourth generation solid state power conversion technology and therefore are mature technology. The efficiencies for the size required are 97 and 94 percent for conversion and inversion, respectively. Future development may take the direction of larger power modules and, if so, ratings higher than 400-500 kW and higher voltages (e.g., 780 VDC) will lead to a cost reduction in the equipment, combined with a 1 to 2 percent increase in operating efficiency.

Lead-acid batteries are mature technology, and no further R&D work is required. Battery makers are currently working on improvements in cycle life, however, present-day lead-acid batteries are simply not a good choice for a commercial SPS plant.

3.2.5.2 Advanced Batteries. Systems studies have shown that advanced batteries have promise of being much more cost effective than the present-day lead-acid version provided, of course, the technology continues to advance. EPRI and DOE are funding studies on various types of advanced batteries and a brief summary of this work for load leveling applications is given below.

The requirements are:

LOAD LEVELING REQUIREMENT

Peak Specific Power (W/kg)	Specific Energy (Wh/kg)	Minimum Cycle Life	Lifetime (Years)	Initial Cost ($/kWh)
60	100	2500-5000	10-20	40

Table 3.27 summarizes the characteristics of the advanced systems currently under development, and Table 3.28 shows the developers of these systems and summarizes the major problem areas. The advanced batteries fall into two general categories of high and low temperature systems. In general, the high temperature batteries have higher energy densities and higher power densities than the low temperature systems. The high temperature batteries currently suffer from problems related to corrosion due to the reactive nature of the chemical constituents of these high temperatures. For this reason, the low temperature batteries, i.e., advanced lead acid and nickel zinc, will be the first to appear in the market place - 1980-81. The high temperature systems are not expected to reach the commercialization stage until after 1985.

3.2.5.3 Other Storage Concepts. Other storage concepts include flywheels, compressed air and a hybrid system using Stirling engines burning fossil fuel. Flywheels appear attractive but breakthroughs will be required. The development work on flywheels is now being funded by various Government agencies.

TABLE 3.27. PROJECTED BATTERY CHARACTERISTICS

	THEOR. CELL ENERGY DENSITY (Wh/kg)	OPERATING TEMPERATURE (°C)	DEMONSTRATED CELL LIFE	PROJECTED		
				ENERGY DENSITY (Wh/kg)	PEAK POWER DENSITY (W/kg)	CYCLE LIFE
LOW TEMPERATURE SYSTEMS						
Lead Acid	247	20 - 30	400	30	80	--
Advanced Lead Acid	247	20 - 30	500	50	150	1000
Lithium-Titanium Sulfide	470	20 - 30	500	130	--	--
Nickel Zinc	130	20 - 30	200 (Cell)	80	150	500 - 1000
Zinc Chlorine	210	50	250	150	70	2500
HIGH TEMPERATURE SYSTEMS						
Sodium-Antimony Trichloride	745	200	350	100	50	2500
Lithium-Iron Sulfide	458	400 - 450	1000 (Cell)	100	30	3000
Sodium Sulfur	790	300 - 350	200	150	75	2500

TABLE 3.28. ADVANCED BATTERY STATUS AND PROBLEM AREAS

	Development Status	Projected Commercialization Date	Principle Technical Problems	Possible Commercialization Problems	Major Developers
LOW TEMPERATURE SYSTEMS					
Zinc Chlorine	early production prototype	1983	system complexity Impurities in eletrolyte	cost of chlorine storage (contaminant). Cost of graphite or rutile electrodes.	Energy Dev. Assoc.
Lithium-Titanium Sulfide*	laboratory cells modules	?	electrolyte instability	cost of lithium low power density	EXXON Ind.
Nickel-Zinc*	prototype battery	1981	dentrite growth cycle life	limited life Nickel Plaque cost	Gould, Inc. GM ESB
HIGH TEMPERATURE SYSTEMS					
Sodium-Sulfur	laboratory cell modules	1985	corrosion cost of β-alumina electrolyte	safety	GE, C.G.E. Ford, Dow, Chloride
Sodium-Antomony Trichloride	laboratory cell	1987	corrosion of current collector. Seals	cost, availability of antimony. Safety	ESB
Lithium-Iron Sulfide	laboratory cell	1985	life corrosion	cost of lithium & fabric separator	Rockwell (Atomic Int'l.) Argonne (Eagle Pitcher Ind., Gould, Inc. Catalytics Res. Grp.) GM

*Development aimed more toward electric vehicles than load leveling.

The only other attractive storage option is using fossil fuel to power Stirling engine/generator sets - attractive, however only if some type of fuel is available. Obviously this option will not require any additional development work over what is now being performed by USS.

3.2.6 CONTROL SUBSYSTEM

Standard, off-the-shelf equipment is proposed for the control system, and no additional R&D is required to bring the system to maturity. However, the entire line of control system hardware is advancing very rapidly and a careful selection was made of a microprocessor which not only uses a high performance microprocessor chip, but one that is well supported by a comprehensive family of peripheral devices, mature program development software and a second source manufacturer. The Cromemco CS-3 computer, which uses the Zilog Z-80A microprocessor chip (second sourced by Mostek), meets all of the above requirements and is the recommended computer for any of the three start-up times.

The current main stream of microprocessor development is being directed toward the design and marketing of machines based on 16-bit microprocessor chips. Complete hardware systems are perhaps a year or two in the future and software maturity will probably lag the availability of hardware in commercial quantities by another year or two. The added processing throughput made possible by 16-bit data paths, more extensive micro-coded arithmetic routines, and probably equal price in OEM quantities makes these machines very attractive for stations to be implemented after 1985, and are recommended.

3.3 SYSTEM CHARACTERIZATION

The three Phase III programs (T_s = 3½, 4½ and 6½ years) will utilize parabolic concentrators, Stirling engines/AC generators and lead-acid batteries as described in previous sections. The 3½ year program will use 11.2m diameter concentrators and the USS P-40 Stirling engines. The 4½ and 6½ year programs will both use 18.6m diameter concentrators and the USS P-75 Stirling engines.

A breakdown of Phase III component weights and subsystem efficiencies is given in Tables 3.29 and 3.30 (JPL Table E-2). For clarity, detailed weight summaries are given in separate Tables 3.31, 3.32, 3.33 and 3.34. Note that component cost estimates are given in paragraph 5.2.

TABLE 3.29 PHASE III ENGINEERING INFORMATION SUMMARY (JPL TABLE E-2)

3½ YEAR PROGRAM

ITEM	EFFICIENCY %	WEIGHTS lb (kg)	ESTIMATE 1978 $K	
			COMPONENTS	SUBTOTALS
COLLECTOR SUBSYSTEM	0.740	12887(5846)		
1. SITE PREPARATION/FOUNDATION				
2. STRUCTURAL FRAMEWORK				
3. REFLECTOR SURFACE AND SUPPORT				
4. DRIVE MECHANISM AND LOCAL CONTROL		TABLE		
5. RECEIVER AND SUPPORT		3.31		
6. PIPES, VALVES, FITTINGS, etc.				
7. MISCELLANEOUS (EXPLAIN)				
8. FIELD INSTALLATION				
9. FIELD SUPERVISION				
10. SUBSYSTEM CHECKOUT/ADJUSTMENT				
POWER CONVERSION SUBSYSTEM	0.336	1601(726)		
1. HEAT ENGINE (η = 0.373)				
2. GENERATOR (η = 0.90)				
3. HEAT EXCHANGER/BOILERS/CONDENSERS				
4. CONTROL VALVES AND LOCAL CONTROL ELEMENTS				
5. PUMPS AND FANS		TABLE		
6. HEAT REJECTION EQUIPMENT		3.32		
7. SUBSYSTEM BUILDINGS AND FACILITIES				
8. SWITCH GEAR, TRANSFORMERS, etc.				
9. CONCEPT PECULIAR (EXPLAIN)				
10. MISCELLANEOUS (EXPLAIN)				
11. FIELD INSTALLATION				
12. FIELD SUPERVISION				
13. SUBSYSTEM CHECKOUT/ADJUSTMENT				
ENERGY TRANSPORT SUBSYSTEM	0.964			
THERMAL				
1. PIPING				
2. INSULATION				
3. CONTROL VALVES AND LOCAL CONTROL ELEMENTS				
4. FLUID PUMPS AND DRIVES				
5. SITE PREPARATION, FOUNDATIONS, AND PIPING SUPPORT ELEMENTS				
6. MISCELLANEOUS (EXPLAIN)				
7. FIELD INSTALLATION				
8. FIELD SUPERVISION				
9. SUBSYSTEM CHECKOUT/ADJUSTMENT				
ELECTRICAL				
1. WIRING (MATERIAL, SUPPORTS, TRENCHES, etc.)				
2. UTILITY INTERFACE SUBSTATION				
3. LOCAL CONTROL ELEMENTS				
4. MISCELLANEOUS (EXPLAIN)				
5. FIELD INSTALLATION				
6. FIELD SUPERVISION				
7. SUBSYSTEM CHECKOUT/ADJUSTMENT				
ENERGY STORAGE SUBSYSTEM	0.775			
1. TANKS, INSULATION, STORAGE MEDIUM				
2. HEAT EXCHANGERS/BOILERS				
3. HEAT TRANSFER FLUID				
4. PUMPS, VALVES, PIPING, etc.				
5. LOCAL CONTROL ELEMENTS				
6. SITE PREPARATION/FOUNDATION				
7. MISCELLANEOUS (EXPLAIN)				
8. FIELD INSTALLATION				
9. FIELD SUPERVISION				
10. SUBSYSTEM CHECKOUT/ADJUSTMENT				
CONTROL SUBSYSTEM	NA			
1. CONTROL SOFTWARE				
2. PROCESSORS/COMPUTERS				
3. SYSTEM CONTROL ELEMENTS FOR PLANT OPERATION				
4. SUBSYSTEM OPERATION CONTROL ELEMENTS				
5. CONTROL LINES TO SUBSYSTEMS AND PLANT CONTROL ELEMENTS				
6. BUILDINGS AND FACILITIES TO HOUSE EQUIPMENT				
7. MISCELLANEOUS (EXPLAIN)				
8. FIELD INSTALLATION				
9. FIELD SUPERVISION				
10. SUBSYSTEM CHECKOUT/ADJUSTMENT				
DETAIL DESIGN				
PLANT CONSTRUCTION MANAGEMENT				
SPECIAL FEATURES				
RELATED ITEMS				
OTHER (BUILDINGS AND OTHER UTILITIES TO SUPPORT SYSTEM FUNCTIONS, etc.)				
TESTING AND EVALUATION				
TOTAL ESTIMATED COST				

TABLE 3.30 PHASE III ENGINEERING INFORMATION SUMMARY (JPL TABLE E-2)
(4½, 6½ YEAR PROGRAMS)

ITEM	EFFICIENCY %	WEIGHTS lb (kg)	ESTIMATE 1978 $K	
			COMPONENTS	SUBTOTALS
COLLECTOR SUBSYSTEM	0.740	32958(14950)		
1. SITE PREPARATION/FOUNDATION		↑		
2. STRUCTURAL FRAMEWORK				
3. REFLECTOR SURFACE AND SUPPORT				
4. DRIVE MECHANISM AND LOCAL CONTROL		TABLE		
5. RECEIVER AND SUPPORT		3.33		
6. PIPES, VALVES, FITTINGS, etc.				
7. MISCELLANEOUS (EXPLAIN)				
8. FIELD INSTALLATION				
9. FIELD SUPERVISION				
10. SUBSYSTEM CHECKOUT/ADJUSTMENT		↓		
POWER CONVERSION SUBSYSTEM	0.354	2530(1147)		
1. HEAT ENGINE (η = 0.393)				
2. GENERATOR (η = 0.90)				
3. HEAT EXCHANGER/BOILERS/CONDENSERS				
4. CONTROL VALVES AND LOCAL CONTROL ELEMENTS				
5. PUMPS AND FANS		TABLE		
6. HEAT REJECTION EQUIPMENT		3.34		
7. SUBSYSTEM BUILDINGS AND FACILITIES				
8. SWITCH GEAR, TRANSFORMERS, etc.				
9. CONCEPT PECULIAR (EXPLAIN)				
10. MISCELLANEOUS (EXPLAIN)				
11. FIELD INSTALLATION				
12. FIELD SUPERVISION				
13. SUBSYSTEM CHECKOUT/ADJUSTMENT		↓		
ENERGY TRANSPORT SUBSYSTEM	0.964			
THERMAL				
1. PIPING				
2. INSULATION				
3. CONTROL VALVES AND LOCAL CONTROL ELEMENTS				
4. FLUID PUMPS AND DRIVES				
5. SITE PREPARATION, FOUNDATIONS, AND PIPING SUPPORT ELEMENTS				
6. MISCELLANEOUS (EXPLAIN)				
7. FIELD INSTALLATION				
8. FIELD SUPERVISION				
9. SUBSYSTEM CHECKOUT/ADJUSTMENT				
ELECTRICAL				
1. WIRING (MATERIAL, SUPPORTS, TRENCHES, etc.)				
2. UTILITY INTERFACE SUBSTATION				
3. LOCAL CONTROL ELEMENTS				
4. MISCELLANEOUS (EXPLAIN)				
5. FIELD INSTALLATION				
6. FIELD SUPERVISION				
7. SUBSYSTEM CHECKOUT/ADJUSTMENT				
ENERGY STORAGE SUBSYSTEM	0.775			
1. TANKS, INSULATION, STORAGE MEDIUM				
2. HEAT EXCHANGERS/BOILERS				
3. HEAT TRANSFER FLUID				
4. PUMPS, VALVES, PIPING, etc.				
5. LOCAL CONTROL ELEMENTS				
6. SITE PREPARATION/FOUNDATION				
7. MISCELLANEOUS (EXPLAIN)				
8. FIELD INSTALLATION				
9. FIELD SUPERVISION				
10. SUBSYSTEM CHECKOUT/ADJUSTMENT				
CONTROL SUBSYSTEM	NA			
1. CONTROL SOFTWARE				
2. PROCESSORS/COMPUTERS				
3. SYSTEM CONTROL ELEMENTS FOR PLANT OPERATION				
4. SUBSYSTEM OPERATION CONTROL ELEMENTS				
5. CONTROL LINES TO SUBSYSTEMS AND PLANT CONTROL ELEMENTS				
6. BUILDINGS AND FACILITIES TO HOUSE EQUIPMENT				
7. MISCELLANEOUS (EXPLAIN)				
8. FIELD INSTALLATION				
9. FIELD SUPERVISION				
10. SUBSYSTEM CHECKOUT/ADJUSTMENT				
DETAIL DESIGN				
PLANT CONSTRUCTION MANAGEMENT				
SPECIAL FEATURES				
RELATED ITEMS				
OTHER (BUILDINGS AND OTHER UTILITIES TO SUPPORT SYSTEM FUNCTIONS, etc.)				
TESTING AND EVALUATION				
TOTAL ESTIMATED COST				

ORIGINAL PAGE IS
OF POOR QUALITY

TABLE 3.31 WEIGHT STATEMENT FOR THE 3½ YEAR PROGRAM: COLLECTOR SUBSYSTEM

COLLECTOR SUBSYSTEM: 11.2m CONCENTRATOR		WEIGHT lb. (kg)
1. Site Preparation/Foundation		NA
2. Structural Framework		4000 (1814)
Pedestal	1600 (726)	
Azimuth bearing support	800 (363)	
Rotating azimuth turret	900 (408)	
Power conversion support tripod	700 (317)	
3. Reflector Surface and Support		5800 (2631)
Reflective panels	2800 (1270)	
Reflector structure	3000 (1361)	
4. Drive Mechanism and Local Control		2100 (952)
Elevation actuator	300 (136)	
Elevation bearings	100 (45)	
Elevation drive motor	100 (45)	
Azimuth bearing with integral gear	700 (318)	
Azimuth speed reducer	800 (363)	
Azimuth drive motor	100 (45)	
5. Receiver and Support		787 (358)
Core and vapor pipe	177 (80)	
Sodium	44 (20)	
Plug valve	21 (10)	
Aperture door/equipment	85 (39)	
Receiver support	150 (68)	
Frame (carries power conversion subsystem & receiver)	196 (89)	
Insulation	114 (52)	
6. Pipes, Valves, Fittings, etc. (included above)		NA
7. Miscellaneous (Tracking control/electrical)		200 (91)
8. - 10. Not Applicable		
TOTAL COLLECTOR SUBSYSTEM WEIGHT		12887 (5846)

TABLE 3.32 WEIGHT STATEMENT FOR THE 3½ YEAR PROGRAM: POWER CONVERSION SUBSYSTEM

POWER CONVERSION SUBSYSTEM	WEIGHT lb.	WEIGHT (kg)
1. Heat Engine (USS-P40) (Including engine power control unit, starter motor, alternator, coolant pump, gel battery.)	496	(225)
2. Generator (AC) (Including shaft coupling, voltage regulator, contactor, circuit breaker, lightning protection.)	570	(259)
3. Heat Exchanger (attached to turret assembly) (Including fan ducting, mounting structure)	150	(68)
4. Control Valves and Local Control Elements (included with engine equipment)	NA	
5. Pumps and Fans (Coolant pump, fan, pulley, electric motor, fan belt assembly)	75	(34)
6. Heat Rejection Equipment (Rigid & flex coolant lines, coolant inventory)	175	(79)
7. Subsystem Buildings and Facilities	NA	
8. Switch Gear, Transformers, etc. (included with Generator)	NA	
9. Concept Peculiar	NA	
10. Miscellaneous (Helium K-bottle for power control)	135	(61)
11. - 13. Not applicable		
TOTAL POWER CONVERSION SUBSYSTEM WEIGHT	1601	(726)

TABLE 3.33 WEIGHT STATEMENT FOR THE 4½ AND 6½ YEAR PROGRAM: COLLECTOR SUBSYSTEMS

COLLECTOR SUBSYSTEM: 18.6m Concentrator			WEIGHT lb.	(kg)
1. Site Preparation/Foundation			NA	
2. Structural Framework			11200	(5081)
Pedestal	4900	(2223)		
Azimuth bearing support	1900	(862)		
Rotating azimuth turret	2700	(1225)		
Power conversion support tripod	1700	(771)		
3. Reflector Surface and Support			16100	(7303)
Reflective panels	7600	(3447)		
Reflector structure	8500	(3856)		
4. Drive Mechanism and Local Control			4200	(1905)
Elevation actuator	700	(317)		
Elevation bearings	200	(91)		
Elevation drive motor	150	(68)		
Azimuth bearing with integral gear	1400	(635)		
Azimuth speed reducer	1600	(726)		
Azimuth drive motor	150	(68)		
5. Receiver and Support			1258	(570)
Core and vapor pipe	245	(111)		
Sodium	73	(33)		
Plug valve	35	(16)		
Aperture door/equipment	142	(64)		
Receiver support	249	(113)		
Frame (carries power conversion subsystem & receiver)	324	(147)		
Insulation	190	(86)		
6. Pipes, Valves, Fittings, etc. (included above)			NA	
7. Miscellaneous (Tracking control/electrical)			200	(91)
8. - 10. Not Applicable				
TOTAL COLLECTOR SUBSYSTEM WEIGHT			32958	(14950)

TABLE 3.34 WEIGHT STATEMENT FOR THE 4½ AND 6½ YEAR PROGRAM: POWER CONVERSION SUBSYSTEM

POWER CONVERSION SUBSYSTEM	WEIGHT lb.	(kg)
1. Heat Engine (USS-P75) (Including engine power control unit, starter motor, alternator, coolant pump, gel battery.)	695	(315)
2. Generator (AC) (Including shaft coupling, voltage regulator, contactor, circuit breaker, lightning protection.)	1150	(522)
3. Heat Exchanger (attached to turret assembly) (Including fan ducting, mounting structure)	200	(91)
4. Control Valves and Local Control Elements (included with engine equipment)	NA	
5. Pumps and Fans (Coolant pump, fan, pulley, electric motor, fan belt assembly)	100	(45)
6. Heat Rejection Equipment (Rigid & flex coolant lines, coolant inventory)	250	(113)
7. Subsystem Buildings and Facilities	NA	
8. Switch Gear, Transformers, etc. (included with Generator)	NA	
9. Concept Peculiar	NA	
10. Miscellaneous (Helium K-bottle for power control)	135	(61)
11. - 13. Not Applicable		
TOTAL POWER CONVERSION SUBSYSTEM WEIGHT	2530	(1147)

SECTION 3

REFERENCES

3-1 Smith, G. A., "Monte Carlo Ray Trace Simulation for Solar Center Receiver Systems," Proceedings of the ERDA Solar Workshop on Methods for Optical Analysis of Central Receiver Systems, pp. 225-242, Houston, Texas, 10-11 August 1977.

3-2 Hankins, J. D., "Description of MIRVAL," Ibid, pp. 243-247.

3-3 Schrenk, G. L., "Fundamental Physics of Cone Optics and the Simulation of Solar-Thermal Systems," Ibid, pp. 19-37.

3-4 Schrenk, G. L., "Simulation of Real Solar Concentrators; Exerpts from a Proposal to National Science Foundation," U. of Pennsylvania (April 1975).

3-5 Clark, T. B., "Flux Distributions and Intercept Factors at the Focal Plane of Parabolic Reflectors," Aeronutronic SPS TR 010, (30 October 1978).

3-6 Umarov, G. Y., "Problems of Solar Energy Concentration," Geliotekhnika (Applied Solar Energy), V. 3, No. 5, (1967).

3-7 Clark, T.B., "Comparisons and Results of Optical Analysis Techniques," Aeronutronic SPS TR 013, (22 December 1978).

3-8 Sweningsen, W. B. and Ihokuchi, L. F., "Preliminary Hazard Evaluation," Aeronutronic SPS Technical Report 015, (17 January 1979)

3-9 Garrigus, W. E., "Solar/Stirling Engine Control Analysis," Aeronutronic SPS TR No. 012, (15 December 1978). (see Appendix E)

3-10 Knorpp, J, "Power Control Subsystem Operating Sequences," WDL SPS TR No. EC-02, February 1979.

3-11 Atomics International Sodium Technology Course, Session VIII, Sodium Safety by R. T. Johnson (1970).

3-12 Symposium on the Thermal and Hydraulic Aspects of Nuclear Reactor Safety; Vol. 2: Liquid Metal Fast Breeder Reactors, Winter Annual meeting of ASMSE, 1977. Published by ASME, (1977).

3-13 Uhlemann, H., Spigt, C. L. and Hermans, H. L., "The Combination of a Stirling Engine with a Remotely Placed Heat Source," 9th IECEC, Paper No. 749051, (1974).

3-14 Meijer, R. J. and Spight, C. L., "The Potential of the Philips Stirling Engine for Pollution Control and Energy Conservation," NATO 2nd Symposium on Low Pollution Power Systems Development, Dusseldorf, Germany, (4-8 November 1974)

REFERENCES (Continued)

3-15 Lia, T. A. and Lagerqvist, R.S.G., "Stirling Engine with Unconventional Heating System," 8th IECEC, Paper No. 739073.

3-16 Dunn, P.D. and Reay, D.A., Heat Pipes, Pergamon Press (1976).

3-17 Pons, R. L. "Preliminary Cylindrical Cavity Performance," Aeronutronic SPS Technical Report 003, August 25, 1978.

3-18 Gubareff, G.G., et.al., Thermal Radiation Properties Survey, Honeywell, (1960).

3-19 Pons, R. L., "Collector Performance Predictions for Various Time Periods," Aeronutronic SPS Technical Report 017, (January 31, 1979).

3-20 Noyes, R.C., "An Experimental Study of Sodium Pool Boiling Heat Transfer," Transactions of the ASME, Series C., Journal of Heat Transfer, V.85, PP. 125-129, (1963).

3-21 Chapman, D.R., "A Theoretical Analysis of Heat Transfer in Regions of Separated Flow," NACA TN3792 (October 1956).

3-22 Wu, Y.C. and Wen, L.C., "Solar Receiver Performance in the Temperature Range of 300°C to 1300°C, JPL Document No. 5102-82 (October 1978).

3-23 Tracked Hovercraft, Ltd., "A Cost Comparison of Three Tracked Air Cushion Vehicles," FRA-RT-71-68 (BP197501), (July 1970).

3-24 Asselman, G.A.A., "Thermal Energy Storage Unit Based on Lithium Flouride," Energy Conversion, Vol. 16, pp. 35-47, Pergamon Press, (1976).

3-25 Pons, R. L., "Stirling Engine Performance Model," Aeronutronic SPS Technical Report 001, Ford Aerospace & Communications Corporation, Aeronutronic Division, Newport Beach, CA. (1978).

3-26 Eichelberger, J.L., "Final Report - Investigation of Metal Fluoride Thermal Energy Storage Materials, Phase I - Study of Availability, Cost, and Components," U.S. ERDA Contract No. EY-76-C-02-2990*000, Pennwalt Corporation, King of Prussia, PA, (1976).

3-27 Boser, O., "Safety Considerations for High Temperature Thermal Energy Storage in Fluoride Salts," 12th IECEC Record, (1977).

3-28 Schroder, J., "Thermal Energy Storage and Control," ASME paper 74-WA/Oct-1, (1974).

3-29 Rohsenow, W. M., and Hartnett, J.P., Handbook of Heat Transfer, McGraw-Hill, (1973).

3-30 McKisson, R. L., "Corrosion and Mass Transfer," Sodium Technology, Atomics International, (1970).

3-31 Thorley, A. W., Tyzack, C., "Corrosion Behavior of Steels and Nicket Alloys in High-Temperature Sodium" Alkai-Metal Coolants, Proceedings of Symposium, Vienna, Austria, (1967).

3-32 Devan, J. H., "Corrosion of Iron- and Nickel-Base Alloys in High Temperature Sodium and NAK," Alkai-Metal Coolants, Proceedings of Symposium, Vienna, Austria, (1966).

3-33 Ratz, G. A., "Effect of Liquid Sodium on Welded AISI type 304 Stainless Steel Pipe," Nuclear Technology, V. 17, No. 2, (1973).

3-34 Spera, D. A., "Comparison of Experimental and Theoretical Thermal Fatigue Lines for Five Nickel-Base Alloys," Fatigue at Elevated Temperatures, ASTM STP 520, ATSM, 1972.

3-35 Hoft, Nicholas J., "Rules and Methods of Stress and Stability Calculations in the Presence of Creep," Sudaar No. 495 published by Stanford University, (May 1975).

3-36 ASME Pressure Vessel Code, Part UG, (1977).

3-37 Roark, R. J. and W. C. Young, Formulas for Stress and Strain, McGraw-Hill Book Company, (1975).

3-38 Bickell, M. B. and Ruiz, C., Pressure Vessel Design and Analysis, MacMillian, St., Martins Press, New York (1967).

3-39 Bushnell, David, "BOSOR4 - Program for Stress, Buckling, and Vibration of Complex Shells of Resolution," Structural Mechanics Lab., Lockheed Missiles & Space Co., Inc., Palo Alto, CA.

3-40 Duvall, G. D., "Operational Evaluation of a Closed Brayton Cycle Laboratory Engine," IECEC, (1976).

3-41 Yao, N. P. and Birk, J. R., "Battery Energy Storage for Utility Load Leveling and Electric Vehicles: A Review of Advanced Secondary Batteries," IECEC, (1975).

3-42 Anon, "Interim Cost Estimates for Advanced Battery Systems," Arthur D. Little, Inc., EM-742, July 1978.

3-43 Birk, J. R. and Yao, N. P., "Batteries for Utility Applications: Progress and Problems", Electrochemical Society Mtg., April 1977.

3-44 O'Donnell, Patricia, etal, "The Redox Flow System for Solar Photovoltaic Energy Storage", STAR Category 44.

3-45 Maskalick, N. J., et al, "The Case For Lead-Acid Storage Battery Peaking Systems", IECEC, 1975.

3-46 Anon., "Economic and Technical Feasibility Study for Energy Storage Flywheels", May 1978, HCP-M1066-01, (previously ERDA 76-65) Space Div., Rockwell International .

3-47 "In-Depth Study of Sodium in High Temperature Applications", Aeronutronic SPS TR No. 019, March 1979. (see Appendix N)

SECTION 4

TASK 2 STUDY RESULTS

SENSITIVITY ANALYSES

In this task, both system (rated) power level and anualized capacity factor were varied. The analysis was applied to both the P-40 and P-75 engine systems, as described in the following paragraphs. Note that the analyses, design and selection of the systems and their components were carried out under Task 1 and are reported in Section 3.

4.1 P-75 STIRLING ENGINE SYSTEM (4½, 6½ YEARS)

Cost/performance input parameters were generalized to account for varying plant size. For example, the annualized capacity factor (ACF) can be written as:

$$ACF^* = 0.3808 + \frac{14.312\ N_1}{\Sigma P_R}$$

where

ΣP_R = Plant size, kW

and

$E_b(MAX)$ = Maximum daily energy delivered to grid from storage, kWh/day

$= 1.585\ \Sigma P_R + (547.25)N_1$

Also, the concentrator unit cost varies to account for economies of scale in erecting and installing the collectors, as summarized below.

P-75 CONCENTRATOR COST

ΣP_R (kW)	C_{CONC} ($/m^2)
500	145
1000	133.8
10,000	124.6

*Presumes advanced battery storage with end-to-end efficiency = 0.775.

The results of the computations are shown in Table 4.1 and Figure 4-1. Note that there is only a small difference in BBEC for power levels above 1 MW_e. This difference is almost entirely due to the savings in concentrator cost since the larger plants are only multiples of the smaller one, i.e., a 10 MW_e plant is essentially 10 one MW_e plants. (As pointed out in Paragraph 3.1.5, the electrical distribution subsystem costs become excessive if a 10 MW_e plant is operated from a single control facility.) Below 1 MW_e, the rate of change of cost is greater, but at 500 kW_e the increase is only ~ 10% above the 1 MW_e value. We conclude, therefore, that a modular, Stirling-based power system is relatively insensitive to size effects. The effect of load factor is sizable, however. Once again, the zero storage case ($P_G \geq P_{G_r}$) is lowest in cost.

TABLE 4.1. SENSITIVITY ANALYSIS RESULTS - P-75

	$\overline{BBEC}$, mills/kWh		
ANNUALIZED CAPACITY FACTOR, ACF	ΣP_R = 500 kW_e	1000 kW_e	10,000 kW_e
ZERO STORAGE	N=9*	N=18	N=180
• 0.404 ($P_G \geq P_{G_r}$)	59.01	53.53	50.83
	N=9	N=18	N=180
• 0.340 ($P_G \leq P_{G_r}$)	70.12	63.61	60.40
ADV BATTERY STORAGE	N=10	N=19	N=190
• 0.4	93.46	77.58	74.67
	N=20	N=40	N=400
• 0.7	123.63	112.04	109.00

* N = Number of modules (collectors).

4.2 P-40 STIRLING ENGINE SYSTEM (3½ YEARS)

The calculations were repeated for the P-40 system and are summarized in Table 4.2 and shown graphically in Figure 4-2. As expected the costs are considerably higher than those for the P-75 system. Note that P-40 system performance could be improved substantially by running at higher RPM

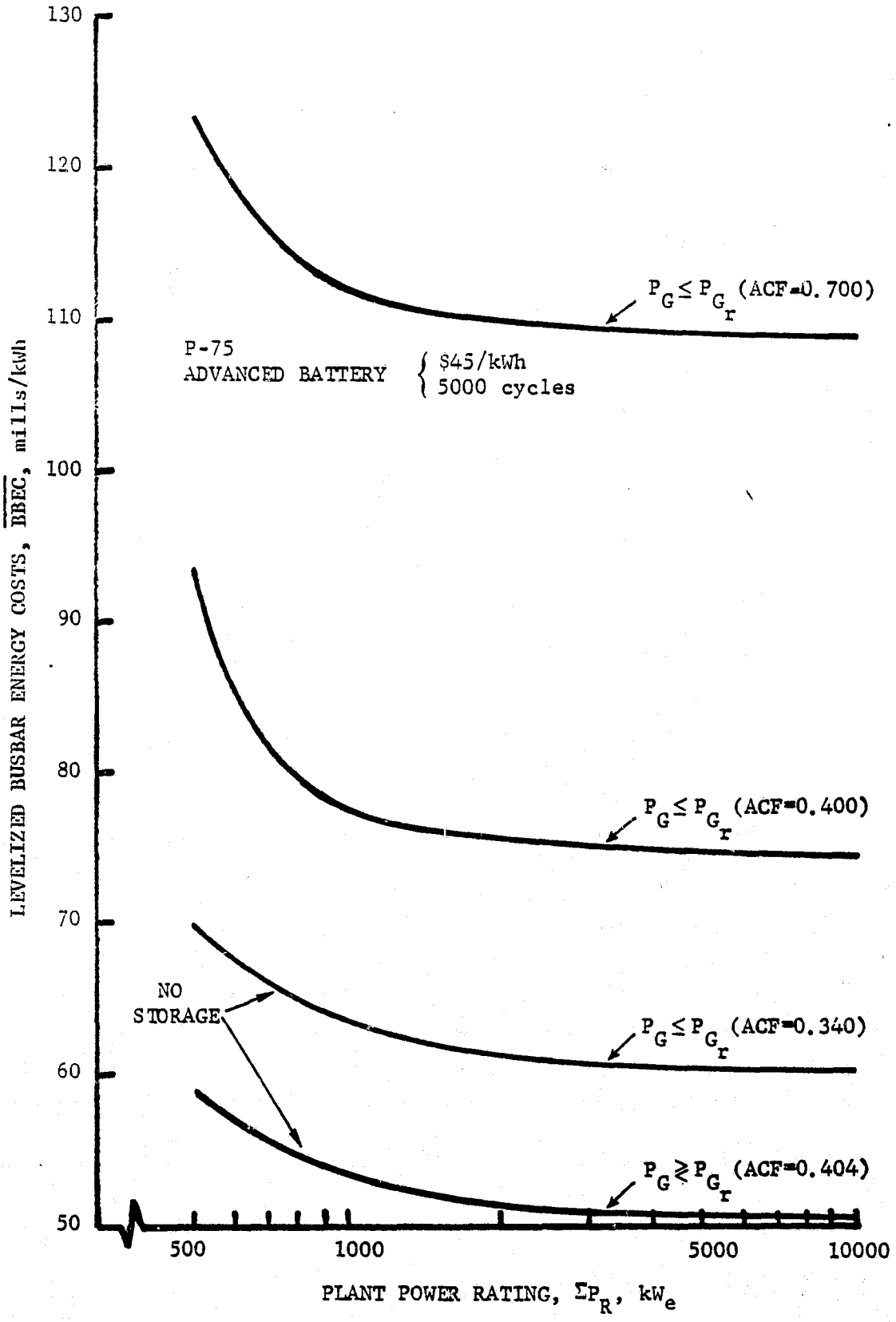

FIGURE 4-1. PLANT SIZE/ACF SENSITIVITY (P-75 SYSTEM)

(higher power and only slightly less efficiency) -- possibly 3600 RPM in order to avoid use of a gearbox -- but USS believes the life of the engine will be shortened. Further study is indicated on this point.

Except for the higher cost, the P-40 system is a mirror image of the P-75 system; it is relatively insensitive to size effects and demonstrates high overall system efficiency. Despite its higher cost, it is cheaper than any of the alternate engine systems of comparable size, i.e., Brayton and Organic Rankine systems. Furthermore, as is the case with the P-75 system, the primary size variant is the concentrator unit cost, since there are economics of scale associated with field erection/installation. Concentrator unit cost for the P-40 system is shown below.

P-40 CONCENTRATOR COST

ΣP_R (kW)	C_{CONC} ($/m^2)
500	115
1000	106
10,000	99

TABLE 4.2. SENSITIVITY ANALYSIS RESULTS - P-40

	$\overline{BBEC}$, mills/kWh		
ANNUALIZED CAPACITY FACTOR, ACF	ΣP_R = 500 kW	1000 kW	10,000 kW
ZERO STORAGE	N=27	N=55	N=550
• 0.399 ($P_G \gtrless P_{G_r}$)	79.85	75.94	73.5
	N=27	N=55	N=550
• 0.355 ($P_G \leq P_{G_r}$)	94.19	89.37	85.49
BATTERY STORAGE	N=29	N=60	N=600
• 0.4	113.38	101.28	95.22
	N=62	N=125	N=1250
• 0.7	152.86	142.42	139.75

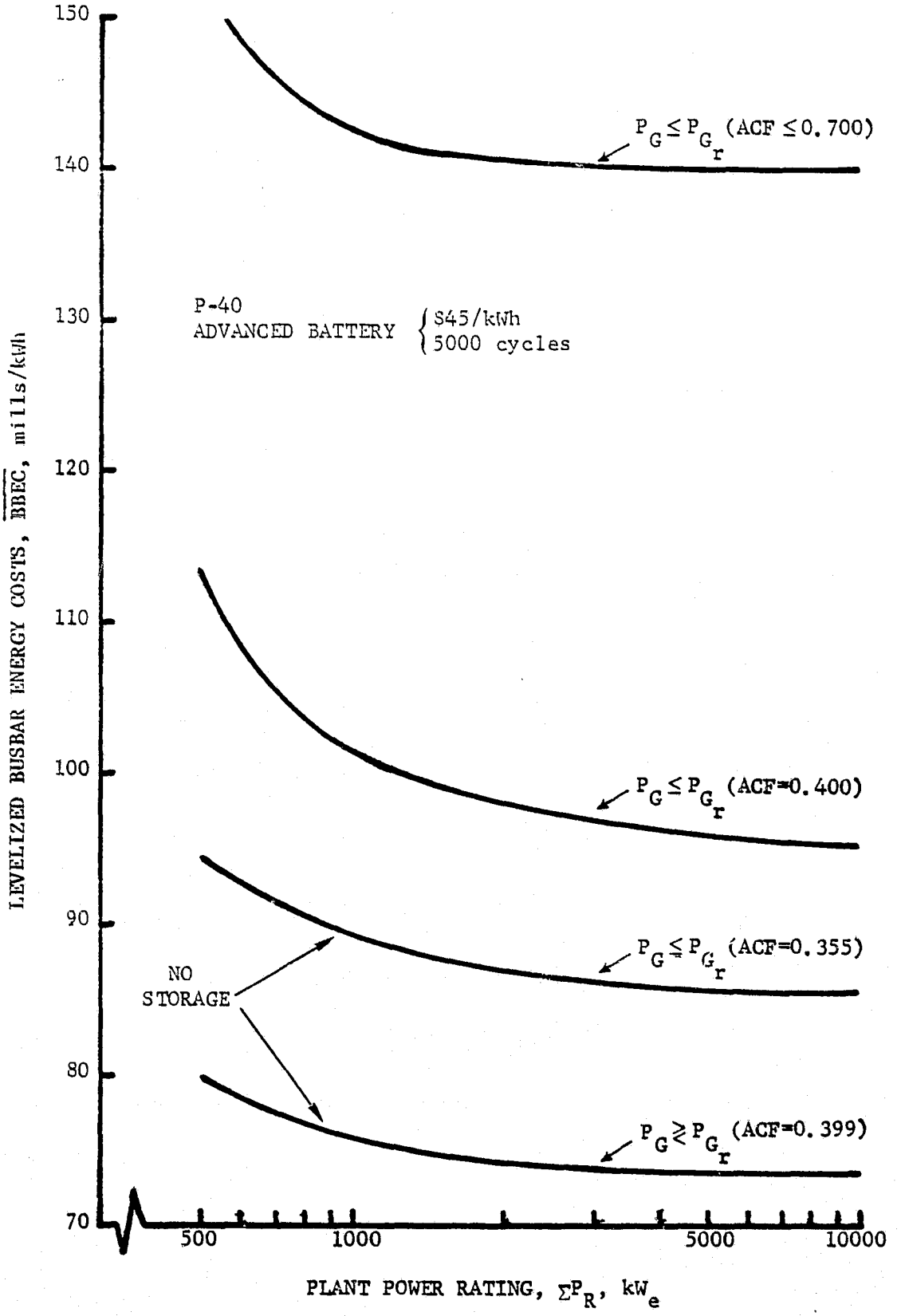

FIGURE 4-2. PLANT SIZE/ACF SENSITIVITY (P-40 SYSTEM)

SECTION 5

CONCLUSIONS

This section of the SPS final report summarizes the results of the Phase I study effort. It includes the Task I/II technical findings as well as Phase II/III cost estimates for each specified plant start-up time at the nominal rated power ($1MW_e$) and annualized capacity factor (ACF = 0.4); in addition, a minimum cost/risk program of 5½ year duration is presented. Finally, a recommendation is made for FACC's choice of the best system to meet the SPS Engineering Experiment No. 1 goals.

5.1 KEY TASK I/II STUDY RESULTS

The major study findings -- which bear on the final selection of an optimum SPS -- are summarized in the following paragraphs.

- Engine - The engine is the major factor in the selection of an optimum system. Its efficiency, together with the collection efficiency (which is effectively determined by the operating temperature of the engine) determines the amount of collector aperture area required; the collector is in turn the largest single cost item in the overall system. In addition, the engine dictates the type, size and cost of the receiver, so this combination of engine/receiver/collector dominates the cost picture. Note that the term "efficiency" refers to the engine part-load efficiency as well as the value at the rated power point since annualized system output is strongly influenced by engine part-load performance in view of the variable nature of solar energy.

  Study results clearly show that the Stirling-cycle machine is a better choice for SPS than any alternate engine available, including the Rankine* and open and closed (recuperated) Brayton cycle machines. Its higher efficiency and projected low production cost result in substantially lower BBEC and it has substantially lower development cost. Major criticism of the engine to date seems to relate to the oft-stated claim that it is not a "mature" power plant. We find it difficult to quantify such an observation for the SPS application, except perhaps to note that none of the candidates in the size range of interest are "mature" in the sense of being readily available hardware with proven performance**. The USS Stirling engines are furthest

*The steam Rankine was not studied, but FACC concurs with the Sundstrand Corp. conclusion that the organic Rankine is a better choice for the SPS application.

**The Brayton open-cycle, non-recuperated engine would fit the definition of ready-availability with proven performance (the 25 hp Solar Gemini engine, for example). The performance is so poor, however, that it was not considered for the SPS application.

along in the development effort. The organic Rankine engine shows some promise -- particularly with the benefit of lower temperature operation -- but it is much more complex than the Stirling and too costly (by about an order of magnitude). Calculated far term BBEC for the organic Rankine system is about 40 to 50% higher than that for the Stirling system; development hardware cost is at least 30% more (100% more if production Stirling engines are employed).

The Brayton cycle engines show poor performance in the SPS application; far term BBEC is nearly twice as much as that of the Stirling. Even allowing for a better receiver design than FACC was able to accomplish within program cost/schedule constraints, both Brayton engines would still finish last in terms of commercialization potential. The situation is exacerbated by very high hardware development costs, that is, a factor of two greater than for the Stirling*.

FACC finds no basis for not selecting the Stirling engine and a host of reasons for selecting it; it is our clear choice for the SPS application.

- Concentrator - Microwave antenna technology is the most effective base for selecting the concentrator. The components constitute available hardware of proven performance. The required conversion to solar use and cost reduction of approximately 10 to 1, however, cannot be achieved except through mass-production techniques. Design changes have been introduced, therefore, for the sole purpose of facilitating mass-production (as well as field assembly and installation) of up to 400,000 units per year. The selected Az-El fixed-leg paraboloidal concentrator with front-braced structure appears capable of meeting the system commercialization goals as well as the near term requirement for low-risk, proven hardware.

- Receiver - The receiver is the component with highest technical risk. However, the selected concept, which employs a sodium pool boiler to transfer heat from the cavity receiver to the engine, has been successfully demonstrated in principle by long-duration, laboratory testing at both N.V. Philips in Holland and United Stirling in Sweden. One of the many advantages of this indirect heating approach is that it provides an inherent buffer capability, that is, for smoothing out short-period variations in solar intensity. Thorough transient analyses of the coupled receiver/thermal transport system show complete stability for all postulated scenarios (transient cloud cover, start-up, shut-down, emergency de-focus, long-term freeze-up, etc.). The unit is quite small, simple to fabricate and uses readily available materials (type 316 stainless steel).

---

*Figures are for the closed cycle engine; the open-cycle engine development cost should be somewhat less but its BBEC is lowest for the group.

- Electrical - The selected AC system is the lowest weight, highest efficiency and lowest cost approach and the requirement for multi-engine synchronization to the utility grid poses no problems. All electrical components comprising the power conversion, energy transport and control subsystems are state-of-art fully developed and proven hardware.

- Storage - The SPS study results show several viable approaches to the storage problem. However, internal storage, that is, where the storage medium is placed between the collector and the power conversion subsystem, doesn't appear feasible. For a typical internal storage concept, for example, thermal storage using phase-change eutectic salts, the required weight for (diurnal) storage puts an excessive load on the concentrator. The thermal store must be placed on the ground and thermal transport accomplished either by 1) piping back and forth between the receiver and the ground or 2) optically transporting the energy to a ground-based receiver. The first approach is infeasible at the high temperatures (~800°C) employed in the Stirling system. The second approach results in multiple reflection optics and attendant high energy losses. We are effectively restricted, therefore, to an external storage concept, for example batteries, flywheels, pumped hydro, compressed air, hydrogen production, etc. Pumped hydro and compressed air concepts have been ruled out primarily due to limitations of available topography. The remaining ones, with the exception of the lead-acid battery, have not yet achieved either the requisite cost or the performance consistent with the schedule requirements of EE No. 1.

  The hybrid concept was briefly investigated, with two different implementations: 1) the simple hybrid, wherein extra Stirling engines are supplied for nighttime use and 2) the integral hybrid, where the solar receivers are provided with combustion equipment and the same engines are used to generate either nighttime energy or energy during periods of inclement weather, cloud passage, etc. In both cases, the results are quite attractive provided fuel cost doesn't exceed about $4 per million BTU. At the present time, the hybrid approach is also the only viable approach for the stand-alone requirement.

  Lowest system $\overline{\text{BBEC}}$ is obtained without storage of any kind, particularly if the grid will accept all power generated. ACF's slightly above 0.4 can be achieved in this manner.

- Size - Lowest-cost systems occur for Stirling engines at rated power levels of 50 to 70 kW with associated concentrator diameters on the order of 18 to 19 m. Although the lowest cost concentrator is about 11m in diameter, the increased engine/receiver/electrical equipment cost (and maintenance cost) is dominant for the large numbers of collectors needed at low power level, that is, at 10 to 30 kW.

  The performance of a Stirling-SPS is virtually insensitive to overall plant size. For plant power in excess of 1MWe, the plant is in

reality a multiple of the $1MW_e$ plant with slight cost reduction due to the economy of scale associated with erecting a larger number of dishes at a single site.

- Site Flexibility - The Stirling SPS concept can be operated effectively on virtually any type of terrain. It exhibits high packing fraction (ratio of collector area to land area) with very low energy loss.

- Reliability - The predicted reliability (and availability) of the proposed concept is substantially higher than that of conventional power plants in this size range. Scheduled maintenance can be carried out at night so that planned downtime does not affect annual output. With regard to unplanned outages, the modular nature of the system assures some plant output -- albeit below rated power -- virtually all the time ("effective" availability of ~99%). Note that this is achieved by making certain that the few "bottleneck" components are either high-reliability parts or made redundant by judicious use of spares.

5.2 PHASE II/III COST ESTIMATES

The following paragraphs present the program schedules and related program costs for the three start-up times specified in the Statement of Work; that is, 3½, 4½ and 6½ years. The major tasks to be accomplished in Phase II are:

- Preliminary and Detail Design
- Subsystem Development
- Fabrication of Subsystem and System Level Verification Test Hardware
- Subsystem and System Level Verification Testing

The Phase III effort includes:

- Fabrication of $1MW_e$, ACF = 0.4 Baseline System
- Installation and Check-out of Baseline System at DOE selected site
- Operation of Baseline System prior to Test and Evaluation Phase

The Test and Evaluation period extends one year subsequent to the completion of system installation and check-out.

5.2.1 SCHEDULE

Schedules for each of the three proposed start-up times, that is, 3½, 4½ and 6½ years are shown in Figures 5-1 through 5-3. The schedules were developed considering hardware availability with technical risk, cost and commercialization potential as additional elements in the planning process. In each

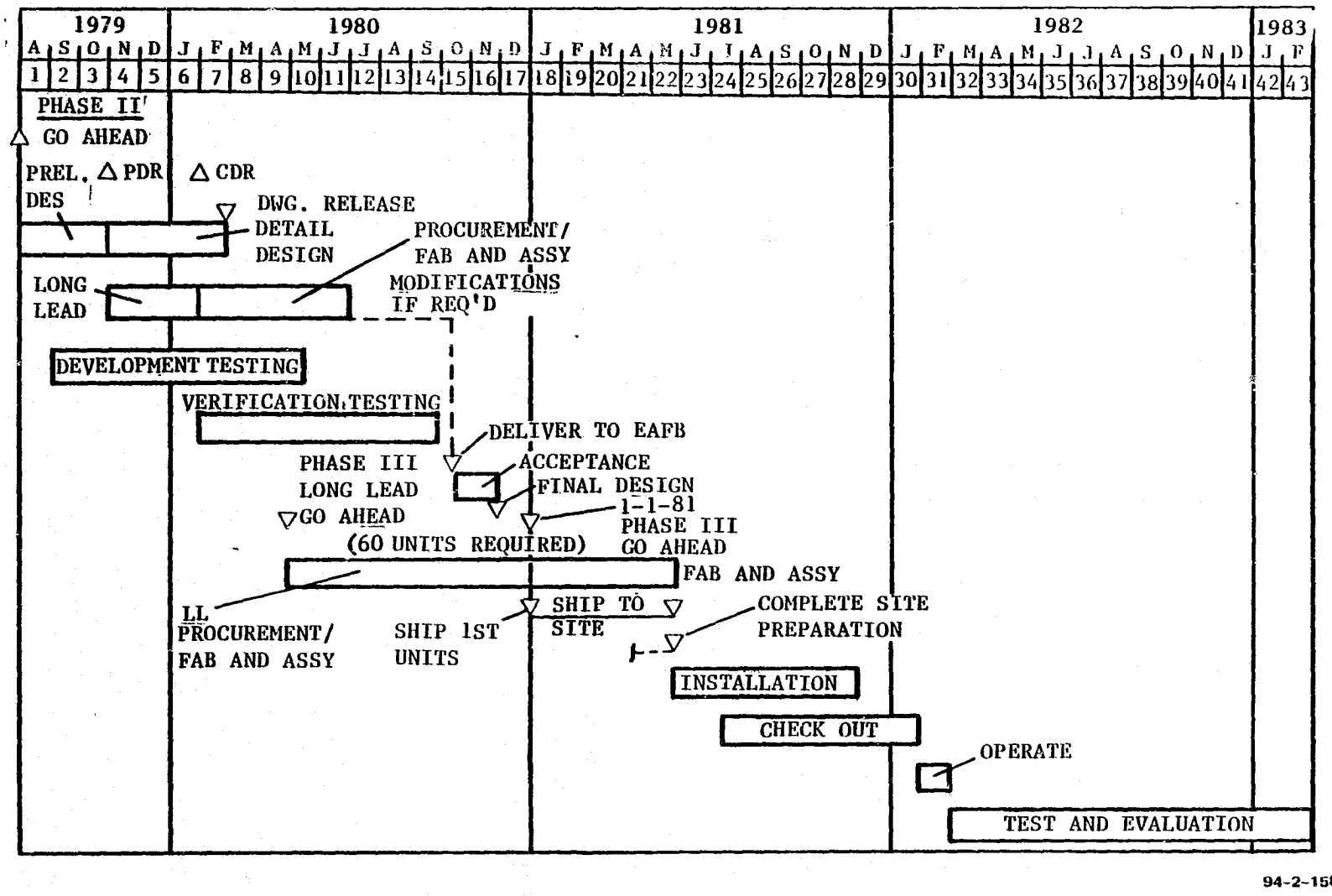

94-2-158

FIGURE 5-1. SMALL POWER SYSTEM (SPS) SCHEDULE 3.5 YEAR PLAN

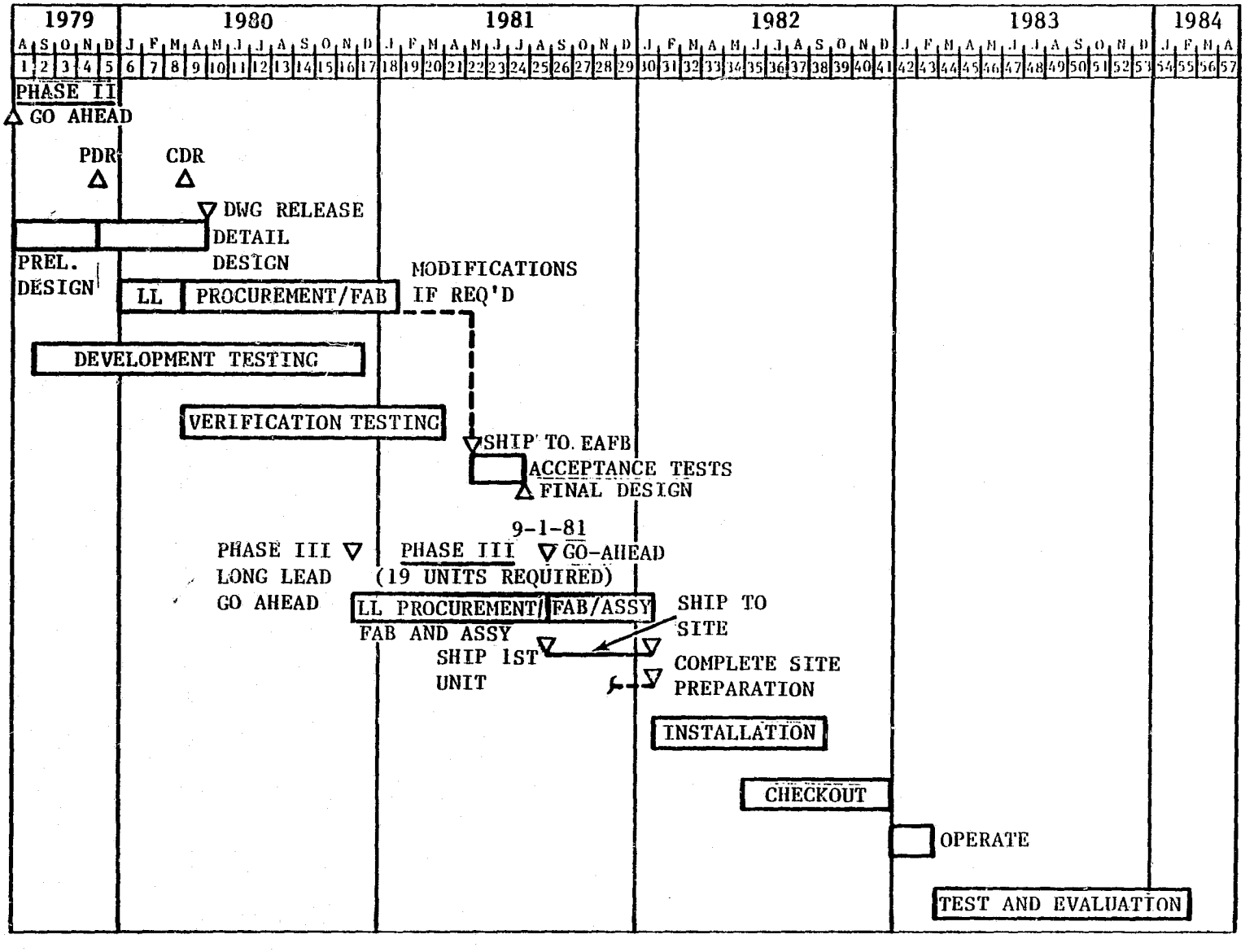

FIGURE 5-2. SPS SCHEDULE FOR A 4.5 YEAR PLAN

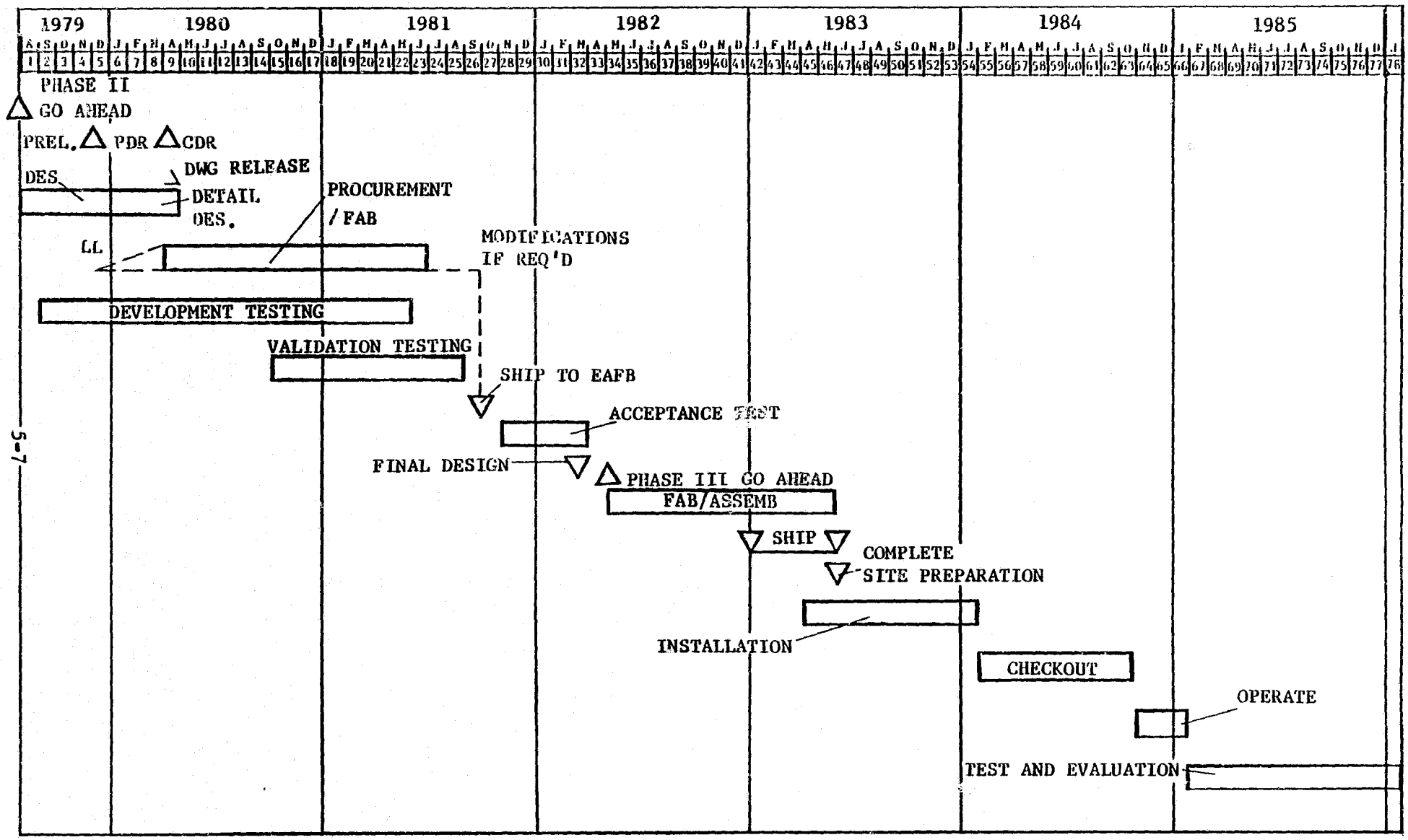

FIGURE 5-3. SPS SCHEDULE FOR A 6.5 YEAR PLAN

program the total length was fixed; the relative time spans between Phases II and III were adjusted to achieve the most favorable overall schedule.

5.2.1.1 Program A (3½ years). A 3½ year effort for the SPS program is considered to be the least desirable by FACC from the standpoint of costs, schedule risk and operational traceability. This schedule shows a short Phase II development and test sequence. At the end of month nine of Phase II, the long-lead procurement effort for Phase III must be started. This early procurement is intended to reduce the schedule risk for Phase III by initiating fabrication of the Stirling engines, collectors and receivers. Due to delivery schedule, the United Stirling P-40 engine is the only viable engine for the 3½ year program. This engine would be used with a 11.2m (diameter) collector, and would suffice to verify feasibility during Phase II of the program. Phase III of the program also utilizes the P-40 engine and would require a 60 collector system to meet the $1MW_e$ requirement with storage. This number of subsystems introduces potential schedule risk due to the extensive collector fabrication which is not relieved in Phase II with the early release of Phase III long-lead items. Furthermore, use of the P-40 engine for Phase III does not provide traceability to the recommended commercial system configuration. The P-40 engine with a 11.2m collector is not considered by FACC as a good prototype for the recommended commercial applications since the P-75 engine with the 18.6m collector which we recommend as a optimum choice for commercialization would not therefore be demonstrated. Another major consideration is the cost of the 3½ year program. The large number of collector systems (60) requires an expenditure of about 3 million dollars more than any other program that FACC has devised. For these reasons, schedule risk, lack of operational traceability and high cost, FACC does not recommend the 3½ year program.

5.2.1.2 Program B (4½ years). A 4½ year program can be accomplished using the P-75 Stirling engine in combination with a 18.6m collector. This program has the advantage of using the P-75 engine, but the Phase II engines would be prototypes and the early limited production engines for Phase III would be acquired at a higher cost than during full production. There is some schedule risk in that the Phase III long lead procurement cycle must be started about nine months prior to Phase III go-ahead (month 16 of Phase II). Overall technical risk for this program is considered low as Phase II is used to demonstrate the operational configuration. Cost for the program would be less than the 3½ year program.

5.2.1.3 Program C (6½ years). A 6½ year program time span virtually eliminates all schedule risk and has the advantage of using full production P-75 Stirling engines which lowers the program costs and is optimum from the standpoint of operational traceability. However, the overall length of the program appears needlessly long. FACC has examined a shorter program (5½ years) which appears to offer advantages over both the 4½ and the 6½ year programs.

5.2.1.4 Preferred Program. FACC recommends a minimum risk program which takes advantage of the production P-75 Stirling engine. The program is 5½ years in duration; the schedule is shown in Figure 5-4. Phase III procurement begins at Phase III go-ahead, eliminating the need for long-lead

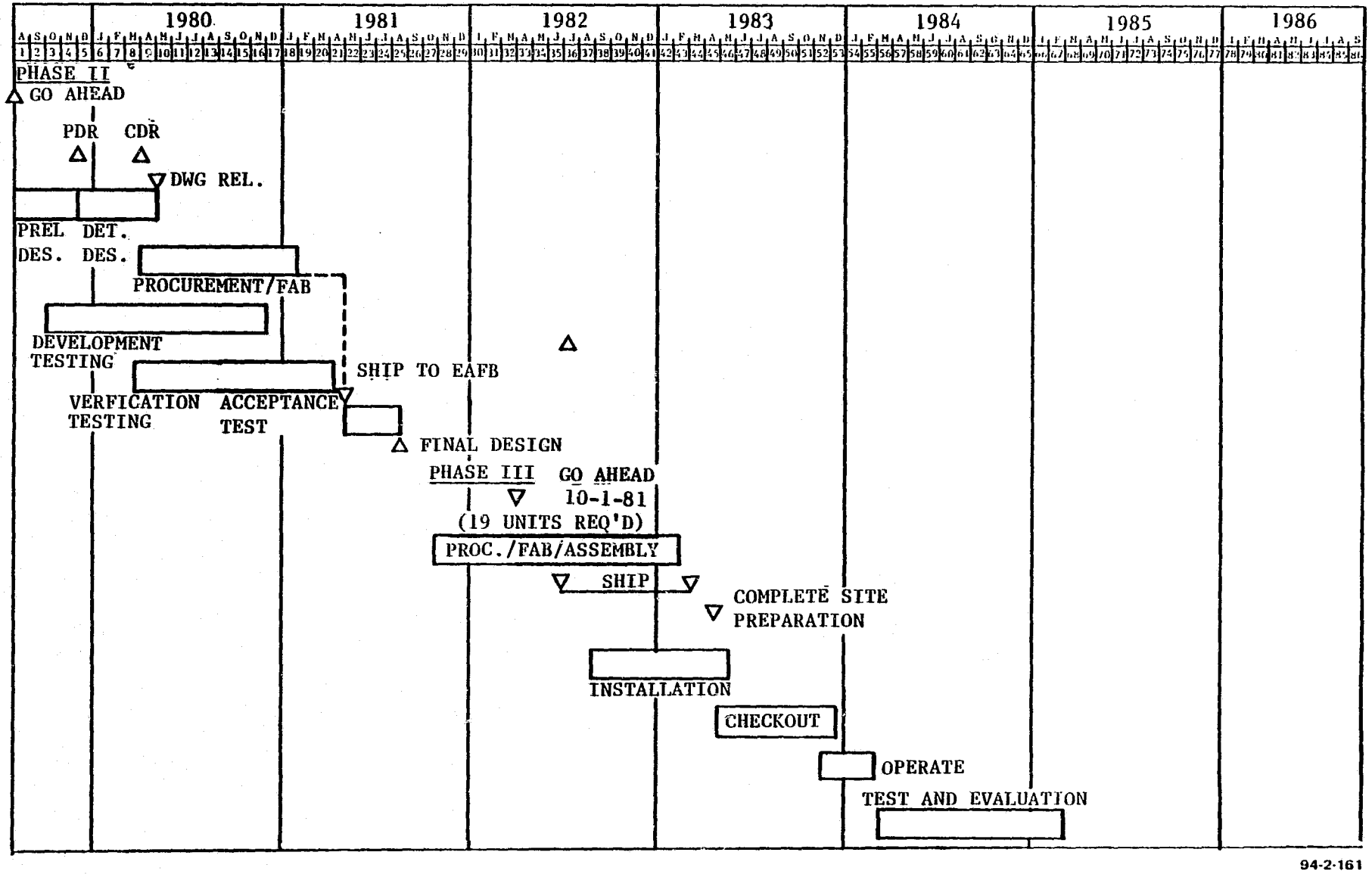

FIGURE 5-4. SPS SCHEDULE FOR A 5.5 YEAR PLAN

procurement and reducing that schedule risk factor. Program risk and costs are minimized by using only full production P-75 Stirling engines. Cost savings for this program are approximately 1.6 million dollars compared to both the 4½ year and the 6½ year plan, making this the lowest cost of all the programs considered.

5.2.2 COSTS

Budgetary and Planning Costs have been prepared for Phases II and III for the baseline Stirling system and for each of the three program start-up times as well as the preferred 5½ year program. The costs for the preferred 5½ year program are:

Phase II	$ 8,983,000
Phase III	11,715,000
TOTAL	$ 20,698,000

Time-phased costs for each program are summarized in Table 5.1. Note that these costs are provided for planning purposes and do not represent a commitment by FACC. (It is expected that firm costs will be supplied in response to the JPL Request for Proposal.) Hardware elements of each of the programs which is the basis for the B and P costs are summarized in Table 5.2.

These B and P costs are based upon the following assumptions:

- Firm cost quotation was received from USS; however, a fixed exchange rate was quoted.
- The JPL Solar Test Site at JPL Edwards Test Station will be used for Phase II.
- An existing building at the JPL Solar Test Site will be used for the control building.
- Facilities at the JPL Solar Test Site will be provided at no cost.
- The Barstow site will be used for Phase III.
- The Phase III site will be provided at no cost.
- Cost for receiver testing at the Advanced Components Test Facility at the Georgia Institute of Technology are included although effort will probably be GFE.

TABLE 5.1. SUMMARY OF PROGRAM COSTS
(THOUSANDS OF DOLLARS)

3 1/2 YEAR PROGRAM

Fiscal Year		1979	1980	1981	1982	1983	1984	1985	1986	1987	Total
Costs	Phase II	1543	5475								7018
	Phase III		6363	5340	5435	901					18039
	Total	1543	11838	5340	5435	901					25057

4 1/2 YEAR PROGRAM

Fiscal Year		1979	1980	1981	1982	1983	1984	1985	1986	1987	Total
Costs	Phase II	2222	3838	1965							8025
	Phase III			5479	6025	2388	397				14289
	Total	2222	3838	7444	6025	2388	397				22314

5 1/2 YEAR PROGRAM

Fiscal Year		1979	1980	1981	1982	1983	1984	1985	1986	1987	Total
Costs	Phase II	848	4957	2585	593						8983
	Phase III				5454	4277	1913	691			11715
	Total	848	4957	2585	6047	4277	1913	691			20698

6 1/2 YEAR PROGRAM

Fiscal Year		1979	1980	1981	1982	1983	1984	1985	1986	1987	Total
Costs	Phase II	887	5197	2686	613						9383
	Phase III				4257	3737	3026	1121	679		12820
	Total	887	5197	2686	4870	3737	3026	1121	679		22203

TABLE 5.2. HARDWARE BASELINE

A - 3 1/2 Year Program

Phase III

- One 11.2 meter concentrator
- Two Power modules including P-40 Stirling engines
- One Reduced size energy distribution S/S
- One Reduced capability storage S/S
- One Control S/S

Phase III

- 60 11.2 meter concentrators
- 60 Power modules including P-40 Stirling engines
- One Energy distribution S/S
- One Storage S/S
- One Control S/S
- One Control Building
- Foundation/Site Preparation

B - 4 1/2 Year Program

Phase II

- One 18.6 meter concentrator
- Two Power modules including pre-production P-75 Stirling engines
- One Reduced size energy distribution S/S
- One Reduced capability storage S/S
- One Control S/S

C - 4

TABLE 5.2. HARDWARE BASELINE (CONT'D)

Phase III

- 19 18.6 meter concentrators
- 19 Power modules including early production P-75 Stirling engines
- One Energy distribution S/S
- One Storage S/S
- One Control S/S
- One Control Building
- Foundation/Site Preparation

C - 5 1/2 and 6 1/2 Year Programs

Phase II

- One 18.6 meter concentrator
- Two Power modules including early production P-75 Stirling engines
- One Reduced size energy distribution S/S
- One Reduced capability storage S/S
- One control S/S

Phase III

- 19 18.6 meter concentrators
- 19 Power modules including full production P-75 Stirling engines
- One Energy distribution S/S
- One Storage S/S
- One Control S/S
- One Control Building
- Foundations/Site Preparation

5.2.3 CONCLUSIONS

The 3½ year program is costly because of the increased quantity of hardware required (60 Stirling engines vs. 19) and is a high risk program due to the necessity of committing Phase III dollars early in Phase II.

The 4½ year program uses P-75 Stirling engines purchased from early production and at a cost of approximately three times that of the 6½ and 5½ year programs. The 4½ year program has an accompanied schedule risk associated with early production release of long-lead items.

The 6½ year program does not contain the objectionable schedule factors associated with the 3½ and 4½ year program. It does, however, have the objectionable characteristic of high costs associated with an unnecessarily long program.

The FACC recommended 5½ year program seems about optimum from a cost standpoint since it takes advantage of the lower engine costs while reducing program support costs. The schedule advantages of the 5½ year program have previously been discussed. Further cost savings are possible, as discussed in paragraph 5.3 below.

Summary Phase III system cost information is given in Tables 5.3, 5.4 and 5.5 (JPL Table E-2).

5.3 RECOMMENDED OPTIMUM SYSTEM

FACC recommends a 5½ year development program for the solar SPS, Engineering Experiment No. 1 employing USS-P-75 Stirling engines. Eighteen (18) parabolic concentrators at 18.6m diameters would be used to develop rated power of $1MW_e$. No storage (other than the buffer storage inherent in the design of the redeiver) would be provided but all energy developed by the system would be delivered to the utility grid regardless of power level. Annualized capacity factor under these conditions is 0.404 including an allowance for an effective system availability of 0.99.

Development costs for this system are reduced by $1,423,000 from the 5½ year system with storage; costs by phase are:

Phase II	$ 8,893,000
Phase III	10,382,000
TOTAL	$ 19,275,000

With mass production and installation techniques, levelized busbar energy cost (BBEC) for the ca. 1990 time period is 53.53 mills/kWh (including maintenance at 7.06 mills/kWh) and capital investment at the time of construction is $975.60/$kW_e$ rated power; the present value of all capital expenditures over the 30-year life of the plant is $1,883,000.

TABLE 5.3. 3 1/2 YEAR PROGRAM

1978 $K

ITEM	EFFICIENCY %	WEIGHTS lb (kg)	ESTIMATE 1978 $K COMPONENTS	ESTIMATE 1978 $K SUBTOTALS
COLLECTOR SUBSYSTEM				5080
1. SITE PREPARATION/FOUNDATION			200	
2. STRUCTURAL FRAMEWORK			975	
3. REFLECTOR SURFACE AND SUPPORT			1500	
4. DRIVE MECHANISM AND LOCAL CONTROL			650	
5. RECEIVER AND SUPPORT			50	
6. PIPES, VALVES, FITTINGS, etc.				
7. MISCELLANEOUS (EXPLAIN) Track Control			425	
8. FIELD INSTALLATION			1280	
9. FIELD SUPERVISION Include in 8				
10. SUBSYSTEM CHECKOUT/ADJUSTMENT Include in 8				
POWER CONVERSION SUBSYSTEM				8565
1. HEAT ENGINE			5800	
2. GENERATOR			350	
3. HEAT EXCHANGER/BOILERS/CONDENSERS			30	
4. CONTROL VALVES AND LOCAL CONTROL ELEMENTS Include in 3				
5. PUMPS AND FANS " "				
6. HEAT REJECTION EQUIPMENT " "				
7. SUBSYSTEM BUILDINGS AND FACILITIES				
8. SWITCH GEAR, TRANSFORMERS, etc.			15	
9. CONCEPT PECULIAR (EXPLAIN)				
10. MISCELLANEOUS (EXPLAIN)				
11. FIELD INSTALLATION			2365	
12. FIELD SUPERVISION Included in 11 "				
13. SUBSYSTEM CHECKOUT/ADJUSTMENT				
ENERGY TRANSPORT SUBSYSTEM				170
THERMAL				
1. PIPING				
2. INSULATION				
3. CONTROL VALVES AND LOCAL CONTROL ELEMENTS				
4. FLUID PUMPS AND DRIVES				
5. SITE PREPARATION, FOUNDATIONS, AND PIPING SUPPORT ELEMENTS				
6. MISCELLANEOUS (EXPLAIN)				
7. FIELD INSTALLATION				
8. FIELD SUPERVISION				
9. SUBSYSTEM CHECKOUT/ADJUSTMENT				
ELECTRICAL				
1. WIRING (MATERIAL, SUPPORTS, TRENCHES, etc.)			20	
2. UTILITY INTERFACE SUBSTATION			25	
3. LOCAL CONTROL ELEMENTS			70	
4. MISCELLANEOUS (EXPLAIN)				
5. FIELD INSTALLATION			55	
6. FIELD SUPERVISION Included in 5				
7. SUBSYSTEM CHECKOUT/ADJUSTMENT " "				
ENERGY STORAGE SUBSYSTEM				885
1. TANKS, INSULATION, STORAGE MEDIUM Batteries			585	
2. HEAT EXCHANGERS/BOILERS				
3. HEAT TRANSFER FLUID				
4. PUMPS, VALVES, PIPING, etc.				
5. LOCAL CONTROL ELEMENTS Inverter-Converter Etc			200	
6. SITE PREPARATION/FOUNDATION				
7. MISCELLANEOUS (EXPLAIN)				
8. FIELD INSTALLATION			100	
9. FIELD SUPERVISION Included in 9				
10. SUBSYSTEM CHECKOUT/ADJUSTMENT " "				
CONTROL SUBSYSTEM				400
1. CONTROL SOFTWARE			50	
2. PROCESSORS/COMPUTERS			300	
3. SYSTEM CONTROL ELEMENTS FOR PLANT OPERATION				
4. SUBSYSTEM OPERATION CONTROL ELEMENTS				
5. CONTROL LINES TO SUBSYSTEMS AND PLANT CONTROL ELEMENTS				
6. BUILDINGS AND FACILITIES TO HOUSE EQUIPMENT				
7. MISCELLANEOUS (EXPLAIN)				
8. FIELD INSTALLATION			50	
9. FIELD SUPERVISION Included in 8 "				
10. SUBSYSTEM CHECKOUT/ADJUSTMENT				
DETAIL DESIGN				
PLANT CONSTRUCTION MANAGEMENT				
SPECIAL FEATURES				
RELATED ITEMS				
OTHER (BUILDINGS AND OTHER UTILITIES TO SUPPORT SYSTEM FUNCTIONS, etc.)				300
TESTING AND EVALUATION				500
TOTAL ESTIMATED COST				15880

ORIGINAL PAGE IS
OF POOR QUALITY

TABLE 5.4. 4 1/2 YEAR PROGRAM

1978 $ K

ITEM	EFFICIENCY %	WEIGHTS lb (kg)	ESTIMATE 1978 $K COMPONENTS	ESTIMATE 1978 $K SUBTOTALS
COLLECTOR SUBSYSTEM				4800
1. SITE PREPARATION/FOUNDATION			170	
2. STRUCTURAL FRAMEWORK			1020	
3. REFLECTOR SURFACE AND SUPPORT			1400	
4. DRIVE MECHANISM AND LOCAL CONTROL			650	
5. RECEIVER AND SUPPORT			60	
6. PIPES, VALVES, FITTINGS, etc.				
7. MISCELLANEOUS (EXPLAIN) Track Control			300	
8. FIELD INSTALLATION			1200	
9. FIELD SUPERVISION Included in 8				
10. SUBSYSTEM CHECKOUT/ADJUSTMENT				
POWER CONVERSION SUBSYSTEM				5640
1. HEAT ENGINE			3870	
2. GENERATOR			250	
3. HEAT EXCHANGER/BOILERS/CONDENSERS			20	
4. CONTROL VALVES AND LOCAL CONTROL ELEMENTS				
5. PUMPS AND FANS				
6. HEAT REJECTION EQUIPMENT				
7. SUBSYSTEM BUILDINGS AND FACILITIES				
8. SWITCH GEAR, TRANSFORMERS, etc.			10	
9. CONCEPT PECULIAR (EXPLAIN)				
10. MISCELLANEOUS (EXPLAIN)				
11. FIELD INSTALLATION			1530	
12. FIELD SUPERVISION Included in 11				
13. SUBSYSTEM CHECKOUT/ADJUSTMENT				
ENERGY TRANSPORT SUBSYSTEM				145
THERMAL				
1. PIPING				
2. INSULATION				
3. CONTROL VALVES AND LOCAL CONTROL ELEMENTS				
4. FLUID PUMPS AND DRIVES				
5. SITE PREPARATION, FOUNDATIONS, AND PIPING SUPPORT ELEMENTS				
6. MISCELLANEOUS (EXPLAIN)				
7. FIELD INSTALLATION				
8. FIELD SUPERVISION				
9. SUBSYSTEM CHECKOUT/ADJUSTMENT				
ELECTRICAL				
1. WIRING (MATERIAL, SUPPORTS, TRENCHES, etc.)			15	
2. UTILITY INTERFACE SUBSTATION			20	
3. LOCAL CONTROL ELEMENTS			60	
4. MISCELLANEOUS (EXPLAIN)				
5. FIELD INSTALLATION			50	
6. FIELD SUPERVISION Included in 5				
7. SUBSYSTEM CHECKOUT/ADJUSTMENT				
ENERGY STORAGE SUBSYSTEM				885
1. TANKS, INSULATION, STORAGE MEDIUM Batteries			585	
2. HEAT EXCHANGERS/BOILERS				
3. HEAT TRANSFER FLUID				
4. PUMPS, VALVES, PIPING, etc.				
5. LOCAL CONTROL ELEMENTS			200	
6. SITE PREPARATION/FOUNDATION				
7. MISCELLANEOUS (EXPLAIN)				
8. FIELD INSTALLATION			100	
9. FIELD SUPERVISION Included in 8				
10. SUBSYSTEM CHECKOUT/ADJUSTMENT				
CONTROL SUBSYSTEM				300
1. CONTROL SOFTWARE			50	
2. PROCESSORS/COMPUTERS			200	
3. SYSTEM CONTROL ELEMENTS FOR PLANT OPERATION				
4. SUBSYSTEM OPERATION CONTROL ELEMENTS				
5. CONTROL LINES TO SUBSYSTEMS AND PLANT CONTROL ELEMENTS				
6. BUILDINGS AND FACILITIES TO HOUSE EQUIPMENT				
7. MISCELLANEOUS (EXPLAIN)				
8. FIELD INSTALLATION			50	
9. FIELD SUPERVISION Included in 8				
10. SUBSYSTEM CHECKOUT/ADJUSTMENT				
DETAIL DESIGN				
PLANT CONSTRUCTION MANAGEMENT				
SPECIAL FEATURES				
RELATED ITEMS				
OTHER (BUILDINGS AND OTHER UTILITIES TO SUPPORT SYSTEM FUNCTIONS, etc.)				300
TESTING AND EVALUATION				500
TOTAL ESTIMATED COST				12570

TABLE 5.5. 6 1/2 YEAR PROGRAM

1978 $ K

ITEM	EFFICIENCY %	WEIGHTS lb (kg)	ESTIMATE 1978 $K COMPONENTS	ESTIMATE 1978 $K SUBTOTALS
COLLECTOR SUBSYSTEM				4800
1. SITE PREPARATION/FOUNDATION			170	
2. STRUCTURAL FRAMEWORK			1020	
3. REFLECTOR SURFACE AND SUPPORT			1400	
4. DRIVE MECHANISM AND LOCAL CONTROL			650	
5. RECEIVER AND SUPPORT			60	
6. PIPES, VALVES, FITTINGS, etc.				
7. MISCELLANEOUS (EXPLAIN) Track Control			300	
8. FIELD INSTALLATION			1200	
9. FIELD SUPERVISION Included in 8				
10. SUBSYSTEM CHECKOUT/ADJUSTMENT " "				
POWER CONVERSION SUBSYSTEM				4350
1. HEAT ENGINE			2600	
2. GENERATOR			250	
3. HEAT EXCHANGER/BOILERS/CONDENSERS			20	
4. CONTROL VALVES AND LOCAL CONTROL ELEMENTS				
5. PUMPS AND FANS				
6. HEAT REJECTION EQUIPMENT				
7. SUBSYSTEM BUILDINGS AND FACILITIES				
8. SWITCH GEAR, TRANSFORMERS, etc.			10	
9. CONCEPT PECULIAR (EXPLAIN)				
10. MISCELLANEOUS (EXPLAIN)				
11. FIELD INSTALLATION			1470	
12. FIELD SUPERVISION Included in 11				
13. SUBSYSTEM CHECKOUT/ADJUSTMENT " "				
ENERGY TRANSPORT SUBSYSTEM				145
THERMAL				
1. PIPING				
2. INSULATION				
3. CONTROL VALVES AND LOCAL CONTROL ELEMENTS				
4. FLUID PUMPS AND DRIVES				
5. SITE PREPARATION, FOUNDATIONS, AND PIPING SUPPORT ELEMENTS				
6. MISCELLANEOUS (EXPLAIN)				
7. FIELD INSTALLATION				
8. FIELD SUPERVISION				
9. SUBSYSTEM CHECKOUT/ADJUSTMENT				
ELECTRICAL				
1. WIRING (MATERIAL, SUPPORTS, TRENCHES, etc.)			15	
2. UTILITY INTERFACE SUBSTATION			20	
3. LOCAL CONTROL ELEMENTS			60	
4. MISCELLANEOUS (EXPLAIN)				
5. FIELD INSTALLATION			50	
6. FIELD SUPERVISION Included in 5				
7. SUBSYSTEM CHECKOUT/ADJUSTMENT " "				
ENERGY STORAGE SUBSYSTEM				885
1. TANKS, INSULATION, STORAGE MEDIUM Batteries			585	
2. HEAT EXCHANGERS/BOILERS				
3. HEAT TRANSFER FLUID				
4. PUMPS, VALVES, PIPING, etc.				
5. LOCAL CONTROL ELEMENTS			200	
6. SITE PREPARATION/FOUNDATION				
7. MISCELLANEOUS (EXPLAIN)				
8. FIELD INSTALLATION			100	
9. FIELD SUPERVISION Included in 8				
10. SUBSYSTEM CHECKOUT/ADJUSTMENT " "				
CONTROL SUBSYSTEM				300
1. CONTROL SOFTWARE			50	
2. PROCESSORS/COMPUTERS			200	
3. SYSTEM CONTROL ELEMENTS FOR PLANT OPERATION				
4. SUBSYSTEM OPERATION CONTROL ELEMENTS				
5. CONTROL LINES TO SUBSYSTEMS AND PLANT CONTROL ELEMENTS				
6. BUILDINGS AND FACILITIES TO HOUSE EQUIPMENT				
7. MISCELLANEOUS (EXPLAIN)				
8. FIELD INSTALLATION			50	
9. FIELD SUPERVISION Included in 8				
10. SUBSYSTEM CHECKOUT/ADJUSTMENT " "				
DETAIL DESIGN				
PLANT CONSTRUCTION MANAGEMENT				
SPECIAL FEATURES				
RELATED ITEMS				
OTHER (BUILDINGS AND OTHER UTILITIES TO SUPPORT SYSTEM FUNCTIONS, etc.)				300
TESTING AND EVALUATION				500
TOTAL ESTIMATED COST				11280

ORIGINAL PAGE IS
OF POOR QUALITY

An external storage concept such as the sodium-sulfur battery (or the advanced composite flywheel) can be added later, depending on the results of the substantial DOE-sponsored current research on this technology. Also, a parallel development is recommended for the integral hybrid concept, that is, where the receiver can be heated by fossil fuel combustion as well as by the sun if there is sufficient interest in a stand-alone capability.

The $1MW_e$ power size is selected since 1) it has a lower $\overline{BBEC}$ than any lower power and 2) all higher powered systems are simple multiples of a $1MW_e$ system.